Doctoral theses at NTNU, 2023:207

Hao Chen

LABORATORY-BASED MODELLING OF VISCOELASTIC PROPERTIES OF ASPHALT PAVEMENT

Doctoral thesis

NTNU
Norwegian University of Science and Technology
Thesis for the Degree of Philosophiae Doctor
Faculty of Engineering
Department of Civil and Environmental Engineering

NTNU
Norwegian University of Science and Technology

Hao Chen

LABORATORY-BASED MODELLING OF VISCOELASTIC PROPERTIES OF ASPHALT PAVEMENT

Thesis for the Degree of Philosophiae Doctor

Trondheim, June 2023

Norwegian University of Science and Technology
Faculty of Engineering
Department of Civil and Environmental Engineering

NTNU
Norwegian University of
Science and Technology

NTNU
Norwegian University of Science and Technology

Thesis for the Degree of Philosophiae Doctor

Faculty of Engineering
Department of Civil and Environmental Engineering

ISBN 978-82-326-7116-8 (printed ver.)
ISBN 978-82-326-7115-1 (electronic ver.)
ISSN 1503-8181 (printed ver.)
ISSN 2703-8084 (online ver.)

Doctoral theses at NTNU, 2023:207

Printed by NTNU Grafisk senter

LABORATORY-BASED MODELLING OF VISCOELASTIC PROPERTIES OF ASPHALT PAVEMENT

PREFACE

This PhD thesis is submitted to the Norwegian University of Science and Technology (NTNU) for the fulfilment of the requirements for the degree of Philosophiae Doctor (PhD).

This work was carried out between August 2019 and June 2023 at the Department of Civil and Environmental Engineering at NTNU, Trondheim.

Professor Inge Hoff, NTNU, has been the main supervisor. Dr Rabbira Garba Saba, Norwegian Public Roads Administration (NPRA), has been the co-supervisor. Professor Gang Liu, Wuhan University of Technology (WUT), has been the co-supervisor.

Hao Chen

ACKNOWLEDGEMENTS

First of all, I would like to express my sincere gratitude to Professor Inge Hoff, my main supervisor, for his support, encouragement and expert guidance throughout my research work. I have learned a lot from his professional knowledge, rigorous scientific attitude and scientific research methods. I am very thankful for the opportunity of working with him.

I would also like to express my thankfulness to Dr. Rabbira Garba Saba, my co-supervisor and the senior principal engineer of the Norwegian Public Roads Administration, for his support and guidance in my experimental work.

Special thanks to Professor Gang Liu, my co-supervisor and the associate dean of the Wuhan University of Technology, for his technical advice and contribution to my thesis.

Thanks to Helge Mork, Alex Klein-Paste and Kelly Pitera for teaching me professional knowledge and skills and invaluable suggestions for my research. I would like to sincerely express my gratitude to Brynhild Snilsberg, Leif Jørgen Bakløkk and Sara Anastasio for their great help and support. I also wish to thank Diego Maria Barbieri for his remarkable assistance in my experimental work. Thanks to Bent Lervik and Jan Erik Molde for your considerable help with the experimental tests.

A warm thanks to my friends Albert Lau, Lei Zhang, Lisa Tronhuus Hannasvik, Fusong Wang, Jianan Liu, Baowen Lou, Seyedali Foroutan Mirhosseini, Wenxiu Jiao, Yang Bi and Ding Peng. Thanks to my friendly and lovely colleagues. Thanks for all the happy moments with you guys in science, party, sports, games and other activities. I would also like to thank all department members, technicians, students and personnel I met at IBM.

Finally, I would like to thank my wife Xuemei Zhang for her unending support throughout my PhD research at NTNU. Thanks to my parents for their support and affection.

ABSTRACT

The Norwegian Public Roads Administration (NPRA) is running a project "VegDim" with the aim of developing and implementing a Mechanistic-Empirical (ME) pavement design system for Norwegian conditions. The traditional empirical method uses resilient modulus to characterise the asphalt material by considering pure elastic properties. However, the asphalt material demonstrates a viscoelastic behaviour in servicing conditions of the flexible pavement. Therefore, the dynamic modulus closer to the real situation, which is time and temperature dependent, is adopted in the ME pavement design. The objective of this study is to investigate the dynamic modulus of various Norwegian asphalt mixtures and model the viscoelastic properties of asphalt mixtures and pavements.

Asphalt mixtures mostly used in Norway are divided into 20 types, based on the kinds of mixture and bitumen. In this study, the Marshall mix design was first conducted to determine the optimum binder contents of 20 types of asphalt mixtures containing Norwegian local aggregate materials. Then the asphalt slabs and gyratory samples based on the required aggregate gradings, and the optimum binder content were created by the roller compactor and the gyratory compactor. The roller compression method was determined as the asphalt sample preparation approach as it is believed to be closer to the paving situation in the field.

Afterwards, the Cyclic Indirect Tensile Test (CITT) and Cyclic Compression Test (CCT) under the same temperature and loading frequency conditions were compared regarding the measured dynamic modulus of asphalt mixtures in the laboratory. The results showed that the two test modes led to similar dynamic modulus values at intermediate temperatures (frequencies) and some differences at extreme conditions. Thus, the CCT was considered to measure the dynamic modulus of asphalt mixtures due to the sample size advantage for both laboratory and field samples in this study.

The master curves were established through the test results to predict the dynamic modulus of asphalt mixtures at any temperature and loading frequencies. Different models, Standard Logistic Sigmoidal (SLS) model, the Generalised Logistic Sigmoidal (GLS) model and the Christensen-Anderson-Marasteanu (CAM) model, for master curve construction were estimated to find an optimum model for Norwegian asphalt mixtures as well as the shifting techniques of log-linear, quadratic polynomial function, Arrhenius, William-Landel-Ferry (WLF) and Kaelble methods. The result indicated that the SLS model had the most suitable fit

for the specimens tested. The WLF equation was recommended for master curve construction due to better fit and convenience of temperature and shift factor transition. Therefore, the SLS model and WLF equation were used to construct the dynamic modulus master curves.

As the modelling method was determined, the dynamic modulus master curves of asphalt mixtures were established as a database for Norwegian materials, which further was the input for the ERAPave program for asphalt pavement structure design.

This research also investigated the relationship between material factors and dynamic modulus. The rheological properties of bitumen were characterised using a dynamic shear rheometer, in which the bitumen viscosity was fitted log-linearly by the temperature and the complex shear modulus master curve of bitumen was constructed by the modified Huet-Sayegh model. The grey relational analysis revealed the correlation existing between material factors and dynamic modulus. A prediction model was established using multiple linear regression based on the material factors to reduce dynamic modulus tests. The results indicated that the dynamic modulus of asphalt mixtures mainly depended on the bitumen type. The correlation between dynamic modulus and the material factors was found to show a good fit of the model with Coefficients of Determination, $R^2 \geq 0.973$.

Finally, the Finite Element (FE) method was implemented to predict the stress-strain response of the asphalt pavement. The viscoelastic behaviour of the materials was described by the generalised Maxwell model. The FE model was established through the relaxation modulus converted from the dynamic modulus master curve. The FE modelling was verified through the stress-strain response of the CITT. The results of the FE model matched the measured values. After validation, the numerical model incorporating the dynamic modulus master curve developed in this study was a very useful tool to predict the stress and strain responses of flexible road pavements.

This research provided a Norwegian material database and proposed the dynamic modulus modelling method and implement the modelling for the stress-strain response of asphalt pavements. This study can reduce huge test processes and provide a more accurate method to predict the viscoelastic behaviour of asphalt materials in cold regions.

TABLE OF CONTENTS

LIST OF FIGURES

LIST OF TABLES

LIST OF ABBREVIATIONS

a	Loading strip width in cyclic indirect tensile test setup
AADT	Annual average daily traffic
AC	Asphalt concrete
AG	Asphalt gravel
a_i	Model parameters in dynamic modulus prediction model based on rheological properties of bitumen
ANOVA	Analysis of variance
AP	Asphalt crushed stone
$\alpha(T)$	Shift factor
B	Binder content
β_c	Model parameter in 2S2P1D model
b_i *and* b_i'	Model parameters in dynamic modulus prediction model based on master curve parameter modelling
C	Model parameter in log-linear equation
CAM	Christensen-Anderson-Marasteanu
CCT	Cyclic compression test
CITT	Cyclic indirect tensile test
CoV	Coefficient of variation
C_1 *and* C_2	Model parameter in William-Landel-Ferry equation
C_1' *and* C_2'	Model parameter in Kaelble equation
C'	Model parameter in Arrhenius equation
δ, α, β *and* γ	Model parameter in standard logistic sigmoidal model
δ_d	Dimensionless coefficient in Huet-Sayegh model
$\Delta H(t)$	Horizontal deformation at a certain time
Δ_{ij}	Difference between material parameter sequence and reference sequence
δ_1, δ_2, m_1, m_2, τ_1 *and* τ_2	Model parameters in modified Huet-Sayegh model
δ', α', β', γ' *and* λ	Model parameter in generalised logistic sigmoidal model
DSR	Dynamic Shear Rheometer
E_a	Activation energy in Arrhenius equation
E_e	Equilibrium elastic modulus
E_i	Relaxation modulus

ε	Strain
$\varepsilon_x(x,t)$	Horizontal strain at a certain position and time
ε_0	Strain amplitude
$\varepsilon(t)$	Strain at a certain time
$\varepsilon^*(t)$	Complex strain at a certain time
ERAPave	Elastic response analysis of pavements
η_e	Equilibrium viscosity
η_i	Viscosity of the *i*th model element
$\eta_{60°C}$	Viscosity at 60 °C
$\eta(T)$	Viscosity at a certain temperature
E_0	Static modulus
E_1	Storage modulus
E_2	Loss modulus
$E(t)$	Relaxation modulus at a certain time
E^*	Complex modulus
$E^*(\omega)$	Complex modulus at a certain angular frequency
E_∞	Glassy modulus
$E'(\omega)$	Storage modulus at a certain angular frequency
$E''(\omega)$	Loss modulus at a certain angular frequency
$\lvert E^*\rvert$	Dynamic modulus
$\lvert E^*\rvert(T,f)$	Dynamic modulus at a certain temperature and frequency
f_c	Location parameter in Christensen-Anderson-Marasteanu model
FE	Finite Element
f_r	Reduced frequency
γ_0	Shear strain amplitude
$\gamma(X_0,X_i)$	Grey relational grade
$\gamma(X_{0j},X_{ij})$	Grey relational coefficient
$\gamma^*(t)$	Complex shear strain at a certain time
$\dot{\gamma}$	Shear rate
GLS	Generalised logistic sigmoidal
G_0	Complex shear modulus at infinitesimal frequency in modified Huet-Sayegh model
$G^*(\omega)$	Complex shear modulus at a certain angular frequency

G_∞	Complex shear modulus at finitesimal frequency in modified Huet-Sayegh model
$\|G_b^*\|$	Complex shear modulus of bitumen
$\|G_g^*\|$	Complex shear modulus at glassy state
$\|G^*\|(T,f)$	Complex shear modulus at certain temperature and frequency
HS	Huet-Sayegh
i	Complex notation
IBM	Department of Civil and Environmental Engineering
k	Number of independent variables
k_c	Critical point in Lorentzian equation
k_g	Growth rate in Lorentzian equation
k_p	Peak value in Lorentzian equation
LVDT	Linear variable differential transformers
LVE	Linear viscoelastic
MA	Soft asphalt
$MAPE$	Mean absolute percentage error
$max(\Delta_{ij})$	Maximum value of Δ_{ij} matrix
$max(x_{ij})$	Maximum value of x_{ij} matrix
ME	Mechanistic-empirical
MEPDG	Mechanistic-empirical pavement design guide
$min(\Delta_{ij})$	Minimum value of Δ_{ij} matrix
$min(x_{ij})$	Minimum value of x_{ij} matrix
MLR	Multiple linear regression
NAT	Nottingham asphalt tester
NPRA	Norwegian Public Roads Administration
NSE	Normalised square error
NTNU	Norwegian University of Science and Technology
v	Poisson's ratio
OBC	Optimum binder content
ω	Angular frequency
$Pen_{25°C}$	Penetration at 25 °C
PhD	Doctor of philosophy
φ	Phase angle

φ_b	Phase angle of bitumen
P_{max}	Maximum aggregate size
PMB	Polymer modified bitumen
p and q	Model parameters in quadratic polynomial equation
P^*	Complex load
R	Radius
R_g	Ideal gas constant
ρ_{mix}	Density of asphalt mixture
ρ_4	Cumulative retained on No. 4 sieve
ρ_{34}	Cumulative retained on 3/4 in sieve
ρ_{38}	Cumulative percent retained on 3/8 in sieve
ρ_{200}	Percentage passing No. 200 sieve
R^2	Coefficient of determination
SAE	Sum of absolute error
$\overline{SAE}$	Average value of sum of absolute error
S_e	Standard error of estimation
S_e/S_y	Standard error ratio
σ	Stress
$\sigma_x(x,t)$	Horizontal stress at certain position and time
$\sigma_y(x,t)$	Vertical stress at certain position and time
σ_0	Stress amplitude
$\sigma^*(t)$	Complex stress at a certain time
$\sigma(t)$	Stress at a certain time
Sig.	p-value
SLS	Standard logistic sigmoidal
SMA	Stone matrix asphalt
SSE	Sum of square error
$\overline{SSE}$	Average value of sum of square error
S_y	Standard error of deviation
t	Time
T	Temperature
τ	Relaxation time
T_g	Glass transition temperature

t_{lag}	Time lag
T_r	Reference temperature
$T_{R\&B}$	Softening point
τ_s	Shear stress
TV	Swedish Transport Administration
τ_0	Shear stress amplitude
$\tau^*(t)$	Complex shear stress at a certain time
UiA	University of Agder
UTM	Universal testing machine
v and w	Model parameters of Christensen-Anderson-Marasteanu modeld
V_a	Air void content
V_{beff}	Effective bitumen content
VFB	Voids filled with binder
VMA	Void in mineral aggregate
VTI	Swedish National Road and Transport Research Institute
WLF	William-Landel-Ferry
WUT	Wuhan University of Technology
X_G	Predicted frequency in global model
X_i	Material parameter sequence
x_{ij}	Material parameters
X_{ij}	Comparability sequence
Y	Measured value
$\hat{Y}$	Predicted value
$\bar{Y}$	Mean value of measured values
z	Specimen thickness
ζ	Resolution coefficient in grey relational analysis

1 INTRODUCTION

1.1 Background

The Norwegian Public Roads Administration (NPRA) is working together with Swedish Transport Administration (TV), Swedish National Road and Transport Research Institute (VTI) and Norwegian University of Science and Technology (NTNU) on a project called "VegDim" with the aim of developing and implementing the Mechanistic-Empirical (ME) pavement design system and creating a material database for Norwegian conditions (Figure 1) [1]. The traditional empirical approach is only applicable for a given set of environmental, material and vehicle loading conditions, which is difficult to estimate the future state of the road pavement. Whereas the ME method considering the characterisation of traffic, climatic effect and structural and material factors provides a unified basis for flexible pavement. It can not only predict a variety of road performances but also establish the relationships between road management systems and materials, road structure design, construction, climate, traffic, which can be widely used and more flexible and accurate to operate by engineers [2, 3].

Figure 1. Illustration of visual communication of VegDim project.

In order to develop a ME pavement design system for Norwegian conditions, a corresponding material database is required. The resilient modulus of both bound and unbound materials under repeated loads was generally applied in the empirical approach. However, asphalt materials show a viscoelastic behaviour when used in flexible road pavements [4-7]. The dynamic modulus taking viscoelasticity into account is used in the asphalt material characterisation of the ME pavement design system. Therefore, the dynamic modulus for asphalt mixtures relates to temperature and loading frequency. The Cyclic Compression Test (CCT) as a standard test method in the Mechanistic-Empirical Pavement Design Guide (MEPDG) is generally used in the laboratory to measure the dynamic modulus of asphalt

mixtures under different temperature and frequency conditions [2]. A cylindrical asphalt specimen with a diameter of 100 mm and a height of 150 mm is usually applied for the CCT. However, the thickness of the asphalt surface layer is usually thin, around 45 mm in Norway. In order to measure the dynamic modulus of field samples, another test method suitable for smaller dimension samples with a diameter of 100 mm and a thickness of 40 mm is applied, which is the Cyclic Indirect Tensile Test (CITT) [8-11]. The indirect tensile mode was developed by Kim et al. to assess the dynamic modulus [12] using both the CCT and CITT for 12 asphalt mixtures used in North Carolina. The results indicated similar dynamic modulus values. However, some studies found the two test modes resulted in a few differences in the dynamic modulus, phase angle and shift factor [13, 14]. The investigation of the influence of the two test modes on Norwegian asphalt mixtures is helpful to verify the dynamic modulus test results and develop the dynamic modulus test method for the ME pavement design system.

Although the CCT and CITT can be used to determine the dynamic modulus of asphalt mixtures in the laboratory, such test requires sophisticated devices and well-trained skills for operators. Since the change of asphalt material at high temperatures is equivalent to the change at low frequencies, and the change at low temperatures is equivalent to the change at high frequencies, the master curve based on the time-temperature superposition principle is established to predict the dynamic modulus of asphalt mixtures at any temperatures and loading frequencies [15, 16]. A smooth curve is obtained from a set of test results shifted through shifting techniques, which is called a master curve. The Standard Logistic Sigmoidal (SLS) model is widely used to fit the master curve of asphalt mixtures [17, 18]. However, the SLS model is more suitable for symmetrical test results. The Generalised Logistic Sigmoidal (GLS) model developed by Rowe et al. is better employed for asymmetric data [19, 20]. Moreover, the Christensen-Anderson-Marasteanu (CAM) model proposed by Marasteanu and Anderson provides a better fit within very low and very high frequencies for unmodified and polymer modified asphalt materials [21]. In addition, to construct the master curve the shifting techniques are considered for the time-temperature superposition relationship related to the viscoelastic properties of asphalt materials. The shifting technique is described by the shift factor, $\alpha(T)$, which is a function of temperature. In terms of mathematical functions, the log-linear equation shows the linear relationship between $log[\alpha(T)]$ and temperature normally used for asphalt materials [17, 22]. The quadratic polynomial equation is another mathematical function that can accurately fit the shift factor with the temperatures [23-25]. Considering that the bitumen consists of polymer is a highly heterogeneous mixture of hydrocarbons, the

temperature dependence of relaxation modes for bituminous materials around glass transition temperature (T_g) can be described by the Williams-Landel-Ferry (WLF) equation [26]. Furthermore, some experimental studies found that the Kaelble equation developed from the WLF equation is a symmetric function to accurately reflect the temperature dependence of viscoelastic properties of asphalt materials below T_g [27]. The Arrhenius equation is another popular model for the shift factor focusing on the thermally activated process [20, 28]. It is therefore necessary to select a proper model for the master curve construction in the development of the ME pavement design system for Norwegian conditions.

Based on the master curve approach, the characterisation of asphalt materials was incorporated into the ERAPave program, which achieved the ME pavement design. The dynamic modulus master curves of 20 asphalt mixture types mostly used in Norway were established in this thesis, which as the material database were input into the program for asphalt pavement structure design.

In addition to the master curve method constructed from experimental tests, the dynamic modulus of asphalt mixtures can be also predicted based on the physical, rheological and mechanical properties of bituminous binder and asphalt mixture itself. For low level road pavements, such a method can predict the dynamic modulus with relative accuracy based on material properties, which can also reduce the number of complex experiments. In the ME pavement design guide, the Witczak 1-37A model is used for Level 2 and Level 3 to predict the dynamic modulus based on the bitumen viscosity, air void content, effective bitumen content, cumulative percentage retained on the sieves and percentage passing the No. 200 sieve [2]. The Witczak 1-40D model was further developed by incorporating the complex shear modulus and phase angle of the binder in the NCHRP 1-40D protocol [29, 30]. Christensen et al. [31] used the Hirsch model to evaluate the dynamic modulus by considering the asphalt stiffness and void properties of the asphalt mixture. Based on the Hirsch model, Al-Khateeb et al. [32] developed a simpler form of the model to overcome the problem of inaccurate high and low temperature predictions. Besides, Sakhaeifar et al. [33] proposed two models based on the viscoelasticity of asphalt materials to predict the dynamic modulus at a wide range of temperatures called global and simplified global models. Although these models can predict the dynamic modulus well in previous studies [34-36], such models are based on test results from hundreds of asphalt mixture types in the United States. Due to differences in environment and materials around the world, these models exhibit different results for different regions in

the world [37-39]. Therefore, a dynamic modulus prediction model suitable for Norwegian conditions considering the material influence on dynamic modulus can be investigated for developing the Norwegian ME pavement design system.

The dynamic modulus as the main parameter characterising the mechanical properties of asphalt materials is used to describe the stress-strain response of flexible road pavement under the vehicle load. In recent years, numerical models based on the Finite Element (FE) method have been developed for estimating the performance of asphalt road pavements. The dynamic modulus is one of the inputs for viscoelastic behaviour simulation of asphalt material in the FE approach. Zhang et al. [40] implemented the generalised Maxwell model to simulate the viscoelasticity of asphalt mixtures with the FE modelling and verified the model. Wang et al. [41] found that the viscoelastic numerical simulation results implementing the Burgers model were in good agreement with the outcomes of the laboratory test. The viscoelasticity of asphalt materials can be well simulated based on the FE method [42]. Such a numerical model can be used to predict the stress-strain response of asphalt pavements. Hasan et al. [43] simulated and analysed the performance of pavement structures containing geosynthetics under different axle loads. The results showed that the tensile, shear and compressive strains increased with higher axle loads and the longitudinal strain in the pavement increased with the thickness of the road structure. Selsal et al. [44] studied the stress distribution at different depths of hot mix asphalt and stone mastic asphalt road pavements using the FE method, demonstrating that the latter is more wearing resistant.

1.2 Research objective and approach

The main objective of this research is to model the viscoelastic properties of asphalt pavement to develop the ME pavement design system for Norwegian conditions. The viscoelasticity of asphalt mixtures is characterised by the dynamic modulus. The measurements of dynamic modulus were discussed due to a variety of test methods. After obtaining the dynamic modulus data, the master curve constructed based on the time-temperature superposition principle with proper models is used to predict the dynamic modulus of asphalt mixtures. Since the dynamic modulus of asphalt mixtures was highly influenced by the material properties, the effect of material factors was also investigated to propose associated prediction models for different types of asphalt mixtures. Finally, the modelling was implemented through the FE method for stress-strain response prediction of asphalt pavements. Above all, this project is divided into five sub-objectives as follows:

(1) Determination of dynamic modulus test method by comparing the compressive and indirect tensile modes.

(2) Development of the master curve based on the evaluation of different models and shift factor equations for Norwegian asphalt mixtures.

(3) Master curve establishment of 20 types of asphalt mixtures mostly used in Norway through the test results to provide the material database for the ME pavement design system.

(4) Investigation of the influence of material factors on the determination of dynamic moduli and development of associated prediction models for different types of asphalt mixtures.

(5) Implementation of the modelling of viscoelastic properties of asphalt mixtures by the FE method to predict the stress-strain response of asphalt pavements.

These sub-objectives and related publications (listed in Section 1.4) are summarised in the following Figure 2.

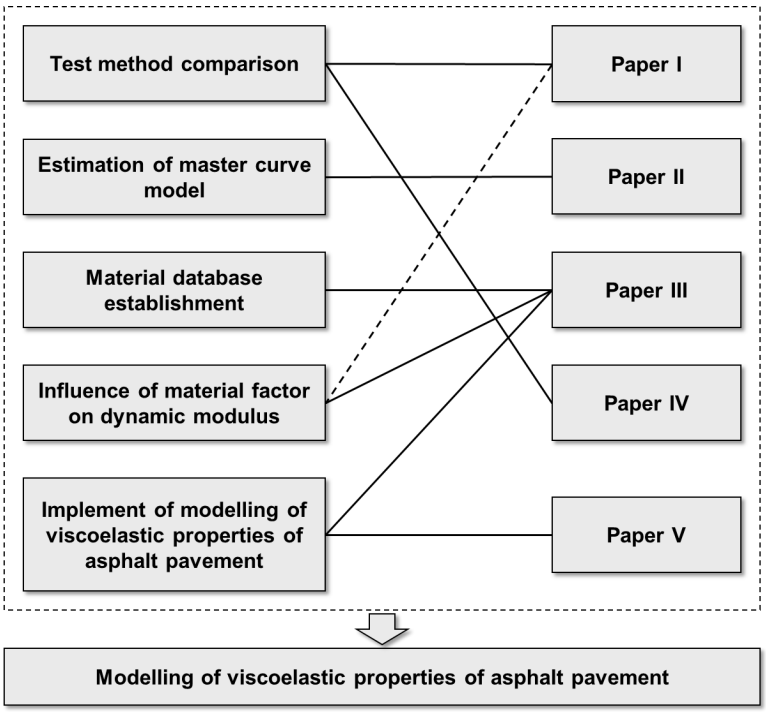

Figure 2. Relations between the papers and the sub-objectives discussed in the thesis.

1.3 Thesis structure

This thesis is divided into five main chapters.

- Chapter 1 introduces the research background and scope.
- Chapter 2 describes the viscoelastic properties of asphalt materials, namely the dynamic modulus.
- Chapter 3 illustrates the source and properties of raw materials, the test modes and the modelling method as well as the FE analysis for the asphalt pavements.
- Chapter 4 discusses the comparison of test methods, the master curve model selection, the master curve parameters required for the ME pavement design system, the influence of material factors on the dynamic modulus and the FE modelling.
- Chapter 5 presents the conclusions, limitations and recommendations for future work.
- The references are listed in Chapter 6.

1.4 Contributions and publications

This research provided the appropriate test method and master curve model for Norwegian conditions and established the material database for the ME pavement design system. The dynamic modulus of asphalt mixtures was mainly affected by the bitumen properties. The prediction model of dynamic modulus based on material factors was proposed for developing the new system. Based on the dynamic modulus and viscoelastic constitutive relationship of asphalt materials, the FE model validated by the CITT results was built as a useful tool to predict the mechanical properties of asphalt pavements. The papers written during the PhD period are listed as follows:

(1) Thesis related publications

Paper I

Chen, Hao; Barbieri, Diego Maria; Hoff, Inge; Mork, Helge; Wathne, Pål; Liu, Gang.

Construction of asphalt mixture master curves for a Norwegian mechanistic-empirical pavement design system.

Published and presented at the Eleventh International Conference on the Bearing Capacity of Roads, Railways and Airfields, Volume 2, 423-434, 2022.

Contribution:

Chen, Hao: Conceptualization, Methodology, Software, Validation, Formal Analysis, Investigation, Data Curation, Writing - Original Draft, Writing - Review & Editing, Visualization. **Barbieri, Diego Maria:** Investigation, Writing - Review & Editing. **Hoff, Inge:** Resources, Writing - Review & Editing, Supervision. **Mork, Helge:** Writing - Review & Editing. **Wathne, Pål:** Investigation, Writing - Review & Editing. **Liu, Gang:** Writing - Review & Editing, Supervision.

Paper II

Chen, Hao*; Barbieri, Diego Maria; Zhang, Xuemei; Hoff, Inge

Reliability of Calculation of Dynamic Modulus for Asphalt Mixtures Using Different Master Curve Models and Shift Factor Equations.

Published in the Journal of Materials, 15(12), 4325, 2022.

Contribution:

Chen, Hao: Conceptualization, Methodology, Software, Validation, Formal Analysis, Investigation, Data Curation, Writing - Original Draft Preparation, Visualization. **Barbieri, Diego Maria:** Methodology, Writing - Review & Editing. **Zhang, Xuemei:** Formal Analysis, Writing - Review & Editing. **Hoff, Inge:** Resources, Writing - Review & Editing, Supervision.

Paper III

Chen, Hao*; Saba, Rabbira Garba; Liu, Gang; Barbieri, Diego Maria; Zhang, Xuemei; Hoff, Inge

Influence of material factors on the determination of dynamic moduli and associated prediction models for different types of asphalt mixtures.

Published in the Journal of Construction and Building Materials, 365, 130134, 2023.

Contribution:

Chen, Hao: Conceptualization, Methodology, Software, Formal Analysis, Investigation, Data Curation, Writing - Original Draft. **Saba, Rabbira Garba:** Project Administration, Resources, Writing - Review & Editing, Supervision. **Liu, Gang:** Methodology, Writing - Review & Editing, Supervision. **Barbieri, Diego Maria:** Investigation, Writing - Review & Editing. **Zhang, Xuemei:** Investigation, Writing - Review & Editing. **Hoff, Inge:** Resources, Writing - Review & Editing, Supervision.

Paper IV

Chen, Hao*; Alamnie, Mequanent Mulugeta; Barbieri, Diego Maria; Zhang, Xuemei; Liu, Gang; Hoff, Inge.

Comparative study of indirect tensile test and uniaxial compression test on asphalt mixtures: Dynamic modulus and stress-strain state.

Published in the Journal of Construction and Building Materials, 366, 130187, 2023.

Contribution:

Chen, Hao: Conceptualization, Methodology, Software, Formal Analysis, Investigation, Data Curation, Writing - Original Draft. **Alamnie, Mequanent Mulugeta:** Conceptualization, Methodology, Investigation, Data Curation, Writing - Review & Editing. **Barbieri, Diego Maria:** Investigation, Writing - Review & Editing. **Zhang, Xuemei:** Investigation, Writing - Review & Editing. **Liu, Gang:** Methodology, Writing - Review & Editing, Supervision. **Hoff, Inge:** Resources, Writing - Review & Editing, Supervision.

Paper V

Chen, Hao; Hoff, Inge; Liu, Gang*; Zhang, Xuemei**; Barbieri, Diego Maria; Wang, Fusong; Liu, Jianan.

Development of finite element model based on indirect tensile test for various asphalt mixtures.

Submitted to the Journal of Construction and Building Materials (Under review).

Contribution:

Chen, Hao: Conceptualization, Methodology, Software, Validation, Formal Analysis, Investigation, Writing - Original Draft, Writing - Review & Editing, Visualization. **Hoff, Inge:** Methodology, Validation, Investigation, Resources, Writing - Review & Editing, Supervision. **Liu, Gang:** Methodology, Investigation, Writing - Review & Editing, Supervision. **Zhang, Xuemei:** Investigation, Writing - Review & Editing, Visualization. **Barbieri, Diego Maria:** Methodology, Investigation, Writing - Review & Editing. **Wang, Fusong:** Investigation, Writing - Review & Editing. **Liu, Jianan:** Investigation, Writing - Review & Editing.

(2) Other significant publications

Paper VI

Zhang, Xuemei; **Chen, Hao***; Barbieri, Diego Maria; Lou, Baowen; Hoff, Inge.

The classification and reutilisation of recycled asphalt pavement binder: Norwegian case study.

Published in the Journal of Case Studies in Construction Materials, 17, e01491, 2022.

Contribution:

Zhang, Xuemei: Conceptualization, Methodology, Formal Analysis, Writing - Original Draft. **Chen, Hao:** Conceptualization, Methodology, Formal Analysis, Writing - Review & Editing. **Barbieri, Diego Maria:** Methodology. **Lou, Baowen:** Methodology. **Hoff, Inge:** Resources, Supervision.

Paper VII

Zhang, Xuemei; **Chen, Hao***; Saba, Rabbira Garba; Hannasvik, Lisa Tronhuus.

Lateral and Longitudinal Variations in Dynamic Modulus of Asphalt Pavement: Surface Layer and Base Layer.

Published in the Journal of Construction and Building Materials, 381, 131304, 2023.

Contribution:

Zhang, Xuemei: Conceptualization, Investigation, Data Curation, Formal Analysis, Writing - Original Draft. **Chen, Hao:** Conceptualization, Methodology, Investigation, Data Curation, Formal Analysis, Writing - Review & Editing. **Saba, Rabbira Garba:** Resources, Investigation, Writing - Review & Editing. **Hannasvik, Lisa Tronhuus:** Methodology, Writing - Review & Editing.

(3) Additional publications (not part of the thesis)

Zhang, Xuemei*; **Chen, Hao**; Hoff, Inge.

The mutual effect and reaction mechanism of bitumen and de-icing salt solution.

Published in the Journal of Construction and Building Materials, 302, 124213, 2021.

Contribution:

Chen, Hao: Methodology, Writing - Original Draft, Writing - Review & Editing.

Barbieri, Diego Maria*; Lou, Baowen; **Chen, Hao**; Shu, Benan; Wang, Fusong; Hoff, Inge.

Organosilane and Lignosulfonate Stabilization of Roads Unbound: Performance during a Two-Year Time Span.

Published in the Journal of Advances in Civil Engineering, 2021, 1-13, 2021.

Contribution:

Chen, Hao: Investigation, Writing - Review & Editing.

Barbieri, Diego Maria*; Lou, Baowen; Dyke, Robert Jason; **Chen, Hao**; Wang, Fusong; Connor, Billy; Hoff, Inge.

Mechanical properties of roads unbound treated with synthetic fluid based on isoalkane and tall oil.

Published in the Journal of Transportation Geotechnics, 32, 100701, 2022.

Contribution:

Chen, Hao: Investigation, Resources, Writing - Review & Editing, Visualization.

Zhang, Xuemei*; Hoff, Inge; **Chen, Hao**.

Characterization of Various Bitumen Exposed to Environmental Chemicals.

Published in the Journal of Cleaner Production, 337, 130610, 2022.

Contribution:

Chen, Hao: Methodology, Writing - Review & Editing.

Lou, Baowen; Sha, Aimin*; Barbieri, Diego Maria; Zhang, Xuemei; **Chen, Hao**; Hoff, Inge.

Evaluation of Microwave Aging Impact on Asphalt Mixtures.

Published in the Journal of Road Materials and Pavement Design, 24(3), 730-743, 2022.

Contribution:

Chen, Hao: Investigation, Writing - Review & Editing.

Zhang, Xuemei*; **Chen, Hao**; Barbieri, Diego Maria; Hoff, Inge.

Laboratory Evaluation of Mechanical Properties of Asphalt Mixtures Exposed to Sodium Chloride.

Published in the Journal of Transportation Research Record, 2676, 03611981221082579, 2022.

Contribution:

Chen, Hao: Conceptualization, Methodology, Investigation, Data Curation, Formal Analysis, Writing - Review & Editing.

Barbieri, Diego Maria*; Lou, Baowen; Dyke, Robert Jason; **Chen, Hao**; Wang, Fusong; Dongmo-Engeland, Berthe; Tingle, Jeb S.; Hoff, Inge.

Stabilization of Coarse Aggregates with Traditional and Nontraditional Additives.

Published in the Journal of Materials in Civil Engineering, 34(9), 04022207, 2022.

Contribution:

Chen, Hao: Investigation, Writing - Review & Editing.

Barbieri, Diego Maria*; Lou, Baowen; Dyke, Robert Jason; Wang, Fusong; **Chen, Hao**; Shu, Benan; Gazder, Uneb; Horpibulsuk, Suksum; Tingle, Jeb S.; Hoff, Inge.

Design and sustainability analyses of road base layers stabilized with traditional and nontraditional additives.

Published in the Journal of Cleaner Production, 372, 133752, 2022.

Contribution:

Chen, Hao: Investigation, Resources, Writing - Review & Editing, Visualization.

Zhang, Xuemei*; Fidai, Tawab; Hoff, Inge; Lerfald, Bjørn Ove; **Chen, Hao**.

Determination of Rejuvenator Proportion within the Recycled Bitumen: Empirical Double-Logarithmic Formula and Calibration.

Published in the Journal of Materials in Civil Engineering, 34(12), 04022350, 2022.

Contribution:

Chen, Hao: Investigation, Methodology, Writing - Review & Editing.

Jing, Haosen[1]; Liu, Jianan[1]; Wang, Zhenjun*; **Chen, Hao**; Zhang, Xuemei; Yuan, Linjian.

X-ray computed tomography analysis of internal voids in steel slag asphalt mixture under freeze–thaw damage and microwave healing process.

Published in the Journal of Construction and Building Materials, 377, 131132, 2023.

Contribution:

Chen, Hao: Writing - Review & Editing.

2 VISCOELASTIC PROPERTIES OF ASPHALT MATERIALS

The asphalt pavement exhibits Linear Viscoelastic (LVE) properties when subject to small strain during service. The mechanical behaviour of asphalt material is time-dependent showing both viscosity and elasticity. Thus, the stress-strain constitutive relationship of asphalt material satisfies the Boltzmann superposition principle, and for a one-dimensional condition it is expressed as follows [45]:

$$\sigma(t) = \int_0^t E(t-\tau)\frac{d\varepsilon}{d\tau}d\tau \tag{1}$$

where σ is the stress, ε is the strain, τ is the integration time variable, t is the time, and $E(t)$ is the relaxation modulus.

2.1 Complex modulus

The complex modulus of asphalt material was mainly discussed in this study, which was also used for the Mechanistic-Empirical (ME) pavement design system. When a sinusoidal load is applied to the asphalt material, the strain response delays relative to stress application as shown in Figure 3.

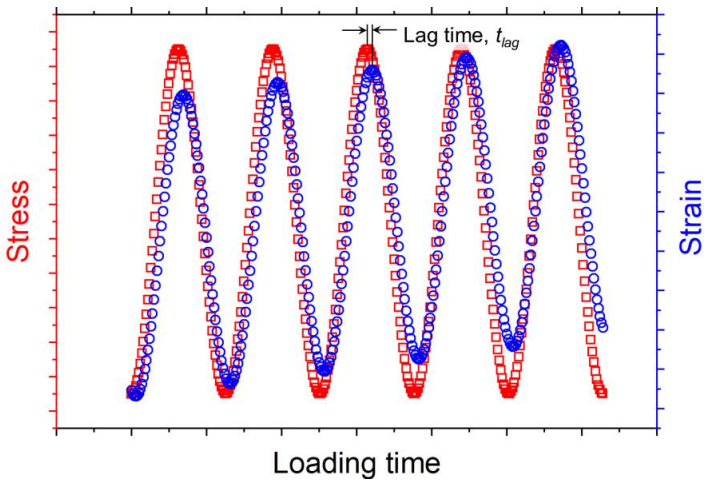

Figure 3. Schematic diagram of stress-strain response of asphalt material under sinusoidal loading.

This lag time, t_{lag}, is described by the phase angle, φ. The time-dependent stress, $\sigma(t)$, and strain, $\varepsilon(t)$, are expressed in Equation 2.

$$\varphi = \omega t_{lag} \tag{2.1}$$

$$\sigma(t) = \sigma_0 \sin(\omega t) \tag{2.2}$$

$$\varepsilon(t) = \varepsilon_0 \sin(\omega t - \varphi) \tag{2.3}$$

where ω is the angular frequency, σ_0 is the stress amplitude, and ε_0 is the strain amplitude.

The complex notation, i, is adopted to define the complex stress, $\sigma^*(t)$, and strain, $\varepsilon^*(t)$, as expressed below:

$$\sigma^*(t) = \sigma_0 e^{i\omega t} \tag{3.1}$$

$$\varepsilon^*(t) = \varepsilon_0 e^{i\omega t - \varphi} \tag{3.2}$$

The complex modulus, $E^*(\omega)$, is calculated as follows:

$$E^*(\omega) = \frac{\sigma^*(t)}{\varepsilon^*(t)} = \frac{\sigma_0 e^{i\omega t}}{\varepsilon_0 e^{i\omega t - \varphi}} = |E^*| e^{i\varphi} \tag{4}$$

where $|E^*|$ is the norm of complex modulus, which is also called the dynamic modulus equal to σ_0 divided by ε_0. Due to the complex form, E^* including real, E_1, and imaginary, E_2, parts is also expressed as follows:

$$E^* = E_1 + iE_2 = |E^*| \cos\varphi + i|E^*| \sin\varphi \tag{5}$$

E_1 is the storage modulus representing the recoverable part of the material during loading and the elasticity of the mechanical behaviour, while E_2 is the loss modulus reflecting the unrecoverable viscous part of the material. Equation 5 indicates that when φ = 0, the material exhibits pure elasticity, while a φ of 90° denotes pure viscous. When $0 < \varphi < 90°$, the material has LVE behaviour. Similar to the $E^*(\omega)$, the complex shear modulus, $G^*(\omega)$, is defined as:

$$G^*(\omega) = \frac{\tau^*(t)}{\gamma^*(t)} = \frac{\tau_0 e^{i\omega t}}{\gamma_0 e^{i\omega t - \varphi}} = |G^*| e^{i\varphi} = G_1 + iG_2 = |G^*| \cos\varphi + i|G^*| \sin\varphi \tag{6}$$

where $\tau^*(t)$ is the complex shear stress, $\gamma^*(t)$ is the complex shear strain, τ_0 is the shear stress amplitude, and γ_0 is the shear strain amplitude.

2.2 LVE models for asphalt materials

The LVE model is employed to simulate the LVE behaviour of asphalt materials, which is defined as a combination of springs (representing elastic behaviour) and dashpots (representing Newtonian viscous behaviour) [46-49]. The LVE models commonly used for asphalt materials are described as follows.

The generalised Maxwell model consists of a number of Maxwell elements in parallel with an isolate spring and an isolate dashpot, which prevents zero relaxation modulus and infinite creep compliance [50], as depicted in Figure 4 [51]. The complex modulus of the generalised Maxwell model is given by:

$$E^*(\omega) = E_e + i\omega\eta_e + \sum_i^n E_i \frac{i\omega\tau_i}{1+i\omega\tau_i} \tag{7}$$

where E_e is the equilibrium elastic modulus of the isolate spring, η_e is the equilibrium viscosity of the isolate dashpot and is infinite for solid materials, E_i is the relaxation modulus of the ith Maxwell element, τ_i is the relaxation time, and $i = 1, 2, \ldots, n$.

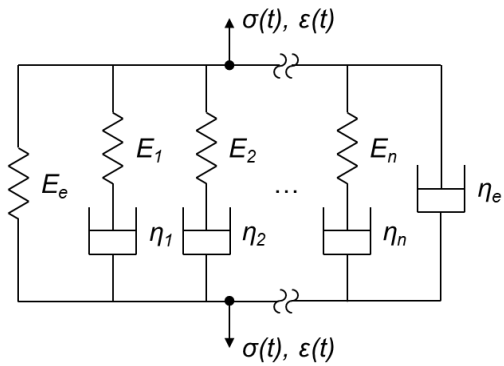

Figure 4. Schematic diagram of generalised Maxwell model.

The generalised Kelvin-Voigt model, illustrated in Figure 5, is composed of several Kelvin-Voigt elements connected in series with an additional spring and an additional dashpot [51]. The complex modulus of the generalised Kelvin-Voigt model is expressed as follows:

$$E^*(\omega)=\left(\frac{1}{E_e}+\frac{1}{i\omega\eta_e}+\sum_i^n\frac{1}{E_i+i\omega\eta_i}\right)^{-1} \tag{8}$$

where η_i is the viscosity of the ith Kelvin-Voigt element.

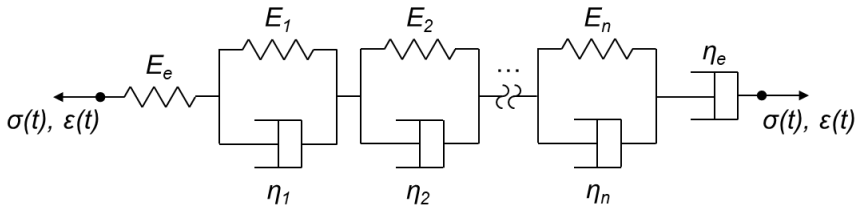

Figure 5. Schematic diagram of generalised Kelvin-Voigt model.

The Huet-Sayegh (HS) model used for asphalt concrete [52, 53] comprises a spring and two parabolic elements connected in series, as well as a spring in parallel [54, 55] as shown in Figure 6. The complex modulus of the Huet-Sayegh model is written as follows:

$$E^*(\omega)=E_0+\frac{E_\infty-E_0}{1+\delta_d(i\omega\tau)^{-m_1}+(i\omega\tau)^{-m_2}} \tag{9}$$

where m_1 is the exponent of the first parabolic element, m_2 is the exponent of the second parabolic element, δ_d is the dimensionless coefficient, E_0 is the static modulus when ω equals 0, and E_∞ is the glassy modulus when ω tends to infinity.

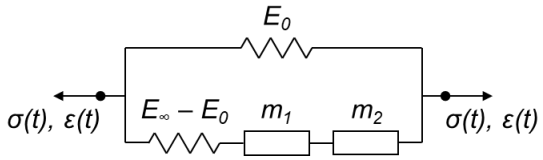

Figure 6. Schematic diagram of HS model.

The 2S2P1D model developed by adding a dashpot to the HS model has shown to be effective in modelling the mechanical behaviour of asphalt materials [56-59] as described in Figure 7. The complex modulus of the 2S2P1D model is expressed as:

$$E^*(\omega)=E_0+\frac{E_\infty-E_0}{1+\delta(i\omega\tau)^{-m_1}+(i\omega\tau)^{-m_2}+(i\omega\beta_c\tau)^{-1}} \tag{10}$$

where $\beta_c = \eta/[(E_0 - E_\infty)\tau]$.

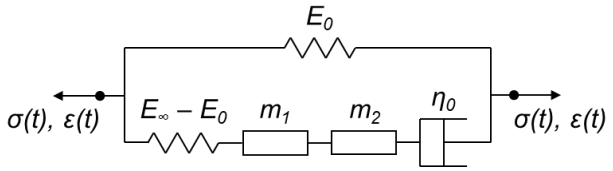

Figure 7. Schematic diagram of 2S2P1D model.

3 RESEARCH METHODOLOGY

3.1 Raw materials

A large number of combinations of different binders and aggregates are in use in Norway, and it is not realistic to test all of them. Since bitumen is believed to be more important the aggregate type was kept constant.

3.1.1 Bitumen

Three classes of bitumen commonly used for Norwegian roads were applied in this thesis. They were the neat bitumen named after the penetration, the Polymer Modified Bitumen (PMB) and the soft bitumen coded by the viscosity, which included nine subclasses of bitumen. The physical properties of nine types of bitumen as given in Table 1 fulfil the requirements set by EN 12591 [60]. The bitumen 70/100 and 160/220 were supplied by the company Veidekke (Trondheim, Norway) and the others were provided by company Nynas (Göteborg, Sweden).

Table 1. Physical properties of bitumen.

Bitumen type		Penetration at 25 °C [0.1 mm] EN 1426 [61]	Softening point [°C] EN 1427 [62]	Dynamic or kinematic viscosity at 60 °C [Pa·s or mm^2/s] EN 13702 [63]
Neat bitumen	70/100	92	46.0	235.7 Pa·s
	160/220	189	38.1	102.6 Pa·s
	330/430	-	-	44.5 Pa·s
PMB	65/105-60	88	62.6	391.8 Pa·s
Soft bitumen	V1500	-	-	1708 mm^2/s
	V3000	-	-	2815 mm^2/s
	V6000	-	-	5450 mm^2/s
	V9000	-	-	8990 mm^2/s
	V12000	-	-	14036 mm^2/s

The bitumen types tested are examples of commonly used bitumen. However, there are significant variations in the groups, e.g., one should be careful to use these results as the representation of a group.

3.1.2 Stone materials

Two kinds of local stone materials as aggregates were adopted in this research. The first type was a crushed rock from the Vassfjell area supplied by the company Franzefoss (Heimdal, Norway), which also presented very good performance and was largely used for road construction in the central part of Norway [64, 65]. The next type of aggregate was natural gravel supplied by the company Forset Grus (Tanem, Norway). This material was characterised by poor mechanical performance and was usually used for low traffic volume roads. Table 2 specifies the wear resistance (abrasion value and Micro-Deval coefficient) and fragmentation (Los Angeles value) of aggregates. The strength of the crushed rock aggregates met the requirements of the Norwegian pavement design handbook N200 with an Annual Average Daily Traffic (*AADT*) of approximately 15000 [66]. The stone materials obtained from the quarry were divided into aggregates of various sizes, i.e., 16 mm – 22.4 mm, 11.2 mm – 16 mm, 8 mm – 11.2 mm, 4 mm – 8 mm, 2 mm – 4 mm, 1 mm – 2 mm, 0.25 mm – 1 mm, 0.063 mm – 0.25 mm and < 0.063 mm, by a sieving machine for the preparation of the mixture. In terms of asphalt mixtures used for roads with a lower *AADT*, 30% to 50% of finely crushed rock aggregates were replaced by natural gravel.

Table 2. Wear resistance and fragmentation of aggregates.

Stone material	Wear resistance		Fragmentation
	Abrasion value [%] EN 1097-9 [67]	Micro-Deval coefficient [%] EN 1097-1 [68]	Los Angeles value [%] EN 1097-2 [69]
Crushed rock	7.8	14.2	18.2
Natural gravel	17.3	17.3	27.7

3.2 Sample preparation for dynamic modulus test

Twenty types of asphalt mixtures mostly used for Norwegian roads were investigated in this study, which involved five grading types of Asphalt Concrete (AC), Stone Matrix Asphalt (SMA), Soft Asphalt (MA) for the low traffic volume road, Asphalt Gravel (AG) and Asphalt Crushed Stone (AP) with a high air void content, and nine kinds of bitumen mentioned above. The grading types of AC, SMA and MA were used for the surface layer and the other two kinds of gradings AG and AP were applied to the base layer. All asphalt mixtures were fabricated in the laboratory with the average values of the upper and lower limits of the required grading curves according to the Norwegian pavement design report No. 670 [70] and the Optimum

Binder Contents (*OBC*) determined by the Marshall mix design method [71]. The used grading curves and the *OBC* of the 20 asphalt mixture types are shown in Table 3.

Table 3. Used grading curves and *OBC* of 20 asphalt mixture types.

Mixture code	Passing percentage [%]									*OBC* [%]
	22.4 mm	16 mm	11.2 mm	8 mm	4 mm	2 mm	1 mm	0.25 mm	0.063 mm	
AC 11-70/100		100	95	70	47.5	33.5	25.5	12.5	7.5	5.1
AC 11-160/220		100	95	77	56	41.5	31.5	15	7.5	5.2
AC 11-330/430		100	95	77	56	41.5	31.5	15	7.5	5.8
AC 11-PMB		100	95	70	47.5	33.5	25.5	12.5	7.5	5.2
AC 16-70/100	100	95	71	58		31.5	24.5	13.5	8	4.9
AC 16-160/220	100	95	76	65		35.5	24.5	12.5	5.5	5.0
AC 16-330/430	100	95	76	65		35.5	24.5	12.5	5.5	5.6
AC 16-PMB	100	95	71	58		31.5	24.5	13.5	8	4.9
SMA 11-70/100		100	95	55.5	37.5	26		16	11	5.3
SMA 11-PMB		100	95	55.5	37.5	26		16	11	5.3
SMA 16-70/100	100	95	56	37		22.5		13.5	10	5.1
SMA 16-PMB	100	95	56	37		22.5		13.5	10	5.2
MA 11-V1500		100	94.5	79.5	60	43.5	34	17	6	4.3
MA 11-V6000		100	94.5	79.5	60	43.5	34	17	6	4.3
MA 16-V3000	100	92.5	80.5		46	31	21	8	5	4.0
MA 16-V9000	100	92.5	80.5		46	31	21	8	5	4.2
MA 16-V12000	100	92.5	80.5		46	31	21	8	5	4.2
AG 16-70/100	100	95	75			35.5		12.5	6	4.7
AG 16-160/220	100	95	75			35.5		12.5	6	4.6
AP 16-70/100	100	95	45	34.5		17		6.5	5	2.8

Based on the grading curves and *OBC*, the corresponding amounts of bitumen and aggregates were first preheated at the conditioning temperature and time according to EN 12697-35 [72]. Then, these materials were mixed in a continuously heated blender for 3 – 5 min to obtain the asphalt mixtures. Considering that the roller compression method was closer to on-site paving, 20 types of asphalt mixtures for the dynamic modulus test were fabricated by the roller compactor. The 305 mm × 305 mm × 60 mm mould with a 3 mm thickness resin plate at the bottom for protecting the mould from the following coring operation was also preheated. The asphalt mixture was poured into the mould with the resin plate to prepare the asphalt slab. The roller compactor manufactured by Cooper Technology (Ripley, UK) was performed to compress the asphalt slab based on four sequences with the table moving velocity of 250 ± 100 mm/s and applying pressures of 2, 4, 6 and 0 bar, respectively [73]. Each stage consisted of four passes and the vibration was used during the last two passes of the fourth stage to ensure an adequate compaction. The cylindrical specimens with a diameter of 100 mm and a height of 40 mm for the dynamic modulus test were cored and cut from the compacted slabs. Therefore, five samples were obtained from one slab, four of which as the parallel

samples were applied to the test. A total of 80 testing specimens were fabricated for 20 asphalt mixture types.

Since different sample preparation methods and dynamic modulus testing methods were compared in this thesis, the gyratory compaction method was also used to prepare the specimens for dynamic modulus test. The gyratory compactor ICT-150RB produced by Invelop oy (Semolina, Finland) was adopted to fabricate the specimens. The asphalt mixture mixed by the same way mentioned earlier was filled into a preheated cylindrical mould with a diameter of 150 mm. The mass of the asphalt mixture added was calculated through the density, which aimed to obtain a cylindrical specimen with a diameter of 150 mm and a height of 180 mm. The compaction pressure was 620 kPa, and the gyratory angle was set to 17 mrad (0.97°) [74]. The specimens of four asphalt mixture types of AC 11-70/100, AC 16-70/100, SMA 11-70/100 and SMA 16-70/100 were prepared by the gyratory compactor. The gyrations of 100 and 115 were applied for the AC mixtures and the SMA mixtures, respectively [75]. All four mixture types were used to compare different sample preparation methods, and AC 11-70/100 and SMA 11-70/100 were also utilised to investigate the differences between dynamic modulus tests. The cylindrical specimens with a diameter of 100 mm and heights of 40 mm and 150 mm were cored and cut from the gyratory samples, which were used for the CITT and CCT respectively. Two testing specimens with a height of 40 mm or one testing specimen with a height of 150 mm were obtained from one gyratory sample. Four replicate specimens were adopted for the dynamic modulus test. A total of 24 testing specimens were prepared by the gyratory compaction method. All specimens used for dynamic modulus tests are given in Table 4. The sample preparation process in the laboratory is shown in Figure 8.

Table 4. All specimens used for dynamic modulus tests.

Investigation	Mixture type	Height of 100mm diameter cylindrical sample [mm]	Number of replicate samples	Sample preparation method	Dynamic modulus test method	Dynamic modulus test condition
Material database establishment and estimation of master curve models	AC 11-70/100 AC 11-160/220 AC 11-330/430 AC 11-PMB AC 16-70/100 AC 16-160/220 AC 16-330/430 AC 16-PMB SMA 11-70/100 SMA 11-PMB SMA 16-70/100 SMA 16-PMB MA 11-V1500 MA 11-V6000 MA 16-V3000 MA 16-V9000 MA 16-V12000 AG 16-70/100 AG 16-160/220 AP 16-70/100	40	4	Roller compression	CITT	-15, -10, 0, 15 and 30 °C 10, 5, 3, 1, 0.3 and 0.1 Hz
Comparison of sample preparation methods	AC 11-70/100 AC 16-70/100 SMA 11-70/100 SMA 16-70/100	40	4	Gyratory compaction	CITT	-15, 0, 15 and 30 °C 10, 5, 3, 1, 0.3 and 0.1 Hz
Comparison of dynamic modulus tests	AC 11-70/100 SMA 11-70/100	40 150 40 150	4	Gyratory compaction	CITT CCT (UiA*) CITT CCT (UiA*)	-10, 5, 21 and 40 °C 10, 5, 2, 1, 0.2 and 0.1 Hz

*The CCT was conducted in the laboratory of University of Agder (UiA).

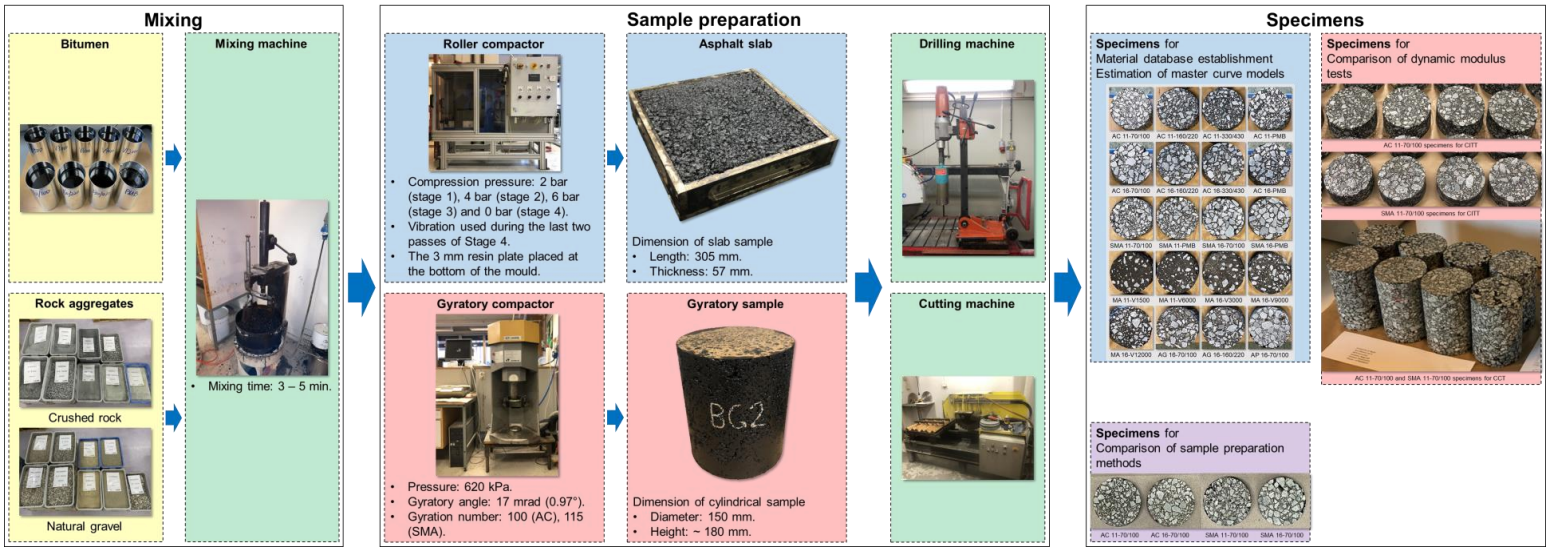

Figure 8. Sample preparation process in the laboratory.

3.3 Experimental procedures

3.3.1 Viscosity test of bitumen

The bitumen properties were characterised to investigate the correlation between material factors and the dynamic modulus of asphalt mixtures. The dynamic viscosity of the bitumen was determined by Dynamic Shear Rheometer (DSR) based on the rotational plate method [63, 76]. The bitumen specimen was placed between two plates of a diameter of 25 mm with a gap distance of 1 mm. The shear rate of 10 rad/s and a shear strain of 1% were set for the rotational process to ensure the bitumen within the LVE range. The shear stress was measured by the DSR. The dynamic viscosity was obtained through Newton's internal friction law:

$$\eta = \frac{\tau_s}{\dot{\gamma}} \tag{11}$$

where η is the dynamic viscosity, τ_s is the shear stress and $\dot{\gamma}$ is the shear rate.

The stiffer bitumen including 70/100, 160/220, 330/430 and PMB were tested at 60, 80 and 100 °C, whereas the soft bitumen of V1500, V3000, V6000, V9000 and V12000 was measured under 40, 60 and 80 °C. The testing temperature selection also aimed to ensure the bitumen was in the LVE range. Three replicate specimens were tested for each bitumen type, and the mean value was calculated as the dynamic viscosity of the bitumen. A total of 27 specimens were measured for nine bitumen types.

3.3.2 Complex shear modulus test of bitumen

The complex shear modulus of bitumen was also investigated to describe the viscoelastic response. The measurements were performed at different loading frequencies swept logarithmically down from 400 rad/s to 0.1 rad/s and temperatures from -10 °C to 80 °C with an interval of 10 °C [77]. The bitumen specimen was placed between two parallel plates with a diameter of 10 mm and a gap of 2 mm at low temperatures (< 30 °C) and with a diameter of 25 mm and with a gap of 1 mm at high temperatures (≥ 30 °C). The shear strain amplitude was controlled to keep all bitumen within the LVE range. The shear strain amplitude of the stiffer bitumen of 70/100, 160/220, 330/430 and PMB was 1%. In terms of soft bitumen of V1500, V3000, V6000, V9000 and V12000, the shear strain amplitudes were 1% and 2% for temperatures lower and higher than 30 °C, respectively. The average values derived from the

three replicate specimens were used. A total of 54 specimens were tested for nine bitumen types at both low and high temperatures.

3.3.3 Dynamic modulus test of asphalt mixture

The CITT and CCT are two commonly used methods to determine dynamic modulus due to the time and temperature dependence of asphalt mixtures. In this study, the former was performed by the Nottingham Asphalt Tester (NAT) produced by Cooper Technology [78]. A harmonic sinusoidal load with a haversine wave controlled by a pneumatic servo as shown in Figure 9. The *x* and *y* axes were defined as the horizontal and vertical directions, respectively. The horizontal strain was recorded by two Linear Variable Differential Transformers (LVDT) on both sides of the specimen. The testing condition set of temperatures of -15, -10, 0, 15 and 30 °C and frequencies of 10, 5, 3, 1, 0.3 and 0.1 Hz was selected for material database establishment and sample preparation comparison. Another sets of testing conditions are the temperatures of -10, 5, 21 and 40 °C and the frequencies of 10, 5, 2, 1, 0.2 and 0.1 Hz for test method comparison as given in Table 4. The applied load amplitude was adjusted to control the initial horizontal strain in a range from 50 με to 100 με for every testing condition, keeping the LVE behaviour of asphalt mixtures. Therefore, the CITT was regarded as a stress-strain dual control test.

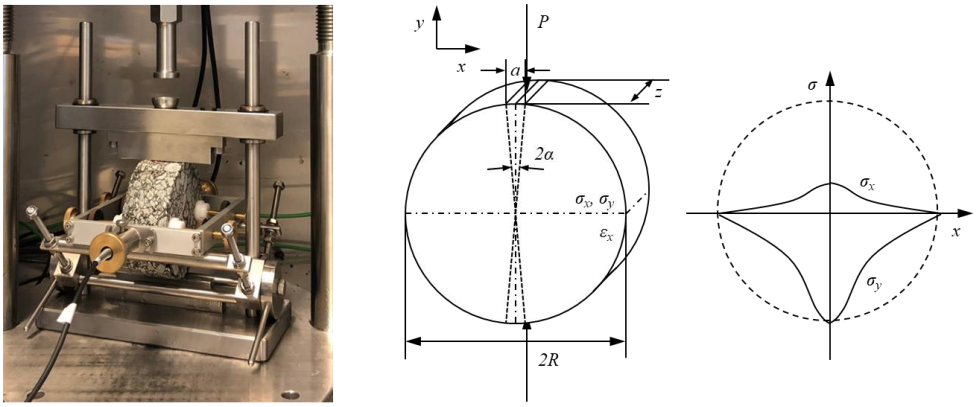

Figure 9. (a) CITT setup using NAT, (b) scheme of CITT specimen subjected to a vertical load and (c) stress distribution.

The dynamic modulus of asphalt mixtures was derived from the deviator stress and strain in the horizontal direction. Based on the viscoelastic solution, a vertical complex load, P^*, is applied as expressed in Equation 12. The stress distribution is shown in Figure 9c and also displayed in Figure 16 by the numerical model. Along the horizontal diameter of the CITT specimen, the horizontal stress, $\sigma_x(x,t)$, and the vertical stress, $\sigma_y(x,t)$, are defined by Equation 13 and Equation 14, respectively [79-81].

$$P^* = P_0 \cdot e^{i\omega t} = P_0\left[\cos(\omega t) + i\sin(\omega t)\right] \tag{12}$$

$$\begin{aligned}\sigma_x(x,t) &= \frac{2P_0}{\pi az}\left[\frac{\left(1-x^2/R^2\right)\sin 2\alpha}{1+2\left(x^2/R^2\right)\cos 2\alpha + x^4/R^4} - \tan^{-1}\left(\frac{1-x^2/R^2}{1+x^2/R^2}\tan\alpha\right)\right] \\ &= \frac{2P_0}{\pi az}\left[f(x) - g(x)\right]\end{aligned} \tag{13}$$

$$\begin{aligned}\sigma_y(x,t) &= -\frac{2P_0}{\pi az}\left[\frac{\left(1-x^2/R^2\right)\sin 2\alpha}{1+2\left(x^2/R^2\right)\cos 2\alpha + x^4/R^4} + \tan^{-1}\left(\frac{1-x^2/R^2}{1+x^2/R^2}\tan\alpha\right)\right] \\ &= -\frac{2P_0}{\pi az}\left[f(x) + g(x)\right]\end{aligned} \tag{14}$$

where x is the distance from the origin along the abscissa, P_0 is the amplitude of the sinusoidal load, a is the loading strip width, z is the thickness of the sample, R is the radius of the sample, and $f(x)$ and $g(x)$ are the substitution expressions for simplifying the formulae. The horizontal strain, $\varepsilon_x(x, t)$, is expressed:

$$\begin{aligned}\varepsilon_x(x,t) &= \frac{1}{E^*}\left[\sigma_x(x) - \nu\sigma_y(x)\right] \\ &= \frac{2P_0}{\left|E^*\right|\pi az}e^{i(\omega t-\varphi)}\left[(\nu+1)f(x) + (\nu-1)g(x)\right]\end{aligned} \tag{15}$$

where ν is the Poisson's ratio. The total deformation between $-R$ and R at the horizontal central axis, $\Delta H(t)$, is given:

$$\begin{aligned}\Delta H(t) &= \int_{-R}^{R} \varepsilon_x(x,t)dx \\ &= \frac{2P_0}{|E^*|\pi az} e^{i(\omega t-\varphi)} \left[(\nu+1)\int_{-R}^{R} f(x)dx + (\nu-1)\int_{-R}^{R} g(x)dx \right] \\ &= \frac{2P_0}{|E^*|\pi az} e^{i(\omega t-\varphi)} A\end{aligned} \tag{16}$$

where A is the substitution expression. Therefore, in the CITT mode, the complex modulus from the horizontal deformation can be expressed as:

$$|E^*| = \frac{2P_0 \sin(\omega t-\varphi)}{\pi az \Delta H(t)} A \tag{17}$$

Another dynamic modulus test method of the CCT was involved in this thesis, which was compared with the CITT. The CCT was performed from the laboratory of UiA using the servo hydraulic Universal Testing Machine (UTM) manufactured by IPC global®. The testing was done by Mequanent Mulugeta Alamnie. The sinusoidal axial load was applied with the testing conditions of temperatures of -10, 5, 21 and 40 °C and the frequencies of 10, 5, 2, 1, 0.2 and 0.1 Hz. Three LVDT with 70 mm gauge lengths were installed at 120° apart of the CCT specimen. The CCT was conducted in a controlled strain mode with a target strain of 50 με or less. Differently from the CITT, the CCT determines the complex modulus uniaxially based on Equation 4 as it measures the vertical stress and strain along the direction of the applied load as shown in Figure 10.

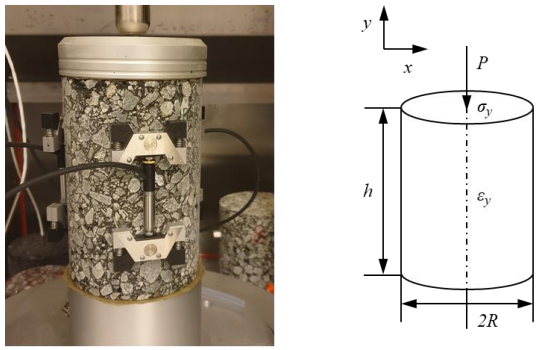

(a) (b)

Figure 10. (a) CCT setup using UTM and (b) scheme of CCT specimen subjected to a vertical load.

3.4 Master curve construction

3.4.1 Master curve models

Bitumen complex shear modulus

In this research, the complex shear modulus master curve of bitumen was constructed based on the modified HS model as expressed:

$$G^*(\omega) = \left\{ \left[G_0 + \frac{G_\infty - G_0}{1 + \delta_1 (i\omega\tau_1)^{-m_1} + \delta_2 (i\omega\tau_2)^{-m_2}} \right]^{-1} - \frac{i}{\eta_3 \omega} \right\}^{-1} \quad (18)$$

where G_0 and G_∞ are the complex shear moduli at the infinitesimal and infinite frequencies, respectively, τ_1 and τ_2 are time constants for the parabolic dashpots and m_1, m_2, δ_1 and δ_2 are model parameters. The number of parameters can be decreased using one time constant $\tau = \tau_1 = \tau_2$.

Asphalt mixture dynamic modulus

The master curve models for the dynamic modulus of asphalt mixtures were estimated in this study. Three models were investigated, which were SLS, GLS and CAM models. The SLS model used in MEPDG is one of the most popular models to describe the rheological properties of asphalt mixture as given by Equation 19.

$$\log\left(\left|E^*\right|\right) = \delta + \frac{\alpha}{1 + e^{\beta - \gamma \cdot \log(f_r)}} \quad (19)$$

where f_r is the frequency at the reference temperature, δ, α, β and γ are the fitting parameters. δ and $\delta + \alpha$ represent the minimum and maximum value of $|E^*|$, respectively. β and γ describe the shape of the SLS model as depicted in Figure 11.

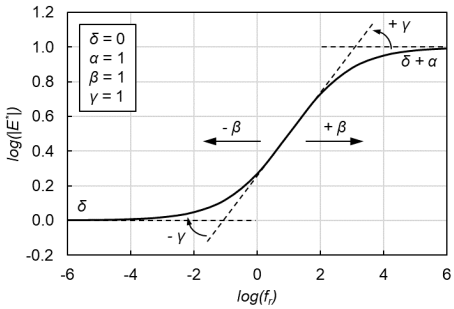

Figure 11. Graphical interpretation of SLS model.

The GLS model is the general form of the SLS function applicable to asymmetric curves as expressed:

$$\log\left(\left|E^*\right|\right) = \delta' + \frac{\alpha'}{\left[1+\lambda\cdot e^{\beta'-\gamma'\cdot\log(f_r)}\right]^{\frac{1}{\lambda}}} \tag{20}$$

where δ', α', β', γ' and λ are the fitting parameters. λ characterises the asymmetric characteristics shown in Figure 12. δ' and $\delta' + \alpha'$ represent the minimum and maximum value of $|E^*|$, respectively. β' and γ' describe the shape of the GLS model.

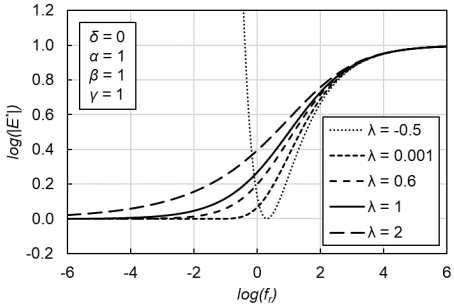

Figure 12. Graphical interpretation of the role of λ coefficient in GLS model.

The CAM model given by Equation 21 also satisfactorily describes the viscoelastic properties of asphalt mixtures.

$$\left|E^*\right| = E_e + \frac{E_\infty - E_e}{\left[1+\left(\frac{f_c}{f_r}\right)^v\right]^{w/v}} \tag{21}$$

where f_c is the location parameter with dimensions of frequency, v and w are fitting parameters and describe the shape of the model as shown in Figure 13.

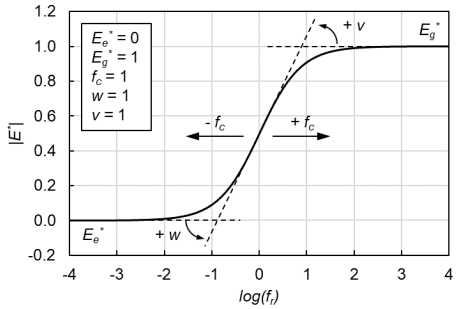

Figure 13. Graphical interpretation of CAM model.

Asphalt mixture phase angle

The phase angle master curve is constructed through the Lorentzian equation, denoted as Equation 22 [82, 83]:

$$\varphi = \frac{k_p \cdot k_g^2}{\left[\log\left(f_r\right) - k_c\right]^2 + k_g^2} \tag{22}$$

where k_p is the peak value, k_g is the growth rate, and k_c is the critical point.

3.4.2 Shift factor techniques

The shift factor, $\alpha(T)$, describes the temperature dependency of the dynamic modulus and the general form is given in Equation 23. It is used to shift the dynamic modulus at different test temperatures to the reduced frequency of the master curve based on the reference temperature.

$$\alpha\left(T\right) = \frac{f_r}{f} \tag{23.1}$$

$$\log\left(f_r\right) = \log\left(f\right) + \log\left[\alpha\left(T\right)\right] \tag{23.2}$$

Five commonly used shift factor equations were compared in this research, which were log-linear, quadratic polynomial, Arrhenius, Williams-Landel-Ferry (WLF) and Kaelble equations.

The log-linear equation is one of the most popular temperature shifting methods for asphalt mixtures, which is expressed as:

$$\log\left[\alpha(T)\right] = C\left(T - T_r\right) \tag{24}$$

where T_r is the reference temperature, and C is the constant which is determined by analysis of the experimental data.

The quadratic polynomial equation well fits the shift factors over a wide range of temperatures and is given in Equation 25.

$$\log\left[\alpha(T)\right] = p\left(T - T_r\right) + q\left(T - T_r\right)^2 \tag{25}$$

where p and q are regression parameters.

The Arrhenius equation for calculating the shift factor is presented in Equation 26.

$$\log\left[\alpha(T)\right] = C'\left(\frac{1}{T} - \frac{1}{T_r}\right) = \frac{0.4347 \cdot E_a}{R_g}\left(\frac{1}{T} - \frac{1}{T_r}\right) \tag{26}$$

where C' is a constant, E_a is the activation energy (J/mol) and R_g is the ideal gas constant (8.314 J/mol·K). Arrhenius equation has only one constant to be determined and can describe the behaviour of the material below the glass transition temperature, T_g [84].

The WLF equation is widely used to describe the relationship between shift factor and temperature above T_g and thereby assess the shift factor of asphalt mixtures:

$$\log\left[\alpha(T)\right] = \frac{-C_1\left(T - T_r\right)}{C_2 + \left(T - T_r\right)} \tag{27}$$

where C_1 and C_2 are two regression parameters.

The Kaelble equation is a modification of the WLF equation and can describe the relationship between shift factor and temperature below T_g as given in Equation 28.

$$\log\left[\alpha(T)\right] = \frac{-C_1'\left(T - T_r\right)}{C_2' + \left|T - T_r\right|} \tag{28}$$

where C_1' and C_2' are two regression parameters.

3.4.3 Fitting procedure and estimation

The Sum of Square Error (*SSE*) between measured values after shifting and predicted values is used to fit the master curve as given by Equation 29. The *SSE* was minimised by the nonlinear least squares regression to obtain the optimal master curve parameters.

$$SSE = \sum \left(\frac{\left|E^*\right|_{measured} - \left|E^*\right|_{predicted}}{\left|E^*\right|_{measured}} \right)^2 \tag{29}$$

The constraint range of variables was not defined due to well fitting results for the cases. The same initial values of master curve parameters were used for each fitting procedure.

The master curve models and shift factor techniques were estimated through the absolute error, Normalised Square Error (*NSE*), Standard Error Ratio (S_e/S_y) and coefficient of determination (R^2). The absolute error formula is expressed as:

$$Absolute\ error = \left|E^*\right|_{predicted} - \left|E^*\right|_{measured} \tag{30}$$

The *NSE* reflecting the relative error is also used to evaluate the models as shown in Equation 31.

$$NSE = \left(\frac{\left|E^*\right|_{predicted} - \left|E^*\right|_{measured}}{\left|E^*\right|_{measured}} \right)^2 \tag{31}$$

The S_e/S_y and R^2 used to evaluate the goodness of fit of the models are defined as:

$$S_e = \sqrt{\frac{\sum \left(Y - \hat{Y}\right)^2}{\left(n-k\right)}} \tag{32}$$

$$S_y = \sqrt{\frac{\sum \left(Y - \bar{Y}\right)^2}{\left(n-1\right)}} \tag{33}$$

$$R^2 = 1 - \frac{(n-k)}{(n-1)} \cdot \left(\frac{S_e}{S_y} \right)^2 \quad (34)$$

where S_e is the standard error of estimation, S_y is the standard error of deviation, n is the sample size, k is the number of independent variables, Y is the measured value, $\hat{Y}$ is the predicted value, and $\bar{Y}$ is the mean value of measured values. Lower S_e/S_y and higher R^2 values indicate better goodness between predicted and measured data.

3.5 Dynamic modulus prediction method based on material factors

3.5.1 Grey relational method

Since it was impossible to compare a single material factor under exactly the same conditions, the grey relational analysis was used to evaluate the influence of material parameters (i.e., maximum aggregate size, binder content, rheological properties of bitumen, bulk density and void characteristics of asphalt mixtures) on the dynamic modulus of asphalt mixtures. The grey relational analysis is a statistical technique, which is mainly used to elaborate the closeness of the relationship between main factors and sub-factors in a system as well as to evaluate the degree of influence that each sub-factor exerts on the main factor [85]. In total, there were m material parameters and n sets of data. The ith material parameters were expressed as x_{ij}, where $i = 1, 2, \ldots, m$ and $j = 1, 2, \ldots, n$. Since the numerical values of the material parameters are in different ranges, the min-max value method is used for the dimensionless processing of variables by Equation 35.

$$X_{ij} = \frac{x_{ij} - \min\left(x_{ij}\right)}{\max\left(x_{ij}\right) - \min\left(x_{ij}\right)} \qquad for\ i = 1,2,\ldots,m\ and\ j = 1,2,\ldots,n \quad (35)$$

where X_{ij} is the comparability sequence from 0 to 1, $min(x_{ij})$ is the minimum value of the x_{ij} matrix and $max(x_{ij})$ is the maximum value of the x_{ij} matrix. The dynamic modulus sequence was defined as the reference sequence X_{0j}. The difference between the material parameter sequence, X_{ij}, and reference sequence, X_{0j}, is $\Delta_{ij} = |X_{0j} - X_{ij}|$. The grey relational coefficient is used to determine how close X_{ij} is to X_{0j}, which is calculated by Equation 36.

$$\gamma\left(X_{0j}, X_{ij}\right) = \frac{\min\left(\Delta_{ij}\right) + \zeta \max\left(\Delta_{ij}\right)}{\Delta_{ij} + \zeta \max\left(\Delta_{ij}\right)} \qquad for\ i = 1,2,\ldots,m\ and\ j = 1,2,\ldots,n \quad (36)$$

where $\gamma(X_{0j},X_{ij})$ is the grey relational coefficient, $min(\Delta_{ij})$ is the minimum value of Δ_{ij} matrix, $max(\Delta_{ij})$ is the maximum value of Δ_{ij} matrix and ζ is the resolution coefficient between 0 and 1 to reflect the difference in the correlation and the value of 0.3 is selected according to the previous study [86]. The grey relational grade between the ith material parameter sequence, X_i, and the dynamic modulus sequence, X_0, is then calculated by Equation 37.

$$\gamma\left(X_0, X_i\right) = \frac{1}{n}\sum_{j}^{n}\gamma\left(X_{0j}, X_{ij}\right) \quad for\ i = 1, 2, \ldots, m \tag{37}$$

where $\gamma(X_0,X_i)$ is the grey relational grade between 0 and 1, and the closer its value is to 1, the better the correlation between the material parameter and the dynamic modulus.

3.5.2 Dynamic modulus prediction from material properties

In addition to the prediction method by constructing the master curve based on the test results, the dynamic modulus can be also calculated through material parameters. The corresponding models investigated in this research are given as follows.

Witczak 1-37A model

The Witczak 1-37A model was developed by Witczak et al. [87]. This model is an empirical model used for predicting the dynamic modulus of Level 2 and Level 3 designs, which is described in the ME pavement design guide [2]. The model takes into account the viscosity of the bitumen and the volumetric properties of asphalt mixtures as expressed:

$$\begin{aligned}\log\left(\left|E^*\right|\right) = {} & 3.750063 + 0.02932\rho_{200} - 0.001767\left(\rho_{200}\right)^2 - 0.002841\rho_4 - 0.058097V_a \\ & -0.802208\left(\frac{V_{beff}}{V_{beff}+V_a}\right) + \frac{3.871977 - 0.0021\rho_4 + 0.003958\rho_{38} - 0.000017\left(\rho_{38}\right)^2 + 0.005470\rho_{34}}{1+e^{\left[-0.603313-0.313351\log(f)-0.393532\log(\eta)\right]}}\end{aligned} \tag{38}$$

where $|E^*|$ is dynamic modulus [psi], η is bitumen viscosity [10^6 Poise], f is the loading frequency [Hz], V_a is the air void content [%], V_{beff} is the effective bitumen content [%], ρ_{34} is the cumulative retained on the 3/4 in sieve [%], ρ_{38} is the cumulative percent retained on the 3/8 in sieve [%], ρ_4 is the cumulative retained on the No. 4 sieve [%], and ρ_{200} is the percentage passing the No. 200 sieve [%].

Witczak 1-40D model

The Witczak 1-40D model incorporating the complex shear modulus and phase angle of the binder was improved by Witczak et al. [88]. This model has been widely adopted in the United States and is one of the most accurate empirical models used for pavement design as given:

$$\begin{aligned}\log\left(\left|E^*\right|\right) &= -0.349 + 0.754\left(\left|G_b^*\right|^{-0.0052}\right) \\ &\times\left[6.65 - 0.032\rho_{200} + 0.0027\left(\rho_{200}\right)^2 + 0.011\rho_4 - 0.0001\left(\rho_4\right)^2 + 0.006\rho_{38} - 0.00014\left(\rho_{38}\right)^2 - 0.08V_a - 1.06\left(\frac{V_{beff}}{V_{beff}+V_a}\right)\right] \\ &+ \frac{2.56 + 0.03V_a + 0.71\left(\frac{V_{beff}}{V_{beff}+V_a}\right) + 0.012\rho_{38} - 0.0001\left(\rho_{38}\right)^2 - 0.01\rho_{34}}{1+e^{\left[-0.7814 - 0.578585\log\left|G_b^*\right| + 0.8834\log\left(\varphi_b\right)\right]}}\end{aligned} \tag{39}$$

where $|G_b^*|$ is the complex shear modulus of binder [psi], and φ_b is the binder phase angle [°].

Hirsch model

The Hirsch model was developed by Hirsch et al. [31]. This empirical model is used to predict the dynamic modulus of asphalt mixtures based on the volumetric properties and the complex shear modulus of the binder as follows.

$$\left|E^*\right| = P_c\left[4200000\left(1-\frac{VMA}{100}\right) + 3\left|G_b^*\right|\left(\frac{VMA\times VFB}{10000}\right)\right] + \frac{1-P_c}{\frac{1-\frac{VMA}{100}}{4200000} + \frac{VMA}{3\left|G_b^*\right|VFB}} \tag{40}$$

$$P_c = \frac{\left(20 + \frac{3\left|G_b^*\right|VFB}{VMA}\right)^{0.58}}{650 + \left(\frac{3\left|G_b^*\right|VFB}{VMA}\right)^{0.58}} \tag{41}$$

Al-Khateeb model

The Al-Khateeb model was proposed by Al-Khateeb et al. [32]. This model uses a regression analysis of dynamic modulus data to material factors, which is expressed as:

$$\left|E^*\right| = 3\left(1-\frac{VMA}{100}\right)\left[\frac{\left(90+\frac{10000\left|G_b^*\right|}{VMA}\right)^{0.66}}{1100+\left(\frac{900\left|G_b^*\right|}{VMA}\right)^{0.66}}\right]\left|G_g^*\right| \quad (42)$$

where $|G_g^*|$ is the binder complex shear modulus at the glassy state (assumed to be 145000 psi).

Global model

This global model is also a regression model developed by Sakhaeifar et al. [33]. This model is applied to predict the dynamic modulus of asphalt mixtures using a large dataset of laboratory test results based on the void characterisation, which is given as follows.

$$\log\left(\left|E^*\right|\right) = 6.1716 - 0.00269\rho_{34} - 0.00137\rho_{38} - 0.10641\rho_{200} - 0.05248V_a - 0.1774V_{beff} + 0.00618V_{beff}^2 + \frac{1.0154 + 0.08395\rho_{200} + 0.0142V_a + 0.17103V_{beff} - 0.00747V_{beff}^2}{1+e^{\left(-0.81189-0.54698X_G\right)}} \quad (43)$$

$$X_G = \log\left\{\frac{2.4392\times10^{-0.0004T^2+0.0135T-0.1003}}{\left[\left(\frac{145000}{\left|G_b^*\right|}\right)^{0.12332}-1\right]^{7.72273}}\right\} \quad (44)$$

where X_G is the predicted frequency as given in Equation 44.

Simplified global model

This model is the simplified version of the global model described in the former section. This model predicts the dynamic modulus of asphalt mixtures considering the air voids, the effective binder content and the complex shear modulus of the binder. It is expressed as follows.

$$\log\left(\left|E^*\right|\right) = 6.4197 - 0.00014\rho_{34}^2 - 0.00547\rho_{38} - 0.11786\rho_{200} - 0.05528V_a - 0.16266V_{beff} - 0.00487V_{beff}^2 + \frac{0.57677 + 0.00713\rho_{38} + 0.16167\rho_{200} - 0.0052\rho_{200}^2 + 0.01889V_a + 0.16031V_{beff} - 0.00592V_{beff}^2}{1+e^{\left[1.8645-0.95991\log\left(\left|G_b^*\right|\right)\right]}} \quad (45)$$

3.5.3 Development of dynamic modulus prediction model

Prediction model based bituminous rheological properties

The correlation between the bitumen rheological properties and the dynamic modulus of asphalt mixtures was investigated using the Multiple Linear Regression (MLR) method as expressed:

$$\log\left[\left|E^*\right|(T, f)\right] = a_1 \cdot \log\left[\eta(T)\right] + a_2 \cdot \log\left[\left|G^*\right|(T, f)\right] + a_3 \quad (46)$$

where $|E^*|(T, f)$ is the dynamic modulus at different temperatures and frequencies, a_1, a_2 and a_3 are model parameters. $\eta(T)$ and $|G^*|(T, f)$ are obtained corresponding prediction models.

Prediction model based on modelling of master curve parameters

A model is developed to predict the dynamic modulus of asphalt mixtures by MLR of the master curve parameters through the material factors. The MLR model is given in Equation 47.

$$Master\ curve\ parameters = \sum_{i=1}^{n} b_i \left(Material\ parameters\right)_i \quad (47)$$

where b_i is the model parameters, and $i = 1, 2, \ldots, n$.

3.6 Finite element (FE) analysis

The FE modelling in this study was performed by the COMSOL Multiphysics program for four types of asphalt mixtures, which were AC 16-70/100, SMA 16-70/100, MA 16-V9000 and AG 16-160/220. The modular structure of the program is shown in Figure 14. The master curve model was incorporated into the parameter module. Therefore, the inputs of temperature and loading frequency were used to determine the dynamic modulus in the material module, which also included the measured density and Poisson's ratio. The Prony series coefficients of relaxation modulus based on the generalised Maxwell model were used as inputs in the viscoelasticity module. The thermal effects were described by the WLF shift function. The viscoelastic behaviour of asphalt mixtures was defined by the master curve models and the relaxation modulus. Afterwards, the FE analysis of the CITT was conducted and the results were compared with the experimental results. Finally, a numerical model was applied for predicting the stress and strain of some asphalt pavement structures.

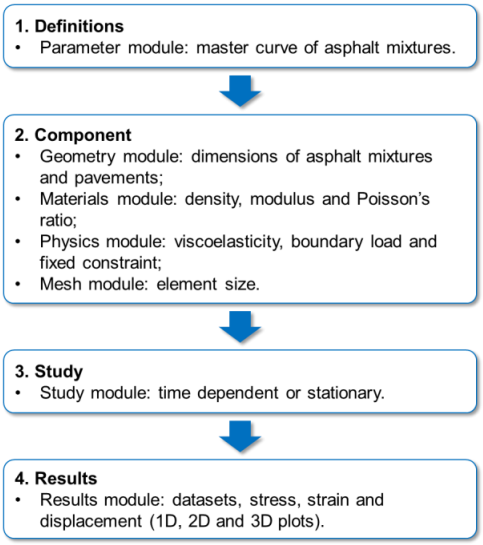

Figure 14. Modular structure of COMSOL Multiphysics program.

3.6.1 Constitutive relationship

The generalised Maxwell model was used to investigate the viscoelastic behaviour of asphalt materials in this study. A Prony series model was used to characterise the relaxation modulus [89].

$$E(t) = E_e + \sum_{i=1}^{n} E_i e^{-t/\tau_i} \tag{48}$$

To determine the coefficients of the relaxation modulus in Equation 48 based on the dynamic modulus test results, the storage modulus, $E'(\omega)$, and the loss modulus, $E''(\omega)$, are calculated as [90]:

$$E'(\omega) = E_e + \sum_{i=1}^{n} \frac{\omega^2 \tau_i^2 E_i}{1+\omega^2 \tau_i^2} \tag{49}$$

$$E''(\omega) = \sum_{i=1}^{n} \frac{\omega \tau_i E_i}{1+\omega^2 \tau_i^2} \tag{50}$$

The dynamic modulus can be expressed as:

$$\left|E^*(\omega)\right| = \sqrt{\left[E'(\omega)\right]^2 + \left[E''(\omega)\right]^2} \tag{51}$$

The least squares regression is used to minimise the *error* as reported in Equation 52 for obtaining the Prony model coefficients of the relaxation modulus.

$$error = \frac{1}{n}\left\{\sum_{i=1}^{n}\left[1-\frac{\left|E^*(\omega_i)\right|_{Predicted}}{\left|E^*(\omega_i)\right|_{Measured}}\right]^2\right\} \tag{52}$$

In this study, the relaxation time was selected from 10^{-8} s to 10^{3} s. The regression coefficients for the four considered types of asphalt mixtures are given in Table 5. The corresponding relaxation moduli are also shown in Figure 15, which were inputs in the LVE domain of the FE modelling for asphalt materials.

Table 5. Prony series coefficients of relaxation modulus for four types of asphalt mixtures.

Serial number	Relaxation time, τ_i [s]	Relaxation modulus, E_i [MPa]			
		AC 16-70/100	SMA 16-70/100	MA 16-V9000	AG 16-160/220
1	10^{-8}	684.258	304.314	1.059	1003.717
2	10^{-7}	2263.211	2163.195	6.879	1705.459
3	10^{-6}	4489.856	4546.179	450.073	2764.411
4	10^{-5}	5739.231	6378.464	3736.190	3648.062
5	10^{-4}	6851.697	7353.890	7254.655	4482.645
6	10^{-3}	7305.593	7288.608	3466.729	5765.889
7	10^{-2}	6297.559	5148.745	439.516	5954.210
8	10^{-1}	2597.327	2783.350	189.400	2415.994
9	10^{0}	1376.162	919.812	28.705	679.442
10	10^{1}	525.526	338.405	0.483	177.008
11	10^{2}	228.401	159.158	0.475	27.059
12	10^{3}	5.653	86.483	150.670	14.454
long-term equilibrium modulus, E_e [MPa]		196.681	95.498	244.800	136.690

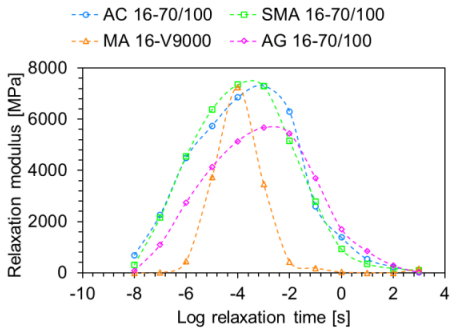

Figure 15. Relaxation moduli for four asphalt mixtures.

3.6.2 Finite element (FE) modelling of cyclic indirect tensile test (CITT)

Figure 16 presents the schematic diagram of FE modelling of the CITT. The geometry of the cylindrical sample was established. The load was applied along a strip with a width of 12.7 mm at the top. The bottom of the geometry was constrained to simulate the CITT. The horizontal tensile stress and strain on the central plane were calculated and their values were compared with the experimental CITT results to verify the reliability.

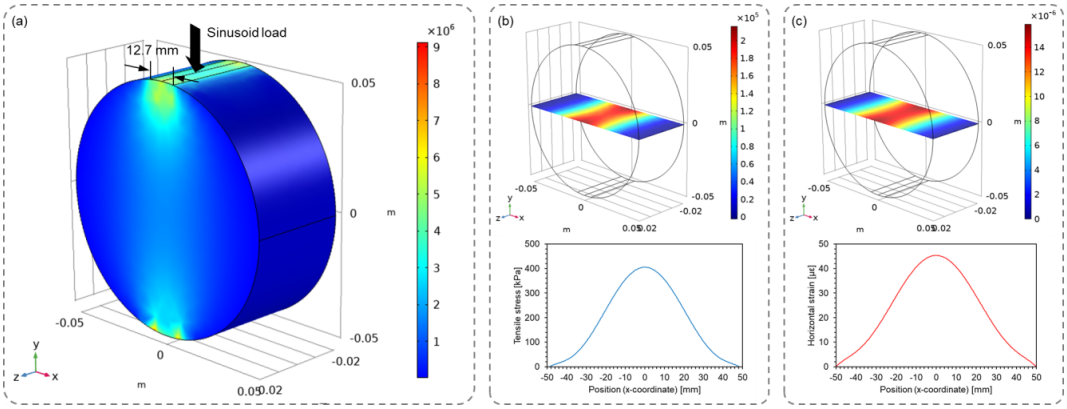

Figure 16. Schematic of FE modelling for CITT: (a) Von Mises stress, (b) Tensile stress and (c) Horizontal strain.

The R^2 and Mean Absolute Percentage Error (*MAPE*) were evaluated. The *MAPE* is expressed as:

$$MAPE = \frac{1}{n}\sum_{i=1}^{n}\left|\frac{Y_i - \hat{Y}}{Y_i}\right| \times 100\% \tag{53}$$

where Y_i is the measured value, $\hat{Y}$ is the simulated value, and i = 1, 2, …, n. The R^2 reflected the goodness of fit of the FE modelling. The *MAPE* reflected the relative difference between the predicted value and the measured value. The FE modelling and test were compared under nine combinations of three temperatures -10, 0 and 15 °C and three loading frequencies 3, 1 and 0.3 Hz.

3.6.3 Finite element (FE) modelling of asphalt pavement

After the validation of the numerical approach, the FE modelling is applied to an asphalt pavement (comprising surface layer, base layer and subbase layer) to predict the stress and

strain responses at the bottom of the surface layer as shown in Figure 17. The information of the pavement structure is given in Table 6. The mechanical response was investigated for seven different values of surface layer thicknesses (40, 60, 80, 100, 120, 140 and 160 mm). The AG 16-160/220 mixture was used as the base layer. The dynamic moduli of the surface layer and the base layer were evaluated according to the master curve model for loading frequency 1 Hz and temperature 0 °C to simulate the low temperature condition in Norway [11]. The contact stress of 0.7 MPa is applied on a circular area having a diameter of 200 mm according to previous studies [91-93]. The corresponding load is approximately 22 kN, which simulates the equivalent single axle load of 100 kN presenting dual wheels.

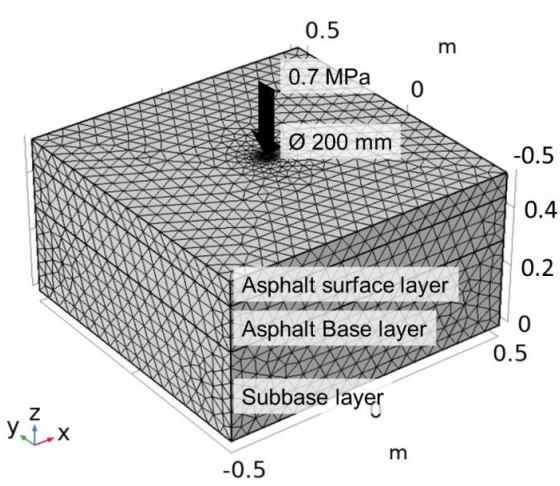

Figure 17. FE modelling of asphalt pavement.

Table 6. Thicknesses and material properties of the pavement structure.

Structure	Thickness [mm]	Material	Material properties	
			Modulus [MPa]	Poisson's ratio [-]
Surface layer	40 – 160	AC 16-70/100	17558	0.35
		SMA 16-70/100	15615	0.35
		MA 16-V9000	2518	0.35
Base layer	150	AG 16-160/220	12537	0.35
Subbase layer	300	Crushed rock	300*	0.4

* The stiffness of the subbase layer was selected based on typical values for Norwegian crushed rock.

In a three-dimensional structure, the directions of tensile stress and strain in the XY plane were various. In this study, the average values of the tensile stress and strain in the *x* and *y* directions in the XY plane shown in Figure 18 are evaluated.

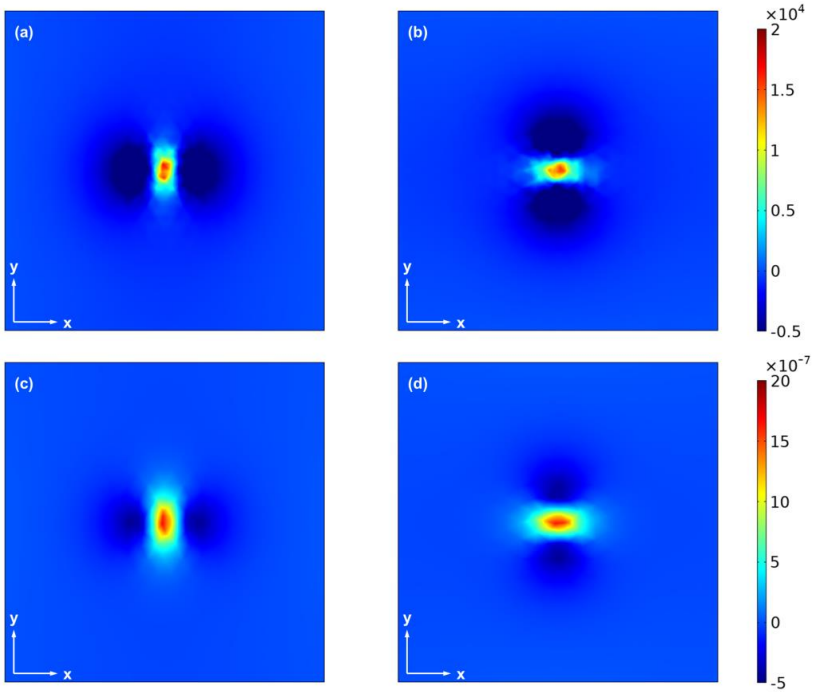

Figure 18. Tensile stress (a) in *x* direction and (b) in *y* direction and strain (c) in *x* direction and (d) in *y* direction of XY plane at the bottom of the 80 mm-thick AC 16-70/100 surface layer in FE modelling.

For this model, it could have been possible to utilise symmetry to reduce the number of elements, but since the calculation time was already quite short this was not done. Some tests were performed also including frost protection/subsoil, but this did not significantly influence the results that were studied.

4 RESULTS AND DISCUSSION

4.1 Test method comparison

4.1.1 Comparison of sample preparation methods

Four types of asphalt mixtures, i.e., AC 11-70/100, AC 16-70/100, SMA 11-70/100 and SMA 16-70/100, were used to compare the sample preparation methods of roller compression and gyratory compaction. The volumetric properties, shift factor, dynamic modulus and phase angle were evaluated as follows. The study on the comparison of sample preparation methods was discussed in detail in Paper I.

Volumetric properties

The volumetric properties reflect how well a specimen is compacted, and the results for the four asphalt mixture types prepared by both roller compactor and gyratory compactor are shown in Figure 19. The void characteristics of an asphalt mixture depend on many factors including compaction mode and effort, binder content, aggregate type, mixture type, etc. As indicated in Figure 19, in this research the gyratory compaction method results in lower Air Void Content (V_a), lower Void in Mineral Aggregate (*VMA*) and higher Voids Filled with Binder (*VFB*) compared to the roller compression method. These findings indicate that gyratory compaction applied a higher degree of compaction when compared to roller compaction.

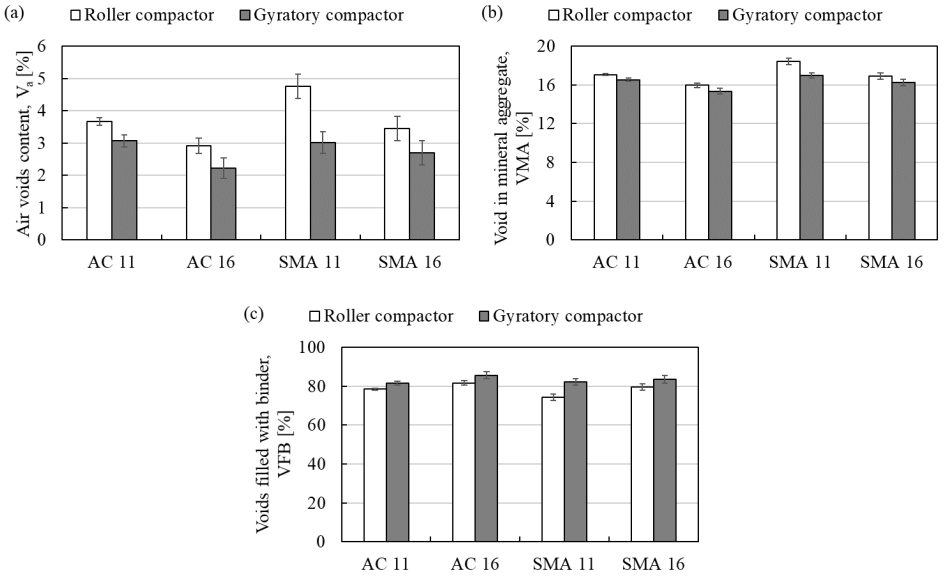

Figure 19. Void characteristics of specimens: (a) V_a, (b) *WMA*, and (c) *VFB*.

Dynamic modulus master curve

The dynamic modulus master curves of specimens fabricated by two preparation methods were constructed based on the SLS model and WLF equation due to a better fit of the model explained in Section 4.2. The fitting parameters, R^2 and *SSE*, are reported in Table 7. The R^2 of all asphalt mixtures ranged from 0.9927 to 0.9997, and the *SSE* values were comprised between 0.0331 and 0.1947, to be concluded that all the experimental values were then satisfactorily fitted.

Table 7. Fitting parameters, *SSE* and R^2 for mixtures.

Mixture	SLS model				WLF equation		R^2	*SSE*
	δ	α	β	γ	C_1	C_2		
AC 11-R	0.406	4.300	-1.070	0.364	17.93	125.21	0.9997	0.0710
AC 11-G	0.830	3.854	-1.097	0.391	18.22	112.91	0.9984	0.0836
AC 16-R	0.529	4.159	-1.070	0.413	12.11	88.71	0.9976	0.1352
AC 16-G	0.313	4.391	-1.254	0.396	13.69	91.34	0.9986	0.0780
SMA 11-R	0.777	3.766	-1.037	0.497	6.91	57.31	0.9962	0.0331
SMA 11-G	0.749	3.776	-1.177	0.469	7.36	55.72	0.9946	0.0413
SMA 16-R	1.562	3.026	-0.589	0.515	8.96	67.63	0.9927	0.1947
SMA 16-G	1.436	3.138	-0.851	0.464	9.78	68.21	0.9973	0.1375

Figure 20 shows the WLF shift factor curves of the different mixtures. It was found that the logarithm of the shift factor linearly decreased with the increase in temperature. The linear regression results are calculated according to the linear equation as given in Table 8, where *x* is the temperature, and *y* is the predicted shift factor. The R^2 of AC 11 and AC 16 were higher than those of SMA 11 and SMA 16, this showed that the logarithm of the shift factor of the AC mixtures tended to be more prone to follow a linear trend than that of the SMA mixtures; furthermore, it also showed that the shifted distances of the dynamic moduli of the AC mixtures per unit temperature were more even than those of the SMA mixtures when the master curves were constructed.

Table 8. Linear regression of shift factors.

Mixture type	Compact method	Linear regression	R^2
AC 11	Roller compaction	*y = -0.159x + 2.602*	0.990
	Gyratory compaction	*y = -0.182x + 3.002*	0.988
AC 16	Roller compaction	*y = -0.161x + 2.721*	0.980
	Gyratory compaction	*y = -0.176x + 2.957*	0.981
SMA 11	Roller compaction	*y = -0.166x + 2.952*	0.946
	Gyratory compaction	*y = -0.184x + 3.291*	0.942
SMA 16	Roller compaction	*y = -0.169x + 2.948*	0.963
	Gyratory compaction	*y = -0.183x + 3.177*	0.963

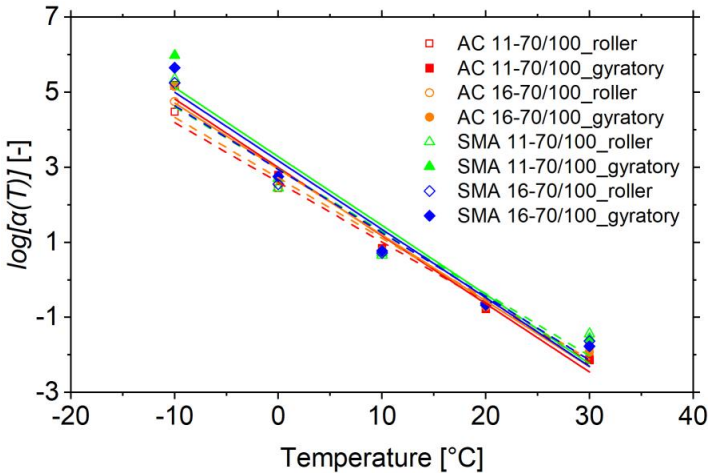

Figure 20. WLF shift factor curves for tested mixtures.

Figure 20 shows that the shift factor of AC 11 prepared by roller compactor is different from the one related to gyratory compaction. At -10 °C, the specimens formed by gyratory compaction had a higher shift factor than those compressed by roller compactor. At 30 °C, the

shift factor of the gyratory compacted specimens was smaller than that of the roller compression method. These results indicated that the shift amplitude of the dynamic modulus curve of the specimens prepared by the gyratory compactor at each temperature was larger than the corresponding values related to roller compaction.

As shown in Table 7, the compaction method, asphalt mixture type, and maximum grain size all exert clear effects on the fitting parameters. The compaction method had a major influence on the fitting parameters of δ and α for AC mixtures. However, there was a smaller difference of δ and α between the two compaction methods for SMA mixtures. This showed that the compaction methods exerted a greater impact on the AC mixtures than the SMA mixtures. The AC and SMA mixtures had different structures causing this result. The AC mixture is composed of a dense gradation. The structural strength of the AC mixture is mainly based on the cohesive force between the mineral aggregate and the binder. The SMA mixture is a semi-dense and semi-inlaid structure. The structural strength of the SMA mixture is composed of the squeezing force, internal friction between the mineral aggregates, and the cohesive force between the mineral aggregate and the binder [94]. The compaction method had a more important influence on the dense structure.

The master curves are portrayed in Figure 21. The dynamic modulus values are then compared at the condition of -10 °C and 10 Hz (low-temperature condition) and at the condition of 40 °C and 0.1 Hz (high-temperature condition) based on the modelling of the dynamic modulus, as shown in Figure 22.

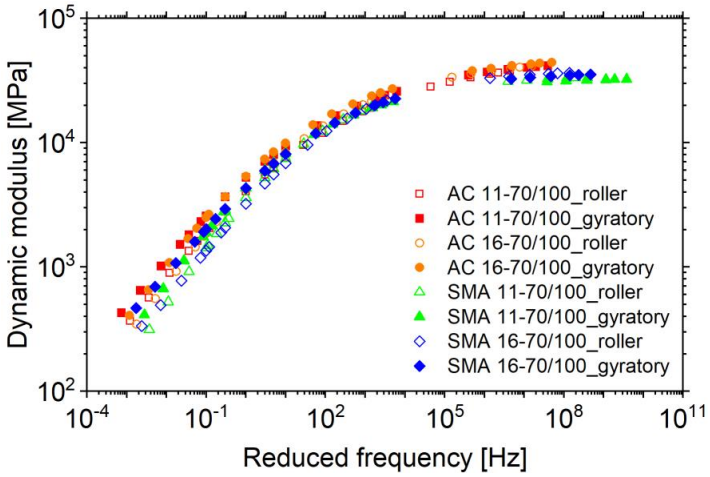

Figure 21. Master curves for tested mixtures.

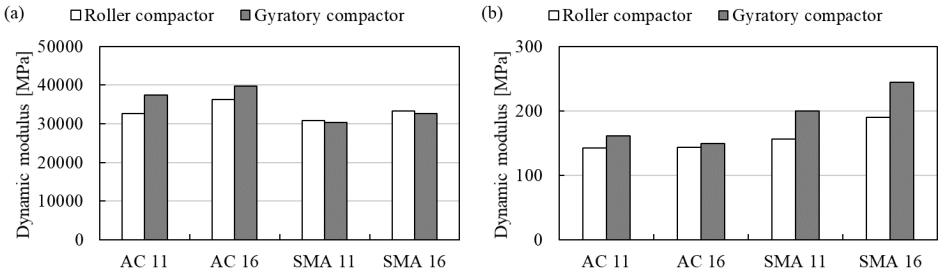

Figure 22. Dynamic modulus at (a) the low-temperature condition -10 °C and 10 Hz and (b) the high-temperature condition 40 °C and 0.1 Hz.

As shown in Figure 22a, the dynamic moduli of AC mixtures prepared by the gyratory compactor are higher than those fabricated by the roller compactor at low-temperature condition. The AC mixtures prepared by the gyratory compactor were denser, leading to a higher dynamic modulus. However, even though the gyratory compaction also made the SMA mixtures denser, the dynamic moduli at the low-temperature condition for SMA mixtures prepared by the gyratory compactor were slightly lower than the corresponding ones attained by the roller compactor. This indicated that the combined effect of the embedded and dense structures caused the dynamic modulus of the SMA mixture at low temperatures to be less affected by the compaction method.

As shown in Figure 22b, the dynamic moduli of gyratory compacted specimens are higher than roller compressed specimens at the high-temperature condition. Considering the findings related to high temperatures, the dynamic moduli of AC mixtures and SMA mixtures were affected the least and the most by the compaction mode, respectively. As the bitumen attains a viscous flow state at high temperatures, the cohesive force between the binder and the aggregate is greatly reduced. Therefore, the dynamic modulus of the AC mixtures was less affected by the compaction method. The structure of the SMA mixture was also improved by the gyratory compactor, which then caused less affected by the temperature at high temperatures.

4.1.2 Comparison of dynamic modulus test methods

Although the CCT was usually employed to develop the ME pavement design, the CITT was considered for the development of the Norwegian ME pavement design system due to the feasibility for both laboratory and field samples. The asphalt mixtures of AC 11-70/100 and SMA 11-70/100 prepared by the gyratory compactor were adopted for the test mode

comparison, which were coded AC 11- or SMA 11-CITT and AC 11- or SMA 11-CCT tested by the CITT and CCT, respectively. The master curves were established based on the SLS model, Lorentzian equation and WLF equation with the reference temperature of 21 °C. The study on comparison of test methods was detailly discussed in Paper IV.

Shift factor

The results of the shift factor are shown in Figure 23. The shift factor reflected how far the measured values moved relative to the dynamic modulus at the reference temperature, resulting in an impact on the modelling values of the master curves. In terms of AC 11 mixtures, the slope of the shift factor of AC 11-CITT was higher than the one of AC 11-CCT, which meant that the curve of AC 11-CITT was shifted more in the construction of the master curve than that of AC 11-UC. However, for the SMA 11 mixtures, the measured values of SMA 11-UC moved more at high frequencies relative to SMA 11-IDT. When the measured values were higher, moving more distance to high and low frequencies widened the difference, reflecting that the difference in dynamic modulus of the two test methods was greater for the AC 11 mixtures than for the SMA 11 mixtures. This result revealed that the structure of the tested asphalt mixture had a great impact on the results obtained with the two test procedures. The SMA mixtures with the embedded structure were less affected by the test than the AC mixtures with the dense structure.

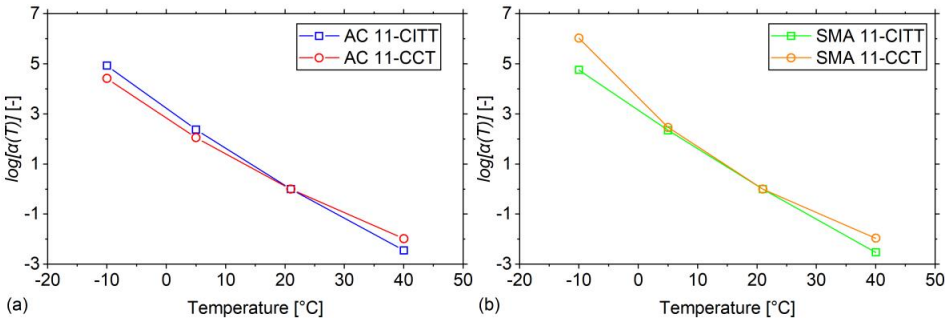

Figure 23. Shift factors for specimens: (a) AC 11 and (b) SMA 11.

Dynamic modulus

The dynamic modulus results of the CITT and CCT are shown in Figure 24. Figure 24a displays that the dynamic moduli of AC 11 mixtures measured by both tests are similar at 5 °C and there are some differences at higher and lower temperatures. The dynamic moduli of SMA 11

mixtures obtained by two tests were similar at low temperatures (-10 and 5 °C) and different at higher temperatures. The Coefficients of Variation (*CoV*) of the dynamic modulus results are given in Figure 25. The *CoV* of AC 11-CITT, AC 11-CCT, SMA 11-CITT and SMA 11-CCT were smaller at -10, 5 and 21 °C, which were around 10% or less. The *CoV* of AC 11-CITT, SMA 11-CITT and SMA 11-CCT were bigger at 40 °C, which was up to 30%. This indicated that the dynamic modulus test had a smaller variation at low temperatures and a bigger variation at high temperatures. Furthermore, the *CoV* of SMA 11 mixtures were lower than the ones of AC 11 mixtures, which displayed that the grading type of mixtures had an influence on the test variation.

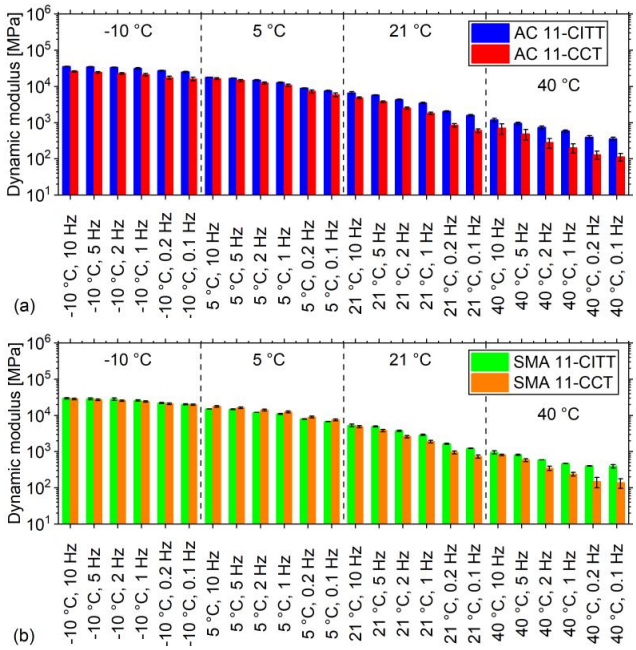

Figure 24. Dynamic modulus results: (a) AC 11 and (b) SMA 11.

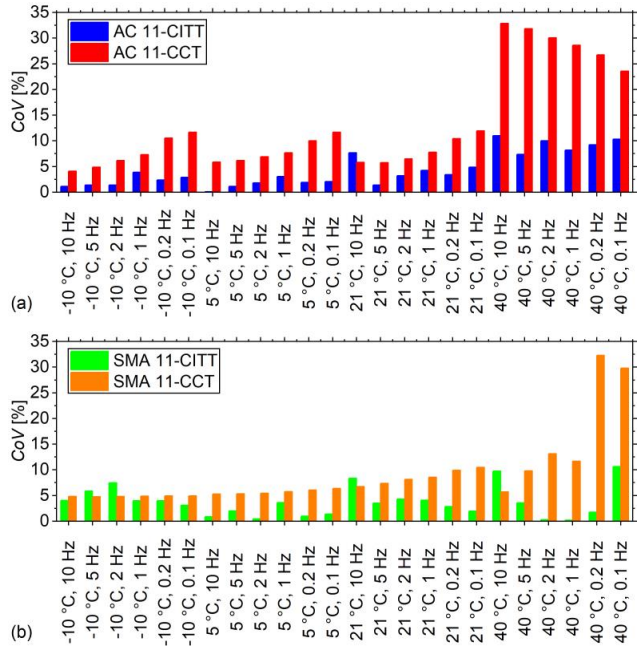

Figure 25. *CoV* of dynamic modulus results: (a) AC 11 and (b) SMA 11.

To compare the two test methods under a wider range of conditions, dynamic modulus master curves of asphalt mixtures were constructed. The dynamic modulus master curves of AC 11-IDT, SMA 11-IDT, AC 11-UC and SMA 11-UC are presented in Figure 26. The fitting parameters and the goodness of fit statistics [95], including the S_e, S_y, S_e/S_y and R^2, are given in Table 9. All master curves had good fits. The R^2 of the dynamic modulus were over 0.988. Both R^2 of dynamic modulus for AC 11-CITT and SMA 11-CITT were bigger than the R^2 values of AC 11-CCT and SMA 11-CCT. Meanwhile, both the S_e/S_y of dynamic modulus for AC 11-CITT and SMA 11-CITT were smaller than the S_e/S_y of AC 11-CCT and SMA 11-CCT. These outcomes indicated that the dynamic modulus master curves had a better fit for IDT test data. Furthermore, it is observed from Figure 26 that the dynamic moduli obtained by the two tests are relatively consistent in the frequency range from 10 Hz to 10^4 Hz. When the frequency was higher than 10^4 Hz or lower than 10 Hz, the dynamic moduli displayed differences. Compared with SMA 11, two tests induced a more severe difference in dynamic modulus at both higher and lower frequencies for AC 11. This result indicated that the AC 11 structure tended to expand the difference in dynamic modulus caused by the two tests compared to SMA 11 structure.

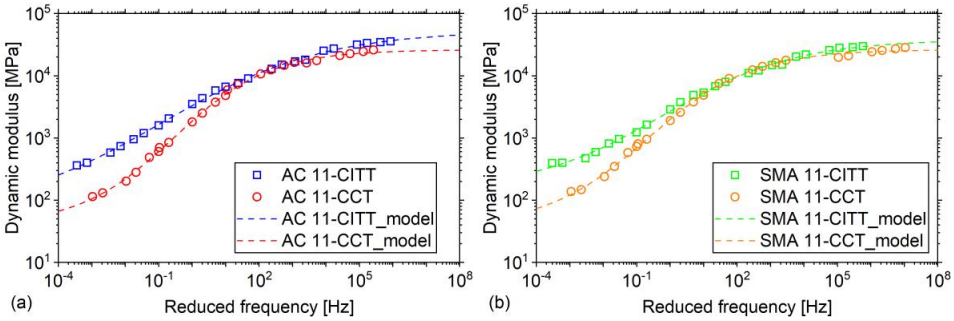

Figure 26. Master curves of dynamic modulus: (a) AC 11 and (b) SMA 11.

Table 9. The fitting parameters and statistical parameters of the dynamic modulus master curves for asphalt mixtures.

Fitting parameter		AC 11-CITT	SMA 11-CITT	AC 11-CCT	SMA 11-CCT
SLS model	δ	1.755	2.152	1.594	1.575
	α	2.974	2.431	2.823	2.847
	β	-0.382	-0.106	-0.385	-0.432
	γ	0.413	0.504	0.701	0.650
WLF equation	C_1	33.802	49.893	19.297	11.018
	C_2	243.539	356.001	166.369	87.622
Goodness of fit statistics					
S_e		724.649	673.983	798.555	1098.795
S_y		12566.958	10345.098	8937.466	10067.358
S_e/S_y		0.058	0.065	0.089	0.109
R^2		0.997	0.996	0.992	0.988

As all the dynamic modulus master curves of the four asphalt mixtures have a good fit, the dynamic modulus predicted by the master curves at each frequency is compared by the *NSE* following Equation 54. The smaller the *NSE* value, the more consistent the two test results.

$$NSE = \frac{\left(\left|E^*\right|_{CITT} - \left|E^*\right|_{CCT}\right)^2}{\left(\left|E^*\right|_{CITT}\right)^2} \tag{54}$$

where $|E^*|_{CITT}$ is the dynamic modulus obtained by the CITT, $|E^*|_{UC}$ is the dynamic modulus obtained by the CCT. The *NSE* between the two tests of AC 11 and SMA 11 is illustrated in Figure 27. The dynamic moduli obtained by the two tests were considered relatively consistent with a *NSE* of less than 0.005.

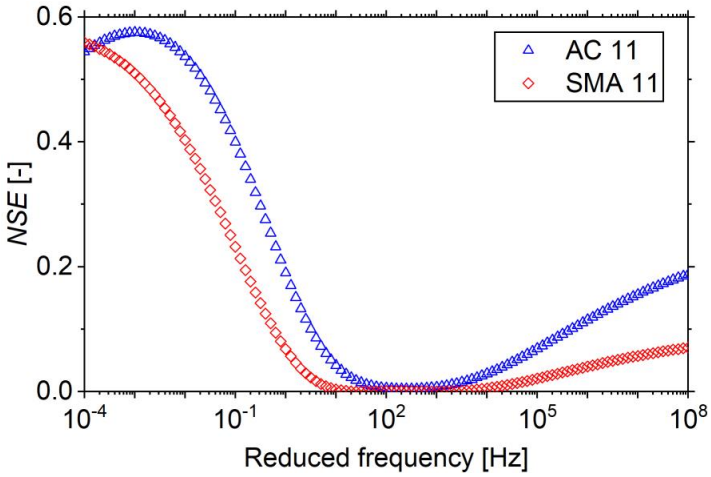

Figure 27. *NSE* of dynamic modulus between two test modes for AC 11 and SMA 11.

As presented in Figure 27, the dynamic moduli obtained from both tests for the AC 11 are consistent in the frequency range from 10^2 Hz to 10^3 Hz. The dynamic modulus evaluated from both tests for the SMA 11 was consistent in the frequency range from 10 Hz to 10^4 Hz. Meanwhile, the *NSE* of the two mixtures increased gradually with the increase of the frequency over 10^4 Hz or the decrease of the frequency less than 10 Hz. The *NSE* of SMA 11 was smaller than that of the *NSE* of AC 11. These results indicated that the dynamic moduli of asphalt mixtures measured by the two tests were almost the same in the reduced frequency range from 10 Hz to 10^4 Hz. However, some differences were found at high and low frequencies (temperatures) where the dynamic moduli measured by the CITT were greater than those obtained with the CCT test. Figure 27 shows that the *NSE* of the two mixtures is large at extreme frequencies, particularly at very low reduced frequencies. This might be connected to the various stress-strain responses of the specimens under the two test modes at relatively high temperatures. The difference in *NSE* between the two asphalt mixtures might be caused by the distinct physical structures. Comparing with the AC 11 mixture, SMA 11 had an embedded structure between large size aggregates and its dynamic modulus is less affected by temperature [96].

Phase angle

Figure 28 presents the phase angle results of the CITT and the CCT. The phase angles obtained by both tests were similar at 21 °C for AC 11 and SMA 11 mixtures. The differences in phase angles between the two tests occurred at higher and lower temperatures. The *CoV* of phase

angle results are smaller at 21 °C as shown in Figure 29, which indicates that the two test modes are stable at 21 °C leading to fewer result differences of both tests in the properties of the same materials.

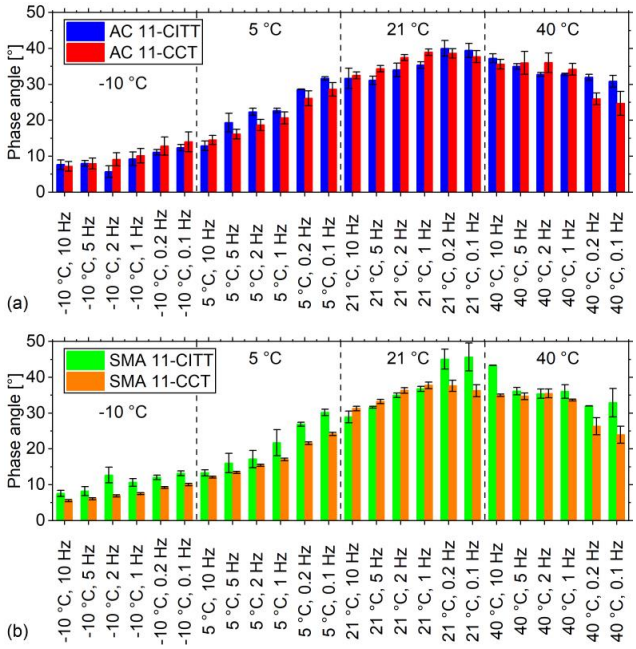

Figure 28. Phase angle results: (a) AC 11 and (b) SMA 11.

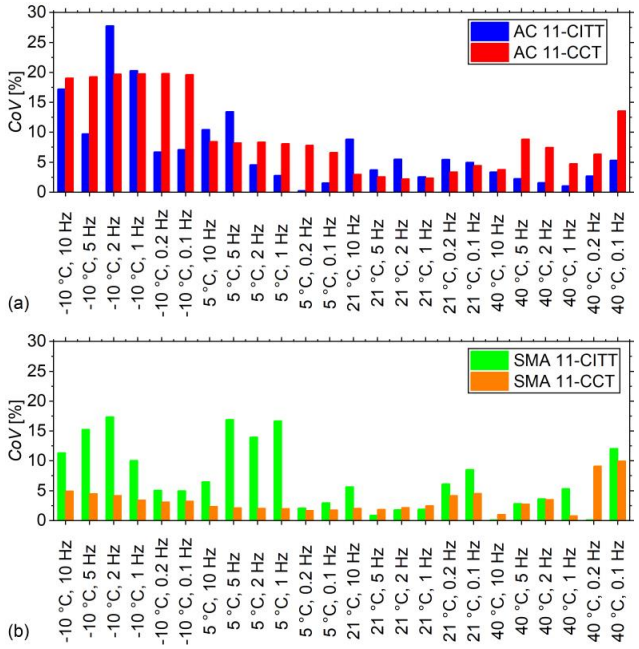

Figure 29. *CoV* of phase angle results: (a) AC 11 and (b) SMA 11.

Similar to the dynamic modulus, phase angle master curves were constructed to compare the differences between the two test methods over a wider range of conditions. The phase angle master curves of AC 11-CITT, SMA 11-CITT, AC 11-CCT and SMA 11-CCT are presented in Figure 30. The fitting parameters and the goodness of fit statistics are given in Table 10. The statistical parameters of phase angle for the two tests were different from the ones of dynamic modulus. Both R^2 of phase angle for AC 11-CITT and SMA 11-CITT were smaller than R^2 of AC 11-UC and SMA 11-UC. Both S_e/S_y of phase angle for AC 11-CITT and SMA 11-CITT exceed S_e/S_y of AC 11-CCT and SMA 11-CCT. Thus, the phase angle master curves of the CCT data have a better fit than that of the CITT data. As shown in Figure 30, the phase angle master curves for both tests are similar at high frequencies and shows differences at lower frequencies. This difference was more severe for the SMA 11 mixtures than for the AC 11 mixtures.

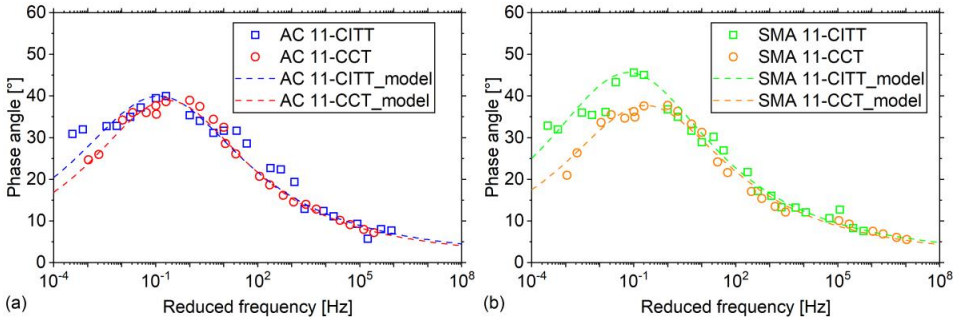

Figure 30. Master curves of phase angle: (a) AC 11 and (b) SMA 11.

Table 10. The fitting parameters and statistical parameters of the phase angle master curves for asphalt mixtures.

Fitting parameter		AC 11-CITT	SMA 11-CITT	AC 11-CCT	SMA 11-CCT
Lorentzian equation	k_p	40.006	45.656	38.960	37.745
	k_g	3.167	3.141	2.946	3.114
	k_c	-0.910	-1.154	-0.639	-0.653
Goodness of fit statistics					
S_e		2.961	2.661	1.299	1.611
S_y		11.358	12.273	11.223	11.934
S_e/S_y		0.261	0.217	0.116	0.135
R^2		0.932	0.953	0.987	0.982

The *NSE* of the phase angle was calculated from the Lorentzian equation and was also utilised to compare the phase angle at each frequency as similar to the comparison of dynamic modulus. Figure 31 presents the *NSE* of the phase angle for AC 11 and SMA 11. A smaller *NSE* value was obtained at a higher frequency and a bigger *NSE* value emerged at a lower frequency. Meanwhile, the *NSE* of AC 11 was less than 0.005 in the range of 0.1 Hz to 10^5 Hz, showing the consistency of the phase angle of the two tests in this range. For the SMA 11 mixtures, the consistent range of phase angles from 10 Hz to 10^5 Hz for both tests was smaller than the range for the AC 11 mixtures. Furthermore, the *NSE* values of SMA 11 mixtures were bigger than the ones of AC 11 mixtures in the low frequency range. This phenomenon indicated that the difference in phase angle between the two test methods was larger for SMA 11 mixtures than for AC 11 mixtures. Besides, the phase angle of the CITT test was larger than that of the CCT, which was consistent with Kim's research [12]. The horizontal phase angles of the CITT were generally higher than the phase angles determined from the CCT. The averaged phase angles from the horizontal direction and vertical direction were close to the values from the

CCT. It can be interpreted that the CITT only considers the phase angle in the horizontal direction.

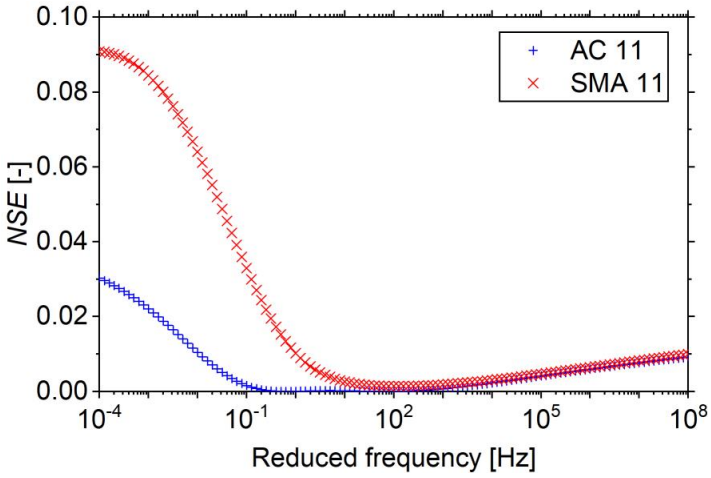

Figure 31. *NSE* of phase angle between two test modes for AC 11 and SMA 11.

Stress-strain response

In order to clarify the fundamental difference between the two test modes, the stress-strain response was investigated. The stress-strain states of AC 11 mixtures for the two tests are represented in Figure 32 at various temperature and frequency conditions. Figure 33 shows the *CoV* of the stress and strain results. As shown in Figure 32a and 32c, the stresses of both test modes for AC 11 decreases as the temperature increases. This was explained that both test modes control the strain in a certain range to ensure that the tested asphalt mixture was in the LVE range. The increase in temperature caused the softening of the asphalt mixture yet the strain range did not change. The strains of two tests for AC 11 are shown in Figure 32b and 32d. It was observed that the strains of the CCT were maintained around 40 με at all temperatures except for 40 °C. However, the strains of the CITT were not stable at a certain value with the temperature changing, and there was no intuitive changing trend between the strain and the temperature. This indicated that the CCT controlled the strain better than the CITT and the strains of both tests were varied at high temperatures.

Figure 32 also shows the changes in stress and strain with the frequency. At low temperatures, the stresses measured for both tests were maintained at a relatively constant stress level as the frequency changed. The stresses were gradually affected by frequency as the temperature increased. For high temperatures, the stress values fluctuated more with various

frequencies for both tests. The variation in the trends of strain and stress with frequency for the CITT was similar, while the strain in the CCT was stable at an average of 40 με. When it came to the changes in strains, the CCT had better deformation control than the CITT. However, both approaches did not control the deformation well at high temperatures due to the viscous properties of the asphalt mixture at high temperatures. The change in the stress-strain state with temperature and frequency can be explained by considering the viscoelastic behaviour of asphalt materials. At low temperatures, the elastic component played a major role; therefore, the dynamic modulus did not change much with frequency, and the stress and strain were stable. At high temperatures, the viscous component played a more important role, and the dynamic modulus, as well as the stress-strain state, were highly related to temperature values. It was worth noting that the strain value measured during the CITT at a high temperature and low frequency was close to the upper limit. Therefore, it was difficult to ensure that the asphalt material specimen was within the LVE range at high temperatures when investigated with the CITT.

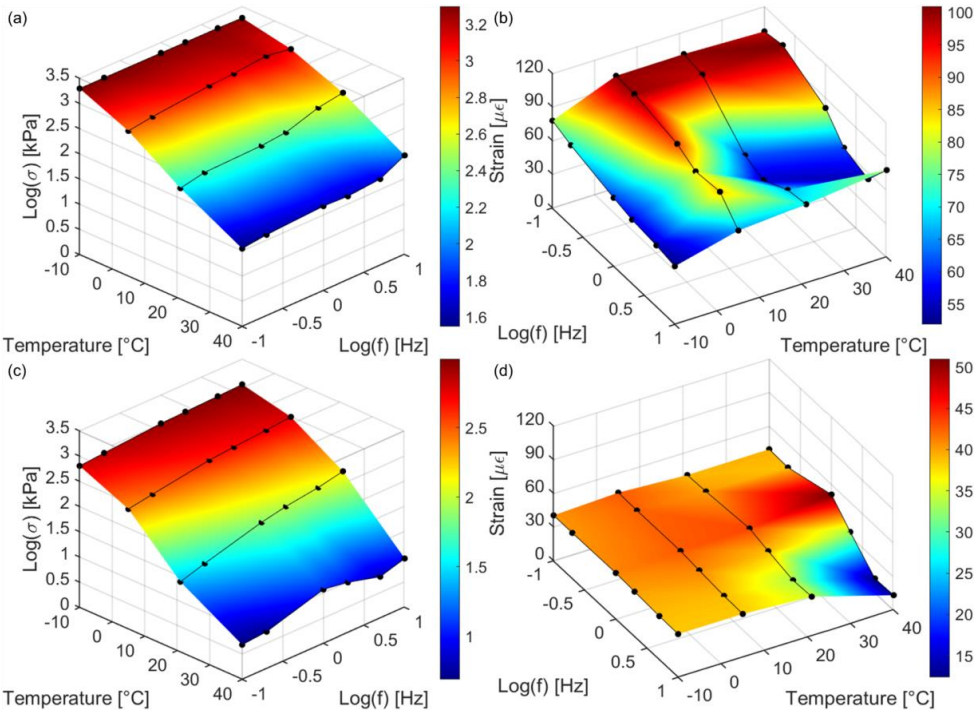

Figure 32. Stress-strain states of AC 11 in CITT and CCT at various conditions: (a) AC 11-CITT stress, (b) AC 11-CITT strain, (c) AC 11-CCT stress and (d) AC 11-CCT strain.

Figure 33 indicates that the *CoV* of stress and strain results for AC 11 mixtures are small at -10, 5 and 21 °C and high at 40 °C, which is consistent with the *CoV* of dynamic modulus results. This result further reflected that the mechanical properties of asphalt mixtures were more stably determined at low and medium temperatures by both two test modes. The larger variations occurred at high temperatures.

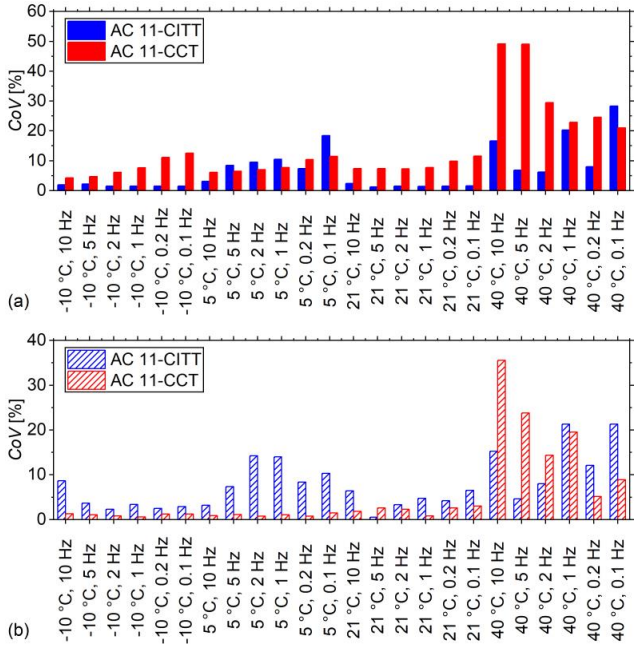

Figure 33. *CoV* of stress and strain results of AC 11 mixtures: (a) stress and (b) strain.

The stress-strain states measured for SMA 11 mixtures are shown in Figure 34. The trend of stress-strain states for SMA 11 was similar to the one for AC 11, indicating the major relevance of the viscoelastic properties of asphalt materials. However, there were still some distinctions between the two asphalt mixtures. At low temperatures, the stress of the SMA 11 was larger than that of the AC 11 except for 10 Hz in the CITT. The strain of the SMA 11 was bigger than that of the AC 11 except for 10 Hz in the CITT. Meanwhile, the stresses of the CCT grew slowly with the increase in frequency, and the strains remained around 40 με for both AC 11 and SMA 11. Thus, this finding illustrated that the CCT had better control of stress and strain than the CITT. Comparing the results depicted in Figure 32a and 32c and Figure 34a and 34c for high temperatures, the CITT stress values measured for the SMA 11 samples are smaller than the ones for the AC 11 specimens. At 40 °C, the stress values of the SMA 11 in the CITT decreased on average by about 15% relative to the AC 11. However, the stress of the

SMA 11 was almost the same as that of the AC 11 in the CCT at 40 °C. The trends of the strain values measured for both SMA 11 and AC 11 asphalt mixtures were similar at high temperatures.

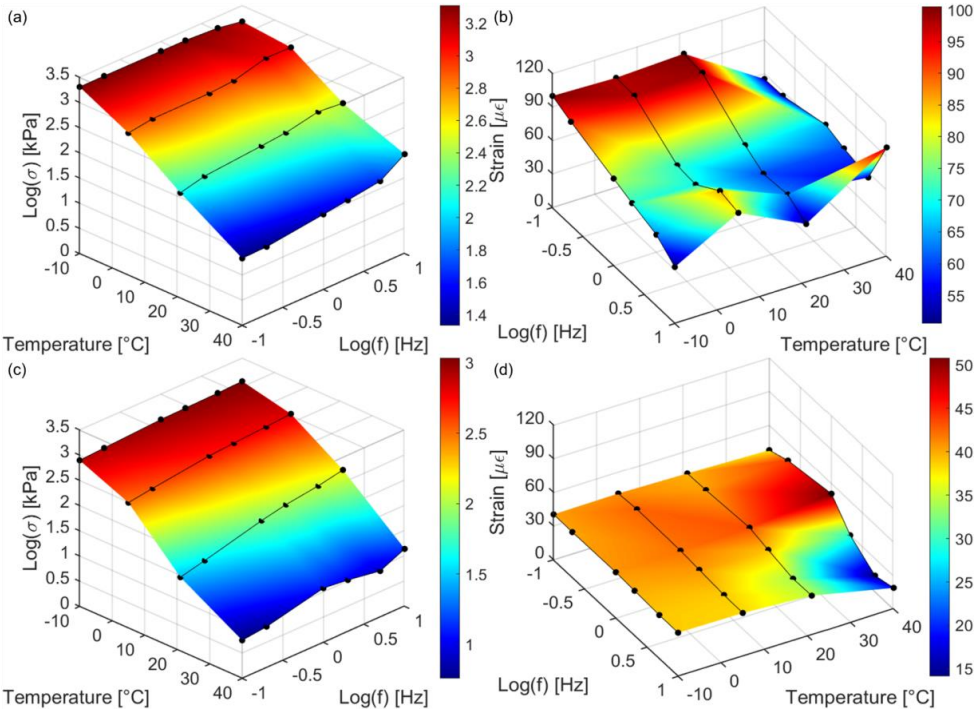

Figure 34. Stress-strain states of SMA 11 in CITT and CCT at various conditions: (a) SMA 11-CITT stress, (b) SMA 11-CITT strain, (c) SMA 11-CCT stress and (d) SMA 11-CCT strain.

The *CoV* of stress and strain results for SMA 11 mixtures have a similar trend to that for AC 11 mixtures as presented in Figure 35. It was worth finding that the *CoV* of the CCT strain was very small at -10, 5 and 21 °C and was relatively large at 40 °C for both asphalt mixtures. This reflected that the CCT had a very stable control on strain at -10, 5 and 21 °C and controlled strain unstably at high temperatures.

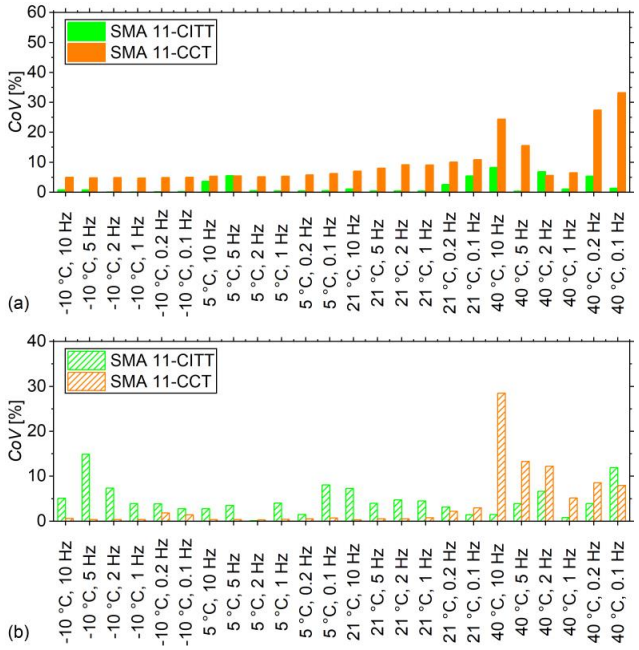

Figure 35. *CoV* of stress and strain results of SMA 11 mixtures: (a) stress and (b) strain.

As the different modes of control strain for the two tests, the stress and the strain were normalised by dividing by the maximum value method for comparison. The normalised stresses at every temperature were used to reflect the changing trend of the stress. The exponential formulations used to fit the experimental values of mean stress and temperature are shown in Figure 36. The high R^2 values validated the reliability of the relationship. The normalised stresses at -10 °C were similar for both tests and the difference occurred at high temperatures. At 40 °C, the values of normalised stresses measured by the CITT were approximately 3.26 and 2.34 times greater than the ones measured by the CCT for AC 11 and SMA 11 mixtures, respectively. Compared with the CCT, the results indicated that the stress level of the CITT was higher and the difference between the two tests of AC 11 was greater than that of SMA 11 in terms of stress.

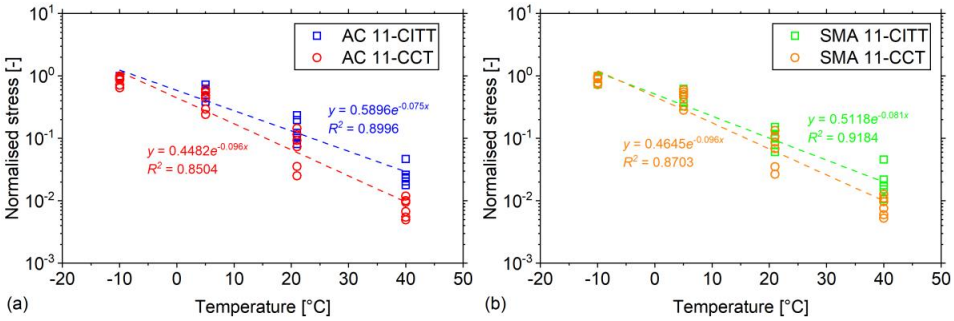

Figure 36. Relationship between normalised stress and temperature: (a) AC 11 and (b) SMA 11.

The relationship between normalised strain and temperature is shown in Figure 37. At -10 °C, the normalized strain of the CCT had a stable value of around 0.8, which corresponded to 40 με. The strain difference with frequencies increased gradually with the increase in temperature. At 40 °C, the strains of the CCT at six frequencies were quite different. The normalised strain of the CITT showed large deviations at all four test temperatures. The strain deviation under different frequencies of the CITT was greater than that of the CCT at -10, 5 and 21 °C and smaller than that of the CCT at 40 °C. The results indicated that the changing trend of strain with temperature for the CCT was smaller than that of the CITT at low and medium temperatures, while higher at high temperatures. This result demonstrated a better control over the strain of the CCT at low and medium temperatures, which was consistent with the *CoV* of strain results.

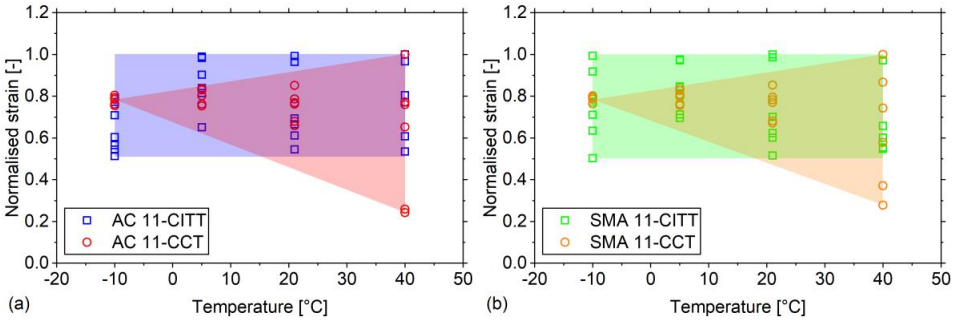

Figure 37. Relationship between normalised strain and temperature: (a) AC 11 and (b) SMA 11.

4.2 Estimation of master curve models

After obtaining test results, the master curves were constructed to predict the dynamic modulus of asphalt mixtures. The different master curve models were estimated in this thesis, which involved four asphalt mixture types of AC 11-70/100, AC 11-PMB, SMA 11-70/100 and SMA 11-PMB prepared by roller compactor. The study on the estimation of master curve models was detailly discussed in Paper II.

4.2.1 Master curve results

The fitting results of master curves are presented in Figure 38, where red represents the SLS model, blue represents the GLS model and green represents the CAM model, moreover, circle markers, square markers, triangle markers, diamond markers and crosses represent the log-linear equation, the polynomial equation, the Arrhenius equation, the WLF equation and the Kaelble equation, respectively. The results of the three model fits were similar for the four types of asphalt mixtures. The differences appeared in the various shift factor equations. No matter whether at a high or low reduced frequency, the dynamic modulus values fitted by the log-linear equation, Arrhenius equation and Kaelble equation were bigger than the ones fitted by the polynomial equation and WLF equation. The fitting parameters of the log-linear equation and the Kaelble equation were similar, and the fitting parameters of the polynomial function and the WLF equation were very close.

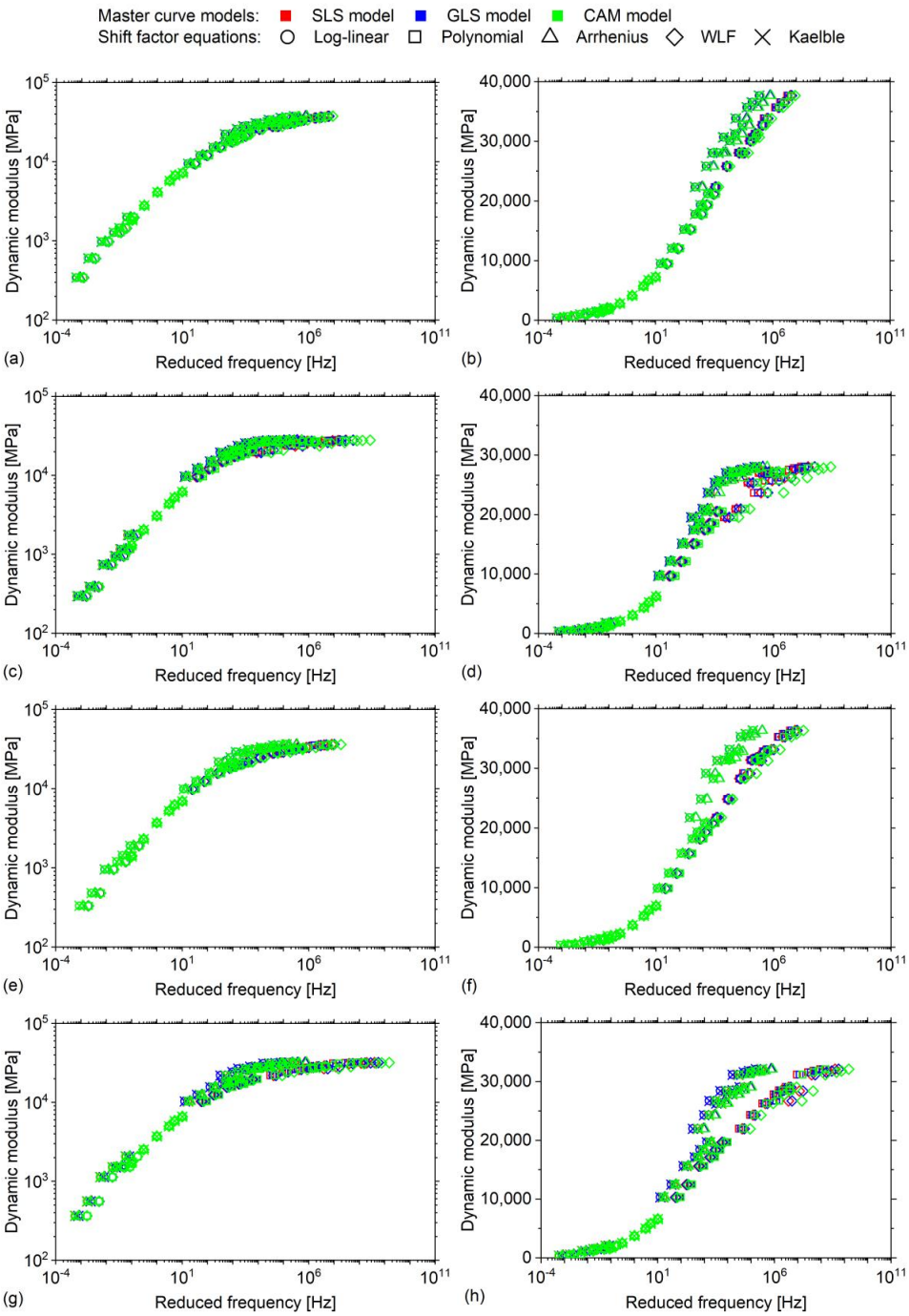

Figure 38. Dynamic modulus master curves of logarithmic scale: (a) AC 11-70/100, (c) AC 11-PMB, (e) SMA 11-70/100 and (g) SMA 11-PMB, and arithmetic scale: (b) AC 11-70/100, (d) AC 11-PMB, (f) SMA 11-70/100 and (h) SMA 11-PMB.

Figure 39 shows the changes in shift factors with temperature, where the colour and shape of the marker represent the same master curve models and shift factor equations as in Figure 38. The curves of the log-linear equation, Arrhenius equation and Kaelble equation were relatively close and show a linear shape, while the curves of the polynomial equation and the WLF equation were similar and more curved than the former ones. This indicates that the polynomial equation and the WLF equation shift the curve more to the right at high reduced frequencies and more to the left at low reduced frequencies in Figure 38 resulting in the dynamic modulus values fitted by the log-linear equation, the Arrhenius equation and the Kaelble equation higher.

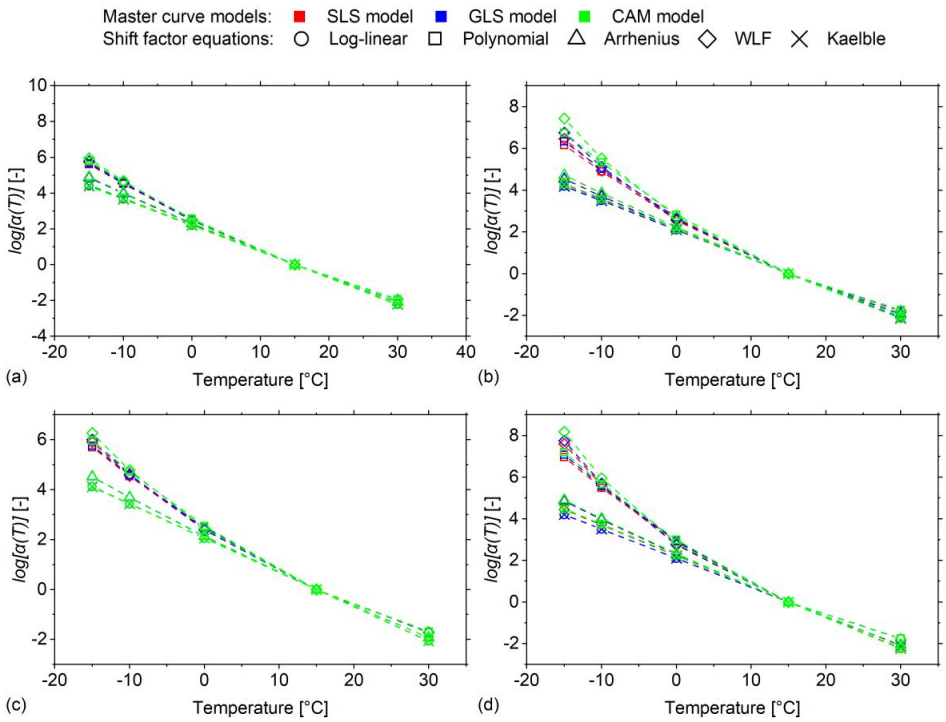

Figure 39. Shift factors of (a) AC 11-70/100, (b) AC 11-PMB, (c) SMA 11-70/100 and (d) SMA 11-PMB.

Figure 40 presents the modelling values of the dynamic modulus at the reduced frequency of 10^4 Hz (T_r = 15 °C) for three master curve models and five shift factor equations. The distinction of dynamic modulus was not greatly affected by the master curve models. The influence of the five shift factor equations was divided into two categories. The first category including the log-linear equation, Arrhenius equation and Kaelble equation showed a higher

value in dynamic modulus. Another category, the polynomial equation and the WLF equation, exhibited a lower dynamic modulus of mixtures. The dynamic modulus of the former category was on average about 23% higher than the one of the latter one.

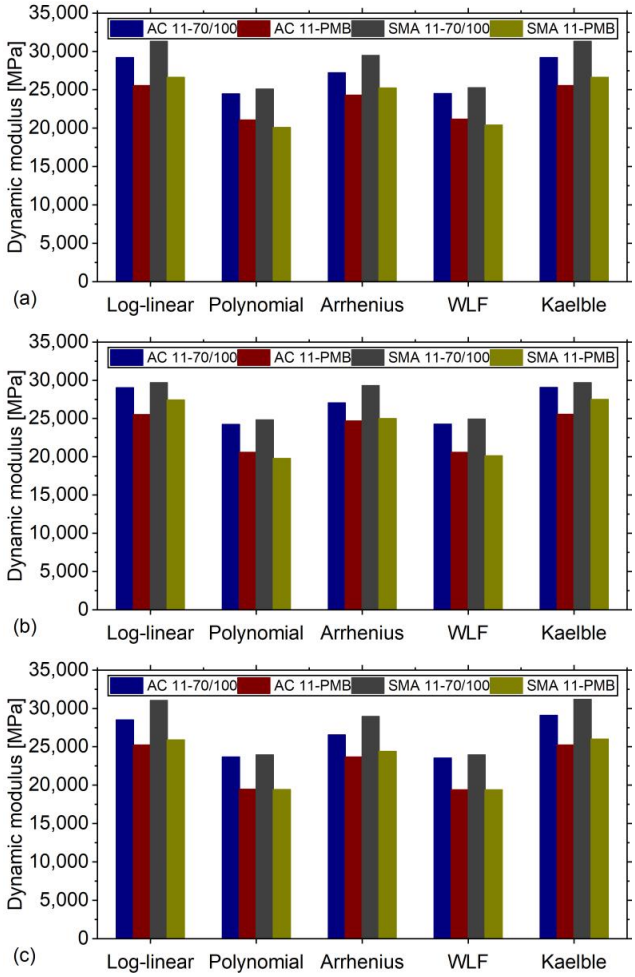

Figure 40. Modelling values of dynamic modulus at the reduced frequency of 10^4 Hz (T_r = 15 °C): (a) SLS model, (b) GLS model and (c) CAM model.

The modelling values of dynamic modulus at the reduced frequency of 10^{-2} Hz (T_r = 15 °C) are given in Figure 41 and had a similar trend as the results at 10^4 Hz, which also were divided into the same two categories. The former has an average 19% higher dynamic modulus than the latter one. The results of Figure 40 and Figure 41 indicate that the modelling values of dynamic modulus fitted by the log-linear equation, Arrhenius equation and Kaelble equation

are approximately 20% higher than the ones fitted by the polynomial equation and the WLF equation both at high and low reduced frequencies.

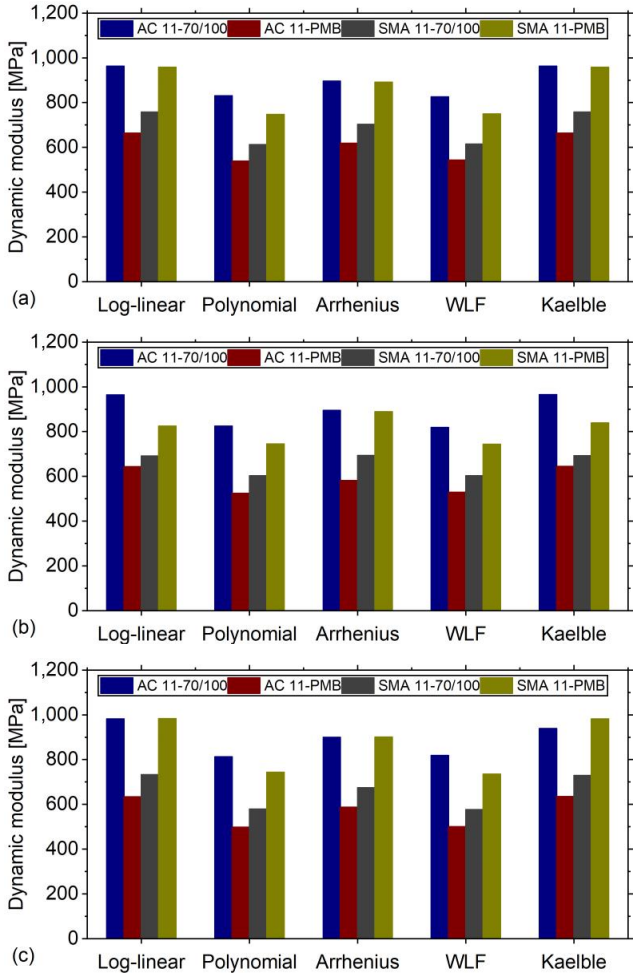

Figure 41. Modelling values of dynamic modulus at the reduced frequency of 10^{-2} Hz (T_r = 15 °C): (a) SLS model, (b) GLS model and (c) CAM model.

4.2.2 Error analysis

Absolute error

After comparing the master curves constructed by different models, the error analysis of each model and shift factor equation was carried out. The absolute errors of dynamic modulus between the modelling values fitted by the three master curve models and the five shift factor equations and the measured values are shown in Figure 42, where the colour and shape of the

marker represent the same master curve models and shift factor equations as in Figure 38. The absolute error was small at high temperatures and relatively big at the temperature range between-15 °C to 0 °C for all mixtures. The maximum absolute error at -10 °C can be explained by the connection between the viscoelastic stage and elastic stage, which in turn changes the mechanical response of mixtures. As the temperature continues to decrease (the reduced frequency increases), the absolute error became smaller again at -15 °C (higher reduced frequency). This result was attributed to the elastomer of asphalt mixture at very low temperatures, resulting in a constant dynamic modulus.

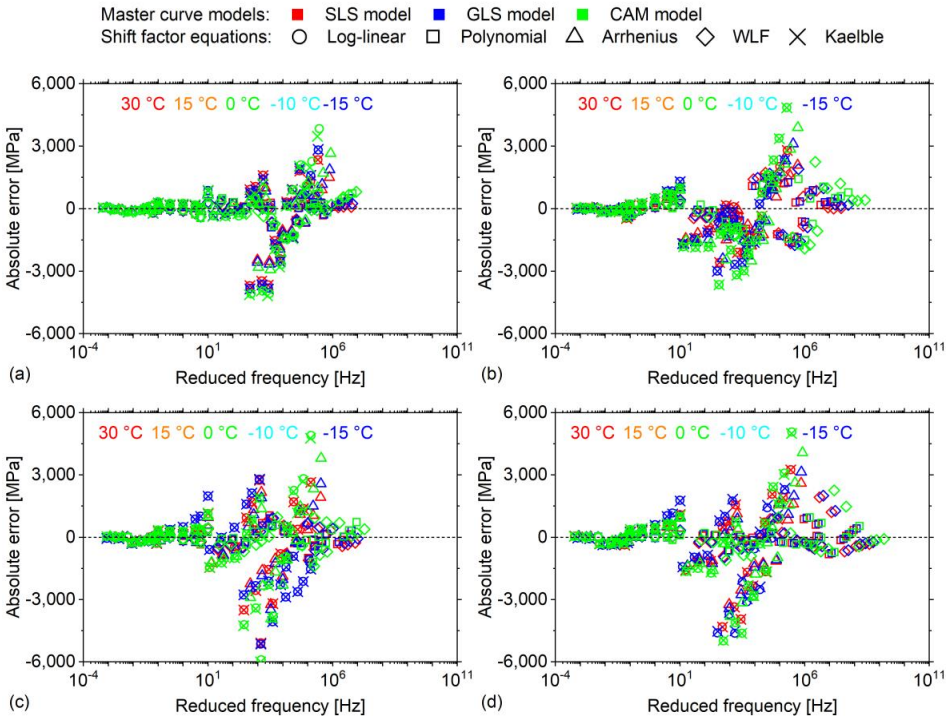

Figure 42. Absolute errors of (a) AC 11-70/100, (b) AC 11-PMB, (c) SMA 11-70/100 and (d) SMA 11-PMB.

The shift factor equation has more influence on the Sum of Absolute Error (*SAE*) than the master curve models as shown in Figure 43. There were 15 master curve model-shift factor equation combinations for four types of mixtures resulting in a total of 60 fitting procedures. The average *SAE* of the fitting procedures with the controlled fitting condition are used for comparing the distinctions of the master curve models, shift factor equations and asphalt mixture types as expressed in Equation 55.

$$\overline{SAE} = \frac{\sum SAE\left(\text{master curve models, shift factor equations, asphalt mixture types}\right)}{n} \quad (55)$$

where $\overline{SAE}$ is the average *SAE*, *n* is the number of fitting procedures. The $\overline{SAE}$ of fitting procedures with the SLS model, the GLS model and the CAM model were 21598 MPa, 23851 MPa and 27244 MPa, respectively. This indicated that the SLS model had the smallest absolute error, the CAM model had the largest absolute error and the GLS model was in between. Regarding the shift factor equations, the *SAE* for the log-linear equation and the Kaelble equation were similar and classified as class 1, the *SAE* for the polynomial equation and the WLF equation were close and grouped into class 2 and the value for the Arrhenius equation lies between them as class 3. The absolute error of class 1 was more than twice the one of class 2. The results revealed that the SLS model and the polynomial function had the smallest absolute errors in three master curve models and five shift factor equations, respectively. For class 1, the absolute error of SMA mixtures was larger than the one of AC mixtures. Comparing four types of mixtures, the AC 11-PMB had the highest absolute error of class 2.

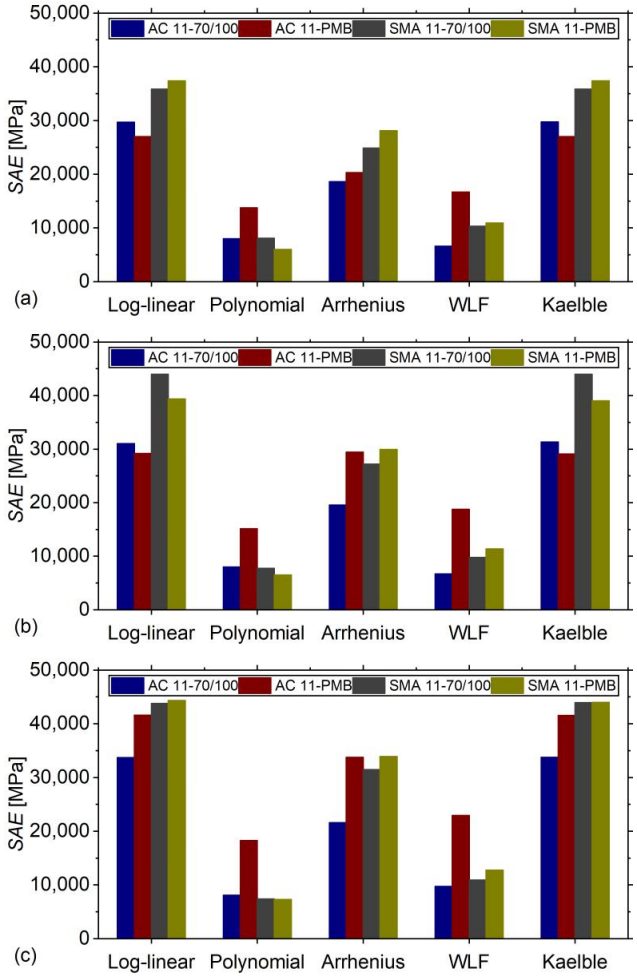

Figure 43. *SAE* of all fitting procedures: (a) SLS model, (b) GLS model and (c) CAM model.

Normalised square error (NSE)

Since the dynamic modulus of asphalt mixtures was distinct at different temperatures and frequencies, it was difficult to compare the error under the same condition over the full frequency range. The *NSE* was analysed to compare different models and shift factor equations at the same condition. From Figure 44, the *NSE* is larger at high temperatures and smaller at low temperatures contrary to the results of the absolute error, which reflects the error of dynamic modulus at high temperatures. The maximum *NSE* appeared at a high temperature of 30 °C. As the temperature increased, the asphalt transitioned to a viscous flow state, and its dynamic modulus was more obviously affected by the loading conditions and became unstable, resulting in an increasing *NSE*. Furthermore, the distinction between different asphalt mixtures

was also found. The *NSE* for asphalt mixtures containing PMB was relatively higher than the one for asphalt mixtures containing bitumen 70/100. Comparing with the bitumen 70/100, the polymer molecular in the PMB also provided a portion of the stiffness modulus for the asphalt mixture. The complex connection between the polymer molecular and the asphalt binder, such as the composition and distribution of the polymer molecular in the asphalt binder, determined the stiffness modulus of the asphalt mixture [97, 98]. Therefore, the dynamic modulus change of the asphalt mixture containing PMB was more complicated than the one of the asphalt mixture with bitumen 70/100, resulting in a larger error. Otherwise, the SMA mixtures had a higher *NSE* than the AC mixtures. The SMA mixture contained more coarse aggregates than the AC mixture, leading to more particle angularity. The more particle angularity, the higher the stiffness modulus of the asphalt mixture [99]. Thus, the change of the dynamic modulus of the SMA mixture was more complex than the one of the AC mixtures, resulting in a larger error.

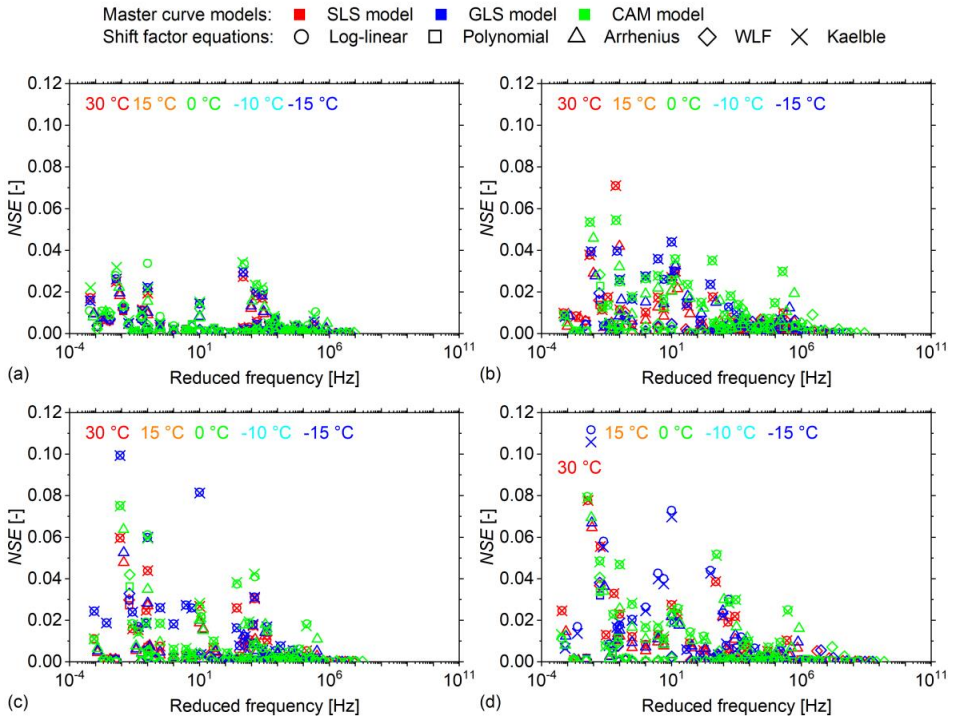

Figure 44. *NSE* of (a) AC 11-NB, (b) AC 11-PMB, (c) SMA 11-NB and (d) SMA 11-PMB.

The *SSE* for different models has the same trend as the *SAE* as shown in Figure 45. The same approach as *SAE* is used for *SSE* as shown in Equation 56.

$$\overline{SSE} = \frac{\sum SSE\left(\text{master curve models, shift factor equations, asphalt mixture types}\right)}{n} \quad (56)$$

where $\overline{SSE}$ is the average *SSE*. The $\overline{SSE}$ of SLS model was 0.20, which was also smaller than the ones of the GLS model (0.25) and the CAM model (0.26). Based on *SSE* values, five shift factor equations were divided into three classes the same as the classification in Section 4.2.2.1. The $\overline{SSE}$ of class 1 is around 5 times the one of class 2. The results showed that the SLS model and the polynomial function had the smallest *SSE* in the three master curve models and the five shift factor equations, respectively. The mixtures containing PMB had a lower *SSE* than the mixtures containing bitumen 70/100, which indicated that the fit of the model for bitumen 70/100 was better than the one for PMB which was explained by the effect of the PMB structure on the dynamic modulus of asphalt mixture.

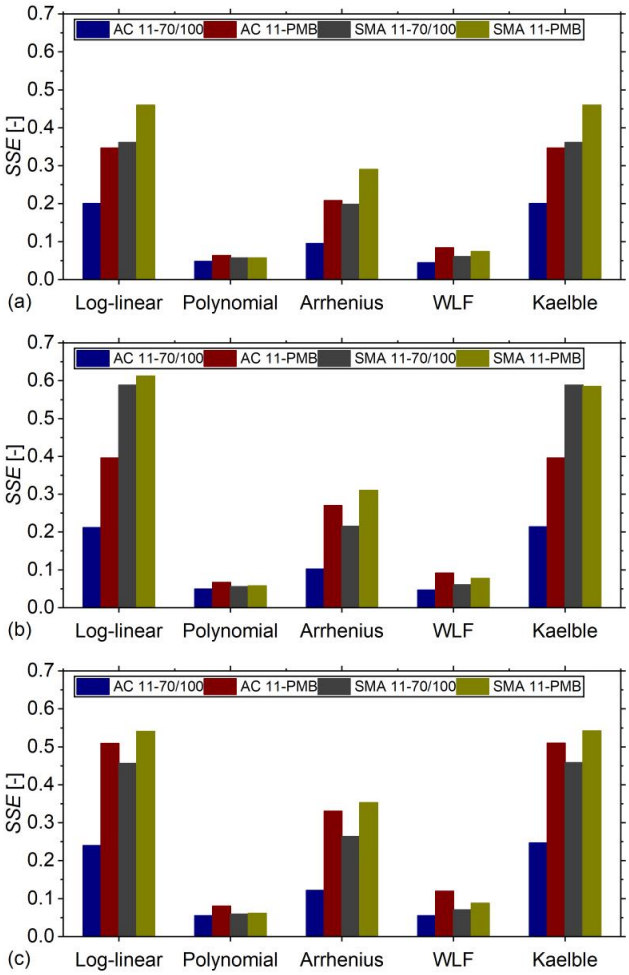

Figure 45. *SSE* of all fitting procedures: (a) SLS model, (b) GLS model and (c) CAM model.

4.2.3 Goodness of fit

The S_e/S_y and R^2 were used to evaluate the quality of the model. From Figure 46, the SLS model has the smallest average value of S_e/S_y (0.0853) and the highest average value of R^2 (0.9915) than the GLS model (0.0951, 0.9906) and the CAM model (0.1090, 0.9859). Otherwise, the average values of S_e/S_y and R^2 for the polynomial equation were the smallest (0.0394) and the largest (0.9982), respectively. While the Kaelble equation had the biggest average value of S_e/S_y (0.1441) and the smallest average value of R^2 (0.9810). These results indicated that the SLS model and the polynomial function had the best goodness of fit in the three master curve models and the five shift factor equations, respectively. Among the 15 kinds of fits, the asphalt mixture containing bitumen 70/100 showed an overall better goodness of fit than the PMB

asphalt mixture. This indicated that the dynamic modulus of the PMB asphalt mixture was affected by more factors than the one of the asphalt mixtures with bitumen 70/100 due to the effect of polymer molecular in the binder.

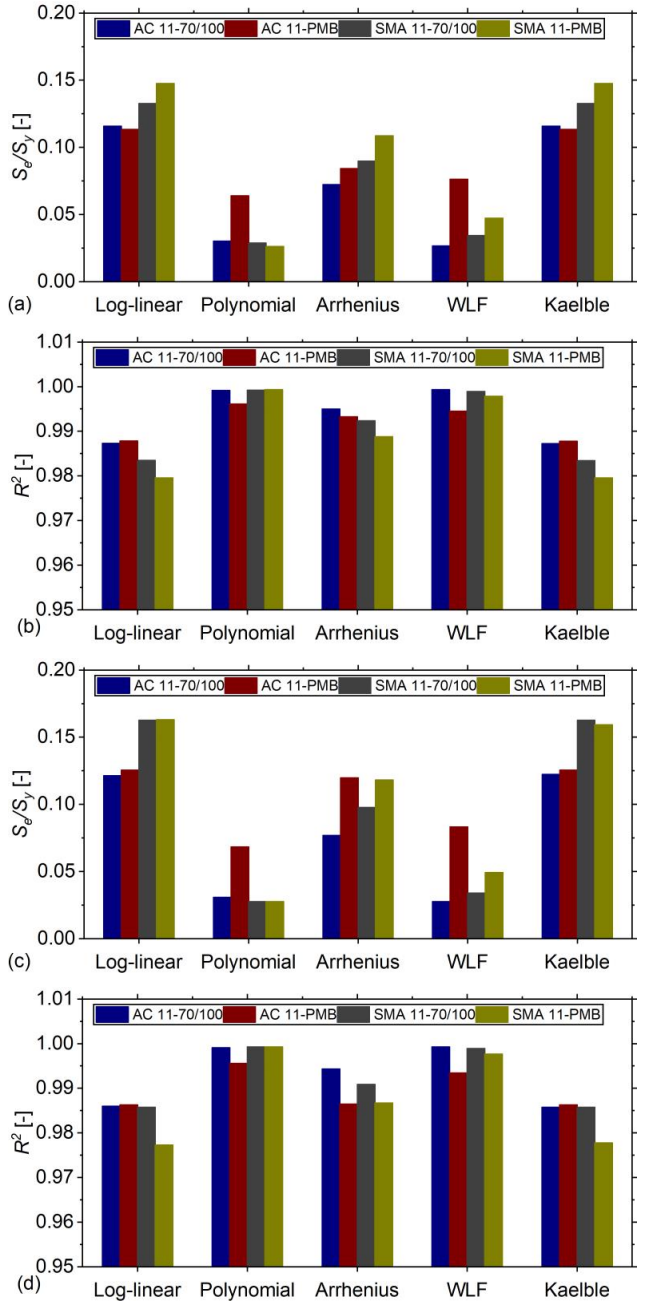

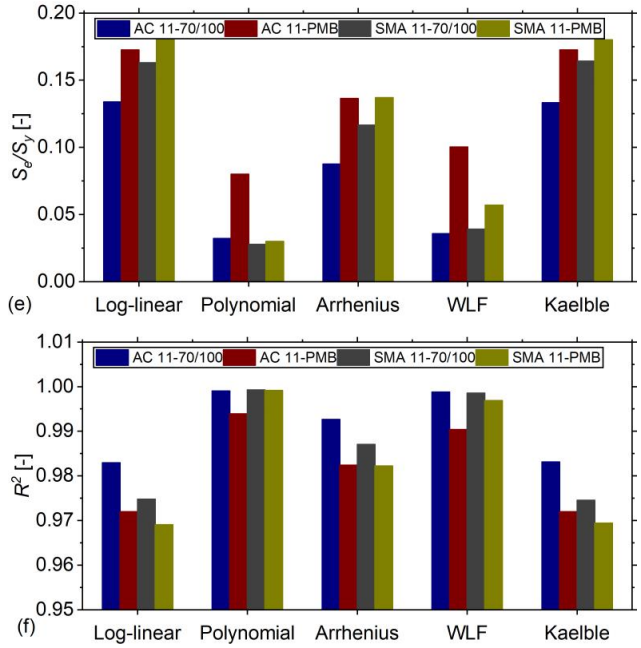

Figure 46. S_e/S_y and R^2 of all fitting procedures: (a) and (b) SLS model, (c) and (d) GLS model and (e) and (f) CAM model.

Master curve model estimation

The comparison of master curve models between measured dynamic modulus and predicted dynamic modulus is shown in Figure 47, where blue represents AC 11-70/100, orange represents AC 11-PMB, grey represents SMA 11-70/100 and yellow represents SMA 11-PMB and the shape of the marker represents the same shift factor equation as in Figure 38. All the models fitted the data satisfactorily according to the goodness of fit ranking criteria. The SLS model had the lowest S_e/S_y of 0.0925 and the highest R^2 of 0.9916, which indicated that this model showed better goodness of fit than the GLS model and CAM model under the test conditions of this study. The S_e/S_y and R^2 of the CAM model were, respectively, 28.2% higher and 0.5% lower than the respective parameters of the SLS model showing the worst correlation in the three models. Therefore, the SLS model with better goodness of fit was considered for modelling the four asphalt mixtures.

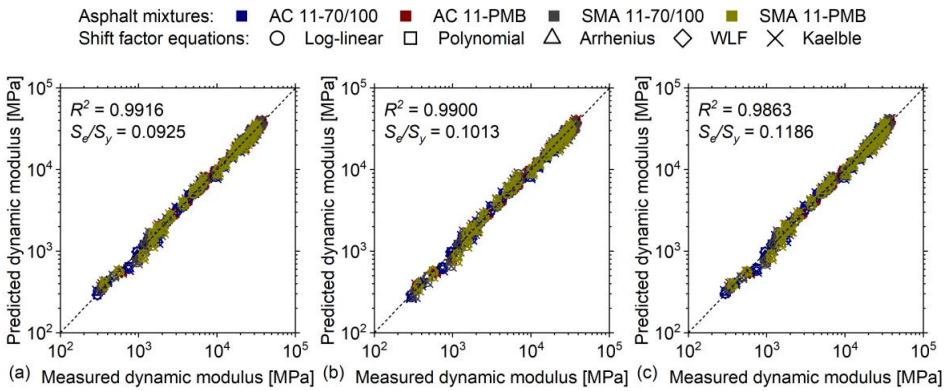

Figure 47. Comparison between measured dynamic modulus and predicted dynamic modulus of three master curve models: (a) SLS model, (b) GLS model and (c) CAM model.

Shift factor equation estimation

The comparison between measured dynamic modulus and predicted dynamic modulus related to the selection of shift factor equation is shown in Figure 48, where the colour represents the same type of asphalt mixtures as in Figure 47, furthermore, circle markers, square markers and triangle markers represent the SLS model, GLS model and CAM model, respectively. The fitting results showed that all the considered five equations fit the data satisfactorily according to the goodness of fit ranking criteria. The *log[α(T)]* of the Kaelble equation showed a linear trend within the test temperature range, the fitting results of the Kaelble equation and log-linear equation were similar and the same findings were also shown in the former Sections. The quadratic polynomial equation displayed the best goodness of fit with the lowest S_e/S_y of 0.0275 and the highest R^2 of 0.9984. The fitting results of the WLF equation and quadratic polynomial equation were similar and showed a good fit. The fit related to the Arrhenius equation was in the middle among the five equations. Furthermore, the transform between frequency and temperature was more convenient for the WLF equation than the quadratic polynomial due to the quadratic form. Therefore, the WLF equation was recommended for modelling the dynamic modulus of the asphalt mixtures.

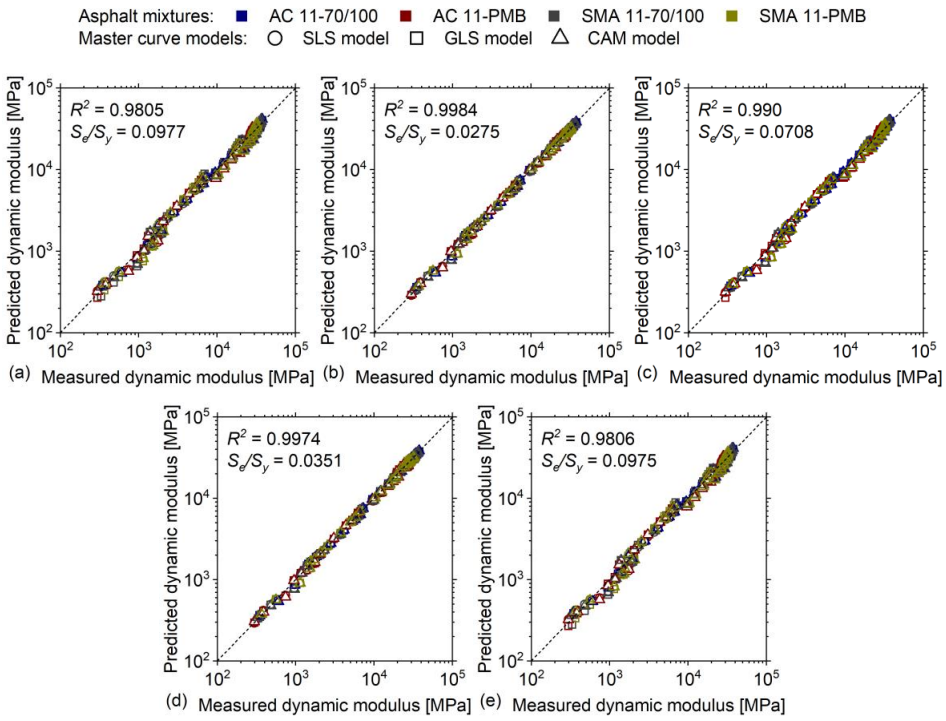

Figure 48. Comparison between measured dynamic modulus and predicted dynamic modulus of five shift factor equations: (a) log-linear equation, (b) quadratic polynomial equation, (c) Arrhenius equation, (d) WLF equation and (e) Kaelble equation.

4.3 Master curves of 20 asphalt mixture types

Based on the above research, Paper III presented the dynamic modulus master curves of asphalt mixtures constructed using the SLS model and the WLF equation as shown in Figure 49. Furthermore, Figure 49 also documents that the dynamic modulus master curves of asphalt mixtures containing the bitumen types belonging to the same group (i.e., neat, PMB, soft) are relatively close. The fitting parameters of both the SLS model and the WLF equation are given in Table 11. All results displayed a high goodness of fit $R^2 \geq 0.973$.

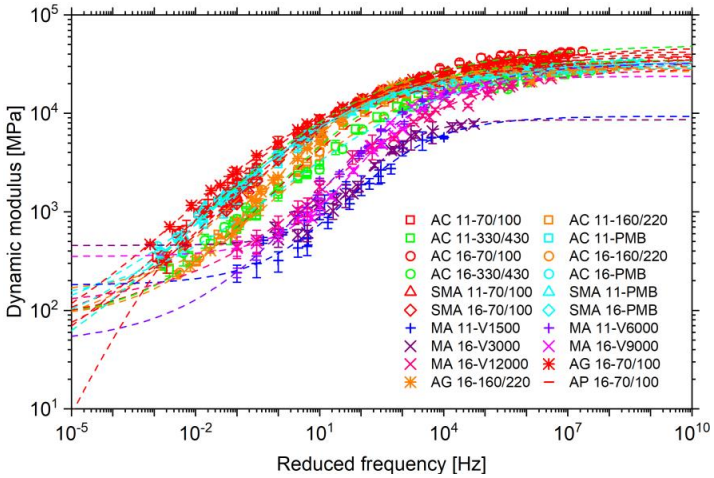

Figure 49. Dynamic modulus master curves of asphalt mixtures.

Table 11. Fitting parameters of SLS model and WLF equation for dynamic modulus.

Mixture code	SLS model				WLF equation		R^2
	δ	α	β	γ	C_1	C_2	
AC 11-70/100	0.72	3.97	-0.98	0.38	17.87	123.47	0.999
AC 11-160/220	1.89	2.60	-0.09	0.63	9.39	82.16	0.995
AC 11-330/430	2.16	2.27	0.23	0.64	10.33	79.76	0.988
AC 11-PMB	1.74	2.73	-0.59	0.57	12.14	86.34	0.994
AC 16-70/100	0.90	3.80	-0.92	0.42	13.20	92.23	0.991
AC 16-160/220	1.87	2.67	-0.08	0.63	8.51	77.17	0.990
AC 16-330/430	2.02	2.46	0.07	0.50	11.60	83.09	0.990
AC 16-PMB	1.76	2.77	-0.65	0.49	11.40	74.07	0.997
SMA 11-70/100	1.40	3.21	-0.71	0.49	12.30	92.50	0.999
SMA 11-PMB	0.85	3.69	-1.04	0.42	9.94	69.26	0.998
SMA 16-70/100	1.74	2.89	-0.46	0.53	12.24	91.17	0.998
SMA 16-PMB	1.59	2.91	-0.78	0.51	12.20	83.56	0.997
MA 11-V1500	2.26	1.71	1.47	0.89	1.11	41.09	0.973
MA 11-V6000	1.65	2.86	0.45	0.61	5.50	70.76	0.977
MA 16-V3000	2.66	1.28	2.53	1.31	1.85	44.84	0.994
MA 16-V9000	2.55	1.83	1.97	1.02	18.41	167.42	0.980
MA 16-V12000	2.05	2.41	0.63	0.56	33705.31	180907.61	0.990
AG 16-70/100	1.17	3.43	-1.06	0.42	23.02	149.73	0.997
AG 16-160/220	1.91	2.53	-0.28	0.76	4.91	50.67	0.981
AP 16-70/100	-4.86	9.43	-2.26	0.36	8.20	57.47	0.996

All master curve parameters are applied in the ERAPave pavement design program to characterise the mechanical properties of asphalt materials as shown in Figure 50. In the structure modular, the pavement structure is defined by the material type and the layer thickness,

where the asphalt material can be chosen from the above 20 asphalt mixture types (the mixture codes in Figure 50 based on the Norwegian codes) and several field core samples.

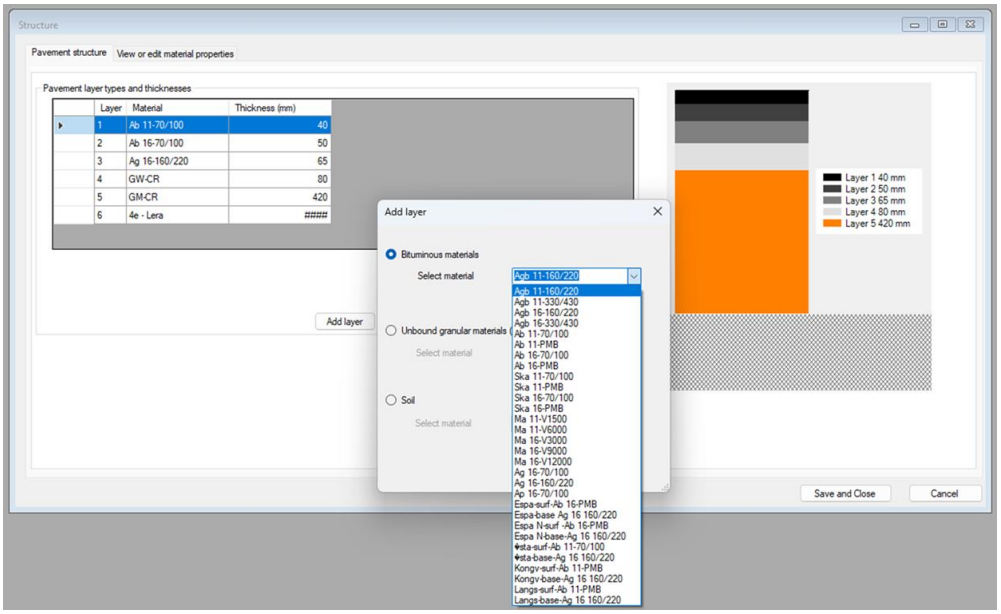

Figure 50. Pavement structure modular in ERAPave pavement design program.

The phase angle master curves are constructed based on the Lorentzian equation as shown in Figure 51. The fitting parameters of the Lorentzian equation are given in Table 12.

Table 12. Fitting parameters of Lorentzian equation for phase angle.

Mixture code	Lorentzian equation			R^2
	k_p	k_g	k_c	
AC 11-70/100	36.57	3.56	-1.01	0.951
AC 11-160/220	39.89	3.59	-1.39	0.957
AC 11-330/430	43.21	2.94	-0.80	0.955
AC 11-PMB	40.35	4.07	-1.74	0.939
AC 16-70/100	40.14	4.12	-0.82	0.940
AC 16-160/220	37.64	4.47	-0.47	0.925
AC 16-330/430	43.79	3.28	-0.77	0.935
AC 16-PMB	40.74	4.12	-0.15	0.922
SMA 11-70/100	44.16	2.91	-1.20	0.964
SMA 11-PMB	37.76	4.71	-1.99	0.959
SMA 16-70/100	45.28	3.01	-1.01	0.960
SMA 16-PMB	38.02	4.64	-2.06	0.926
MA 11-V1500	43.47	2.30	2.50	0.818
MA 11-V6000	40.55	2.50	1.67	0.894
MA 16-V3000	47.56	3.72	2.83	0.747
MA 16-V9000	50.02	2.35	1.54	0.896
MA 16-V12000	47.50	3.12	1.51	0.773
AG 16-70/100	41.77	3.01	-1.66	0.974
AG 16-160/220	43.00	3.71	-1.17	0.964
AP 16-70/100	46.27	3.52	-2.39	0.935

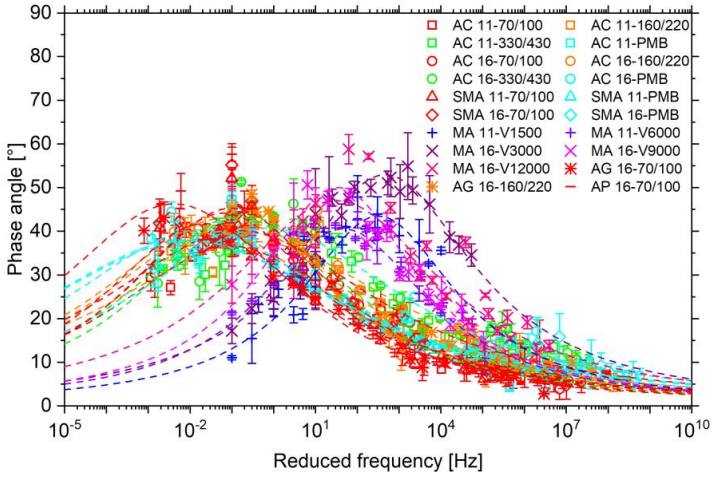

Figure 51. Phase angle master curves of asphalt mixtures.

Based on these test results, the Norwegian material database was established, which was also input into the ERAPave program for the asphalt pavement structure design.

4.4 Impact factor of materials on the dynamic modulus of asphalt mixtures

The influence of material factors including maximum aggregate size, binder content, rheological properties of bitumen, bulk density and void characteristics of asphalt mixtures on the dynamic modulus of asphalt mixtures was discussed detailed discussed in Paper III. The rheological properties of bitumen, i.e., viscosity and complex shear modulus were first characterised by the DSR method to reveal the correlation between material factors and dynamic modulus and to develop the prediction model.

4.4.1 Bitumen viscosity

The viscosities of the nine types of bitumen are presented in Figure 52, with PMB being associated with the highest values in the range of 40 °C to 100 °C due to the network structure of the polymer in the bitumen [100, 101]. Soft bitumen had the lowest viscosity, which presented a flow state at room temperature. The neat bitumen was characterised by average values, and its viscosity decreases as the penetration increases. The log value of viscosity is linear with temperature, as shown in Table 13. All R^2 were higher than 0.989, which indicated almost perfect fits. Therefore, the viscosity of the bitumen at a given temperature can be predicted by the linear regression model, which is used as a material factor influencing the dynamic modulus of asphalt mixtures.

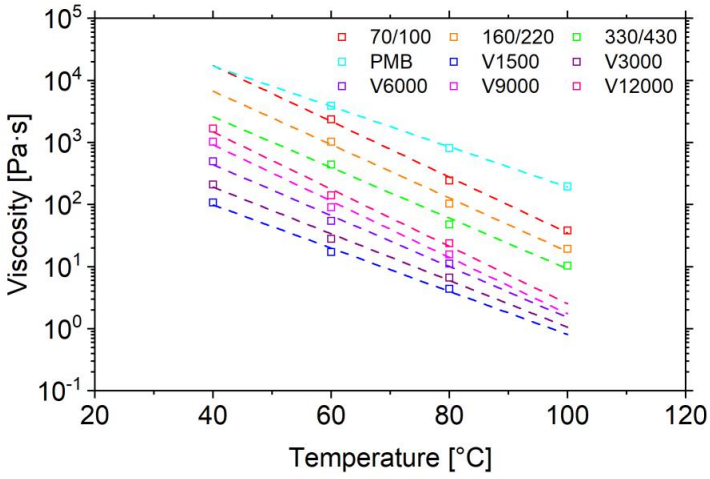

Figure 52. Relationship between viscosity of bitumen and temperature.

Table 13. Linear regression of viscosity, η, with temperature, T.

Bitumen		Linear regression equation	R^2
Neat bitumen	70/100	$log(\eta) = -0.0448 \cdot T + 6.0315$	0.997
	160/220	$log(\eta) = -0.0430 \cdot T + 5.5481$	0.992
	330/430	$log(\eta) = -0.0408 \cdot T + 5.0483$	0.989
PMB	65/105-60	$log(\eta) = -0.0325 \cdot T + 5.5327$	0.999
Soft bitumen	V1500	$log(\eta) = -0.0348 \cdot T + 3.3888$	0.992
	V3000	$log(\eta) = -0.0376 \cdot T + 3.7867$	0.991
	V6000	$log(\eta) = -0.0411 \cdot T + 4.2923$	0.991
	V9000	$log(\eta) = -0.0454 \cdot T + 4.7810$	0.991
	V12000	$log(\eta) = -0.0461 \cdot T + 5.0168$	0.991

4.4.2 Bitumen complex shear modulus

The complex shear moduli of the nine types of bitumen are shown in Figure 53. The complex shear modulus of neat bitumen was higher than the one of soft bitumen. In terms of neat bitumen, the values of complex shear modulus decreased with increasing penetration. Regarding the soft bitumen, the values of complex shear modulus decreased with decreasing viscosity. The complex shear modulus of PMB was lower than the one of neat bitumen at high frequencies (low temperatures) and higher than that of neat bitumen at low frequencies (high temperatures). This is connected that the polymer increases the flexibility of the binder at low temperatures and the network structure of the polymer provides the elasticity in neat bitumen at high temperatures [102, 103]. The modified HS model and WLF equation parameters of nine bitumen are given in Table 14. The results displayed good goodness of fit as all R^2 values were higher than 0.968. Therefore, the complex shear modulus of bitumen at an arbitrary condition can be obtained by the master curves and used as a material factor for evaluating the dynamic modulus.

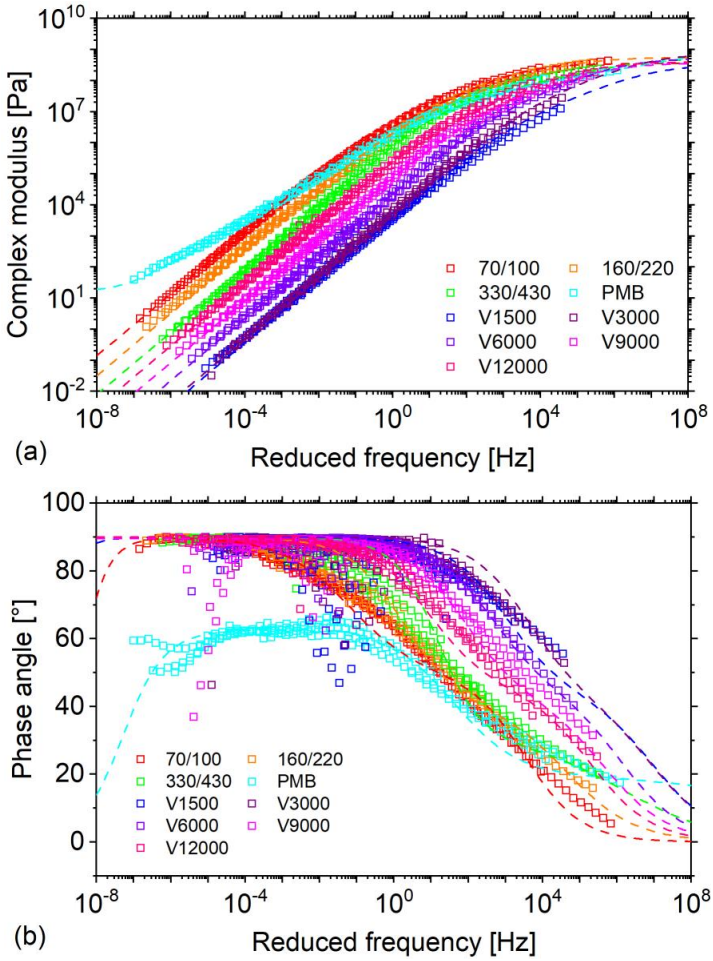

Figure 53. (a) Complex shear modulus and (b) phase angle master curves of bitumen.

Table 14. Modified HS model and WLF equation parameters of complex shear modulus.

Bitumen		Modified HS model								WLF equation		R^2
		G_0	G_∞	τ	m_1	m_2	δ_1	δ_2	η_3	C_1	C_2	
Neat bitumen	70/100	4.51×10^{-2}	3.52×10^{8}	6.30×10^{-3}	0.55	1.00	15.04	1.00	1.00×10^{50}	13.44	108.37	0.968
	160/220	4.01×10^{-103}	5.59×10^{8}	9.16×10^{-4}	0.45	1.00	12.57	1.00	9.97×10^{49}	14.23	125.06	0.994
	330/430	3.54×10^{-97}	5.82×10^{8}	2.18×10^{-4}	0.34	1.00	13.25	6.55	3.60×10^{50}	11.26	100.32	0.985
PMB	65/105-60	1.62×10^{1}	3.48×10^{9}	3.35×10^{-6}	0.22	0.70	29.03	5.59	1.00×10^{300}	13.53	104.01	0.984
Soft bitumen	V1500	1.09×10^{-6}	3.30×10^{8}	1.76×10^{-6}	0.49	1.00	10.11	1.00	3.24×10^{49}	8.34	100.91	0.991
	V3000	2.15×10^{-16}	7.70×10^{8}	9.86×10^{-7}	0.48	1.00	7.17	1.00	1.83×10^{49}	7.53	92.78	0.988
	V6000	3.23×10^{-163}	5.22×10^{8}	6.83×10^{-6}	0.5	1.00	7.98	1.00	8.64×10^{105}	9.34	102.05	0.987
	V9000	1.60×10^{-205}	3.71×10^{8}	3.22×10^{-5}	0.48	0.99	9.00	1.00	9.98×10^{49}	9.6	92.97	0.984
	V12000	5.46×10^{-281}	3.99×10^{8}	1.17×10^{-4}	0.5	1.00	12.42	1.04	1.10×10^{50}	10.95	99.83	0.978

4.4.3 Grey relational analysis of material factors

In this research, only bitumen 70/100, 160/220 and PMB were characterised by the following parameters of the penetration at 25 °C, $Pen_{25\ °C}$, and softening point tested in the water, $T_{R\&B}$. Thus, the grey relational grad was assessed regarding the correlation between the dynamic modulus of asphalt mixtures and the following available material parameters: maximum aggregate size, P_{max}, binder content, B, bitumen viscosity, $\eta(T)$, bitumen complex shear modulus, $|G^*|(T,f)$, asphalt mixture density, ρ_{mix}, V_a, VMA and VFB. The bitumen viscosity and complex shear modulus obtained at the same testing conditions adopted for the evaluation of the dynamic modulus were calculated according to the regression and modified HS models illustrated in Section 4.4.1 and Section 4.4.2, respectively. The 20 asphalt mixtures were analysed, and their dynamic moduli were measured for 30 combinations of frequencies and temperatures for neat bitumen and PMB and 24 combinations for soft bitumen. Thus, the grey relational analysis is conducted for a total of 570 sets of data leading to the result shown in Figure 54. The grey relational degree was ranked as follows in descending order: $|G^*|(T,f)$, $\eta(T)$, VFB, V_a, $\eta_{60°C}$, B, ρ_{mix}, P_{max}, and VMA. The result indicated that the dynamic modulus was greatly affected by the bitumen complex shear modulus and its viscosity as the two corresponding factors were higher than 0.7, followed by the void characteristics of VFB and V_a with values of 0.595 and 0.592. Other factors, such as bitumen properties and binder content, had a relatively low effect on the dynamic modulus since their values range from 0.428 to 0.562. On the one hand, this outcome was explained considering that the rheological properties of bitumen dominate the viscoelastic behaviour of asphalt mixtures. On the other hand, the factors of bitumen complex shear modulus and viscosity, resembling dynamic modulus, changed with frequency and temperature, whereas others were not dependent on these two conditions and therefore did not vary, e.g., VFB, V_a, $\eta_{60\ °C}$, B, ρ_{mix}, P_{max}, and VMA.

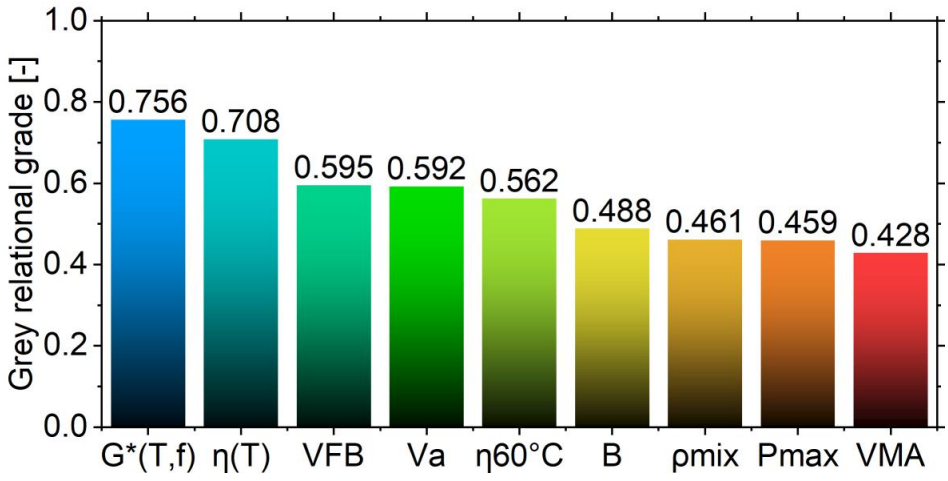

Figure 54. Grey relational grade of material parameters except $Pen_{25\,°C}$ and $T_{R\&B}$.

Considering the effect of $Pen_{25\,°C}$ and $T_{R\&B}$, 13 asphalt mixtures with these two parameters were selected for the grey relational analysis; the corresponding 390 sets of data were analysed. The results are presented in Figure 55, which are similar to the findings already reported in Figure 54. The effect of $Pen_{25\,°C}$ and $T_{R\&B}$ on the dynamic modulus of asphalt mixtures were close to $\eta_{60\,°C}$, and were ranked according to the descending order: $|G^*|(T,f)$, $\eta(T)$, *VFB* and V_a.

The results of the grey relational analysis illustrated that the most influential factor in the determination of the dynamic modulus of asphalt mixtures was represented by the rheological properties of the bitumen, which changed with frequency and temperature. The void characteristics of *VFB* and V_a as well as $\eta_{60\,°C}$, $Pen_{25°C}$ and $T_{R\&B}$ of the binders were the other parameters exerting the largest influence.

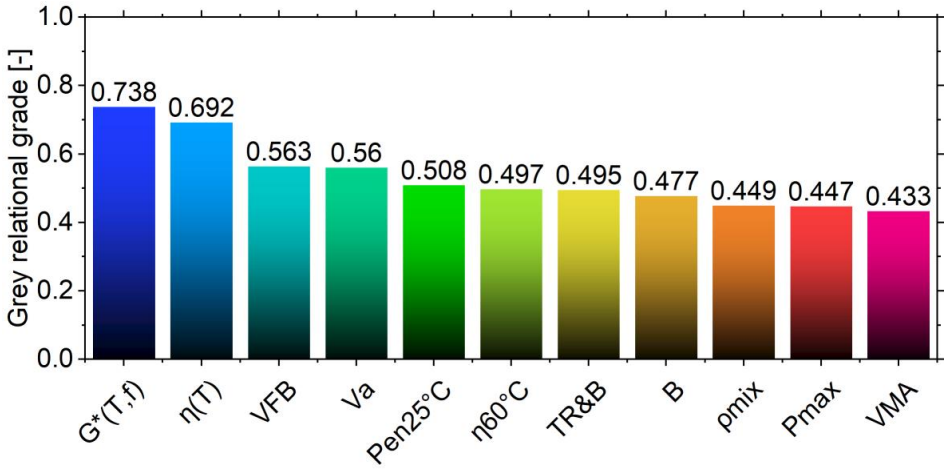

Figure 55. Grey relational grade of material parameters containing $Pen_{25\,°C}$ and $T_{R\&B}$.

4.4.4 Development of dynamic modulus prediction model

Prediction model based on rheological properties of bitumen

Based on the results of the grey relational analysis, the correlation between bitumen viscosity, bitumen complex shear modulus and dynamic modulus of asphalt mixtures was investigated. As shown in Figure 49, the dynamic modulus of asphalt mixtures containing the different types of bitumen belonging to the same group is relatively close. Therefore, the asphalt mixtures were divided into nine types according to the type of bitumen. Based on the experimental data of the asphalt mixture dynamic modulus and the modelling data of the viscosity and complex shear modulus of the bitumen, Multiple Linear Regression (MLR) was performed to evaluate the correlation. The MLR model is given in Equation 57.

$$\log\left[\left|E^*\right|(T,f)\right] = a_1 \cdot \log\left[\eta(T)\right] + a_2 \cdot \log\left[\left|G^*\right|(T,f)\right] + a_3 \tag{57}$$

where $|E^*|(T, f)$ is the dynamic modulus at different temperatures and frequencies, a_1, a_2 and a_3 are model parameters. The model parameters are displayed in Table 15 and the results are illustrated in Figure 56. All nine bitumen types had a good fit with $R^2 \geq 0.901$. The value of *Sig.* is the p-value, which indicates the significance of the independent variable in the model. The lower p-value showed the greater significance of the variable. Analysis of Variance (ANOVA) was used to verify the significance of the model. As shown in Table 15, the p-values of a_2 are all 0, reflecting the significance of bitumen complex shear modulus in the model. Whereas the p-values of a_1 are from 0 to 0.837, and neat bitumen showed a lower value than

the other bitumen. This result indicated that the effect of viscosity on dynamic modulus depended on bitumen types. The ANOVA results indicated that the models for all bitumen had a good correlation with the test results. The R^2 of soft bitumen was more variable when compared to neat bitumen and PMB. This might be caused by the relatively unstable test results of the asphalt mixtures containing the soft bitumen, causing fluctuations, especially at high temperatures [104]. Nevertheless, the dynamic modulus of asphalt mixtures was predicted with high reliability by the viscosity and complex shear modulus of the bitumen for certain loading frequency and temperature conditions. This method can save testing time and the required materials for performing the dynamic modulus test.

Table 15. MLR model parameters of Equation 57 calculated for the nine bitumen types.

Bitumen type		Coefficient						ANOVA		Model summary
		a_1	*Sig.*	a_2	*Sig.*	a_3	*Sig.*	*F*	*Sig.*	R^2
Neat bitumen	70/100	0.041	0.057	0.463	0.000	6.385	0.000	7614.192	0.000	0.989
	160/220	0.086	0.039	0.452	0.000	6.212	0.000	2309.521	0.000	0.982
	330/430	0.300	0.000	0.320	0.000	6.385	0.000	2269.337	0.000	0.988
PMB	65/105-60	-0.009	0.837	0.501	0.000	6.442	0.000	4041.070	0.000	0.986
Soft bitumen	V1500	-0.131	0.411	0.336	0.000	38.213	0.000	95.217	0.000	0.901
	V3000	0.111	0.369	0.259	0.000	7.453	0.000	124.104	0.000	0.922
	V6000	0.024	0.719	0.429	0.000	6.858	0.000	1095.766	0.000	0.991
	V9000	0.093	0.437	0.407	0.000	6.511	0.000	285.341	0.000	0.965
	V12000	0.258	0.019	0.370	0.000	6.128	0.000	364.748	0.000	0.972

Table 16. MLR model parameters of Equation 58.

Master curve parameter		Coefficient																				ANOVA		Model summary
		b_1	*Sig.*	b_2	*Sig.*	b_3	*Sig.*	b_4	*Sig.*	b_5	*Sig.*	b_6	*Sig.*	b_7	*Sig.*	b_8	*Sig.*					*F*	*Sig.*	R^2
MLR without *Pen* and $T_{R\&B}$	δ	0.129	0.049	-4.738	0.350	0.001	0.564	-0.018	0.193	-5.533	0.026	-0.647	0.001	2.580	0.234	99.76	0.027					24.08	0.000	0.934
	α	-0.145	0.069	8.730	0.171	-0.001	0.615	0.028	0.119	7.176	0.021	0.646	0.003	-4.188	0.124	-118.0	0.033					17.12	0.000	0.909
	β	0.118	0.039	-14.79	0.004	0.000	0.856	-0.038	0.006	-7.602	0.002	-0.303	0.029	6.063	0.005	121.9	0.004					16.30	0.000	0.905
	γ	0.024	0.271	-2.481	0.175	0.000	0.831	-0.007	0.160	-1.303	0.117	-0.063	0.234	0.970	0.207	24.66	0.104					2.906	0.050	0.629
		b_1'	*Sig.*	b_2'	*Sig.*	b_3'	*Sig.*	b_4'	*Sig.*	b_5'	*Sig.*	b_6'	*Sig.*	b_7'	*Sig.*	b_8'	*Sig.*	b_9'	*Sig.*	b_{10}'	*Sig.*	*F*	*Sig.*	R^2
MLR with *Pen* and $T_{R\&B}$	δ	0.107	0.163	8.187	0.005	125.7	0.029	0.062	0.041	-	-	0.011	0.119	-	0.942	-0.575	0.027	-2.375	0.038	11.52	0.571	43.01	0.000	0.984
	α	-0.110	0.176	-8.242	0.006	-150.0	0.020	-0.074	0.029	-	-	-0.010	0.156	-	0.963	0.576	0.034	2.3655	0.048	-7.046	0.744	38.06	0.000	0.982
	β	0.036	0.430	1.248	0.302	72.37	0.041	0.005	0.724	-	-	0.001	0.828	-	0.683	-0.064	0.613	-0.294	0.608	-0.714	0.955	9.808	0.012	0.932
	γ	0.005	0.728	0.093	0.799	31.67	0.013	0.005	0.314	-	-	0.001	0.636	-	0.678	-0.002	0.954	0.024	0.893	-2.381	0.562	3.669	0.086	0.837

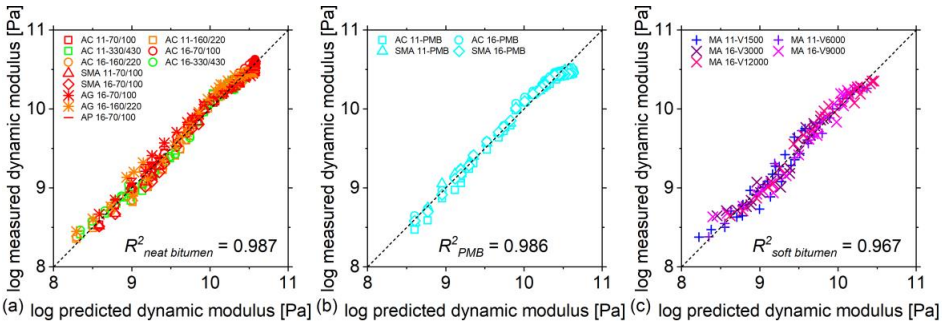

Figure 56. Results of multiple linear regression of Equation 57: (a) Neat bitumen, (b) PMB and (c) Soft bitumen.

Prediction model based on master curve parameter modelling

Although the method of Equation 57 can well predict the dynamic modulus of asphalt mixtures, it is necessary to assess the viscosity and complex shear modulus of bitumen, which are evaluated by means of laboratory devices requiring highly specialized equipment and well-trained operating skills. While the dynamic modulus varied with loading frequency and temperature, some other material parameters (i.e., P_{max}, B, $\eta_{60\,°C}$, ρ_{mix}, V_a, VMA, VFB, Pen and $T_{R\&B}$) did not vary. The sigmoidal function fitted the dynamic modulus well and its fitting parameters were also fixed for one material. Thus, the material parameters can be used to predict the fitting parameters of the sigmoidal function and thus estimate the dynamic modulus. In this case, the selected material parameters were P_{max}, B, $\eta_{60\,°C}$, ρ_{mix}, V_a, VMA, VFB, Pen and $T_{R\&B}$, while δ, α, β and γ were chosen as the fitting parameters of the sigmoidal function. The MLR is also used to find the correlation between material parameters and fitting parameters of the sigmoidal function as expressed in Equation 58 in two ways: one for the material parameters without Pen and $T_{R\&B}$ (Equation 58.1) and another one for all obtained material parameters (Equation 58.2).

For material parameters without Pen and $T_{R\&B}$

$$\delta,\alpha,\beta \text{ and } \gamma = b_1 P_{\max} + b_2 B + b_3 \eta_{60°C} + b_4 \rho_{\text{mix}} + b_5 V_a + b_6 VMA + b_7 VFB + b_8 \qquad (58.1)$$

For material parameters with Pen and $T_{R\&B}$

$$\delta,\alpha,\beta \text{ and } \gamma = b_1' P_{\max} + b_2' B + b_3' Pen_{25\,°C} + b_4' T_{\text{R\&B}} + b_5' \eta_{60°C} + b_6' \rho_{\text{mix}} + b_7' \cdot V_a + b_8' VMA + b_9' VFB + b_{10}' \qquad (58.2)$$

where $b_{1\text{-}10}{}'$ and $b_{1\text{-}8}$ are the regression parameters and all material parameters are in the international system of units. The MLR model parameters of Equation 58 are given in Table 16. The results indicated that there was a good fit between parameters δ, α, β and material parameters. The correlation between γ and material parameters was relatively poor. This reflected the γ was less affected by the material properties. Nevertheless, in the MLR model with material parameters containing *Pen* and $T_{R\&B}$, the R^2 of γ was also as high as 0.837, showing a certain dependence of γ on the material parameters. Furthermore, in this MLR model, the variables of $\eta_{60\,^\circ C}$ and V_a were excluded. This was due to the small correlation between $\eta_{60\,^\circ C}$ and fitting parameters of the master curve, which was also verified by small values of b_3 for the MLR model without *Pen* and $T_{R\&B}$. The variable of V_a was excluded due to a higher variance inflation factor, which was caused by the correlation between V_a, *VMA* and *VFB*.

The dynamic modulus of the asphalt mixtures predicted by the SLS model fitted with the material parameters and Witczak 1-37A, Witczak 1-40D, Hirsch, Al-Khateeb, global and simplified global models for comparison are shown in Figure 57. The R^2 of the MLR without and with *Pen* and $T_{R\&B}$ are 0.973 and 0.993, respectively, which can reasonably predict the dynamic modulus for more types of asphalt mixtures [86]. The soft bitumen displayed a lower R^2 than the other types, especially at low frequencies (high temperatures). This can be interpreted by taking into consideration the small contribution of soft bitumen to the elasticity of the asphalt mixture at high temperatures. In this condition, the stiffness was provided mainly by the aggregate skeleton, thus defining estimated actual stiffness, which deviated from the dynamic modulus predicted by the material parameters. Compared with the Witczak 1-37A (R^2 = 0.707), Witczak 1-40D (R^2 = 0.926), Hirsch (R^2 = 0.815), Al-Khateeb (R^2 = 0.814), global (R^2 = 0.906) and simplified global (R^2 = 0.891) models, the prediction results of the MLR model in this research showed a better fit. Furthermore, the empirical model of Witczak 1-40D was more suitable for Norwegian asphalt mixtures.

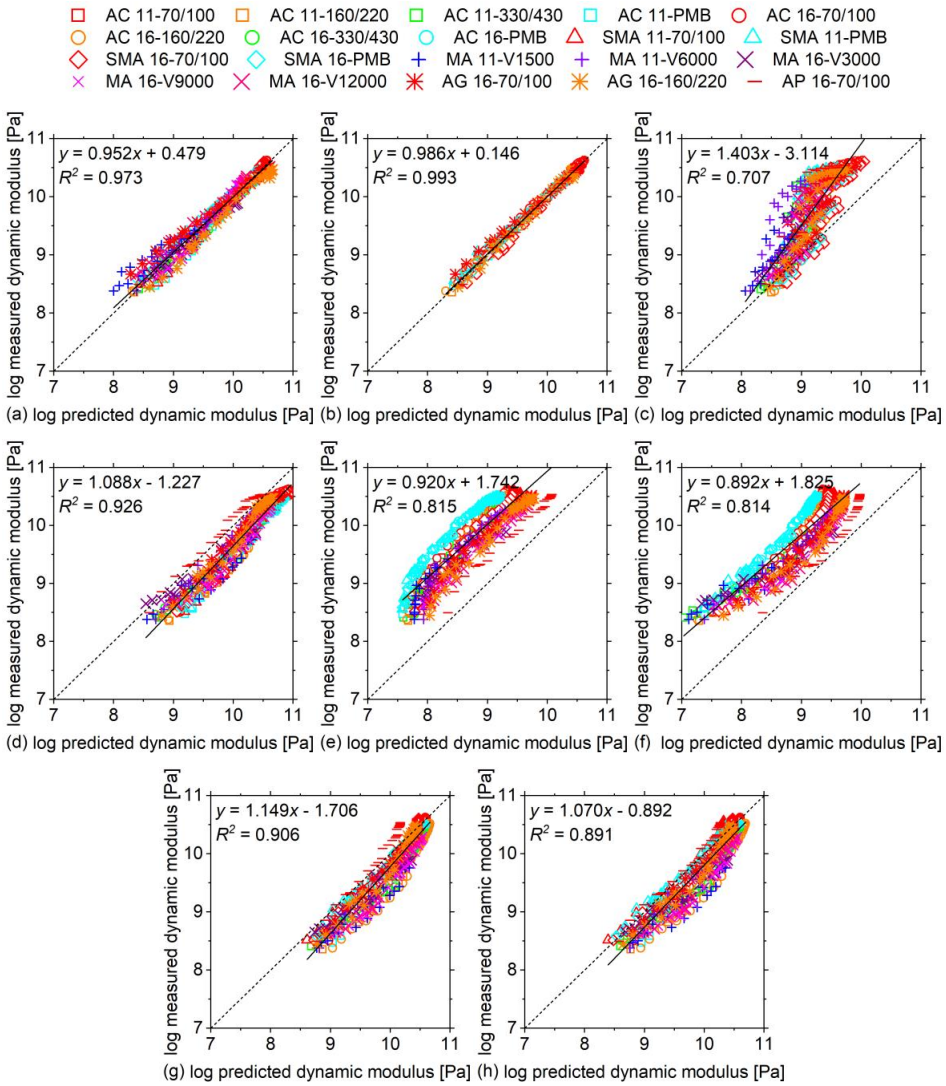

Figure 57. Comparison between the predicted and measured dynamic modulus: (a) MLR model without *Pen* and $T_{R\&B}$, (b) MLR model with *Pen* and $T_{R\&B}$, (c) Witczak 1-37A model, (d) Witczak 1-40D model, (e) Hirsch model, (f) Al-Khateeb model, (g) Global model and (h) Simplified global model.

For each type of asphalt mixture, Figure 58 shows that the MLR model offers a better fit for stiffer bitumen. This was related to the larger variation in the dynamic modulus test for the asphalt mixtures containing soft bitumen. In summary, the dynamic modulus of asphalt mixtures can be predicted based on the material parameters by this MLR model.

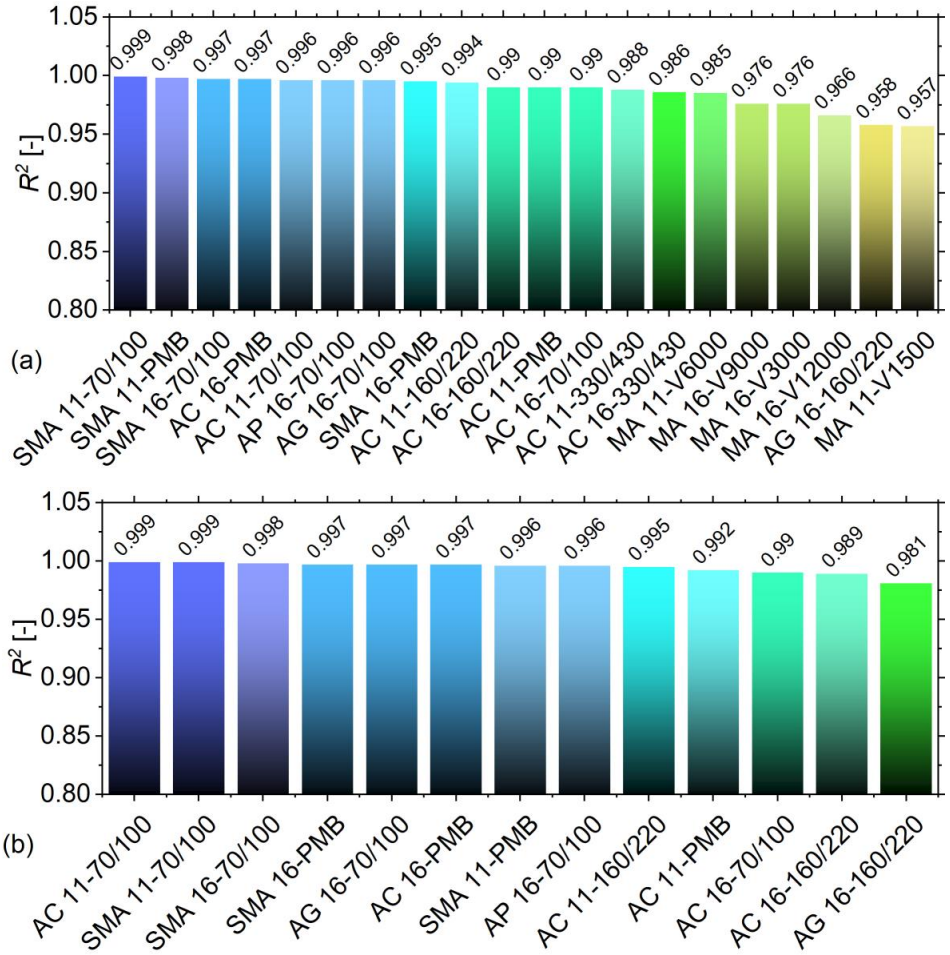

Figure 58. Goodness of fit R^2 for each type of asphalt mixture: (a) MLR model without *Pen* and $T_{R\&B}$ and (b) MLR model with *Pen* and $T_{R\&B}$.

4.5 FE modelling

The modelling of the dynamic modulus of asphalt mixture can be implemented into the FE model to predict the mechanical behaviour of asphalt pavement. The asphalt mixtures of AC 16-70/100, SMA 16-70/100, MA 16-V9000 and AG 16-160/220 were investigated in the FE modelling. The development of the FE model for mechanical behaviour prediction of asphalt pavements was detailly discussed in Paper V.

4.5.1 Validation of cyclic indirect tensile test (CITT)

The FE model was first validated through the test results of the CITT. The tensile stress at 0 °C and 1 Hz of the FE modelling and the CITT are compared as shown in Figure 59. The five analytical cycles were selected. The waveform of tensile stress simulated by the FE modelling was similar to the measured values of the CITT.

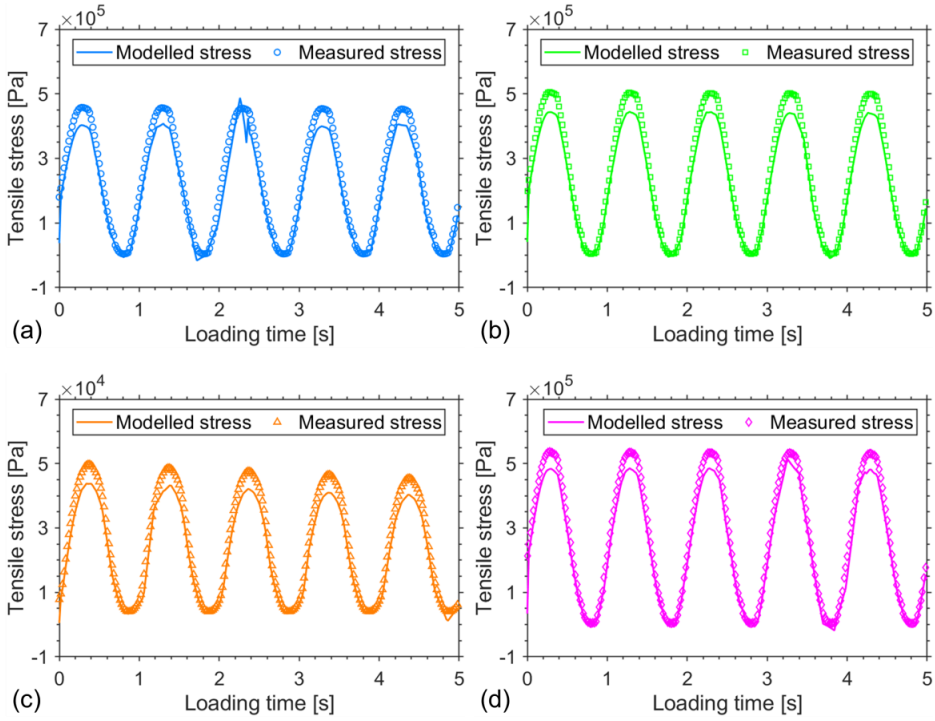

Figure 59. Comparison of tensile stress between FE modelling and the CITT at 0 °C and 1 Hz: (a) AC 16-700/100, (b) SMA 16-70/100, (c) MA 16-V9000 and (d) AG 16-160/220.

The R^2 and *MAPE* of tensile stress for the four types of asphalt mixtures at nine temperature and frequency combinations are presented in Figure 60a and 60b, respectively. The results indicated that most R^2 were higher than 0.99 and the minimum value was 0.95, which displayed a good fit of the FE modelling. The results also showed small relative errors for most comparisons. Very few large *MAPE* reflected big relative errors at certain test times (around the peak of the wave) under the corresponding condition.

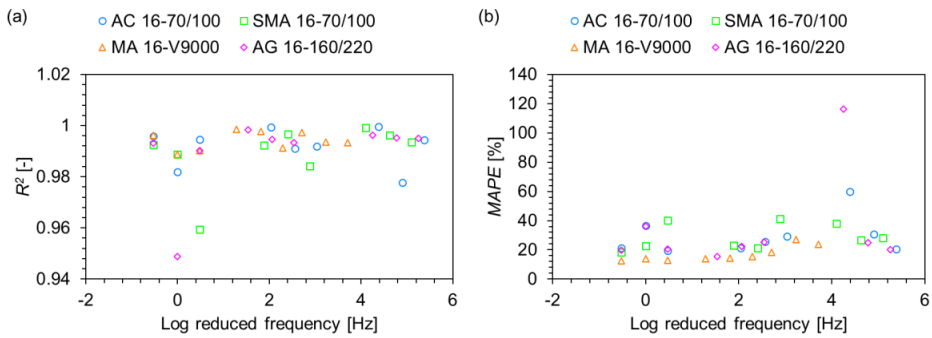

Figure 60. (a) R^2 and (b) *MAPE* of tensile stress between FE modelling and the CITT.

Since the applied load was controlled in the CITT, the tensile stress value of the FE modelling had high goodness of fit. However, the horizontal strain was a response to stress based on the viscoelastic behaviour of asphalt materials. The differences between the predicted and measured horizontal strain values were larger than the tensile stress results. The comparison of horizontal strain at 0 °C and 1 Hz between FE modelling and the CITT are displayed in Figure 61. The R^2 and *MAPE* of the FE modelling for the four types of asphalt mixtures at nine temperature and frequency combinations are shown in Figure 62a and 62b, respectively. The R^2 and *MAPE* of horizontal strain were obviously smaller and higher than those of tensile stress, respectively. Moreover, with the increase of the reduced frequency, the R^2 and *MAPE* of horizontal strain became larger and smaller, respectively. This result indicated that the FE modelling had a better fit at the reduced frequency higher than 100 Hz representing the low temperature (high loading frequency) conditions. This phenomenon can be explained by considering the viscoelastic behaviour of asphalt materials, which become more viscous when temperature increases. However, the calculation in the FE modelling was still based on linear viscoelasticity, which caused the differences.

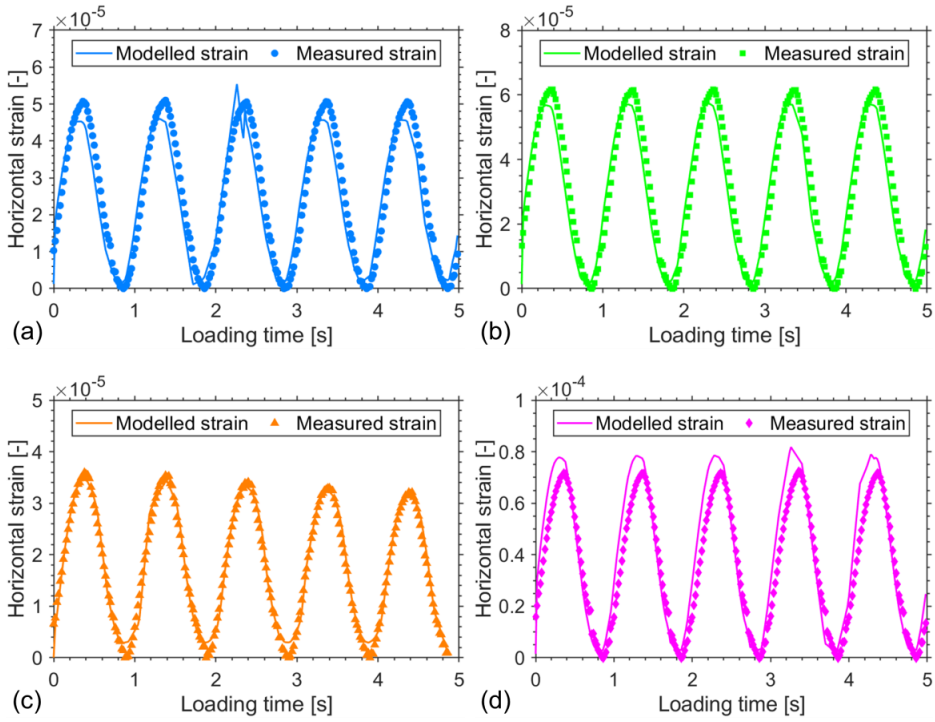

Figure 61. Comparison of horizontal strain between FE modelling and the CITT at 0 °C and 1 Hz: (a) AC 16-700/100, (b) SMA 16-70/100, (c) MA 16-V9000 and (d) AG 16-160/220.

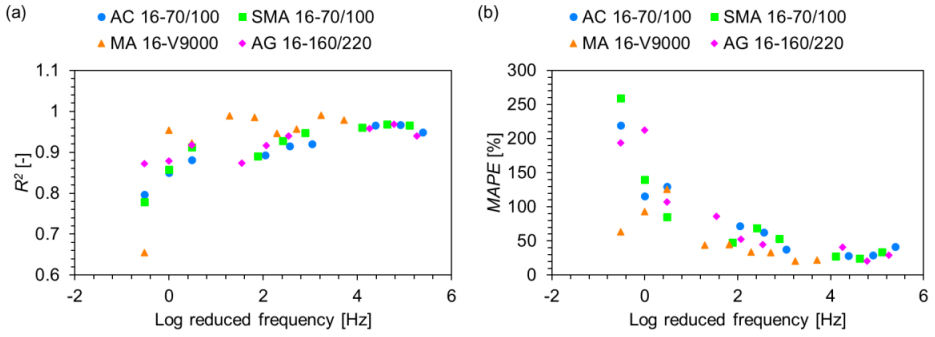

Figure 62. (a) R^2 and (b) *MAPE* of horizontal strain between FE modelling and the CITT.

Based on Equation 4, the dynamic modulus was calculated by the amplitudes of stress and strain in analytical cycles. The comparison between the predicted and measured values for the four types of asphalt mixtures at nine temperature and frequency combinations is shown in Figure 63. The R^2 was 0.98, thus showing that the FE modelling can properly simulate the viscoelasticity.

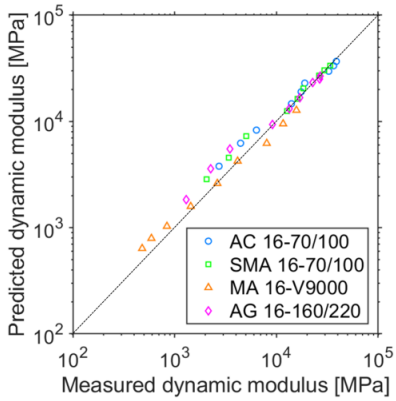

Figure 63. Comparison of dynamic modulus between FE modelling values and the testing results.

4.5.2 Stress and strain prediction for asphalt pavements

In practice, it is difficult to measure the stress and strain of the internal pavement structure, especially for very small strains [105]. Based on the above validation, the FE modelling performed with the COMSOL Multiphysics program had the potential to predict the stress and strain for asphalt pavements. Figure 64 shows the von Mises stress and displacement magnitude on *x* and *y* cross sections of pavements with an 80 mm-thick surface layer. The stress and displacement depended on the dynamic modulus of asphalt mixtures. Under the same load condition, the displacement of MA 16-V9000 was the most remarkable due to the lowest dynamic modulus of 2518 MPa, and the displacements of AC 16-70/100 and SMA 16-70/100 were similar because of the close values of dynamic moduli (17558 and 15616 MPa).

When a flexible road pavement is subjected to vehicle load, the bottom of the asphalt layer is prone to crack under tensile stress leading to thermal fatigue damage [106]. Therefore, the stress and strain at the bottom of both the asphalt surface and base layers were investigated in the following sections. Furthermore, their variation as a function of the surface layer thickness was also investigated.

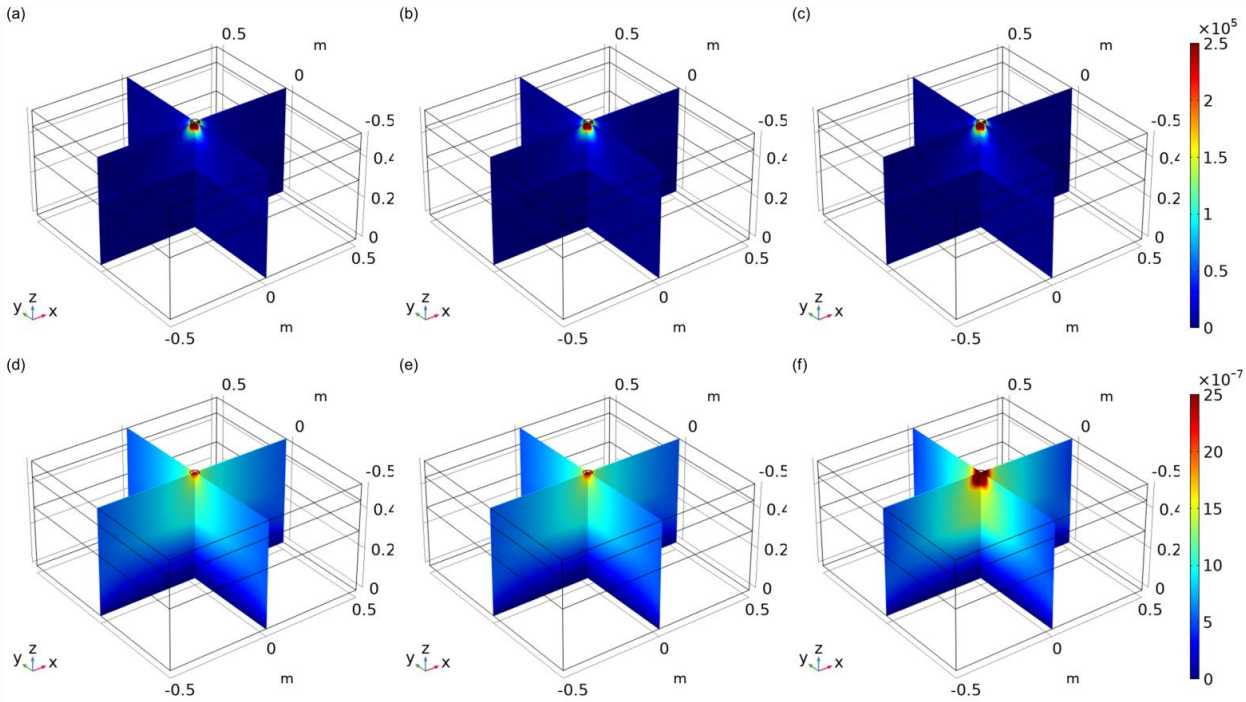

Figure 64. Von Mises stress (a) AC 16-70/100, (b) SMA 16-70/100 and (c) MA 16-V9000 and displacement magnitude (d) AC 16-70/100, (e) SMA 16-70/100 and (f) MA 16-V9000 of FE modelling on *x* and *y* cross-sections of pavements with an 80 mm-thick surface layer.

Stress prediction

The compressive and tensile stresses at the bottom of surface layers predicted by the FE modelling are shown in Figure 65 for different thicknesses. The result displayed that both compressive and tensile stresses decreased when augmenting surface thickness. The compressive stresses of AC 16-70/100 and SMA 16-70/100 were smaller than the ones of MA 16-V9000 due to the values of dynamic moduli. Generally, asphalt layers with larger dynamic moduli showed smaller stresses response at the bottom of the asphalt layers under the same vehicle load. As the variation trend of stress depended on the viscoelasticity of the asphalt mixture, soft bitumen with lower viscosity showed a wider range of stress changes for MA 16-V9000. Comparing Figure 65a and 65b, the compressive stress at this position is greater than the tensile stress. When the thickness of the surface layer reached 100 mm, the influence of increasing surface thickness on stress reduction gradually became smaller. For example, the reduction in compressive stress of AC 16-70/100 caused by thickness increasing from 100 mm to 140 mm was 15.8% of that led to by increasing the thickness from 60 mm to 100 mm.

Moreover, a strong correlation between the thickness of the surface layer and the stress was found, which fulfilled the power function well. The regression analysis for stress predictions of asphalt surface layers is given in Table 17, where *x* is the surface thickness and *y* is the stress. The R^2 was higher than 0.94 showing a good fit of the regression equations. Therefore, this outcome confirmed the common practice adopted in pavement structure design to reduce the stress at the bottom of the surface layer by increasing its thickness. However, the most appropriate value of the layer thickness should also be defined based on economic and energy costs as well other environmental considerations.

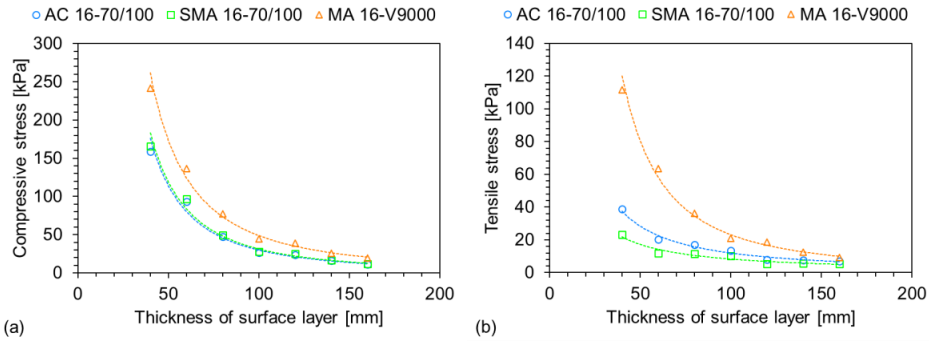

Figure 65. (a) Compressive and (b) Tensile stress predictions at the bottom point of asphalt surface layers with different thicknesses.

Table 17. Regression analysis for stress predictions of asphalt surface layers with different thicknesses.

Stress type	Surface layer	Regression equation (power function)	R^2
Compressive stress	AC 16-70/100	$y = 225348x^{-1.94}$	0.9806
	SMA 16-70/100	$y = 226557x^{-1.93}$	0.9819
	MA 16-V9000	$y = 226348x^{-1.83}$	0.9901
Tensile stress	AC 16-70/100	$y = 3720x^{-1.25}$	0.9828
	SMA 16-70/100	$y = 1081x^{-1.06}$	0.9400
	MA 16-V9000	$y = 91932x^{-1.80}$	0.9905

Figure 66 presents the compressive and tensile stress predictions of the FE modelling at the bottom point of the asphalt base course for different thickness values of surface layers. The stress of the base course showed a trend which was similar to the one already found for the surface layer. The stress of the base course was affected by the dynamic modulus of the asphalt surface layer. This phenomenon was explained by the different capacities of transferring the vehicle load to the base course for different asphalt mixtures. AG 16-160/220

was subjected to greater stress under the surface layer of MA 16-V9000 with a smaller dynamic modulus and viscosity. As the asphalt mixtures of the base course were the same, the stress variation trends with the surface thickness under different asphalt surface layers were similar. However, the compressive stress of the base course is smaller than the tensile stress from the comparison between Figure 66a and 66b, which is different from the results of the surface layer. This result indicated that the compressive stress decreased faster during transmission down due to the support at the bottom of the pavement structure, while the tensile stress was not supported on both sides resulting in a larger value. This outcome further reflected that the tensile stress at the bottom of the asphalt layer was more prone to cracking. Moreover, the changing trend of stress for the base course did not have an obvious inflexion point with the decrease of the surface thickness compared to the asphalt surface layer. The trend is better fitted by a logarithmic function than by a power function shown in Table 18. This result indicated that the stress response of the base course was different from the surface layer due to the reduction of compressive stress.

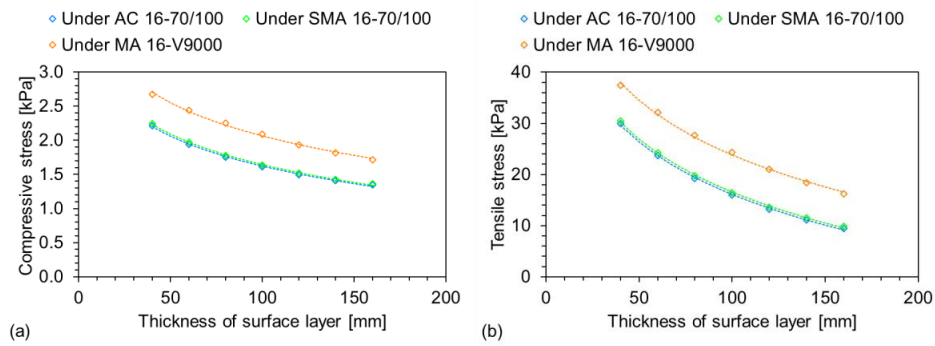

Figure 66. (a) Compressive and (b) Tensile stress predictions at the bottom point of asphalt base course under different thickness surface layers.

Table 18. Regression analysis for stress predictions of asphalt base course under different thickness surface layers.

Stress type	Surface layer	Regression equation (logarithmic function)	R^2
Compressive stress	AC 16-70/100	$y = -0.635\ln(x) + 4.546$	0.9982
	SMA 16-70/100	$y = -0.646\ln(x) + 4.619$	0.9985
	MA 16-V9000	$y = -0.704\ln(x) + 5.307$	0.9948
Tensile stress	AC 16-70/100	$y = -14.86\ln(x) + 84.528$	0.9991
	SMA 16-70/100	$y = -14.96\ln(x) + 85.493$	0.9993
	MA 16-V9000	$y = -15.45\ln(x) + 94.999$	0.9969

Strain prediction

Figure 67 shows the compressive and tensile strain predictions of the FE modelling at the bottom point of asphalt surface layers with different thicknesses. Similarly, to the variation trend of the stresses, the strains also became smaller with the increase in surface thickness. It was worth noting that the tensile strains at the bottom of the three asphalt surface layers were very close in numerical values. The tensile strain might be influenced by the relatively stiffer asphalt layer at the interface between the courses. The tensile strains of AC 16-70/100 and SMA 16-70/100 surface layers depended on their dynamic modulus, while the stiffer AG 16-70/100 base course reduced the tensile strain of the MA 16-V9000 surface layer. Similar to the stress of the asphalt surface layer, when the thickness reached 100 mm, the influence of increasing the thickness on reducing the strain became smaller. The strains of asphalt surface layers with the change of thickness can be also fitted by the power function shown in Table 19, where x is the surface thickness and y is the strain.

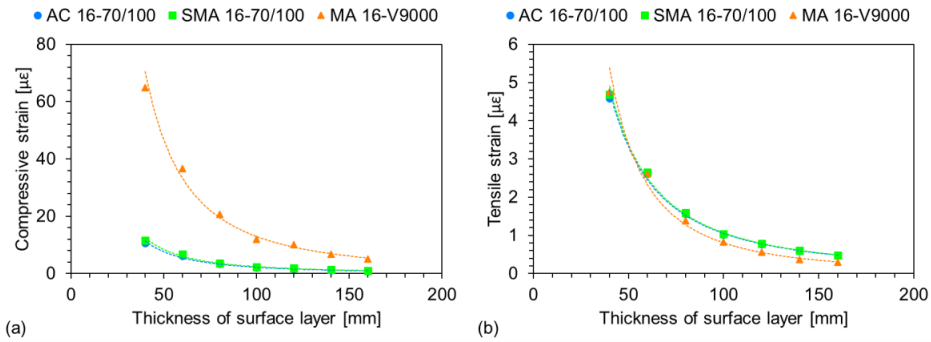

Figure 67. (a) Compressive and (b) Tensile strain predictions at the bottom point of asphalt surface layers with different thicknesses.

Table 19. Regression analysis for strain predictions of asphalt surface layers with different thicknesses.

Strain type	Surface layer	Regression equation (power function)	R^2
Compressive strain	AC 16-70/100	$y = 8613x^{-1.80}$	0.9896
	SMA 16-70/100	$y = 9777x^{-1.81}$	0.9895
	MA 16-V9000	$y = 64829x^{-1.85}$	0.9899
Tensile strain	AC 16-70/100	$y = 2194x^{-1.66}$	0.9961
	SMA 16-70/100	$y = 2281x^{-1.67}$	0.9960
	MA 16-V9000	$y = 11317x^{-2.07}$	0.9848

The strain predictions of the FE modelling for the base course for different thickness surface layers are presented in Figure 68. The trend of the strains of the base course was consistent with the trend of the surface layer. The compressive strain was reduced to about the same as the tensile strain. The base courses under different surface layers had different tensile strain values. This was because the subbase layer was soft, resulting in the tensile strain of the interface between the base and the subbase layers depending on the stiffer asphalt base course. In addition, the correlation between the strain and the thickness of the surface layer is also fitted well by the logarithmic function given in Table 20.

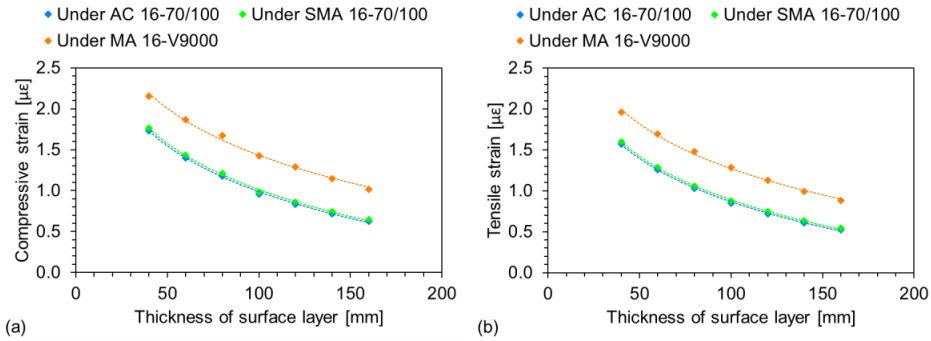

Figure 68. (a) Compressive and (b) Tensile strain predictions at the bottom point of asphalt base course under different thickness surface layers.

Table 20. Regression analysis for strain predictions of asphalt base course under different thickness surface layers.

Strain type	Surface layer	Regression equation (logarithmic function)	R^2
Compressive strain	AC 16-70/100	*y = -0.807ln(x) + 4.703*	0.9986
	SMA 16-70/100	*y = -0.812ln(x) + 4.754*	0.9987
	MA 16-V9000	*y = -0.827ln(x) + 5.239*	0.9942
Tensile strain	AC 16-70/100	*y = -0.762ln(x) + 4.377*	0.9992
	SMA 16-70/100	*y = -0.768ln(x) + 4.425*	0.9994
	MA 16-V9000	*y = -0.789ln(x) + 4.903*	0.9965

5 FINAL CONSIDERATIONS

5.1 Conclusions

The objective of this research was to model the viscoelastic properties of asphalt pavements for developing the Norwegian Mechanistic-Empirical (ME) pavement design system.

Based on the standard testing setting, comparing with the gyratory compaction, the roller compression method resulted in lower Air void content (V_a), lower Void in Mineral Aggregate (*VMA*) and higher Voids Filled with Binder (*VFB*), as well as leading to a little higher dynamic modulus at both low and high temperature situations. *Since the roller compression method was closer to pavement paving and five specimens with similar volumetric properties can be obtained from one asphalt slab, the roller compression was recommended to develop the Norwegian ME pavement design system and for modelling the dynamic modulus of asphalt mixtures*.

Two laboratory tests of Cyclic Indirect Tensile Test (CITT) and Cyclic Compression Test (CCT) for dynamic modulus determination were investigated in this study. The dynamic moduli measured using both tests at the intermediate frequency (temperature) range were the same. The values obtained from CITT were higher than the ones assessed by CCT at extreme frequencies (temperatures). The stress level pertaining to the CITT was bigger than the one achieved during CCT. The CITT strain values were various at all four test temperatures. Although the variation of strain obtained from the CCT was based on the frequency largens as the temperature increased, the stress-strain states were stable at low and medium temperatures, showing a better stain control than the CITT. In general, both tests can be used to properly characterise the dynamic modulus of asphalt materials. The CITT can be efficiently used for the characterisation of road surfaces built in cold regions. Moreover, the CITT plays an important role when it comes to the mechanical characterisation of existing asphalt pavements since the dimensions of the field samples normally meet the size requirements. The CCT controls strain better for low and medium temperature ranges compared with CITT, resulting in more accurate results. A confining pressure can be applied for CCT, which better simulates real field conditions. *For Norwegian conditions as a basis for practical design, the CITT seems to be the best choice due to easier/more realistic sample preparation and to compare with field cored samples*.

FINAL CONSIDERATIONS

Three master curve models of Standard Logistic Sigmoidal (SLS), Generalised Logistic Sigmoidal (GLS) and Christensen-Anderson-Marasteanu (CAM) models and five shifting techniques of log-linear, quadratic polynomial, Arrhenius, Williams-Landel-Ferry (WLF) and Kaelble equations were estimated in this research. *The SLS model showed the best fitting quality and was considered to model the dynamic modulus of asphalt mixtures. Due to better goodness of fit and more convenience for temperature and frequency transform, the WLF equation was considered for the dynamic modulus modelling.*

The dynamic modulus database of 20 asphalt mixture types commonly used in Norway was established. All master curves had good fits with the $R^2 \geq 0.973$. The corresponding master curve parameters were utilised in the ERAPave program for asphalt pavement structure design.

The influence of different material factors (i.e., maximum aggregate size, binder content, rheological properties of bitumen, bulk density and void characteristics of asphalt mixtures) on the dynamic modulus was investigated. According to the grey relational analysis results, *the dynamic modulus of asphalt mixtures is greatly affected by the viscosity and complex shear modulus of bitumen*, followed by the void characteristics of *VFB* and V_a, and then by the bitumen penetration and softening point. *The dynamic modulus can be well predicted by the bitumen viscosity and complex shear modulus using Multiple Linear Regression (MLR)*, showing the goodness of fit values $R^2 \geq 0.901$. Moreover, *the MLR was also used to predict the SLS model parameters through the material factors aiming to obtain the dynamic modulus.* This method had a better fit than the existing models.

After the viscoelastic properties of asphalt mixtures were modelled, the dynamic modulus was implemented into the Finite Element (FE) model. The FE model incorporated the dynamic modulus master curve and the viscoelastic constitutive model was established. The model was validated through the CITT results with a high goodness of fit at low temperature conditions. Furthermore, the mechanical properties were simulated by this FE model, which gave reasonable results of stress and strain at the bottom of the asphalt layers for a generic road pavement structure comprising surface, base and subbase layers. *Therefore, based on the modelling of viscoelastic properties of asphalt mixtures the FE modelling was a very useful tool to predict the performance of asphalt pavements*.

5.2 Limitation of this research and recommendations for future work

The findings from this thesis imply the test method selection for the Norwegian situation, the Norwegian material database establishment based on 20 asphalt mixture types, the development of the model for predicting the dynamic modulus according to the material factors and the FE model for the asphalt pavement mechanical properties prediction. However, some limitations of this research and recommendations for future work are considered as follows.

- There is a certain difference between the CITT and the CCT under extreme conditions. The connection of the CITT and CCT under such conditions should be established to develop the wide application of the CITT in the ME pavement design.
- There are many new simulation methods now available. Besides the regression method, other machine learning methods can be developed to predict the dynamic modulus of different asphalt materials under various temperature and frequency conditions based on a large amount of experimental data.
- In the long term, the Norwegian material database needs to be replenished due to a large number of other types of asphalt mixtures in Norway and the use of new materials.
- The MLR results for master curve parameters show that some material factors have a significant influence on the prediction model for some asphalt mixtures, while they have little effect on other asphalt mixtures. Therefore, the types of material factors can be further optimised for a specific asphalt mixture to improve the accuracy of the prediction model and reduce the workload in future studies.
- The FE model proposed in this research only considered linear viscoelastic behaviour for asphalt materials and limited pavement structure and material type. In order to simulate their stress-strain response more accurately, more advanced FE models with more accurate geometric structures implementing material nonlinear viscoelasticity and plasticity can be further developed. Furthermore, based on a large scale of field test database, the FE model can be incorporated into the flexible pavement design system such as the VegDim project in Norway. Engineers can conveniently perform the computation remotely once the interface is defined by the input such as temperatures, loading frequencies, material parameters etc. and the output like stress-strain responses, pavement structure and distress condition etc.

6 REFERENCES

[1] R.G. Saba, Analytical Design of Pavement Structures, NPRA reports, Nowegian Public Roads Administration, Oslo, Norway, 2019.

[2] I. ARA, ERES Consultants Division, Guide for Mechanistic-Empirical Design of New and Rehabilitated Pavement Structures, Final report, NCHRP Project 1-37A, Transportation Research Board, Washington D.C., 2004.

[3] T. Officials, Mechanistic-empirical pavement design guide: A manual of practice, AASHTO: Washington, DC, USA (2008).

[4] D. Lesueur, J.F. Gerard, P. Claudy, J.M. Letoffe, J.P. Planche, D. Martin, A structure-related model to describe asphalt linear viscoelasticity, Journal of Rheology 40(5) (1996) 813-836.

[5] D.D. Li, M.L. Greenfield, Viscosity, relaxation time, and dynamics within a model asphalt of larger molecules, The Journal of chemical physics 140(3) (2014) 034507.

[6] X. Zhang, H. Chen, D.M. Barbieri, B. Lou, I. Hoff, The classification and reutilisation of recycled asphalt pavement binder: Norwegian case study, Case Studies in Construction Materials 17 (2022) e01491.

[7] B. Rahimzadeh, Linear and non-linear viscoelastic behaviour of binders and asphalts, University of Nottingham Nottingham, UK, 2002.

[8] D.W. Christensen, R.F. Bonaquist, Evaluation of indirect tensile test (IDT) procedures for low-temperature performance of hot mix asphalt, Transportation Research Board2004.

[9] M. Zaumanis, M.C. Cavalli, L.D. Poulikakos, How not to design 100% recycled asphalt mixture using performance-based tests, Road Materials and Pavement Design 21(6) (2020) 1634-1646.

[10] K. Mollenhauer, P. Plachkova-Dzhurova, Categories for stiffness and fatigue based on cyclic indirect tensile tests and their applicability in construction contracts, 6th Eurasphlat & Eurobitumen Congress, 2016.

[11] X. Zhang, H. Chen, D.M. Barbieri, I. Hoff, Laboratory evaluation of mechanical properties of asphalt mixtures exposed to sodium chloride, Transportation Research Record 2676(8) (2022) 90-98.

[12] Y.R. Kim, Y. Seo, M. King, M. Momen, Dynamic modulus testing of asphalt concrete in indirect tension mode, Transportation Research Record 1891(1) (2004) 163-173.

[13] X. Qin, L. Ma, H. Wang, Comparison analysis of dynamic modulus of asphalt mixture: indirect tension and uniaxial compression test, Transportmetrica A: Transport Science 15(1) (2019) 165-178.

[14] H. Cheng, Y. Wang, L. Liu, L. Sun, Y. Zhang, R. Yang, Estimating tensile and compressive moduli of asphalt mixture from indirect tensile and four-point bending tests, Journal of Materials in Civil Engineering 33(1) (2021) 04020402.

[15] G. Chehab, Y. Kim, R. Schapery, M. Witczak, R. Bonaquist, Time-temperature superposition principle for asphalt concrete with growing damage in tension state, Journal of the Association of Asphalt Paving Technologists 71 (2002).

[16] C.W. Schwartz, N. Gibson, R.A. Schapery, Time-temperature superposition for asphalt concrete at large compressive strains, Transportation Research Record 1789(1) (2002) 101-112.

[17] T.K. Pellinen, M.W. Witczak, R.F. Bonaquist, Asphalt mix master curve construction using sigmoidal fitting function with non-linear least squares optimization, Recent advances in materials characterization and modeling of pavement systems2004, pp. 83-101.

[18] T.K. Pellinen, M.W. Witczak, Stress dependent master curve construction for dynamic (complex) modulus (with discussion), Journal of the Association of Asphalt Paving Technologists 71 (2002).

[19] G. Rowe, G. Baumgardner, M. Sharrock, Functional forms for master curve analysis of bituminous materials, Advanced testing and characterization of bituminous materials, two volume set, CRC Press2009, pp. 97-108.

[20] F. Zhang, L. Wang, C. Li, Y. Xing, Predict the phase angle master curve and study the viscoelastic properties of warm mix crumb rubber-modified asphalt mixture, Materials 13(21) (2020) 5051.

[21] D.W. Christensen, D.A. Anderson, Interpretation of dynamic mechanical test data for paving grade asphalt cements (with discussion), Journal of the Association of asphalt paving technologists 61 (1992).

[22] G. Garcia, M. Thompson, HMA dynamic modulus predictive models (a review), FHWA-ICT-07-005 (2007).

[23] S. Angelone, M. Borghi, M.C. Casaux, F. Martinez, Evaluation of Different Procedures and Models for the Construction of Dynamic Modulus Master Curves of Asphalt Mixtures, Proceedings of the international conferences on the bearing capacity of roads, railways and airfields, 2013, pp. 647-657.

[24] P. Tavassoti-Kheiry, I. Boz, X. Chen, M. Solaimanian, Application of ultrasonic pulse velocity testing of asphalt concrete mixtures to improve the prediction accuracy of dynamic modulus master curve, Proceedings, Airfield and Highway Pavements (2017).

[25] M. Kim, L.N. Mohammad, M.A. Elseifi, Effects of various extrapolation techniques for abbreviated dynamic modulus test data on the MEPDG rutting predictions, Journal of Marine Science and Technology 23(3) (2015) 12.

[26] M.L. Williams, R.F. Landel, J.D. Ferry, The temperature dependence of relaxation mechanisms in amorphous polymers and other glass-forming liquids, Journal of the American Chemical society 77(14) (1955) 3701-3707.

[27] S.A. Forough, F.M. Nejad, A. Khodaii, A comparative study of temperature shifting techniques for construction of relaxation modulus master curve of asphalt mixes, Construction and Building Materials 53 (2014) 74-82.

[28] M.A. Bohn, The connection between the parameters of wlf equation and of arrhenius equation, Propellants, Explosives, Pyrotechnics 44(6) (2019) 696-705.

[29] M. Witczak, O. Fonseca, Revised predictive model for dynamic (complex) modulus of asphalt mixtures, Transportation Research Record 1540(1) (1996) 15-23.

[30] Z. You, S. Adhikari, S.W. Goh, Q. Dai, Dynamic Moduli for ME Design of Asphalt Pavements, Plan, Build, and Manage Transportation Infrastructure in China2008, pp. 841-850.

[31] D. Christensen Jr, T. Pellinen, R. Bonaquist, Hirsch model for estimating the modulus of asphalt concrete, Journal of the Association of Asphalt Paving Technologists 72 (2003).

[32] G. Al-Khateeb, A. Shenoy, N. Gibson, T. Harman, A new simplistic model for dynamic modulus predictions of asphalt paving mixtures, Journal of the Association of Asphalt Paving Technologists 75 (2006).

[33] M.S. Sakhaeifar, Y.R. Kim, P. Kabir, New predictive models for the dynamic modulus of hot mix asphalt, Construction and Building Materials 76 (2015) 221-231.

[34] N. Solatifar, A. Kavussi, M. Abbasghorbani, Dynamic modulus predictive models for in-service asphalt layers in hot climate areas, Journal of Materials in Civil Engineering 33(2) (2021) 04020438.

[35] I.D. Uwanuakwa, A. Busari, S.I.A. Ali, M.R. Mohd Hasan, A. Sani, S. Abba, Comparing Machine Learning Models with Witczak NCHRP 1-40D Model for Hot-Mix Asphalt Dynamic Modulus Prediction, Arabian Journal for Science and Engineering 47(10) (2022) 13579-13591.

[36] H. Zhu, L. Sun, J. Yang, Z. Chen, W. Gu, Developing master curves and predicting dynamic modulus of polymer-modified asphalt mixtures, Journal of Materials in Civil Engineering 23(2) (2011) 131-137.

[37] S. Yousefdoost, B. Vuong, I. Rickards, P. Armstrong, B. Sullivan, Evaluation of dynamic modulus predictive models for typical Australian asphalt mixes, Proceedings of the 15th AAPA International Flexible Pavements Conference, 2013, pp. 22-25.

[38] C. Zhang, S. Shen, X. Jia, Modification of the Hirsch dynamic modulus prediction model for asphalt mixtures, Journal of Materials in Civil Engineering 29(12) (2017) 04017241.

[39] Y. Ali, M. Irfan, S. Ahmed, S. Khanzada, T. Mahmood, Investigation of factors affecting dynamic modulus and phase angle of various asphalt concrete mixtures, Materials and Structures 49 (2016) 857-868.

[40] Y. Zhang, B. Birgisson, R.L. Lytton, Weak form equation–based finite-element modeling of viscoelastic asphalt mixtures, Journal of Materials in Civil Engineering 28(2) (2016) 04015115.

[41] H. Wang, P. Hao, Numerical simulation of indirect tensile test based on the microstructure of asphalt mixture, Journal of Materials in Civil Engineering 23(1) (2011) 21-29.

[42] M. Koohmishi, Comparison of pavement layers responses with considering different models for asphalt concrete viscoelastic properties, Slovak Journal of Civil Engineering 21(2) (2013) 15-20.

[43] H. Taherkhani, M. Jalali, Investigating the performance of geosynthetic-reinforced asphaltic pavement under various axle loads using finite-element method, Road Materials and Pavement Design 18(5) (2017) 1200-1217.

[44] Z. Selsal, A.S. Karakas, B. Sayin, Effect of pavement thickness on stress distribution in asphalt pavements under traffic loads, Case Studies in Construction Materials 16 (2022) e01107.

[45] L. Boltzmann, Zur theorie der elastischen nachwirkung, Annalen der Physik 241(11) (1878) 430-432.

[46] C. Gallegos, F. Martínez-Boza, Linear viscoelasticity, Rheology: encyclopaedia of life support systems (EOLSS), UNESCO. Eolss, Oxford (2010) 120-143.

[47] S. Tiouajni, H. Di Benedetto, C. Sauzéat, S. Pouget, Approximation of linear viscoelastic model in the 3 dimensional case with mechanical analogues of finite size: Application to bituminous materials, Road Materials and Pavement Design 12(4) (2011) 897-930.

[48] Y. Sun, B. Huang, J. Chen, A unified procedure for rapidly determining asphalt concrete discrete relaxation and retardation spectra, Construction and Building Materials 93 (2015) 35-48.

[49] Y. Zhao, Y. Ni, W. Zeng, A consistent approach for characterising asphalt concrete based on generalised Maxwell or Kelvin model, Road Materials and Pavement Design 15(3) (2014) 674-690.

[50] J.D. Ferry, Viscoelastic properties of polymers, John Wiley & Sons1980.

[51] N.W. Tschoegl, The phenomenological theory of linear viscoelastic behavior: an introduction, Springer Science & Business Media2012.

[52] Q. Xu, M. Solaimanian, Modelling linear viscoelastic properties of asphalt concrete by the Huet–Sayegh model, International Journal of Pavement Engineering 10(6) (2009) 401-422.

[53] E. Behzadfar, S.G. Hatzikiriakos, Viscoelastic properties and constitutive modelling of bitumen, Fuel 108 (2013) 391-399.

[54] A.C. Pronk, The Huet-Sayegh model: A simple and excellent rheological model for master curves of asphaltic mixes, Asphalt concrete: simulation, modeling, and experimental characterization2006, pp. 73-82.

[55] C. Huet, Etude par une méthode d'impédance du comportement viscoélastique des matériaux hydrocarbonés, 1965.

[56] F. Olard, H. Di Benedetto, General "2S2P1D" model and relation between the linear viscoelastic behaviours of bituminous binders and mixes, Road materials and pavement design 4(2) (2003) 185-224.

[57] H. Di Benedetto, F. Olard, C. Sauzéat, B. Delaporte, Linear viscoelastic behaviour of bituminous materials: From binders to mixes, Road Materials and Pavement Design 5(sup1) (2004) 163-202.

[58] H.D. Benedetto, B. Delaporte, C. Sauzéat, Three-dimensional linear behavior of bituminous materials: experiments and modeling, International Journal of Geomechanics 7(2) (2007) 149-157.

[59] H. Di Benedetto, N. Mondher, C. Sauzéat, F. Olard, Three-dimensional thermo-viscoplastic behaviour of bituminous materials: The DBN model, Road Materials and Pavement Design 8(2) (2007) 285-315.

[60] EN 12591 Bitumen and bituminous binders Specifications for paving grade bitumens, European Committee for Standardization, Brussels, Belgium, 2011.

[61] EN 1426 Bitumen and bituminous binders Determination of needle penetration, European Committee for Standardization, Brussels, Belgium, 2015.

[62] EN 1427 Bitumen and bituminous binders Determination of the softening point Ring and Ball method, European Committee for Standardization, Brussels, Belgium, 2015.

[63] EN 13702 Bitumen and bituminous binders Determination of dynamic viscosity of bitumen and bituminous binders by the cone and plate method, European Committee for Standardization, Brussels, Belgium, 2018.

[64] D. Barbieri, I. Hoff, H. Mork, Laboratory investigation on unbound materials used in a highway with premature damage, Bearing capacity of Roads, Railways and Airfields, CRC Press2017, pp. 101-108.

[65] D.M. Barbieri, I. Hoff, M.B.E. Mørk, Mechanical assessment of crushed rocks derived from tunnelling operations, Tunneling in Soft Ground, Ground Conditioning and Modification Techniques: Proceedings of the 5th GeoChina International Conference 2018–Civil Infrastructures Confronting Severe Weathers and Climate Changes: From Failure to Sustainability, held on July 23 to 25, 2018 in HangZhou, China, Springer, 2019, pp. 225-241.

[66] Road construction, Handbook N200, Norwegian Public Roads Administration, Oslo, Norway, 2018.

[67] EN 1097-9 Tests for mechanical and physical properties of aggregates Part 9: Determination of the resistance to wear by abrasion from studded tyres Nordic test, European Committee for Standardization, Brussels, Belgium, 2014.

[68] EN 1097-1 Tests for mechanical and physical properties of aggregates Part 1: Determination of the resistance to wear (micro-Deval), European Committee for Standardization, Brussels, Belgium, 2011.

[69] EN 1097-2 Tests for mechanical and physical properties of aggregates Part 2: Methods for the determination of resistance to fragmentation, European Committee for Standardization, Brussels, Belgium, 2020.

[70] R.E. Asbjørn Arnevik, Nils Sigurd Uthus, Joralf Aurstad, Jostein Aksnes, Torbjørn Jørgensen, Guidelines asphalt 2019, NPRA reports, Norwegian Public Roads Administration, Oslo, Norway, 2018.

[71] S. Anastasio, I. Hoff, C.C. Thodesen, H.U. Bahia, Laboratory testing methods for evaluating the moisture damage on the aggregate-asphalt system, 8th RILEM International Symposium on Testing and Characterization of Sustainable and Innovative Bituminous Materials, Springer, 2016, pp. 533-543.

[72] EN 12697-35 Bituminous mixtures Test methods Part 35: Laboratory mixing, European Committee for Standardization, Brussels, Belgium, 2016.

[73] EN 12697-33 Bituminous mixtures Test method Part 33: Specimen prepared by roller compactor, European Committee for Standardization, Brussels, Belgium, 2019.

[74] EN 12697-31 Bituminous mixtures Test methods Part 31: Specimen preparation by gyratory compactor, European Committee for Standardization, Brussels, Belgium, 2019.

[75] M.M. Alamnie, E. Taddesse, I. Hoff, Thermo-piezo-rheological characterization of asphalt concrete, Construction and Building Materials 329 (2022) 127106.

[76] H. Luo, X. Huang, T. Rongyan, H. Ding, J. Huang, D. Wang, Y. Liu, Z. Hong, Advanced method for measuring asphalt viscosity: Rotational plate viscosity method and its application to asphalt construction temperature prediction, Construction and Building Materials 301 (2021) 124129.

[77] EN 14770 Bitumen and bituminous binders Determination of complex shear modulus and phase angle Dynamic Shear Rheometer (DSR), European Committee for Standardization, Brussels, Belgium, 2012.

[78] EN 12697-26 Bituminous mixtures Test methods Part 26: Stiffness, European Committee for Standardization, Brussels, Belgium, 2018.

[79] G. Cerni, E. Bocci, F. Cardone, A. Corradini, Correlation between asphalt mixture stiffness determined through static and dynamic indirect tensile tests, Arabian Journal for Science and Engineering 42(3) (2017) 1295-1303.

[80] F. Olard, F. Noël, F. Loup, Modulus testing in indirect tension mode, Road materials and pavement design 7(4) (2006) 543-554.

[81] P. Ghasemi, S. Lin, D.K. Rollins, R.C. Williams, Predicting dynamic modulus of asphalt mixture using data obtained from indirect tension mode of testing, arXiv preprint arXiv:1905.06810 (2019).

[82] R. Nemati, E.V. Dave, Nominal property based predictive models for asphalt mixture complex modulus (dynamic modulus and phase angle), Construction and Building Materials 158 (2018) 308-319.

[83] A.R. Archilla, J.P. Corrales-Azofeifa, J.P. Aguiar-Moya, Comprehensive Model for the Prediction of the Phase Angle Master Curve of Asphalt Concrete Mixes, Proceedings of the RILEM International Symposium on Bituminous Materials: ISBM Lyon 2020 1, Springer, 2022, pp. 473-479.

[84] S. Hutcheson, G. McKenna, The measurement of mechanical properties of glycerol, m-toluidine, and sucrose benzoate under consideration of corrected rheometer compliance: An in-depth study and review, The Journal of chemical physics 129(7) (2008) 074502.

[85] Y. Kuo, T. Yang, G.-W. Huang, The use of grey relational analysis in solving multiple attribute decision-making problems, Computers & industrial engineering 55(1) (2008) 80-93.

[86] M. Zhang, H. Zhao, L. Fan, J. Yi, Dynamic modulus prediction model and analysis of factors influencing asphalt mixtures using gray relational analysis methods, Journal of Materials Research and Technology 19 (2022) 1312-1321.

[87] D. Andrei, M. Witczak, W. Mirza, Appendix CC-4: Development of a revised predictive model for the dynamic (complex) modulus of asphalt mixtures, Development of the 2002 Guide for the Design of New and Rehabilitated Pavement Structures (1999) 66-204.

[88] M. Witczak, M. El-Basyouny, S. El-Badawy, Incorporation of the new (2005) E* predictive model in the MEPDG, NCHRP 1-40D Final Report (2007).

[89] S. Park, Y. Kim, Fitting Prony-series viscoelastic models with power-law presmoothing, Journal of materials in civil engineering 13(1) (2001) 26-32.

[90] R. Schapery, S. Park, Methods of interconversion between linear viscoelastic material functions. Part II—An approximate analytical method, International Journal of Solids and Structures 36(11) (1999) 1677-1699.

[91] P. Liu, Q. Xing, Y. Dong, D. Wang, M. Oeser, S. Yuan, Application of finite layer method in pavement structural analysis, Applied Sciences 7(6) (2017) 611.

[92] Z. Liu, X. Gu, H. Ren, X. Wang, Q. Dong, Three-dimensional finite element analysis for structural parameters of asphalt pavement: A combined laboratory and field accelerated testing approach, Case Studies in Construction Materials 17 (2022) e01221.

[93] D. Swan, R. Tardif, J.J. Hajek, D.K. Hein, Development of regional traffic data for the mechanistic–empirical pavement design guide, Transportation Research Record 2049(1) (2008) 54-62.

[94] Y. Jiang, Y. Zhang, J. Xue, C. Deng, T. Tian, Performance of Stone Mastic Asphalt Mixtures Fabricated by Different Compaction Methods, Applied Sciences 10(7) (2020) 2523.

[95] M.W. Witzcak, Simple performance test for superpave mix design, Transportation Research Board2002.

[96] I.M. Asi, Laboratory comparison study for the use of stone matrix asphalt in hot weather climates, Construction and Building Materials 20(10) (2006) 982-989.

[97] A. Veeraragavan, Dynamic mechanical characterization of asphalt concrete mixes with modified asphalt binders, Materials science and engineering: A 528(21) (2011) 6445-6454.

[98] F. Dong, W. Zhao, Y. Zhang, J. Wei, W. Fan, Y. Yu, Z. Wang, Influence of SBS and asphalt on SBS dispersion and the performance of modified asphalt, Construction and Building Materials 62 (2014) 1-7.

[99] H. Yu, S. Shen, Impact of aggregate packing on dynamic modulus of hot mix asphalt mixtures using three-dimensional discrete element method, Construction and Building Materials 26(1) (2012) 302-309.

[100] G. Liu, G. Leegwater, E. Nielsen, J. Komacka, M. van de Ven, Evaluating the rheological properties of PMB-containing RA binders from surface-layer asphalt mixtures to be recycled, Construction and Building Materials 49 (2013) 8-14.

[101] F. Guo, J. Zhang, J. Pei, B. Zhou, A.C. Falchetto, Z. Hu, Investigating the interaction behavior between asphalt binder and rubber in rubber asphalt by molecular dynamics simulation, Construction and Building Materials 252 (2020) 118956.

[102] V. Bulatović, V. Rek, K. Marković, Polymer modified bitumen, Materials research innovations 16(1) (2012) 1-6.

[103] G. Liu, Y. Liang, H. Chen, H. Wang, J. Komacka, X. Gu, Influence of the chemical composition and the morphology of crumb rubbers on the rheological and self-healing properties of bitumen, Construction and Building Materials 210 (2019) 555-563.

[104] J. Ekblad, R. Lundström, Soft bitumen asphalt produced using RAP, Materials and Structures 50 (2017) 1-14.

[105] Z. Liu, X. Gu, C. Wu, H. Ren, Z. Zhou, S. Tang, Studies on the validity of strain sensors for pavement monitoring: A case study for a fiber Bragg grating sensor and resistive sensor, Construction and Building Materials 321 (2022) 126085.

[106] S. Li, X. Liu, Z. Liu, Interlaminar shear fatigue and damage characteristics of asphalt layer for asphalt overlay on rigid pavement, Construction and Building Materials 68 (2014) 341-347.

APPENDIX A – PAPER I

Chen, Hao; Barbieri, Diego Maria; Hoff, Inge; Mork, Helge; Wathne, Pål; Liu, Gang.

Construction of asphalt mixture master curves for a Norwegian mechanistic-empirical pavement design system.

Published and presented at the Eleventh International Conference on the Bearing Capacity of Roads, Railways and Airfields, Volume 2, 423-434, 2022.

Eleventh International Conference on the Bearing Capacity of Roads, Railways and Airfields, Volume 2 – Hoff, Mork & Saba (eds)

Construction of asphalt mixture master curves for a Norwegian mechanistic-empirical pavement design system

Hao Chen, Diego Maria Barbieri, Inge Hoff & Helge Mork
Department of Civil and Environmental Engineering, Norwegian University of Science and Technology, Trondheim, Norway

Pål Wathne
Norconsult AS, Trondheim, Norway

Gang Liu
School of Materials Science and Technology, Wuhan University of Technology, Wuhan, China

ABSTRACT: As part of the development of a mechanistic-empirical pavement design system for Norwegian conditions, this paper presents the results of a laboratory study assessing asphalt mixture master curves based on Cyclic Indirect Tensile Tests (CITT). Specimens were prepared by means of a gyratory Intensive Compactor Tester (ICT), as well as by means of a roller compactor. The four asphalt mixtures of AC (asphalt concrete) 11, AC 16, SMA (stone mastic asphalt) 11, and SMA 16 with bitumen 70/100 commonly used as the surface layer in Norway were investigated. The dynamic modulus of the asphalt mixture samples was determined by frequency-sweep CITT at different temperatures. Based on the time-temperature superposition principle, the master curves were constructed and they are an important input for the mechanistic-empirical pavement design system to be implemented in the country. The voids characteristics, shift factor, and dynamic modulus of the four types of asphalt mixtures were compared. Besides, the effect of different compaction methods in the laboratory was investigated and recommendations regarding the specimen preparation were given.

Keywords: Asphalt mixture, cyclic indirect tensile test, dynamic modulus, master curve

1 INTRODUCTION

The Norwegian Public Roads Administration (NPRA) in cooperation with Swedish Transport Administration (TV), Swedish National Road and Transport Research Institute (VTI) and Norwegian University of Science and Technology (NTNU) is developing and implementing a new mechanistic design system for Norwegian roads adopting the mechanistic-empirical approach, which is based on the mechanics of materials for evaluating the pavement response (Huang, 1993). The characterization of asphalt mixtures is a central task to achieve this. The asphalt materials have viscoelastic behavior with distinctive temperature- and frequency-dependent properties (Lesueur et al. 1996). The dynamic modulus at different temperatures and frequencies characterizes the mechanical properties of asphalt mixtures, and can be evaluated in the laboratory by performing the uniaxial compression test (NCHRP, 2004) and the Cyclic Indirect Tensile Test (CITT) (Kim et al. 2004). The dynamic modulus master curve can then be constructed according to the time-temperature superposition principle within the Linear ViscoElastic (LVE) range by

DOI: 10.1201/9781003222897-39

horizontally shifting the test results measured based on a selected reference temperature (Chehab et al. 2002, Schwartz et al. 2002). A dynamic modulus master curve is constructed by fitting a sigmoidal function to the data, by using a time-temperature shift factor based on the Mechanistic-Empirical Pavement Design Guide (MEPD Guide) (NCHRP, 2004). The shift factor for asphalt materials can be accurately described by using the Williams, Landel and Ferry (WLF) equation at temperatures above the glass transition temperature (Williams et al. 1955). The dynamic modulus master curve can be used to predict the mechanical properties of the asphalt material for a wider frequency and temperature range than included in the actual test conditions.

The compaction of the asphalt pavement is an important factor affecting the overall performance of the material (Hunter et al. 2009). The roller compression method and gyroscopic compression method are two most commonly preparation methods of asphalt mixtures in the laboratory. Therefore, many studies have compared the influence of two laboratory compression methods on the asphalt mixture performance. Consuegra et al. (Consuegra et al. 1988) compared the engineering properties (resilient moduli, indirect tensile strengths and strains at failure, and tensile creep data) of laboratory-compacted samples prepared by roller compactor and gyratory compactor. The results related to the resilient modulus of laboratory specimens created with roller compactor were closer to the performance of field core samples than those created with gyratory compactor. Later, Button et al. (Button et al. 1994) investigated the physical properties of laboratory samples created by different compaction methods, and compared the results to the ones pertaining to pavement cores. The specimens prepared by both gyratory compactor and roller compactor were more similar to the pavement cores than the specimens prepared by the Marshall method. Besides, the roller compactor exhibited better air-void distribution than the gyratory compactor. Other researchers also indicate that the selected compaction methods exert different responses in terms of void characteristics and mechanical properties of asphalt mixtures (Sarsam and Jumaah 2016, Renken, 2000). However, the effect of the compaction methods on the dynamic modulus of asphalt mixtures has been studied less: ie. a comparison of the influence of the roller compactor method and the gyratory compactor method on the dynamic modulus of asphalt mixtures can provide recommendations regarding the specimen preparation procedures to be used in the development of the new Norwegian pavement design system.

In this research study, four asphalt mixtures were selected; AC 11, AC 16 (asphalt concrete), SMA 11 and SMA 16 (stone mastic asphalt), being the most commonly used surface layers of Norwegian asphalt pavements. The roller compactor and the gyratory Intensive Compactor Tester (ICT) were used to prepare the asphalt mixture specimens. The dynamic modulus was measured by the CITT employing the Nottingham Asphalt Tester (NAT). The sigmoidal function based on the MEPD Guide and the WLF equation were used to construct the dynamic modulus master curves, and the influence of the different types of asphalt mixtures and the different compaction methods on the dynamic modulus master curve was evaluated. Hence, the objective of this study is to provide data support for the development of the mechanistic-empirical design system for Norwegian conditions, and to recommend a proper compaction approach.

2 MATERIALS AND METHODS

2.1 *Materials*

A 70/100 bitumen supplied by the Veidekke company (Trondheim, Norway) was used and its main physical properties are given in Table 1.

Table 1. Physical properties of bitumen 70/100.

Physical properties	Unit	Value	Test standard
Penetration at 25 °C	0.1 mm	91.6	EN 1426 (CEN, 2015)
Softening point (Ring and Ball)	°C	46.0	EN 1427 (CEN, 2015)

The crushed rocks and limestone filler supplied by the Franzefoss company (Heimdal, Norway) were adopted, and their resistance to wear and fragmentation is specified in Table 2. The aggregates used in this study fulfil the requirements for AC and SMA mixtures considering an Annual Average Daily Traffic (AADT) bigger than 15000 (NPRA, 2018).

Table 2. Resistance to wear and fragmentation of crushed rock aggregates.

Test	Value	Requirements for AADT > 15000	Test standard
Los Angeles value	18.2	≤ 20	EN 1097-2 (CEN, 2020)
Micro-Deval coefficient	14.2	≤ 15	EN 1097-1 (CEN, 2011)

2.2 *Specimen preparation*

The asphalt mixture specimens were prepared in the laboratory based on the gradation curves of AC 11, AC 16, SMA 11, and SMA 16 shown in Figure 1 (NPRA, 2019), and the Optimum Binder Content (OBC) was determined by the Marshall mixture design and specific requirements of the Air Voids Content (V_a) and the Voids Filled with Binder (VFB) (NPRA, 2005).

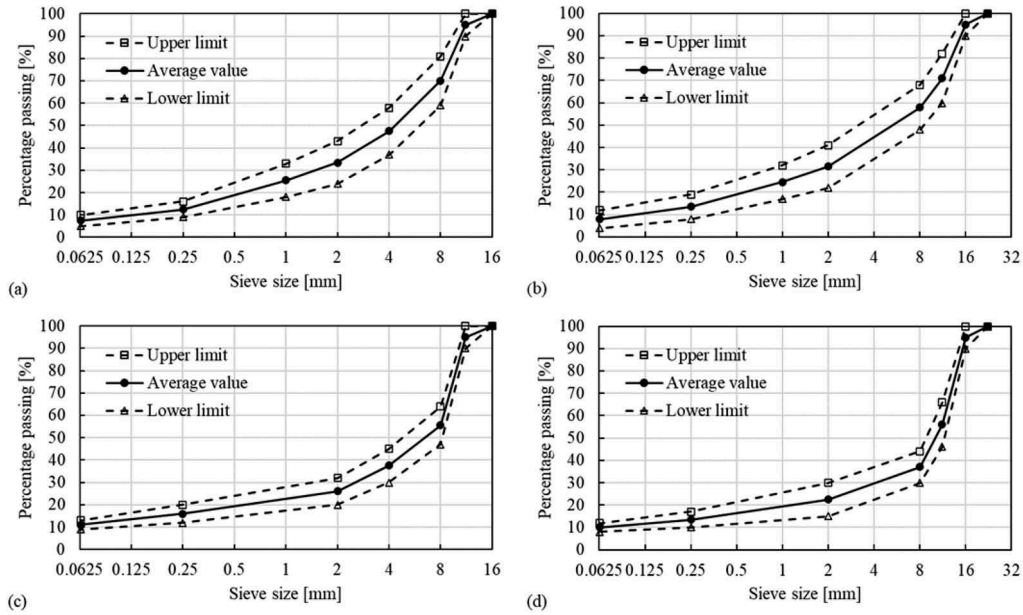

Figure 1. Gradation curves of (a) AC 11, (b) AC 16, (c) SMA 11, and (d) SMA 16.

The void characteristics of the Marshall specimens impacted by 50 blows per side were verified to meet the requirements of the design criteria (NPRA, 2019). The OBCs were 5.1%, 4.9%, 5.3%, and 5.1% for AC 11, AC 16, SMA 11, and SMA 16, respectively.

The specimens were prepared by both a roller compactor (manufactured by Cooper Technology, Ripley, UK) and a gyratory compactor (ICT-150RB produced by Invelop oy, Semolina, Finland). Referring to the former one (CEN, 2019), the space inside a mold correspond to a rectangular parallelepiped with dimensions 305 mm × 305 mm × 57 mm. The compaction process was divided into four stages further subdivided into four passes. The pressure in the first, second stage, and the third stage is 2 bar, 4 bar and 6 bar, respectively.

No pressure was provided during the fourth stage, only the weight of the roller was applied to the specimen; meanwhile, the vibration was applied at the last two passes of the fourth stage for sufficient and effective compaction.

For the gyratory compactor, the cylindrical asphalt mixture specimens had a diameter of 150 mm and a height of 180 mm. The compaction pressure was 620 kPa, and the gyratory angle was set to 17 mrad (0.97°) (CEN, 2019). To ensure sufficient compaction, 100 and 115 gyrations were applied for the AC mixtures and SMA mixtures, respectively.

Afterwards, cylindrical specimens with a diameter of 100 mm and a height of 40 mm were drilled and cut from the asphalt slabs and gyratory specimens to be tested by the CITT. The eight mixture types designated in Table 3 were investigated in this study and four parallel specimens were prepared for each type, ie. a total of 32 specimens was tested. The preparation process of specimens is shown in Figure 2. The void characteristics of NAT test specimens were also recorded (CEN, 2018).

Table 3. Designation of the tested specimens according to selected mixture type and compaction method.

Mixture type	Compaction method	Designation
AC 11	Roller compaction	AC 11-R
	Gyratory compaction	AC 11-G
AC 16	Roller compaction	AC 16-R
	Gyratory compaction	AC 16-G
SMA 11	Roller compaction	SMA 11-R
	Gyratory compaction	SMA 11-G
SMA 16	Roller compaction	SMA 16-R
	Gyratory compaction	SMA 16-G

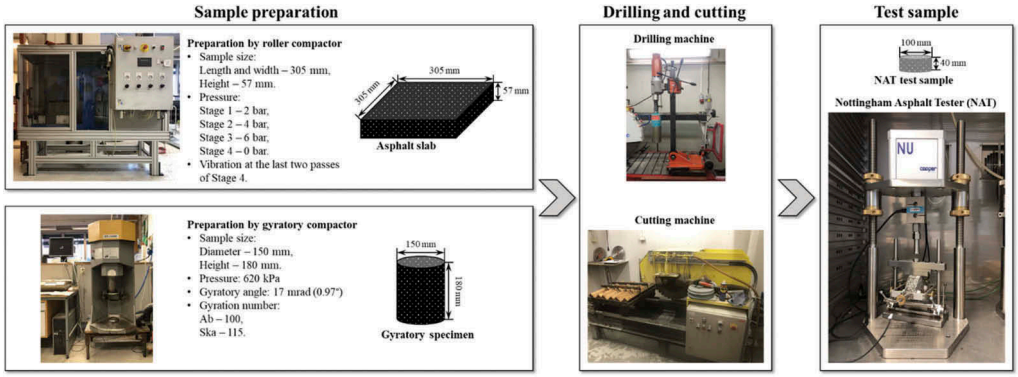

Figure 2. Preparation process of specimens.

2.3 *Cyclic indirect tensile test*

The cyclic indirect tensile test was performed by a servo-pneumatic universal testing machine produced by Cooper Technology exerting a controlled harmonic sinusoidal load without rest periods according to the relevant standard (CEN, 2018). The applied load ensured that the sample was in the LVE range as the initial horizontal strain was in a range between 50 με to 100 με for each test temperature and frequency. This research study presents the mean results corresponding to the CITT testing of four parallel specimens for each asphalt mixture.

The CITT was performed at temperatures of -15 °C, 0 °C, 15 °C and 30 °C and at frequencies of 10 Hz, 5 Hz, 3 Hz, 1 Hz, 0.3 Hz and 0.1 Hz for each specimen.

The dynamic modulus was determined for each load pulse in the CITT using the following equation:

$$|E^*| = \frac{F \cdot (\nu + 0.27)}{z \cdot h} \tag{1}$$

where $|E^*|$ is the dynamic modulus, in megapascal (MPa), v is the Poisson's ratio, F is the maximum load, in Newton (N), z is the sample thickness, in millimeter (mm), and h is the horizontal deformation, in millimeter (mm).

2.4 *Master curve construction*

The sigmoidal function described in MEPD Guide (NCHRP, 2004) and the WLF equation as the shift factor (Williams, 1955) were referred to in this study. The sigmoidal function is given by equation (2):

$$\log(|E^*|) = \delta + \frac{\alpha}{1 + e^{\beta - \gamma(\log f_r)}} \tag{2}$$

where $|E^*|$ is the dynamic modulus, in megapascal (MPa), f_r is the frequency at the reference temperature, in hertz (Hz), δ, α, β and γ are the fitting parameters, where δ represents the minimum value of $|E^*|$. $\delta + \alpha$ represents the maximum values of $|E^*|$, β and γ describe the shape of the sigmoidal function as shown in Figure 3 (Pellinen et al. 2004).

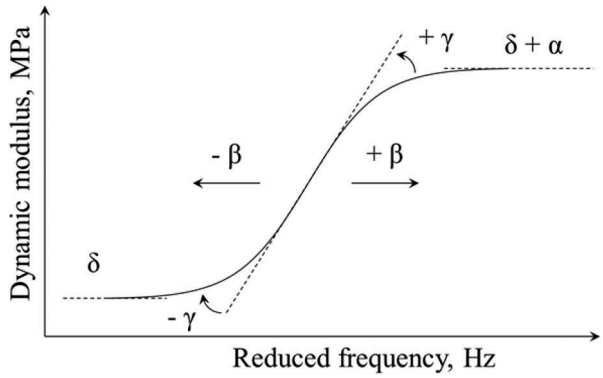

Figure 3. Shape description of dynamic modulus considering the parameters of sigmoidal function.

The shift factor, α_T, describes the temperature dependency of the dynamic modulus and Equation (3) provides the general form.

$$\alpha_T = \frac{f_r}{f} \tag{3a}$$

$$\log(f_r) = \log(f) + \log(\alpha_T) \tag{3b}$$

where f_r is the reduced frequency at the reference temperature, in hertz (Hz), f is the frequency at the test temperature, in hertz (Hz), and T is the test temperature, in degrees Celsius (°C).

The Williams-Landel-Ferry (WLF) equation is widely used to describe the relationship between the shift factor and the temperature and thereby assess the shift factor of asphalt mixtures:

$$\log[\alpha(T)] = \frac{-C_1(T - T_r)}{C_2 + (T - T_r)} \tag{4}$$

where T is the temperature, in degrees Celsius (°C), T_r is the reference temperature chosen to construct the compliance master curve, in degrees Celsius (°C), C_1 and C_2 are two empirical constants adjusted to fit the values of the shift factor.

The fitting procedure to construct the dynamic modulus master curve was conducted by using the Microsoft Excel Solver tool, in which optimization of the data with non-linear least squares regression techniques was performed. The Sum of Square Error (SSE) between measured values after shifting, $|E^*|_{measured}$, and predicted values, $|E^*|_{predicted}$, as shown in Equation (5) was used to optimize the fitting procedure. To define the optimum results of the master curves, the values of δ, α, β, γ, C_1 and C_2 were fitted to minimize SSE.

$$SSE = \sum \frac{(|E^*|_{measured} - |E^*|_{predicted})^2}{(|E^*|_{measured})^2} \tag{5}$$

3 RESULTS AND DISCUSSION

3.1 *Void characteristics*

The void characteristics reflect how well a specimen is compacted, and the results for the four asphalt mixture types prepared by both roller compactor and gyratory compactor are shown in Figure 4. The void characteristics of an asphalt mixture depend on many factors including compaction mode and effort, binder content, aggregate type, mixture type, etc. As indicated in Figure 4, the V_a of AC 11-G, AC 16-G, SMA 11-G and SMA 16-G were 0.6%, 0.7%, 1.7% and 0.8% lower than for the corresponding specimens prepared by roller compactor, respectively. The Void in Mineral Aggregate (VMA) of AC 11-G, AC 16-G, SMA 11-G and SMA 16-G were 0.5%, 0.6%, 1.5% and 0.6% lower than for the corresponding specimens prepared by roller compactor, respectively. The VFB of AC 11-G, AC 16-G, SMA 11-G and SMA 16-G were 3.0%, 3.9%, 8.0% and 3.8% higher than for the corresponding specimens prepared by roller compactor, respectively. These findings indicate that gyratory compaction applied a higher degree of compaction when compared to roller compaction. Based on the Marshall mix design performed in this study, the AC mixtures had lower V_a and VMA, and higher VFB than the SMA mixtures. Meanwhile, the specimens with larger particle size had lower V_a and VMA, and higher VFB than the specimens with smaller maximum grain size.

3.2 *Shift factors*

Figure 5 shows the WLF shift factor curves of the different mixtures. It was found that the logarithm of the shift factor linearly decreased with the increase in temperature. The linear regression results are calculated according to an equation of the form $y = ax + b$, where x is the temperature, y is the predicted shift factor, a is the slope of the line, and b is the intercept (Table 4). The coefficients of determination (R^2) of AC 11 and AC 16 were higher than those of SMA 11 and SMA 16, this shows that the logarithm of the shift factor of the AC mixtures tends to be more prone to follow a linear trend than that of the SMA mixtures; furthermore, it also shows that the shifted distances of the dynamic moduli of the AC mixtures per unit temperature were more even than those of the SMA mixtures when the master curves were constructed.

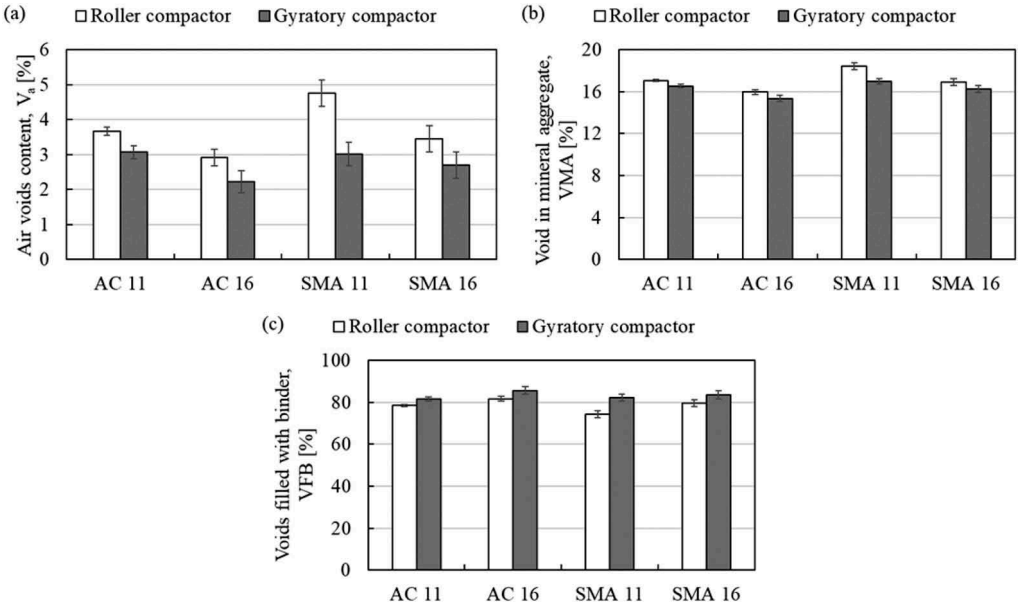

Figure 4. Void characteristics of specimens: (a) V_a, (b) WMA, and (c) VFB.

Table 4. Linear regression of shift factors.

Mixture	Linear regression		
	a	b	R^2
AC 11-R	-0.159	2.602	0.990
AC 11-G	-0.182	3.002	0.988
AC 16-R	-0.161	2.721	0.980
AC 16-G	-0.176	2.957	0.981
SMA 11-R	-0.166	2.952	0.946
SMA 11-G	-0.184	3.291	0.942
SMA 16-R	-0.169	2.948	0.963
SMA 16-G	-0.183	3.177	0.963

Figure (b) shows that the shift factor of AC 11 prepared by roller compactor is different from the one related to gyratory compaction. At -10 °C, the shift factors of AC 11-G, AC 16-G, SMA 11-G and SMA 16-G were 15.8%, 8.5%, 11.9% and 7.7% higher than for the corresponding specimens prepared by roller compactor, respectively. At 30 °C, the shift factors of AC 11-G, AC 16-G, SMA 11-G and SMA 16-G were 11.4%, 10.2%, 8.8%, and 8.4% lower than for the corresponding specimens prepared by roller compactor, respectively. These results indicate that the shift amplitude of the dynamic modulus curve of the specimens prepared by the gyratory compactor at each temperature is larger than the corresponding values related to roller compaction.

Figure (c) indicates that SMA 11-R has higher shift factors at both low temperatures and high temperatures than that of AC 11-R. The shift factors of SMA 11-R, SMA 11-G, SMA 16-R, and SMA 16-G were 19.6%, 15.5%, 10.5%, and 9.7% higher than that of AC 11-R, AC 11-G, AC 16-R, and AC 16-G, respectively, at -10 °C, and 25.2%, 27.0%, 7.2%, and 8.7% higher at 30 °C. These results indicate that the dynamic modulus curves of the SMA mixtures shifted more at the low temperature (high frequency) and less at the high temperature (low frequency) than that of the AC mixtures.

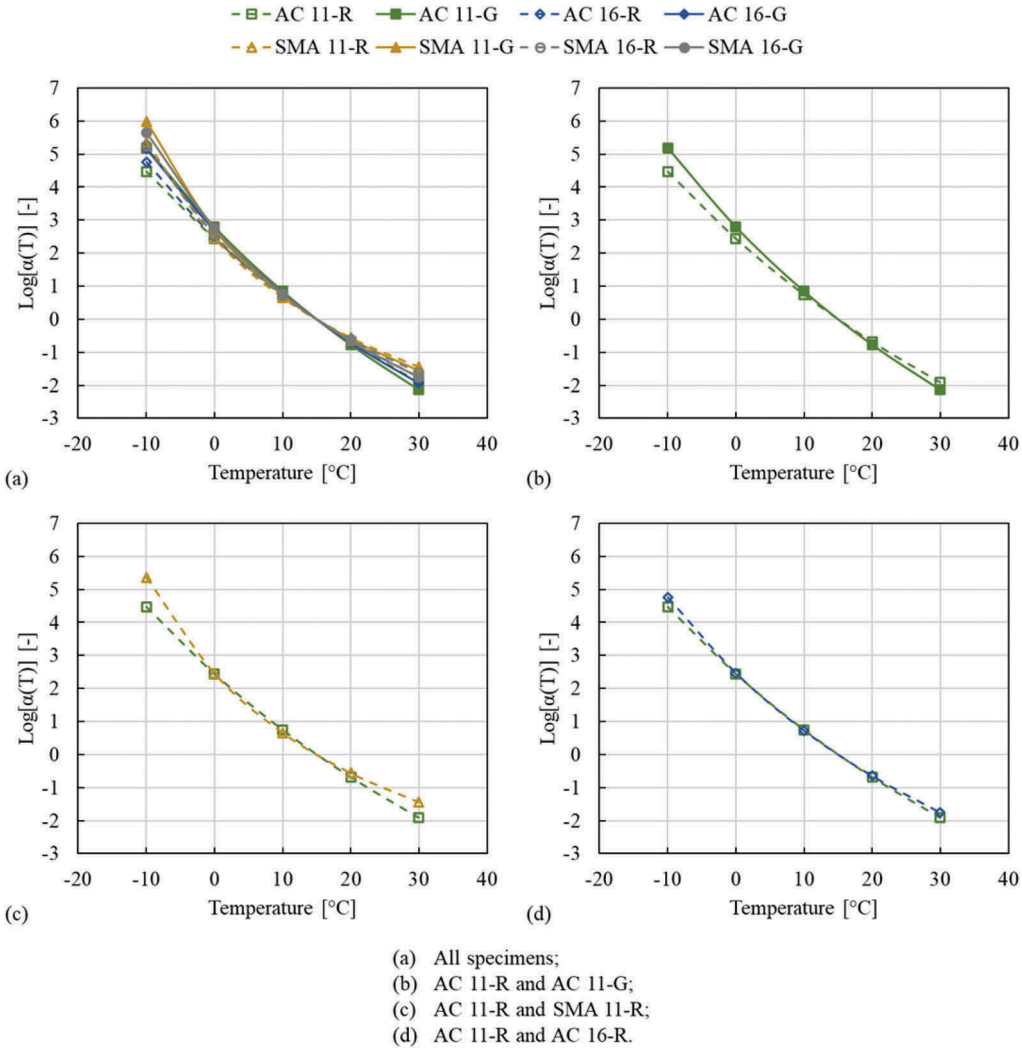

(a) All specimens;
(b) AC 11-R and AC 11-G;
(c) AC 11-R and SMA 11-R;
(d) AC 11-R and AC 16-R.

Figure 5. WLF shift factor curves for tested mixtures.

Figure (d) illustrate that there are just slight differences in the shift factors between AC 11-R and AC 16-R. The shift factor did not change much with the maximum grain size of the asphalt mixture, thus indicating the minor role played by the particle size of the aggregates.

3.3 *Master curves*

The fitting parameters, R^2 and SSE, are reported in Table 5. The R^2 of all asphalt mixtures ranged from 0.9927 to 0.9997, and the SSE values were comprised between 0.0331 and 0.1947, to be concluded that all the experimental values were then satisfactorily fitted.

As shown in Table 4, the compaction method, asphalt mixture type, and maximum grain size all exerted clear effects on the fitting parameters. The compaction method had a major influence on the fitting parameters of δ and α for AC mixtures. However, there was a smaller difference of δ and α between the two compaction methods for SMA mixtures. This shows that the compaction methods exerted a greater impact on the AC mixtures than the SMA mixtures. The AC and SMA mixtures have different structures causing this result. The AC mixture is composed of a dense gradation. The structural strength of the AC mixture is mainly based on the cohesive

Table 5. Fitting parameters, SSE and R^2 for mixtures.

Mixture	Sigmoidal function				WLF equation		R^2	SSE
	δ	α	β	γ	C_1	C_2		
AC 11-R	0.406	4.300	-1.070	0.364	17.93	125.21	0.9997	0.0710
AC 11-G	0.830	3.854	-1.097	0.391	18.22	112.91	0.9984	0.0836
AC 16-R	0.529	4.159	-1.070	0.413	12.11	88.71	0.9976	0.1352
AC 16-G	0.313	4.391	-1.254	0.396	13.69	91.34	0.9986	0.0780
SMA 11-R	0.777	3.766	-1.037	0.497	6.91	57.31	0.9962	0.0331
SMA 11-G	0.749	3.776	-1.177	0.469	7.36	55.72	0.9946	0.0413
SMA 16-R	1.562	3.026	-0.589	0.515	8.96	67.63	0.9927	0.1947
SMA 16-G	1.436	3.138	-0.851	0.464	9.78	68.21	0.9973	0.1375

force between the mineral aggregate and the binder. The SMA mixture is a semi-dense and semi-inlaid structure. The structural strength of the SMA mixture is composed of the squeezing force, internal friction between the mineral aggregates, and the cohesive force between the mineral aggregate and the binder (Jiang et al. 2020). The compaction method has a more important influence on the dense structure.

The range of the dynamic modulus reflects the temperature sensitivity of asphalt mixtures. The δ values for AC mixtures were generally lower than those for SMA mixtures while the δ + α values for AC mixtures tended to be higher than those for SMA mixtures. These results indicate that the AC mixtures were more sensitive to temperature than the SMA mixtures. This phenomenon can be explained by considering their structures: for AC mixtures, the cohesiveness of the binder exerts more influence on the structural strength; therefore, their temperature sensitivity is stronger than for SMA mixtures.

The fitting parameters also varied for each considered aggregate grading curve. As the coarse grains constitute the three-dimensional matrix structure of the asphalt mixture and are directly related to the stiffness, the different aggregate sizes form a skeleton structure of various qualities resulting in different values and trends of the dynamic modulus.

The master curves are portrayed in Figure 6. The dynamic modulus values are then compared at the condition of -10 °C and 10 Hz (low-temperature condition) and at the condition of 40 °C and 0.1 Hz (high-temperature condition) based on the modeling of the dynamic modulus, as shown in Figure 7.

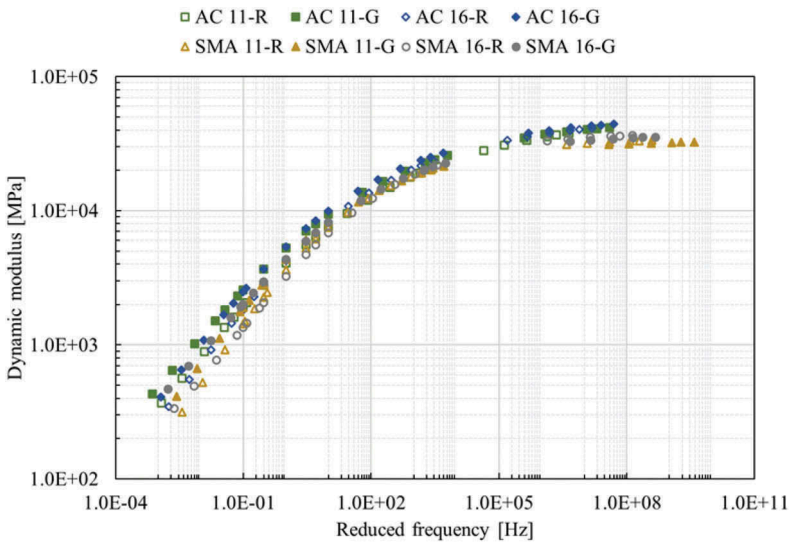

Figure 6. Master curves for tested mixtures.

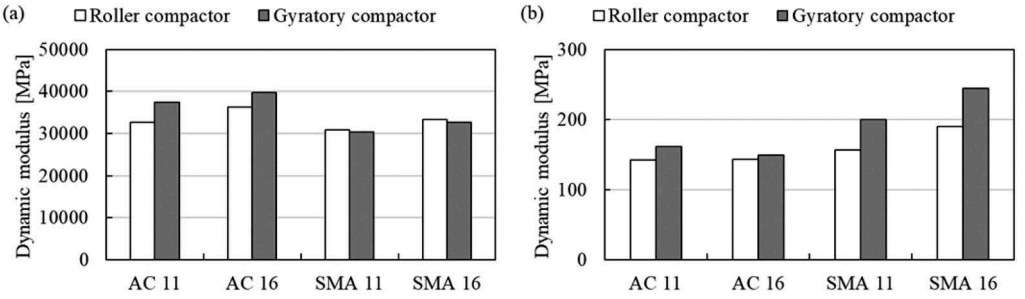

Figure 7. Dynamic modulus at (a) the low-temperature condition -10 °C and 10 Hz and (b) the high-temperature condition 40 °C and 0.1 Hz.

As shown in Figure 7 (a), the dynamic moduli of AC 11-G and AC 16-G were 14.6% and 9.4% higher than those of AC 11-R and AC 16-R at the low-temperature condition. The AC mixtures prepared by the gyratory compactor were denser, leading to a higher dynamic modulus. However, even though the gyratory compaction also made the SMA mixtures denser, the dynamic moduli at the low-temperature condition for SMA mixtures prepared by the gyratory compactor were slightly lower than the corresponding ones attained by the roller compactor. This indicate that the combined effect of the embedded and dense structures caused the dynamic modulus of the SMA mixture at low temperature to be less affected by the compaction method.

As shown in Figure 7 (b), the dynamic moduli of AC 11-G, AC 16-G, SMA 11-G, and SMA 16-G were 13.4%, 4.3%, 27.7%, and 28.3%, respectively, higher than those of AC 11-R, AC 16-R, SMA 11-R, and SMA 16-R at the high-temperature condition. Considering the findings related to high temperatures, the dynamic moduli of AC mixtures and SMA mixtures were affected the least and the most by the compaction mode, respectively. As the bitumen attains a viscous flow state at high temperatures, the cohesive force between the binder and the aggregate is greatly reduced. Therefore, the dynamic modulus of the AC mixtures was less affected by the compaction method. The structure of the SMA mixture was also improved by the gyratory compactor, which then caused less affected by the temperature at high temperatures.

The dynamic modulus of SMA 16-G decreased by 17.7% at the low-temperature condition and increased by 63.6% at the high-temperature condition compared to that of AC 16-G. The lower dynamic modulus at low temperatures can prevent thermal cracking of an asphalt pavement, while a higher dynamic modulus at high temperatures is beneficial for protecting an asphalt pavement from permanent deformations (Zhang et al, 2012). This outcome documents that the SMA mixture has a better performance than the AC mixtures at both high and low temperatures.

At high temperatures, the dynamic moduli of AC 16-R and SMA 16-R were 11.0% and 8.4% higher than those of AC 11-R and SMA 11-R, respectively. As thoroughly documented in other studies, the scaling effect of the aggregates including particle shape and particle size has a significant impact on its strength (Thuro et al. 2001) and thereby on the modulus of the asphalt mixture. In this study, as the particle shapes were the same for all asphalt mixtures, the large-sized mineral aggregates improved the quality of the skeleton structure showing a higher dynamic modulus.

4 CONCLUSIONS

In this laboratory study, the asphalt mixtures that are most commonly employed in Norway were prepared using two different compaction methods, namely gyratory compaction and roller compaction. The corresponding dynamic moduli at different temperatures and frequencies were obtained using the Cyclic Indirect Tensile Test (CITT). The dynamic modulus master curves for these mixtures were constructed by the Sigmoidal function and the Williams, Landel and Ferry (WLF) equation. Based on the results attained, the conclusions are as follows:

- Gyratory compaction made both AC and SMA mixtures denser compared to the case of roller compaction, resulting in lower Air voids content (V_a), lower Void in Mineral Aggregate (VMA), and higher Voids Filled with Binder (VFB), as well as leading to a higher dynamic modulus of AC mixtures at low temperatures and of SMA mixtures at high temperatures. The shift factors of specimens prepared by the gyratory compactor were higher at low temperatures and lower at high temperatures than those related to the samples prepared by the roller compactor.
- The SMA mixtures were characterized by a lower dynamic modulus at low temperature and higher dynamic modulus at high temperature when compared to the AC mixtures, thus showing better performance than the AC mixture. The shift factors of SMA mixtures were significant higher at both high and low temperatures than those of AC mixtures.
- The asphalt mixtures with a larger maximum grain size displayed better compact ability, resulting in lower V_a, lower VMA, and higher VFB, as well as higher dynamic modulus than the asphalt mixtures with a smaller maximum grain size. The grain size had little effect on the shift factor.

According to these key-findings, the SMA mixture can be recommended for asphalt pavements carrying a high traffic volume because of its better mechanical properties at both high and low temperatures from the perspective of asphalt stiffness. Besides, the volumetric properties and dynamic modulus of specimens prepared by roller compactor and gyratory compactor were different. Considering that the roller compactor method is closer to on-site paving, the roller compaction is thus recommended to develop the new Norwegian pavement design system and for modeling the dynamic modulus of asphalt pavements.

ACKNOWLEDGMENTS

This research work was supported by the VegDim project of the Norwegian Public Roads Administration. The financial support provided by China Scholarship Council (No. 201806950077) and Department of Civil and Environmental Engineering, Norwegian University of Science and Technology (No. K-649105) is highly acknowledged. The support kindly provided by the laboratory technicians Bent Lervik and Jan Erik Molde is greatly acknowledged.

REFERENCES

Button, J. et al., 1994. *Correlation of Selected Laboratory Compaction Methods with Field Compaction*. Transportation Research Record, 1454.

CEN, 2011. *NS-EN 1097-1 Tests for Mechanical and Physical Properties of Aggregates - Part 1: Determination of the Resistance to Wear (Micro-Deval)*. European Standard, Brussels, Belgium.

CEN, 2015. *NS-EN 1426 Bitumen and Bituminous Binders - Determination of Needle Penetration*. European Standard, Brussels, Belgium.

CEN, 2015. *NS-EN 1427 Bitumen and Bituminous Binders - Determination of Softening Point - Ring and Ball Method*. European Standard, Brussels, Belgium.

CEN, 2018. *NS-EN 12697-8 Bituminous Mixtures - Test methods - Part 8: Determination of Void Characteristics of Bituminous Specimens*. European Standard, Brussels, Belgium.

CEN, 2018. *NS-EN 12697-26 Bituminous Mixtures - Test Methods - Part 26: Stiffness*. European Standard, Brussels, Belgium.

CEN, 2019. *NS-EN 12697-31 Bituminous Mixtures - Test methods - Part 31: Specimen Prepared by Gyratory Compactor*. European Standard, Brussels, Belgium.

CEN, 2019. *NS-EN 12697-33 Bituminous Mixtures - Test method - Part 33: Specimen Prepared by Roller Compactor*. European Standard, Brussels, Belgium.

CEN, 2020. *NS-EN 1097-2 Tests for Mechanical and Physical Properties of Aggregates - Part 2: Methods for the Determining of Resistance to Fragmentation*. European Standard, Brussels, Belgium.

Chehab, G. R. et al., 2002. *Time-Temperature Superposition Principle for Asphalt Concrete with Growing Damage in Tension State*. Journal of the Association of Asphalt Paving Technologists, 71.

Consuegra, A. et al., 1988. *Comparative Evaluation of Laboratory Compaction Devices Based on Their Ability to Produce Mixtures with Engineering Properties Similar to Those Produced in the Field*. Master's thesis, Texas A&M University.

Huang, Y., 1993. *Pavement Analysis and Design*.
Hunter, A. et al., 2009. *Effect of Compaction Mode on the Mechanical Performance and Variability of Asphalt Mixtures*. Journal of Transportation Engineering, 135(11), 839–851.
Jiang, Y. et al., 2020. *Performance of Stone Mastic Asphalt Mixtures Fabricated by Different Compaction Methods*. Applied Sciences, 10(7), 2523.
Kim, Y. et al., 2004. *Dynamic Modulus Testing of Asphalt Concrete in Indirect Tension Mode*. The 83rd Transportation Research Board, Washington, DC, United States.
Lesueur, D. et al., 1996. *A Structure-Related Model to Describe Asphalt Linear Viscoelasticity*. Journal of Rheology, 40(5), 813–836.
NCHRP, 2004. *Guide for Mechanistic-Empirical Design of New and Rehabilitated Pavement Structures*. National Cooperative Highway Research Program, Washington, DC, United States.
NPRA, 2005. *Håndbok 018 Vegbygging*. Vegdirektoratet, Norway.
NPRA, 2018. *Håndbok N200 vegbygging*. Vegdirektoratet, Norway.
NPRA, 2019. *STATENS VEGVESENS RAPPORTER Nr. 670 Retningslinjer asfalt 2019*. Vegdirektoratet, Norway.
Pellinen, T. et al., 2004. *Asphalt Mix Master Curve Construction Using Sigmoidal Fitting Function with Non-Linear Least Squares Optimization*.Recent Advances in Materials Characterization and Modeling of Pavement Systems, 83–101.
Renken, P., 2000. *Influence of Specimen Preparation onto the Mechanical Behaviour of Asphalt Aggregate Mixtures*. The 2nd Eurasphalt and Eurobitume Congress, Barcelona, Spain.
Sarsam, S. and Jumaah, M., 2016. *Modeling of Comparative Performance of Asphalt Concrete under Hammer, Gyratory, and Roller Compaction*. Journal of Engineering, 22(11), 1–15.
Schwartz, C. W. et al., 2002. *Time-Temperature Superposition for Asphalt Concrete at Large Compressive Strains*. Transportation Research Record, 1789(1), 101–112.
Thuro, K. et al., 2001. *Scale Effects in Rock Strength* Properties. *Part 1: Unconfined Compressive Test and Brazilian Test*. ISRM Regional Symposium, EUROCK, 169–174.
Williams, M. L. et al., 1955. *The Temperature Dependence of Relaxation Mechanisms in Amorphous Polymers and Other Glass-Forming Liquids*. Journal of the American Chemical society, 77(14), 3701–3707.
Zhang, Y. et al., 2012. *Characterizing Permanent Deformation and Fracture of Asphalt Mixtures by Using Compressive Dynamic Modulus Tests*. Journal of Materials in Civil Engineering, 24(7), 898–906.

APPENDIX B – PAPER II

Chen, Hao*; Barbieri, Diego Maria; Zhang, Xuemei; Hoff, Inge

Reliability of Calculation of Dynamic Modulus for Asphalt Mixtures Using Different Master Curve Models and Shift Factor Equations.

Published in the Journal of Materials, 15(12), 4325, 2022.

materials

MDPI

Article

Reliability of Calculation of Dynamic Modulus for Asphalt Mixtures Using Different Master Curve Models and Shift Factor Equations

Hao Chen [1,*], Diego Maria Barbieri [1,2], Xuemei Zhang [1] and Inge Hoff [1]

[1] Department of Civil and Environmental Engineering, Norwegian University of Science and Technology, Høgskoleringen 7A, 7491 Trondheim, Norway; diegomb271@gmail.com (D.M.B.); xuemei.zhang@ntnu.no (X.Z.); inge.hoff@ntnu.no (I.H.)

[2] Department of Mechanical and Structural Engineering and Materials Science, University of Stavanger, Kristine Bonnevies vei 22, 4021 Stavanger, Norway

* Correspondence: hao.chen@ntnu.no

Abstract: To develop a mechanistic-empirical pavement design system for Norwegian conditions, this paper evaluates the influence of the adoption of different models and shifting techniques on the determination of dynamic modulus master curves of asphalt mixtures. Two asphalt mixture types commonly used in Norway, namely Asphalt Concrete (AC) and Stone Mastic Asphalt (SMA) containing neat bitumen and polymer-modified bitumen, were prepared by the roller compactor, and their dynamic moduli were determined by the cyclic indirect tensile test. The dynamic modulus master curves were constructed using the standard logistic sigmoidal model, a generalized logistic sigmoidal model and the Christensen–Anderson–Marasteanu model. The shifting techniques consisted of log-linear, quadratic polynomial function, Arrhenius, William–Landel–Ferry and Kaelble methods. The absolute error, normalised square error and goodness-of-fit statistics encompassing standard error ratio and coefficient of determination were used to appraise the models and shifting methods. The results showed that the standard logistic sigmoidal model and the Williams–Landel–Ferry equation had the most suitable fits for the specimens tested. The asphalt mixtures containing neat bitumen had a better fit than the ones containing polymer-modified bitumen. The Kaelble equation and log-linear equation led to similar results. These findings provide a relevant recommendation for the mechanistic-empirical pavement design system.

Keywords: asphalt mixture; dynamic modulus; master curve model; shift factor; goodness of fit

Citation: Chen, H.; Barbieri, D.M.; Zhang, X.; Hoff, I. Reliability of Calculation of Dynamic Modulus for Asphalt Mixtures Using Different Master Curve Models and Shift Factor Equations. *Materials* **2022**, *15*, 4325. https://doi.org/10.3390/ma15124325

Academic Editor: Francesco Canestrari

Received: 27 May 2022
Accepted: 17 June 2022
Published: 18 June 2022

1. Introduction

To develop the mechanistic–empirical pavement design system for Norwegian conditions envisaged by the Norwegian Public Roads Administration (NPRA) [1], the mechanical characterization of asphalt pavement is of primary importance. The asphalt material is sensitive to the temperature and the rate-of-load due to its viscoelastic properties [2,3]. Based on the Mechanistic–Empirical Pavement Design Guide (MEPDG) [4], the dynamic modulus is a relevant parameter to characterise the mechanical properties of asphalt pavements. Due to the time-consuming process of specimen preparation and testing, master curves were developed according to the time–temperature superposition principle [5,6]. It is necessary to select an appropriate method to evaluate the dynamic modulus master curve among all the formulated extrapolation methodologies in order to develop a proper mechanistic–empirical pavement design system.

The Standard Logistic Sigmoidal (SLS) model used in the MEPDG is widely used to construct the dynamic modulus master curve of asphalt materials. The SLS model can more accurately fit the dynamic modulus test data in a wider temperature range than a single polynomial model [7,8]. However, the SLS model is more applicable when test

data are symmetrical, whereas the Generalized Logistic Sigmoidal (GLS) model developed by Rowe et al. is better employed to fit asymmetric data [9,10]. Moreover, Marasteanu and Anderson proposed a Christensen–Anderson–Marasteanu (CAM) model based on the Christensen–Anderson (CA) formulation [11], which provides a better fit of the dynamic modulus of asphalt mixtures within very low and very high frequencies for unmodified and polymer modified bituminous binders [12–14].

To construct the dynamic modulus master curve, different shifting techniques (shift factor, α_T) were used to model the time–temperature superposition relationship related to the viscoelastic properties of asphalt materials. Traditionally, the temperature dependence of relaxation modes in the vicinity of glass transition temperature (T_g) is modelled with the Williams–Landel–Ferry (WLF) equation [15]. However, recent experimental studies [16,17] found that the temperature dependence of viscoelastic properties deviate from the WLF equation below T_g. To address this issue, the Kaelble equation based on the WLF formulation was proposed [18–20]. The Kaelble equation is a symmetric function devised to reflect the temperature dependence of viscoelastic properties below T_g [21]. The Arrhenius equation is another popular model used to describe the temperature dependence of viscoelastic properties of materials. The WLF and Arrhenius equations focus on the volume processes and the thermally activated processes, respectively [10,22]. In addition to the above two methods, the log-linear equation can also describe the temperature dependence of asphalt materials [7]. The log-linear equation presents the straight-line relationship between $log(\alpha_T)$ and temperature, and is normally used for asphalt mixtures [23]. The quadratic polynomial equation is another well-known shift factor equation that can accurately fit the shift factors over a wide range of temperatures [24–26].

The objective of this study is to adopt various models and shift factor equations to evaluate the dynamic modulus of four types of asphalt mixtures commonly used in Norwegian highway by means of Cyclic Indirect Tensile Tests (CITTs) conducted in the laboratory. The three master curve models and five shift factor equations were employed to assess the dynamic modulus master curve. The quality of the extrapolation calculations was assessed by error analysis and goodness-of-fit statistics. The results can provide recommendations for the selection of the proper master curve model and shift factor equation for developing the mechanistic–empirical pavement design system.

2. Materials and Methods

2.1. Materials

The Neat Bitumen (NB) of Pen 70/100 and the Polymer Modified Bitumen (PMB) of Pen 65/105 were supplied by Veidekke company (Trondheim, Norway) and Nynas company (Göteborg, Sweden), respectively. Their main physical properties are given in Table 1. In PMB, the critical network structure is formed between the polymer molecule and the asphalt binder, which enhances its deformation resistance at high temperature, resulting in a lower penetration and a higher softening point [27].

Table 1. Physical properties of neat bitumen and PMB.

Physical Properties	Bitumen		Test Standard
	NB	PMB	
Penetration at 25 °C [0.1 mm]	92	86	EN 1426:2015 [28]
Softening point (Ring and Ball) [°C]	46.0	62.6	EN 1427:2015 [29]

Crushed rock aggregates supplied by Franzefoss company (Heimdal, Norway) were adopted, and their resistance to wear and fragmentation are specified in Table 2. The aggregates fulfilled the requirements for AC and SMA mixture with an Annual Average Daily Traffic (AADT) higher than 15,000 [30].

Table 2. Resistance to wear and fragmentation of crushed rock aggregates.

Test	Value	Requirements for AADT > 15,000	Test Standard
Micro-Deval coefficient	14.2	≤20	EN 1097-1:2011 [31]
Los Angeles value	18.2	≤15	EN 1097-2:2020 [32]

2.2. Cyclic Indirect Tensile Test

2.2.1. Sample Preparation

The asphalt mixture specimens were prepared in the laboratory based on the average value of the upper limit and lower limit in the gradation curves of AC 11 and SMA 11 shown in Figure 1 [30], and the Optimum Binder Contents (OBC, by asphalt mixture weight) were determined by the Marshall mix design. Therefore, four types of mixtures were used in this study, as shown in Table 3. The OBC of AC 11-NB, AC 11-PMB, SMA 11-NB and SMA 11-PMB were, respectively, 5.1%, 5.2%, 5.3% and 5.3%.

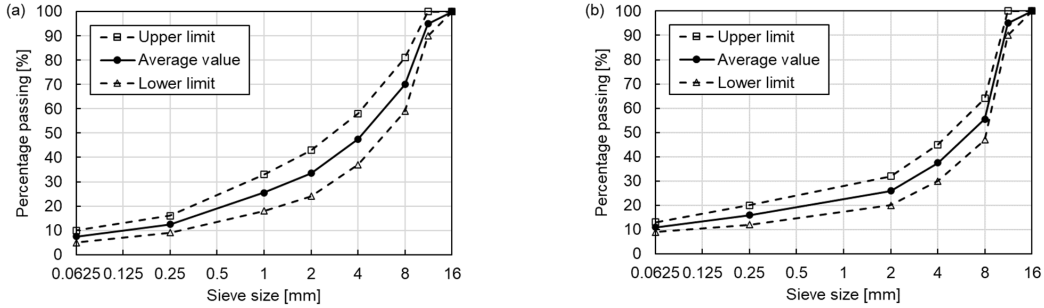

Figure 1. Gradation curves of (**a**) AC 11 and (**b**) SMA 11.

Table 3. Designation of the tested specimens according to selected mixture types and bitumen types.

Mixture Type	Bitumen Type	Designation
AC 11	NB	AC 11-NB
	PMB	AC 11-PMB
SMA 11	NB	SMA 11-NB
	PMB	SMA 11-PMB

The asphalt slabs were compacted using a roller compactor based on the gradation curves and OBC of asphalt mixtures. Then, designated specimens with a diameter of 100 mm and a height of 40 mm were drilled, cut and further used to perform CITT. A total of 16 specimens were prepared (four replicate specimens for each type of mixture). The maximum density of each asphalt mixture was determined by its aggregate density and its bitumen density based on the mathematic procedure method. The void characteristics of specimens are given in Table 4.

Table 4. Maximum density and void characteristics of specimens.

Mixture	Maximum Density [Mg/m^3]	Air Voids Content [%]		Voids in Mineral Aggregate [%]		Voids Filled with Bitumen [%]	
		Value	Standard Deviation	Value	Standard Deviation	Value	Standard Deviation
AC 11-NB	2.753	3.5	0.197	16.9	0.170	79.1	0.947
AC 11-PMB	2.748	2.9	0.314	16.6	0.269	82.8	1.636
SMA 11-NB	2.740	4.4	0.252	18.1	0.216	75.8	1.101
SMA 11-PMB	2.740	3.1	0.296	17.1	0.254	81.6	1.438

2.2.2. Testing Procedure

The CITT was performed using the Nottingham Asphalt Tester (NAT) produced by Cooper Technology Company (Ripley, United Kingdom). The controlled harmonic sinusoidal load was applied without rest period through a servo-controlled double acting pneumatic actuator. The horizontal deformation was detected by two Linear Variable Differential Transformers (LVDT). The sets of frequencies and temperatures were, respectively, 10 Hz, 5 Hz, 3 Hz, 1 Hz, 0.3 Hz, 0.1 Hz and −15 °C, −10 °C, 0 °C, 15 °C, 30 °C for each test. The applied load ensured that the tested samples were in the linear viscoelastic range as the initial horizontal strain was in a range between 50 με to 100 με for each temperature and frequency. This research presents the average results deriving from the testing of four replicate specimens.

2.3. Master Curve Construction

2.3.1. Master Curve Models

SLS Model

The SLS model used in the MEPDG is one of the most popular models used to describe the rheological properties of asphalt mixture. The SLS model is given by Equation (1).

$$\log(|E^*|) = \delta + \frac{\alpha}{1 + e^{\beta - \gamma \cdot \log(f_r)}} \quad (1)$$

where $|E^*|$ is the dynamic modulus, f_r is the frequency at the reference temperature of 15 °C in this research, and δ, α, β and γ are the fitting parameters. δ and $\delta + \alpha$ represent the minimum and maximum values of $|E^*|$, respectively. β and γ describe the shape of the SLS model as depicted in Figure 2.

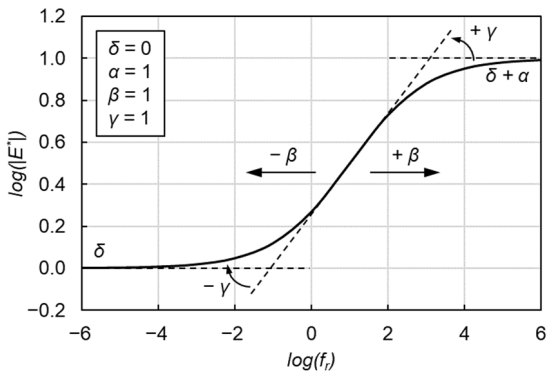

Figure 2. Graphical interpretation of SLS model.

GLS Model

The SLS model provides an excellent fit to symmetric experimental data points, but it cannot acceptably fit non-symmetric curves. Therefore, the use of a GLS model was recommended by Rowe et al., as it is the general form of sigmoidal function applicable to asymmetric curves [33] as given by Equation (2).

$$\log(|E^*|) = \delta' + \frac{\alpha'}{\left[1 + \lambda \cdot e^{\beta' - \gamma' \cdot \log(f_r)}\right]^{\frac{1}{\lambda}}} \quad (2)$$

where δ', α', β', γ' and λ are the fitting parameters. λ characterizes the asymmetric characteristics shown in Figure 3. δ' and $\delta' + \alpha'$ represent the minimum and maximum values of $|E^*|$, respectively. β' and γ' describe the shape of the GLS model.

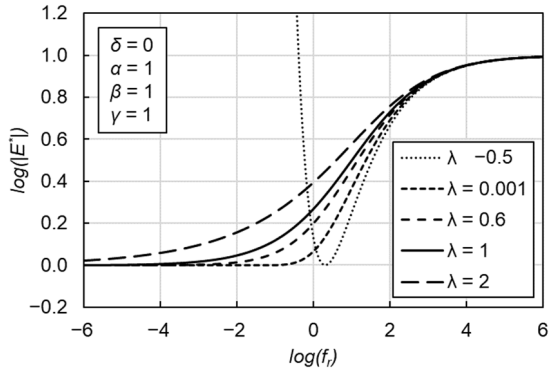

Figure 3. Graphical interpretation of the role of λ coefficient in GLS model.

CAM Model

The CAM model given by Equation (3) can also satisfactorily describe the viscoelastic properties of asphalt mixtures.

$$|E^*| = E_e^* + \frac{E_g^* - E_e^*}{\left[1 + \left(\frac{f_c}{f_r}\right)^v\right]^{w/v}} \tag{3}$$

where E_e^* is the equilibrium modulus representing the minimum modulus, E_g^* is the glassy modulus representing maximum asymptotic modulus, f_c is the location parameter with dimensions of frequency, v and w are fitting parameters and describe the shape of the model as shown in Figure 4.

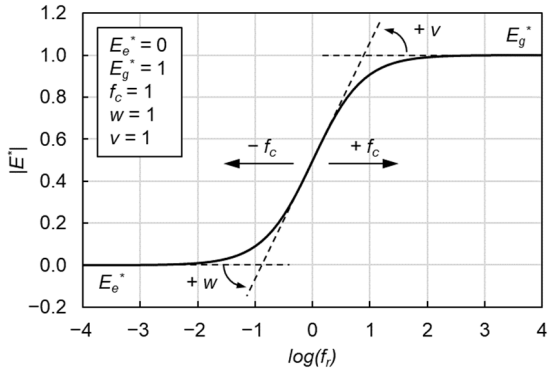

Figure 4. Graphical interpretation of CAM model.

2.3.2. Shift Factor Equations

The shift factor describes the temperature dependency of the dynamic modulus and the general form is given in Equation (4). It can be used to shift the dynamic modulus at different test temperatures to the reduced frequency of the master curve based on the reference temperature of 15 °C.

$$f_r = f \cdot \alpha_T \tag{4a}$$

$$\log(f_r) = \log(f) + \log(\alpha_T) \tag{4b}$$

Five commonly used shift factor equations were adopted in this research, which were the log-linear equation, quadratic polynomial equation, Arrhenius equation, WLF equation and Kaelble equation.

Log-Linear Equation

The log-linear equation is one of the most popular temperature-shifting methods for asphalt mixtures. Christensen and Anderson [11] suggested that below 0 °C, $log(\alpha_T)$ varies linearly with temperature for many binders, and this same relationship has been deemed suitable for asphalt mixture at low to intermediate temperatures [34]. The log-linear equation for calculating the shift factor is:

$$\log(\alpha_T) = C \cdot (T - T_r) \tag{5}$$

where α_T is the shift factor, T is the temperature, T_r is the reference temperature (15 °C), C is the constant which is determined by analysis of the experimental data.

Quadratic Polynomial Equation

The quadratic polynomial equation can well fit the shift factors over a wide range of temperatures, and is expressed as:

$$\log(\alpha_T) = a \cdot (T - T_r) + b \cdot (T - T_r)^2 \tag{6}$$

where a and b are regression parameters.

Arrhenius Equation

The Arrhenius equation for calculating the shift factor is presented in Equation (7):

$$\log(\alpha_T) = C' \cdot \left(\frac{1}{T} - \frac{1}{T_r}\right) = \frac{0.4347 \cdot E_a}{R} \cdot \left(\frac{1}{T} - \frac{1}{T_r}\right) \tag{7}$$

where C' is a constant, E_a is the activation energy (J/mol) and R is the ideal gas constant (8.314 J/mol·K). The Arrhenius equation has only one constant to be determined and can describe the behaviour of the material below T_g [16].

WLF Equation

The WLF equation is widely used to describe the relationship between shift factor and temperature above T_g and thereby assess the shift factor of asphalt mixtures:

$$\log(\alpha_T) = \frac{-C_1 \cdot (T - T_r)}{C_2 + (T - T_r)} \tag{8}$$

where C_1 and C_2 are two regression parameters.

Kaelble Equation

The Kaelble equation is a modification of the WLF equation and can describe the relationship between shift factor and temperature below T_g as given in Equation (9).

$$\log(\alpha_T) = \frac{-C_1' \cdot (T - T_r)}{C_2' + |T - T_r|} \tag{9}$$

where C_1' and C_2' are two regression parameters.

2.3.3. Fitting Procedure

To construct the master curves deriving from the experimental data, the nonlinear least squares regression analysis was integrated in the Microsoft Excel Solver tool. The Sum

of Square Error (*SSE*) between measured values after shifting, $|E^*|_{measured}$, and predicted values, $|E^*|_{predicted}$, as shown in Equation (10) was used for the fitting procedure.

$$SSE = \sum \frac{\left(|E^*|_{measured} - |E^*|_{predicted}\right)^2}{\left(|E^*|_{measured}\right)^2} \quad (10)$$

To define the optimal results of master curves, the coefficients of the models and shift factor equations were fitted to minimize *SSE*. The constraint range of variables was not defined due to well fitting results for the cases. The selection of solving method was GRG Nonlinear. Furthermore, the same initial values of fitting parameters were used for each fitting procedure.

2.4. Goodness of Fit Statistics

The standard error ratio and coefficient of determination (R^2) were used to evaluate the goodness of fit between measured and predicted values. The standard error of estimation and standard error of deviation are defined as follows [35]:

$$S_e = \sqrt{\frac{\sum(Y - \hat{Y})^2}{(n-k)}} \quad (11)$$

$$S_y = \sqrt{\frac{\sum(Y - \overline{Y})^2}{(n-1)}} \quad (12)$$

where S_e is the standard error of estimation, S_y is the standard error of deviation, n is sample size, k is the number of independent variables, Y is the measured value, $\hat{Y}$ is the predicted value and $\bar{Y}$ is the average value of measured values. The standard error ratio is defined as S_e/S_y. R^2 is determined as follows:

$$R^2 = 1 - \frac{(n-k)}{(n-1)} \cdot \left(\frac{S_e}{S_y}\right)^2 \quad (13)$$

Lower S_e/S_y and higher R^2 values indicate better goodness between predicted and measured data. Based on the criteria of the goodness of fit from previous research [36], S_e/S_y and R^2 of this research are lower than 0.35 and higher than 0.90, respectively, which indicates that all results have a good fit.

3. Results and Discussion

3.1. Dynamic Modulus Master Curve

The fitting results of master curves are presented in Figure 5, where red represents the SLS model, blue represents the GLS model and green represents the CAM model, moreover, circle markers, square markers, triangle markers, diamond markers and crosses represent the log-linear equation, the polynomial equation, the Arrhenius equation, the WLF equation and the Kaelble equation, respectively. The results of the three model fits are similar for the four types of asphalt mixtures. The differences appear in the various shift factor equations. No matter at high or low reduced frequency, the dynamic modulus values fitted by the log-linear equation, Arrhenius equation and Kaelble equation are bigger than the ones fitted by the polynomial equation and WLF equation. The fitting parameters of the log-linear equation and the Kaelble equation are similar, and the fitting parameters of the polynomial function and the WLF equation are very close.

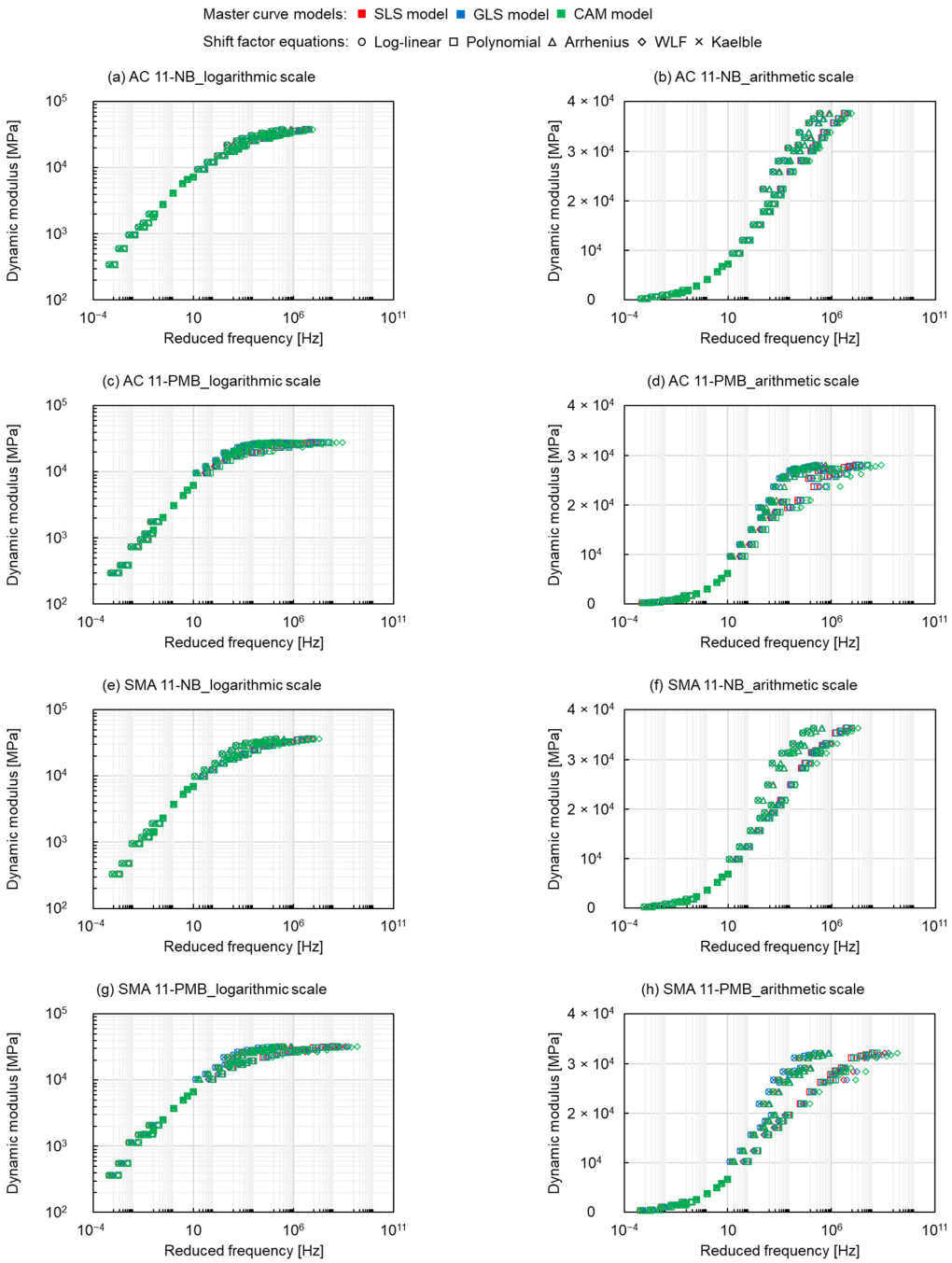

Figure 5. Dynamic modulus master curves of (**a**) and (**b**) AC 11-NB, (**c**) and (**d**) AC 11-PMB, (**e**) and (**f**) SMA 11-NB and (**g**) and (**h**) SMA 11-PMB.

Figure 6 shows the changes in shift factors with temperature, where the colour and shape of the marker represent the same master curve models and shift factor equations as in Figure 5. The curves of the log-linear equation, Arrhenius equation and Kaelble equation are relatively close and show a linear shape, while the curves of the polynomial equation and the WLF equation are similar and more curved than the former ones. This indicates that the polynomial equation and the WLF equation shift the curve more to the right at high reduced frequency and more to the left at low reduced frequency, as shown in Figure 5, resulting in the higher dynamic modulus values fitted by the log-linear equation, the Arrhenius equation and the Kaelble equation. Meanwhile, the difference in the shift factor of the PMB asphalt mixtures is more obvious than the one of the NB asphalt mixtures, and the SMA mixtures have a more pronounced effect on the difference between shift factors than the AC mixtures. This indicates that the PMB and the SMA mixtures are more sensitive to the shift factor equations. This can be explained considering that the different cross-linked structures of the NB and the PMB and the different skeleton structures of the SMA and the AC mixtures lead to the distinction in the mechanical response of the asphalt mixtures, which causes the difference in the shift factor equations on the modelling of dynamic modulus.

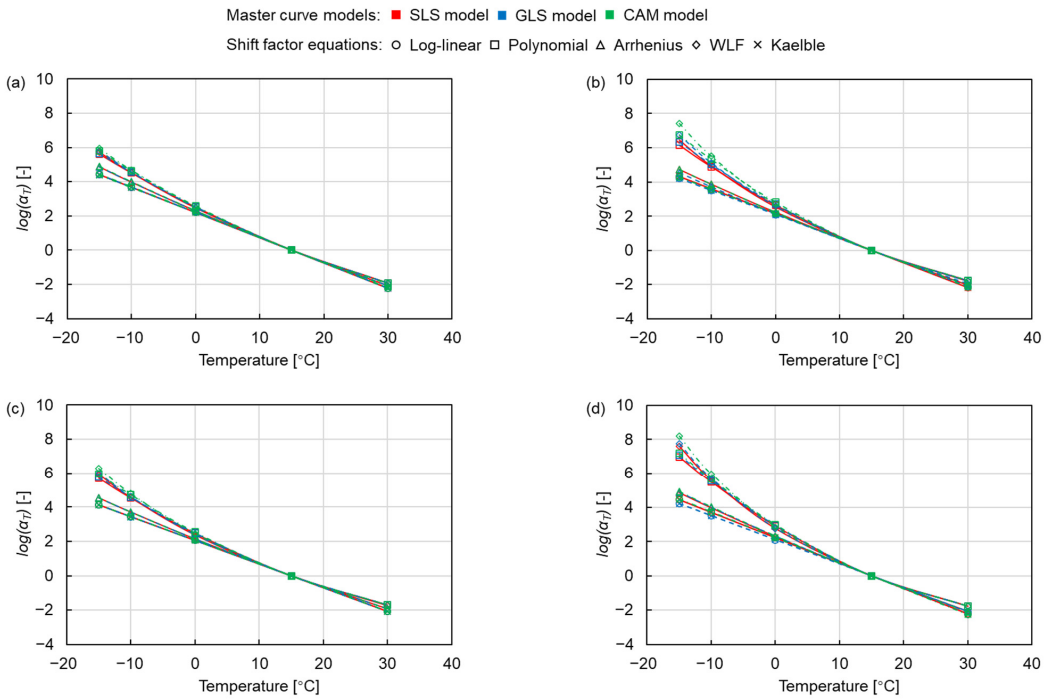

Figure 6. Shift factors of (**a**) AC 11-NB, (**b**) AC 11-PMB, (**c**) SMA 11-NB and (**d**) SMA 11-PMB.

Figure 7 presents the modelling values of the dynamic modulus at the reduced frequency of 10^4 Hz (T_r = 15 °C) for three master curve models and five shift factor equations. The distinction of dynamic modulus is not greatly affected by the master curve models. The influence of the five shift factor equations can be divided into two categories. The first category including the log-linear equation, Arrhenius equation and Kaelble equation, shows a higher value in dynamic modulus. Another category including the polynomial equation and the WLF equation exhibits a lower dynamic modulus of mixtures. The dynamic modulus of the former category is on average about 23% higher than that of the latter one.

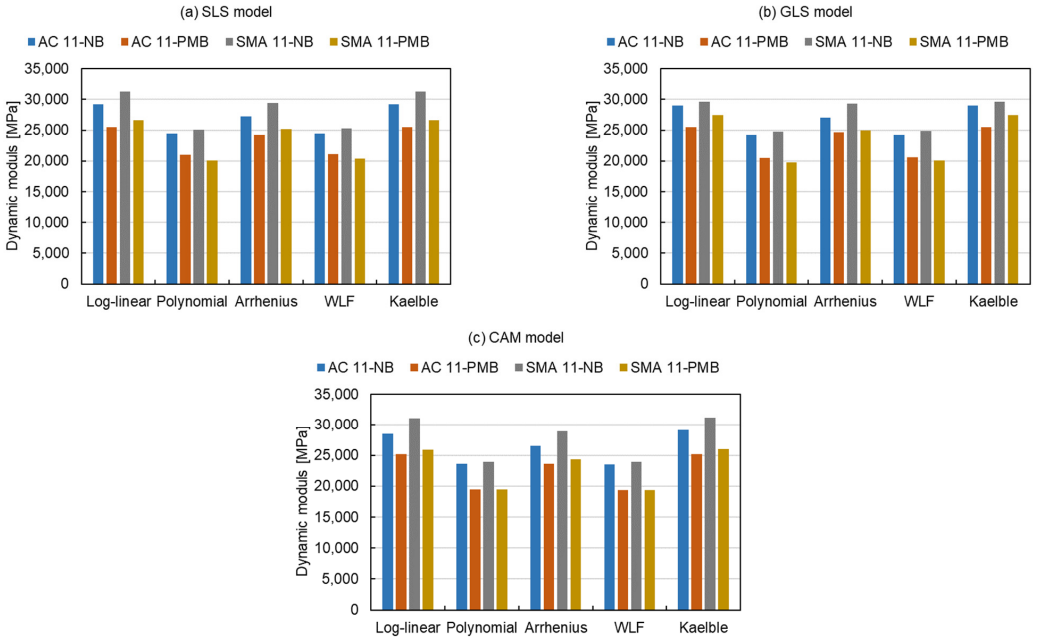

Figure 7. Modelling values of dynamic modulus at the reduced frequency of 10^4 Hz (T_r = 15 °C).

The modelling values of the dynamic modulus at the reduced frequency of 10^{-2} Hz (T_r = 15 °C) are given in Figure 8 and have a similar trend as the results at 10^4 Hz, which can also be divided into the same two categories. The former one has an average 19% higher dynamic modulus than the latter one. The results of Figures 7 and 8 indicate that the modelling values of dynamic modulus fitted by the log-linear equation, Arrhenius equation and Kaelble equation are approximately 20% higher than the ones fitted by the polynomial equation and the WLF equation, both at high and low reduced frequencies.

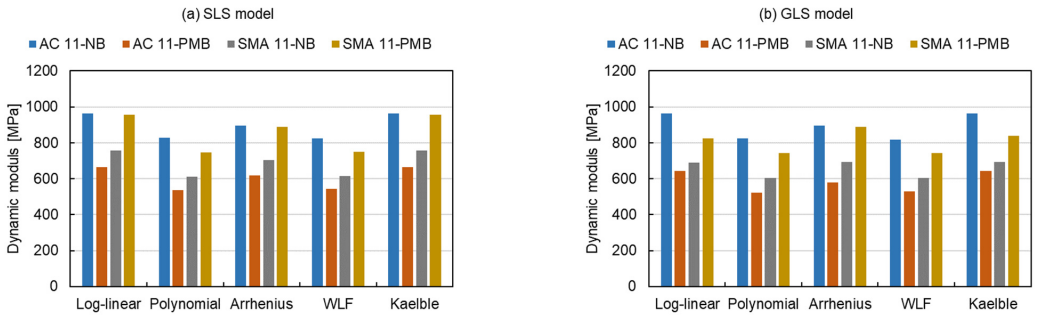

Figure 8. *Cont.*

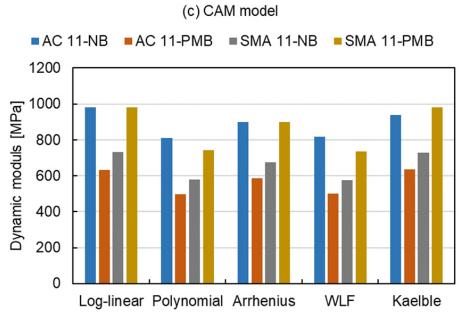

Figure 8. Modelling values of dynamic modulus at the reduced frequency of 10^{-2} Hz (T_r = 15 °C).

3.2. Error Analysis

3.2.1. Absolute Error

After comparing the master curves constructed by different models, the error analysis of each model and shift factor equation was carried out. The absolute errors of the dynamic modulus between the modelling values fitted by the three master curve models and the five shift factor equations, and the measured values are shown in Figure 9, where the colour and shape of the marker represent the same master curve models and shift factor equations as in Figure 5. The absolute error is small at high temperatures and relatively big at the temperature range between −15 °C to 0 °C for all mixtures. The maximum absolute error at −10 °C can be explained by the connection between viscoelastic stage and elastic stage, which in turn changes the mechanical response of mixtures. As the temperature continues to decrease (the reduced frequency increases), the absolute error becomes smaller again at −15 °C (higher reduced frequency). This result is attributed to the elastomer of asphalt mixture at very low temperature, resulting in a constant dynamic modulus.

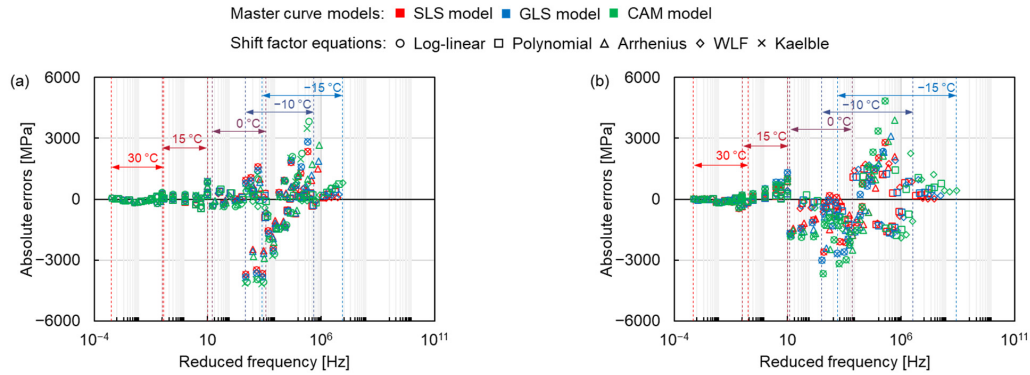

Figure 9. *Cont.*

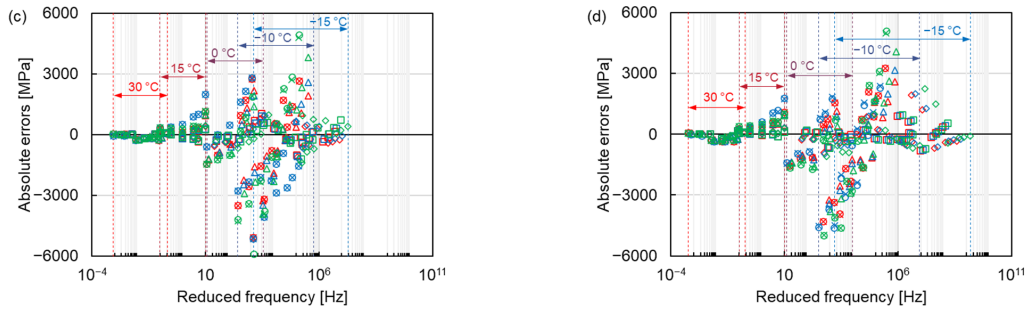

Figure 9. Absolute errors of (**a**) AC 11-NB, (**b**) AC 11-PMB, (**c**) SMA 11-NB and (**d**) SMA 11-PMB.

The shift factor equation has more influence on the Sum of Absolute Error (*SAE*) than the master curve models, as shown in Figure 10. There are 15 master curve model-shift factor equation combinations for 4 types of mixtures resulting in a total of 60 fitting procedures. The average *SAE* of the fitting procedures with the controlled fitting condition are used for comparing the distinctions of the master curve models, shift factor equations and asphalt mixture types as expressed in Equation (14).

$$\overline{SAE} = \frac{\sum SAE(\text{master curve models, shift factor equations, asphalt mixture types})}{n} \quad (14)$$

where $\overline{SAE}$ is the average *SAE* and *n* is the number of fitting procedures. The $\overline{SAE}$ of the fitting procedures with the SLS model, the GLS model and the CAM model are 21,598 MPa, 23,851 MPa and 27,244 MPa, respectively. This indicates that the SLS model has the smallest absolute error, the CAM model has the largest absolute error and the GLS model is in between. Regarding the shift factor equations, the *SAE* for the log-linear equation and the Kaelble equation are similar and classified as class 1, the *SAE* for the polynomial equation and the WLF equation are close and grouped into class 2 and the value for the Arrhenius equation lies between them as class 3. The absolute error of class 1 is more than twice that of class 2. The results reveal that the SLS model and the polynomial function have the smallest absolute errors in three master curve models and five shift factor equations, respectively. For class 1, the absolute error of SMA mixtures is larger than the one of AC mixtures. Comparing four types of mixtures, the AC 11-PMB has the highest absolute error of class 2.

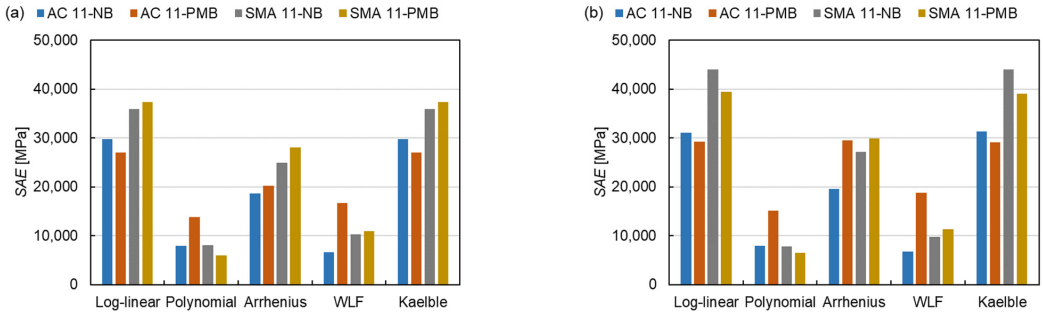

Figure 10. *Cont.*

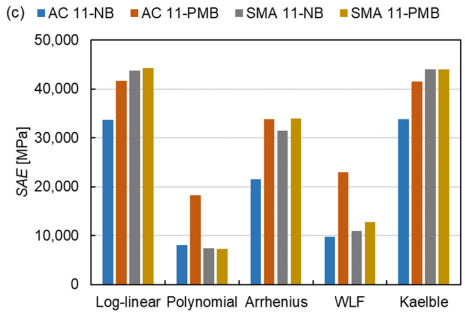

Figure 10. *SAE* of all fitting procedures: (**a**) SLS model, (**b**) GLS model and (**c**) CAM model.

3.2.2. Normalised Square Error

Since the dynamic modulus of asphalt mixtures is distinct at different temperatures and frequencies, it is difficult to compare the error under the same condition over the full frequency range. The normalised square error was analysed to compare different models and shift factor equations at the same condition. From Figure 11, the normalised square error is larger at high temperatures and smaller at low temperatures, contrary to the results of the absolute error, which reflects the error of dynamic modulus at high temperatures. The maximum normalised error appears at the high temperature of 30 °C. As the temperature increases, the asphalt transitions to a viscous flow state, and its dynamic modulus is more obviously affected by the loading conditions, becoming unstable, resulting in an increasing normalised square error. Furthermore, the distinction between different asphalt mixtures can also be found. The normalised square error for asphalt mixtures containing PMB is relatively higher than the one for asphalt mixtures containing NB. Compared to the NB, the polymer molecular in the PMB also provides a portion of the stiffness modulus for the asphalt mixture. The complex connection between the polymer molecular and the asphalt binder, such as the composition and distribution of the polymer molecular in the asphalt binder, determines the stiffness modulus of the asphalt mixture [37,38]. Therefore, the dynamic modulus change of the asphalt mixture containing PMB is more complicated than that of the NB asphalt mixture, resulting in a larger error. Otherwise, the SMA mixtures have a higher normalised square error than the AC mixtures. The SMA mixture contains more coarse aggregates than the AC mixture, leading to more particle angularity. The greater the particle angularity, the higher the stiffness modulus of the asphalt mixture [39]. Thus, the change of the dynamic modulus of the SMA mixture is more complex than that of the AC mixture, resulting in a larger error.

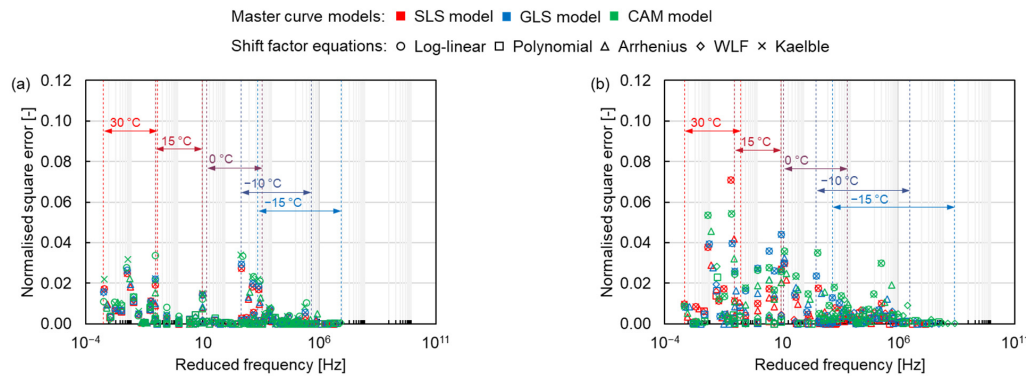

Figure 11. *Cont.*

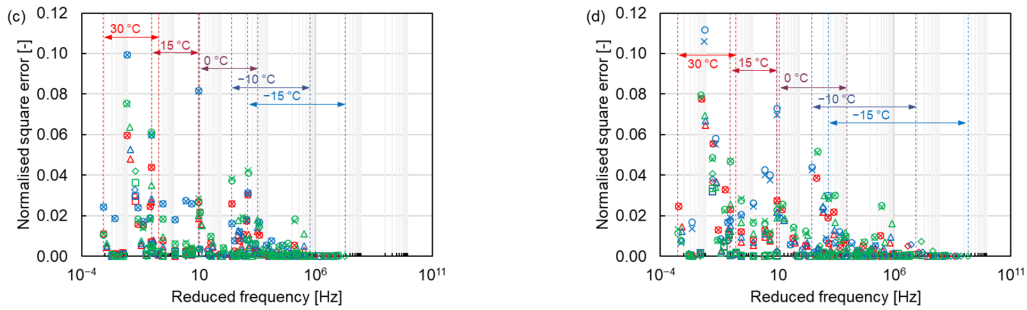

Figure 11. Normalised square errors of (**a**) AC 11-NB, (**b**) AC 11-PMB, (**c**) SMA 11-NB and (**d**) SMA 11-PMB.

The *SSE* for different models has the same trend as the *SAE* as shown in Figure 12. The same approach as *SAE* is used for *SSE* as shown in Equation (15).

$$\overline{SSE} = \frac{\sum SSE(\text{master curve models, shift factor equations, asphalt mixture types})}{n} \quad (15)$$

where $\overline{SSE}$ is the average *SSE*. The $\overline{SSE}$ of the SLS model is 0.20, which is also smaller than those of the GLS model (0.25) and the CAM model (0.26). Based on *SSE* values, five shift factor equations are divided into three classes, the same as the classification in Section 3.2.1. The $\overline{SSE}$ of class 1 is around five times that of class 2. The results show that the SLS model and the polynomial function have the smallest normalised square errors in the three master curve models and the five shift factor equations, respectively. The mixtures containing PMB have a lower *SSE* than the mixtures containing NB, which indicates that the fit of the model for NB is better than the one for PMB, which can be explained by the effect of the PMB structure on the dynamic modulus of the asphalt mixture.

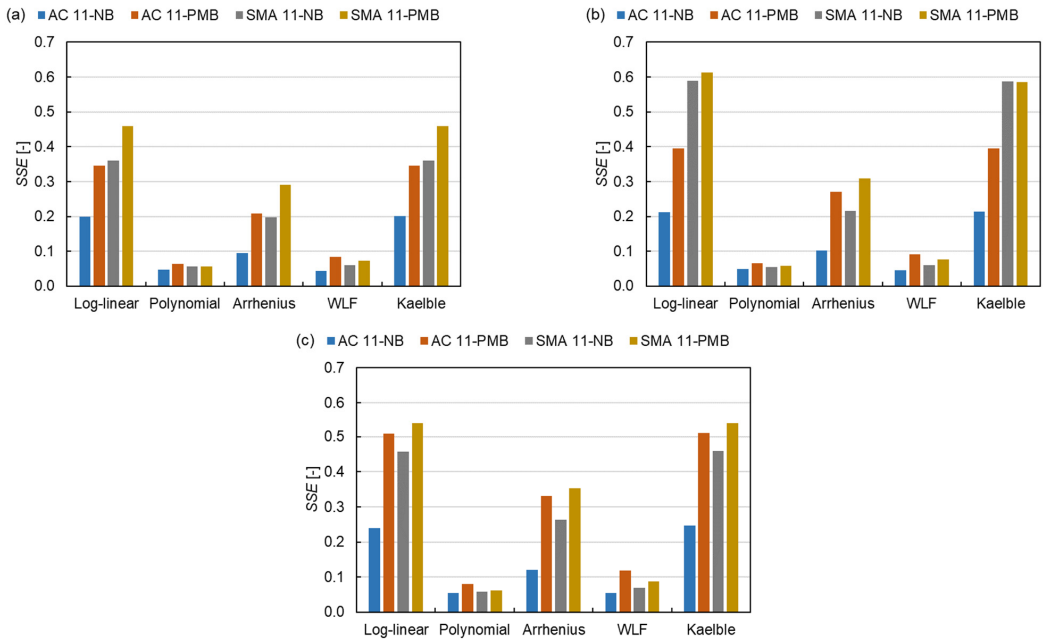

Figure 12. *SSE* of all fitting procedures: (**a**) SLS model, (**b**) GLS model and (**c**) CAM model.

3.3. Goodness of Fit

The S_e/S_y and R^2 are used to evaluate the quality of the model. From Figure 13, the SLS model has the smallest average value of S_e/S_y (0.0853) and the highest average value of R^2 (0.9915) compared to the GLS model (0.0951, 0.9906) and the CAM model (0.1090, 0.9859). Otherwise, the average values of S_e/S_y and R^2 for the polynomial equation are the smallest (0.0394) and the largest (0.9982), respectively. While the Kaelble equation has the biggest average value of S_e/S_y (0.1441) and the smallest average value of R^2 (0.9810). These results indicate that the SLS model and the polynomial function have the best goodness-of-fit in the three master curve models and the five shift factor equations, respectively. Among the 15 kinds of fits, the NB asphalt mixture shows an overall better goodness-of-fit than the PMB asphalt mixture. This indicates that the dynamic modulus of PMB asphalt mixture is affected by more factors than that of NB asphalt mixture due to the effect of polymer molecular in the binder.

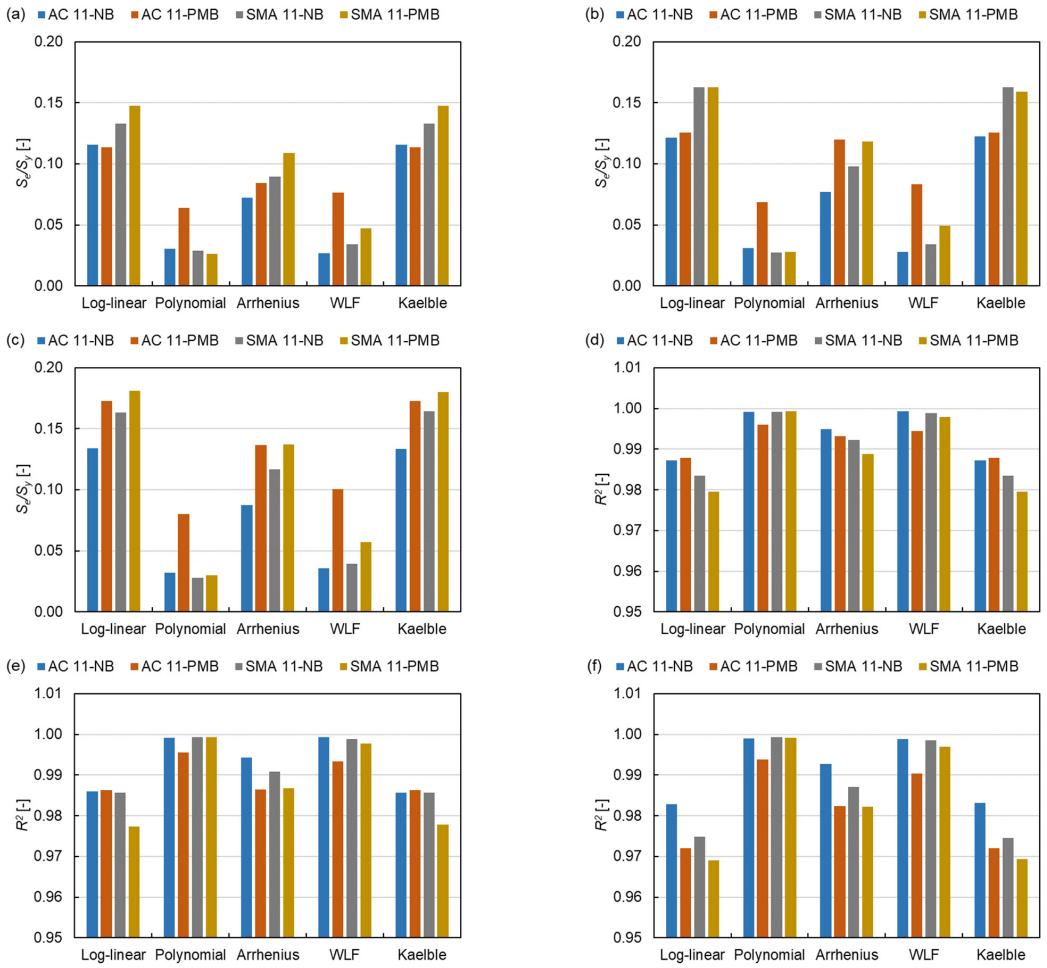

Figure 13. S_e/S_y of (**a**) SLS model, (**b**) GLS model and (**c**) CAM model and R^2 of (**d**) SLS model, (**e**) GLS model and (**f**) CAM model.

3.3.1. Master Curve Models

The comparison of master curve models between measured dynamic modulus and predicted dynamic modulus is shown in Figure 14, where blue represents AC 11-NB, orange represents AC 11-PMB, gray represents SMA 11-NB and yellow represents SMA 11-PMB, and the shape of the marker represents the same shift factor equation as in Figure 5. All the models fit the data satisfactorily according to the goodness-of-fit ranking criteria. The SLS model had the lowest S_e/S_y of 0.0925 and the highest R^2 of 0.9916, which indicates that this model shows a better goodness-of-fit than the GLS model and the CAM model under the test conditions of this study. The S_e/S_y and R^2 of the CAM model were, respectively, 28.2% higher and 0.5% lower than the respective parameters of the SLS model, showing the worst correlation in the three models. Therefore, the SLS model with better goodness-of-fit can be considered for modelling the four asphalt mixtures.

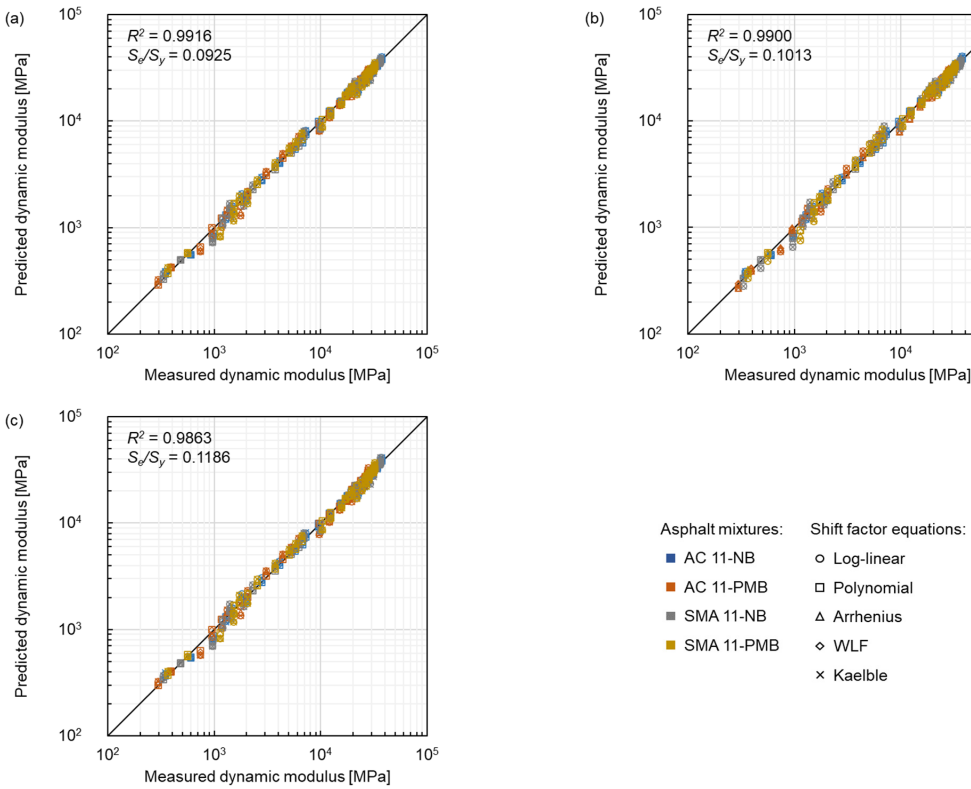

Figure 14. Comparison between measured dynamic modulus and predicted dynamic modulus of three master curve models: (**a**) SLS model, (**b**) GLS model and (**c**) CAM model.

3.3.2. Shift Factor Equations

The comparison between measured dynamic modulus and predicted dynamic modulus related to the selection of shift factor equation is shown in Figure 15, where the colour represents the same type of asphalt mixtures as in Figure 14. Furthermore, circle markers, square markers and triangle markers represent the SLS model, GLS model and CAM model, respectively. The fitting results showed that all the considered five equations had fit the data satisfactorily according to the goodness-of-fit ranking criteria. The $log(\alpha_T)$ of the Kaelble equation showed a linear trend within the test temperature range, the fitting results of the Kaelble equation and the log-linear equation were similar, and the same findings were also shown in the former sections. The quadratic polynomial equation displayed

the best goodness-of-fit with the lowest S_e/S_y of 0.0275 and the highest R^2 of 0.9984. The fitting results of the WLF equation and the quadratic polynomial equation were similar and showed a good fit. The fit related to the Arrhenius equation was in the middle among the five equations. Furthermore, the transform between frequency and temperature was more convenient for the WLF equation than the quadratic polynomial due to the quadratic form. Therefore, the WLF equation was recommended for modelling the dynamic modulus of the asphalt mixtures.

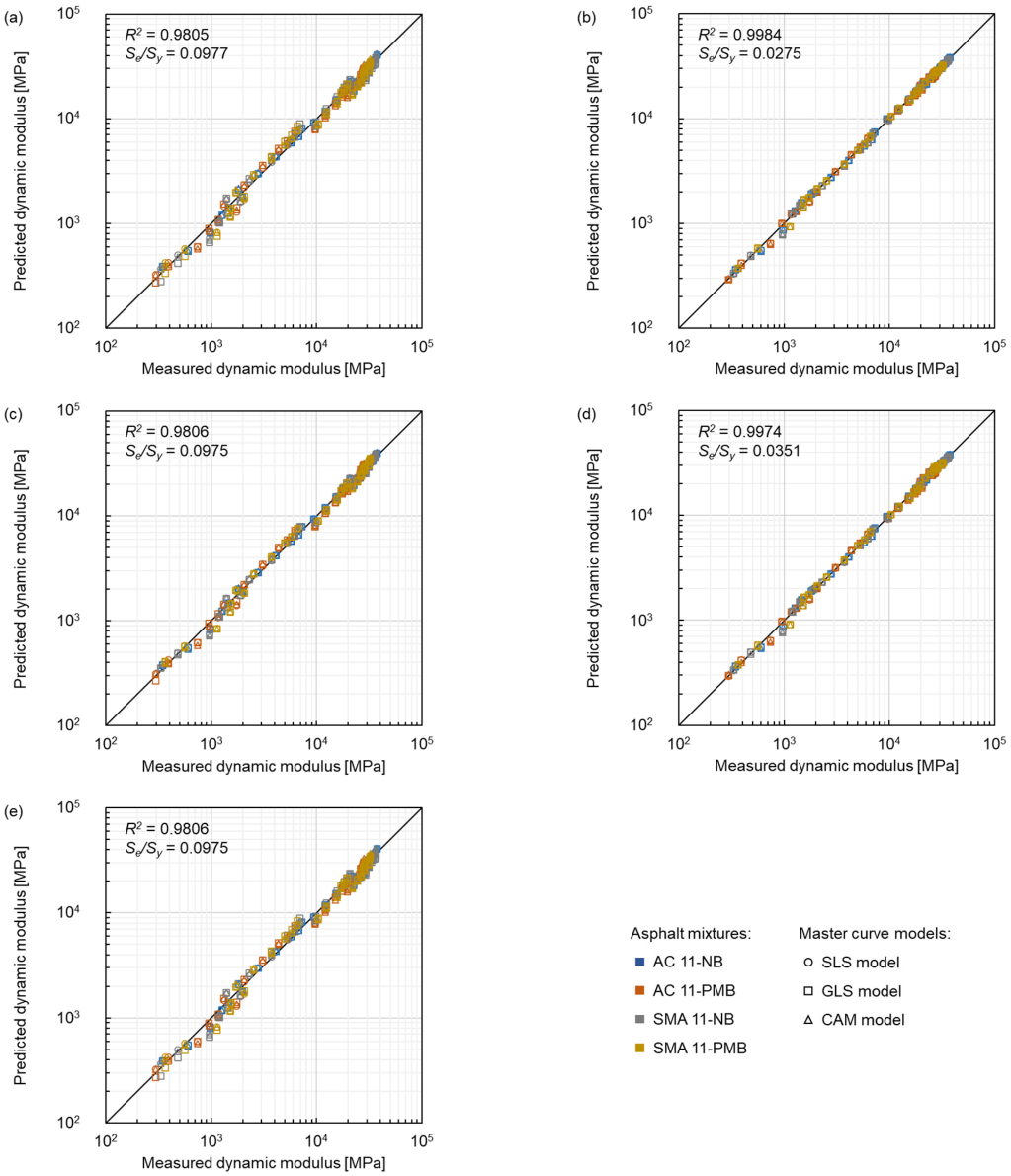

Figure 15. Comparison between measured dynamic modulus and predicted dynamic modulus of five shift factor equations: (**a**) log-linear equation, (**b**) quadratic polynomial equation, (**c**) Arrhenius equation, (**d**) WLF equation and (**e**) Kaelble equation.

3.4. Comparison of Fits

In this study, four indicators of absolute error, normalised square error, S_e/S_y and R^2 were used to evaluate the fitting quality of the models. The 15 permutations of the three master curve models and five shift factor equations for the four types of asphalt mixtures were ranked from good to poor (from 1 to 15), and the index of fitting quality is expressed by Equation (16).

$$I_{fq} = \frac{\overline{A_{ae}}+\overline{A_{nse}}+\overline{A_{S_e/S_y}}+\overline{A_{R^2}}}{4}$$
$$\overline{A_{ae}},\ \overline{A_{nse}},\ \overline{A_{S_e/S_y}}\ and\ \overline{A_{R^2}} = \frac{A_{AC11-NB}+A_{AC11-PMB}+A_{SMA11-NB}+A_{SMA11-PMB}}{4} \quad (16)$$
$$A_{AC11-NB},\ A_{AC11-PMB},\ A_{SMA11-NB}\ and\ A_{SMA11-PMB} = 1,\ 2,\ \ldots,\ 15$$

where I_{fq} is the index of fitting quality, $\bar{A}_{ae}$, $\bar{A}_{nse}$, $\bar{A}_{Se/Sy}$ and $\bar{A}_{R2}$ are the average arrays of absolute error, normalised square error, S_e/S_y and R^2, respectively, $A_{AC\ 11\text{-}NB}$, $A_{AC\ 11\text{-}PMB}$, $A_{SMA\ 11\text{-}NB}$ and $A_{SMA\ 11\text{-}PMB}$ are the arrays of the order in 15 permutations. The average values of sequences are summarised in Table 5. The shift factor equation has a more significant effect on the dynamic modulus modelling than the master curve model. The modelling of the SLS model with the polynomial equation has the best fitting quality, while the result fitted by the CAM model with the Kaelble equation is the worst in this study. Among the five shift factor equations, the polynomial equation has the best fit, followed by the WLF equation. The intertransform between frequency and temperature is more convenient for the WLF equation than the quadratic polynomial due to the quadratic form. Therefore, the SLS model and the WLF equation were recommended for modelling the dynamic modulus of these mixture types.

Table 5. Comparison of fits for three master curve models and five shift factor equations.

Shift Factor Equation	Master Curve Model		
	SLS Model	GLS Model	CAM Model
Log-linear	9.75	12.56	14.00
Polynomial	1.94	2.31	3.44
Arrhenius	6.81	8.50	9.75
WLF	3.31	4.00	6.19
Kaelble	10.75	12.44	14.25

Colour bar of fitting quality: Good (1) Poor (15).

The same method was used to compare the models and how well the models fit different asphalt mixtures. The degree-of-fit for the four types of asphalt mixtures was ranked from good to poor (from 1 to 4) as shown in Table 6. The results indicate that the models have a better fit for asphalt mixtures containing NB than the ones containing PMB. The fitting results of AC mixtures are better than those of SMA mixtures when the bitumen is the same. These results are caused by more impact factors of the PMB asphalt mixture and the SMA mixture on the dynamic modulus.

Table 6. Comparison of fits for different asphalt mixtures.

Mixture Type	Bitumen Type	
	NB	PMB
AC 11	1.45	2.92
SMA 11	2.38	3.25

Colour bar of fitting quality: Good (1) Poor (4).

4. Conclusions

In this study, the reliability of calculation of dynamic modulus using the three master curve models and the five shift factor equations was evaluated by the absolute error, normalised error and the goodness-of-fit encompassing S_e/S_y and R^2 for four types of asphalt mixtures. The conclusions are summarised as follows.

- The selected shift factor equations were more influent with respect to the employed models in determining the final fitting reliability.
- The relationship between $log(\alpha_T)$ and temperature of both the log-linear equation and the Kaelble equation were linear in the testing temperature range. These two shift factor equations had similar goodness-of-fit when extrapolating dynamic modulus master curves.
- Considering the results of absolute error, normalised square error, S_e/S_y and R^2, the combination of the SLS model and the polynomial equation had the best fitting quality index (1.94), while the combination of the CAM model and the Kaelble equation had the worst fitting quality index (14.25). Regarding the different asphalt mixtures, the fitting quality index of AC 11-NB (1.45) was the best, whereas the one of SMA 11-PMB (3.25) was the worst.
- The SLS model showed the best fitting quality and was considered to model the dynamic modulus of the asphalt mixtures most used as surface layer for Norwegian highway within the investigated CITT temperature range.
- Due to better goodness-of-fit and more convenience for temperature and frequency transform, the WLF equation was considered for modelling the dynamic modulus of the asphalt mixtures most adopted in Norway.
- The master curves constructed according to all the models and all shifting techniques were characterized by better goodness-of-fit for the asphalt mixtures containing NB than the ones comprised of PMB due to the effect of PMB structure on the dynamic modulus of the asphalt mixture. The modelling of dynamic modulus master curves for SMA mixtures has a better fit than the one for SMA mixtures because of the influence of more particle angularity on the dynamic modulus of the asphalt mixture. Therefore, the models can be developed further to be suitable for the asphalt mixtures containing the PMB and SMA types of asphalt mixtures.

Author Contributions: Conceptualization, H.C.; methodology, H.C. and D.M.B.; software, H.C.; validation, H.C.; formal analysis, H.C. and X.Z.; investigation, H.C.; resources, I.H.; data curation, H.C.; writing-original draft preparation, H.C.; writing-review and editing, D.M.B., X.Z. and I.H.; visualization, H.C.; supervision, I.H. All authors have read and agreed to the published version of the manuscript.

Funding: This research was funded by China Scholarship Council, grant number 201806950077 and Norwegian University of Science and Technology, grant number K-649105.

Institutional Review Board Statement: Not applicable.

Informed Consent Statement: Not applicable.

Data Availability Statement: Not applicable.

Acknowledgments: This research was supported by the VegDim project of Norwegian Public Roads Administration. The financial support provided by China Scholarship Council (No. 201806950077) and Department of Civil and Environmental Engineering, Norwegian University of Science and Technology (No. K-649105) is acknowledged. The support kindly provided by the laboratory assistants Bent Lervik and Jan Erik Molde is greatly acknowledged.

Conflicts of Interest: The authors declare no conflict of interest.

References

1. NPRA. VegDim. Available online: https://www.vegvesen.no/fag/fokusomrader/forskning-innovasjon-og-utvikling/pagaende-programmer-og-prosjekter/vegdim/ (accessed on 12 March 2022).
2. Bahia, H.U.; Zhai, H.; Onnetti, K.; Kose, S. Non-linear viscoelastic and fatigue properties of asphalt binders. *J. Assoc. Asph. Paving Technol.* **1999**, *68*, 1–34.
3. Lesueur, D.; Gerard, J.F.; Claudy, P.; Letoffe, J.M.; Planche, J.P.; Martin, D. A structure-related model to describe asphalt linear viscoelasticity. *J. Rheol.* **1996**, *40*, 813–836. [CrossRef]
4. NCHRP. *Guide for Mechanistic-Empirical Design of New and Rehabilitated Pavement Structures*; National Cooperative Highway Research Program 1-37A: Washington, DC, USA, 2004.
5. Schwartz, C.W.; Gibson, N.; Schapery, R.A. Time-temperature superposition for asphalt concrete at large compressive strains. *Transp. Res. Rec.* **2002**, *1789*, 101–112. [CrossRef]
6. Chehab, G.; Kim, Y.; Schapery, R.; Witczak, M.; Bonaquist, R. Time-temperature superposition principle for asphalt concrete with growing damage in tension state. *J. Assoc. Asph. Paving Technol.* **2002**, *71*, 559–593.
7. Pellinen, T.K.; Witczak, M.W.; Bonaquist, R.F. Asphalt mix master curve construction using sigmoidal fitting function with non-linear least squares optimization. In *Recent Advances in Materials Characterization and Modeling of Pavement Systems*; American Society of Civil Engineers: Reston, VA, USA, 2004; pp. 83–101.
8. Pellinen, T.K.; Witczak, M.W.; Marasteanu, M.; Chehab, G.; Alavi, S.; Dongre, R. *Stress Dependent Master Curve Construction for Dynamic (Complex) Modulus*; Asphalt Paving Technology: Association of Asphalt Paving Technologists-Proceedings of the Technical Sessions; Association of Asphalt Paving Technologist: Colorado Springs, CO, USA, 2002; pp. 281–309.
9. Rowe, G.; Baumgardner, G.; Sharrock, M. Functional forms for master curve analysis of bituminous materials. In *Advanced Testing and Characterization of Bituminous Materials, Two Volume Set*; CRC Press: London, UK, 2009; pp. 97–108.
10. Zhang, F.; Wang, L.; Li, C.; Xing, Y. Predict the Phase Angle Master Curve and Study the Viscoelastic Properties of Warm Mix Crumb Rubber-Modified Asphalt Mixture. *Materials* **2020**, *13*, 5051. [CrossRef]
11. Christensen, D.W.; Anderson, D.A. Interpretation of dynamic mechanical test data for paving grade asphalt cements (with discussion). *J. Assoc. Asph. Paving Technol.* **1992**, *61*, 67–116.
12. Marasteanu, M.; Anderson, D. *Improved Model for Bitumen Rheological Characterization*; Eurobitume workshop on performance related properties for bituminous binders; European Bitumen Association: Brussels, Belgium, 1999.
13. Wathne, P. *Evaluation of Different Models for Construction of Master Curves for Dynamic E-module for Asphalt Materials*; Norwegian University of Science and Technology: Trondheim, Norway, 2020.
14. CholewiŃSka, M.; IwaŃSki, M.; Mazurek, G. The Impact of Ageing on the Bitumen Stiffness Modulus Using the Cam Model. *Balt. J. Road Bridge Eng.* **2018**, *13*, 34–39. [CrossRef]
15. Williams, M.L.; Landel, R.F.; Ferry, J.D. The temperature dependence of relaxation mechanisms in amorphous polymers and other glass-forming liquids. *J. Am. Chem. Soc.* **1955**, *77*, 3701–3707. [CrossRef]
16. Hutcheson, S.; McKenna, G. The measurement of mechanical properties of glycerol, m-toluidine, and sucrose benzoate under consideration of corrected rheometer compliance: An in-depth study and review. *J. Chem. Phys.* **2008**, *129*, 074502. [CrossRef]
17. O'Connell, P.A.; McKenna, G.B. Arrhenius-type temperature dependence of the segmental relaxation below T g. *J. Chem. Phys.* **1999**, *110*, 11054–11060. [CrossRef]
18. Kaelble, D.H. *Computer Aided Design of Polymers and Composites*; CRC Press: New York, NY, USA, 1985; Volume 7.
19. Rowe, G.M.; Sharrock, M.J. Alternate Shift Factor Relationship for Describing Temperature Dependency of Viscoelastic Behavior of Asphalt Materials. *Transp. Res. Rec. J. Transp. Res. Board* **2011**, *2207*, 125–135. [CrossRef]
20. Laukkanen, O.-V.; Winter, H.H. The dynamic fragility and apparent activation energy of bitumens as expressed by a modified Kaelble equation. *J. Non-Cryst. Solids* **2018**, *499*, 289–299. [CrossRef]
21. Forough, S.A.; Nejad, F.M.; Khodaii, A. A comparative study of temperature shifting techniques for construction of relaxation modulus master curve of asphalt mixes. *Constr. Build. Mater.* **2014**, *53*, 74–82. [CrossRef]
22. Bohn, M.A. The Connection Between the Parameters of WLF Equation and of Arrhenius Equation. *Propellants Explos. Pyrotech.* **2019**, *44*, 696–705. [CrossRef]
23. Garcia, G.; Thompson, M. *HMA Dynamic Modulus Predictive Models (A Review)*; IDEALS: Urbana, IL, USA, 2007.
24. Angelone, S.; Borghi, M.; Casaux, M.C.; Martinez, F. Evaluation of Different Procedures and Models for the Construction of Dynamic Modulus Master Curves of Asphalt Mixtures. In Proceedings of the International Conferences on the Bearing Capacity of Roads Railways and Airfields, Trondheim, Norway, 25–27 June 2013; pp. 647–657.
25. Tavassoti-Kheiry, P.; Boz, I.; Chen, X.; Solaimanian, M. Application of ultrasonic pulse velocity testing of asphalt concrete mixtures to improve the prediction accuracy of dynamic modulus master curve. In Proceedings of the Airfield and Highway Pavements, Philadelphia, PA, USA, 13 August 2017.
26. Kim, M.; Mohammad, L.N.; Elseifi, M.A. Effects of various extrapolation techniques for abbreviated dynamic modulus test data on the MEPDG rutting predictions. *J. Mar. Sci. Technol.* **2015**, *23*, 12.
27. Yildirim, Y. Polymer modified asphalt binders. *Constr. Build. Mater.* **2007**, *21*, 66–72. [CrossRef]
28. *CEN, EN 1426:2015*; Bitumen and Bitumen Binders-Determination of Needle Penetration. European Committee for Standardization: Brussels, Belgium, 2015.

29. *CEN, EN 1427:2015*; Bitumen and Bituminous Binders-Determination of the Softening Point-Ring and Ball Method. European Committee for Standardization: Brussels, Belgium, 2015.
30. Arnevik, R.E.; Uthus, N.S.; Aurstad, J.; Aksnes, J.; Jørgensen, T. *Guidelines Asphalt 2019*; Norwegian Public Roads Administration: Oslo, Norway, 2019.
31. *CEN, EN 1097-1:2011*; Tests for Mechanical Physical Properties of Aggregates-Part 1: Determination of the Resistance to Wear (Micro-Deval). European Committee for Standardization: Brussels, Belgium, 2011.
32. *CEN, EN 1097-2:2020*; Tests for Mechanical and Physical Properties of Aggregates-Part 2: Methods for the Determination of Resistance to Fragmentation. European Committee for Standardization: Brussels, Belgium, 2020.
33. Rowe, G. Phase angle determination and interrelationships within bituminous materials. In *Advanced Testing and Characterization of Bituminous Materials, Two Volume Set*; CRC Press: London, UK, 2009; pp. 59–68.
34. Fan, B.; Kazmer, D.O. Low-temperature modeling of the time-temperature shift factor for polycarbonate. *Adv. Polym. Technol.* **2005**, *24*, 278–287. [CrossRef]
35. Tran, N.; Hall, K. Evaluating the predictive equation in determining dynamic moduli of typical asphalt mixtures used in Arkansas. *SAGE* **2005**, *2210*, 7.
36. Witczak, M.W. *Simple Performance Test for Superpave Mix Design*; Transportation Research Board: Washington, DC, USA, 2002; Volume 465.
37. Veeraragavan, A. Dynamic mechanical characterization of asphalt concrete mixes with modified asphalt binders. *Mater. Sci. Eng. A* **2011**, *528*, 6445–6454.
38. Dong, F.; Zhao, W.; Zhang, Y.; Wei, J.; Fan, W.; Yu, Y.; Wang, Z. Influence of SBS and asphalt on SBS dispersion and the performance of modified asphalt. *Constr. Build. Mater.* **2014**, *62*, 1–7. [CrossRef]
39. Yu, H.; Shen, S. Impact of aggregate packing on dynamic modulus of hot mix asphalt mixtures using three-dimensional discrete element method. *Constr. Build. Mater.* **2012**, *26*, 302–309. [CrossRef]

APPENDIX C – PAPER III

Chen, Hao*; Saba, Rabbira Garba; Liu, Gang; Barbieri, Diego Maria; Zhang, Xuemei; Hoff, Inge

Influence of material factors on the determination of dynamic moduli and associated prediction models for different types of asphalt mixtures.

Published in the Journal of Construction and Building Materials, 365, 130134, 2023.

Construction and Building Materials 365 (2023) 130134

Contents lists available at ScienceDirect

Construction and Building Materials

journal homepage: www.elsevier.com/locate/conbuildmat

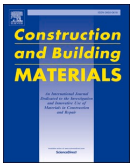

Influence of material factors on the determination of dynamic moduli and associated prediction models for different types of asphalt mixtures

Hao Chen [a,*], Rabbira Garba Saba [b], Gang Liu [c], Diego Maria Barbieri [a,d], Xuemei Zhang [a], Inge Hoff [a]

[a] Department of Civil and Environmental Engineering, Norwegian University of Science and Technology, Høgskoleringen 7A, 7491 Trondheim, Norway
[b] Norwegian Public Roads Administration, Abels Gate 5, 7030 Trondheim, Norway
[c] School of Materials Science and Engineering, Wuhan University of Technology, 122 Luoshi Road, 430070 Wuhan, China
[d] Department of Mechanical and Structural Engineering and Materials Science, University of Stavanger, Kristine Bonnevies vei 22, 4021 Stavanger, Norway

ARTICLE INFO

Keywords:
Asphalt mixture
Dynamic modulus
Prediction model
Grey relational analysis
Cyclic indirect tensile tests

ABSTRACT

In a Mechanistic-Empirical (ME) pavement design system, the dynamic modulus is used to characterise asphalt mixtures, which are affected by many factors including environmental conditions and material properties. This study examined twenty types of asphalt mixtures containing nine types of bituminous binders that are commonly used for construction of road pavements in Norway. The objective of the study was to investigate the relationship between material factors and dynamic modulus. The dynamic moduli of asphalt mixtures were experimentally determined employing cyclic indirect tensile tests and were modelled with master curves implementing the sigmoidal function. The rheological properties of bitumen were characterised using a dynamic shear rheometer. The viscosity was simulated using a temperature-based log-linear relationship and the complex modulus was obtained based on the modified Huet-Sayegh model. The grey relational analysis revealed the correlation existing between the material factors and the dynamic modulus. A prediction model was established using a Multiple Linear Regression (MLR). The results indicate that the dynamic modulus of asphalt mixtures is greatly affected by the following parameters ranked in order of decreasing significance: viscosity and complex modulus of the binder, void filled with bitumen, air void content, bitumen penetration and softening point. Based on the MLR model, the correlation between the dynamic modulus and the bitumen viscosity and complex modulus fit well with Coefficient of Determination (R^2) $\geq$ 0.901. The determination of the sigmoidal function parameters to predict the dynamic modulus had good reliability with $R^2 \geq 0.973$. This study contributes to the development of an accurate and convenient method to predict the dynamic moduli of asphalt mixtures based on the material factors for a ME pavement design system.

1. Introduction

Asphalt pavement is widely used in highways, urban roads and airport runways due to the advantages of comfortable driving, low noise, anti-skid and short construction period, etc. [1–3]. Over the past decades, road construction in Norway has been dominated by an empirical design approach. With increasing traffic volumes, axial loads and new materials being used in road construction, the Norwegian Public Roads Administration (NPRA) is working together with Swedish Transport Administration (TV), Swedish National Road and Transport Research Institute (VTI) and Norwegian University of Science and Technology (NTNU) on a project called “VegDim” with the aim of developing and implementing a Mechanistic-Empirical (ME) pavement design system and to create a material database for Norwegian materials [4]. The ME pavement design approach provides a unified basis for the design of flexible pavements. Based on this method, the performance of a road is affected by a number of different factors, e.g., management systems, construction materials, structural design, environmental conditions, traffic type and volume [5,6]. In this regard, the dynamic modulus is important for asphalt material characterisation and generally determined by Cyclic Compression Test (CCT) or Cyclic Indirect Tensile Test (CITT) performed at different loading frequencies and temperatures

* Corresponding author.
E-mail addresses: hao.chen@ntnu.no (H. Chen), rabbira.saba@vegvesen.no (R.G. Saba), liug@whut.edu.cn (G. Liu), diegomb271@gmail.com (D.M. Barbieri), xuemei.zhang@ntnu.no (X. Zhang), inge.hoff@ntnu.no (I. Hoff).

https://doi.org/10.1016/j.conbuildmat.2022.130134
Received 26 September 2022; Received in revised form 4 November 2022; Accepted 17 December 2022
Available online 23 December 2022

[7–10]. Since the wearing and binder courses in Norway are commonly around 40 mm, the dimension of core samples derived from fields can meet the requirement of CITT (i.e. a diameter of 100 mm and a thickness of 40 mm) instead of CCT (i.e. a diameter of 100 mm and a height of 150 mm). Thus, the CITT was used in this study. However, the dynamic modulus test requires sophisticated devices and well-trained operational skills. Furthermore, the procedure is time-consuming and needs a cumbersome amount of the material to be tested. Therefore, the establishment of correlations between the properties of asphalt material factors and corresponding dynamic moduli is useful to make a reasonably accurate prediction of dynamic modulus for ME pavement design system.

In the ME pavement design guide, the prediction of the dynamic modulus for an asphalt mixture is based on the physical, rheological and mechanical properties of bituminous binder (e.g., viscosity, penetration, content), aggregates (e.g., grading curve) and asphalt mixture itself (e.g., air void) in the Witczak 1-37A model for the Level 2 and Level 3 conditions [11]. This model was further developed by incorporating the complex modulus of binder and the binder phase angle in the NCHRP 1-40D protocol, which was called Witczak 1-40D model [12]. Christensen et al. [13] used the Hirsch model to evaluate the dynamic modulus by taking into account bitumen stiffness and void characteristics of asphalt mixtures. Based on the Hirsch model, Al-Khateeb et al. [14] developed a simpler form of the model to overcome the problem of inaccurate prediction at high and low temperatures. Sakhaeifar et al. [15] developed two models based on the viscoelastic and time–temperature superposition principles to predict the dynamic moduli at a wide range of temperatures (e.g., −10, 4.4, 37.8 and 54.4 °C) named global and simplified global models. Although these models were established based on hundreds of asphalt mixture types in the United States, the materials in different regions of the world exhibit different properties [16–18].

In addition, the determination of the factors affecting dynamic modulus has received more attention from researchers. Shu et al. [19] developed a new micromechanical model based on the particulate-filled composite theory to predict the dynamic modulus of asphalt mixtures. The results showed that the stiffer binder, lower binder content and lower air void content lead to a higher dynamic modulus. Zhang et al. [20] analysed the influence of some material factors on the dynamic modulus by using grey relational analysis and established a prediction model to simulate the dynamic modulus based on the material parameters. The softening point of bitumen and the air void content of the asphalt mixture were highly correlated with the dynamic modulus. A regression model of dynamic modulus was proposed based on the loading rate and material parameters; results show that a higher Coefficient of Determination (R^2) was found for the conditions of the Chinese province Jilin compared to the outcomes of Witczak model. Whereas the viscosity and complex modulus of bitumen changing with different environmental conditions were not considered in this research. Bi et al. [21] compared the master curves of different types of asphalt mixtures to find the correlation between binder/mastic properties and dynamic modulus. The results indicated that the type of bitumen and the filler-to-binder ratio had a clear effect on the dynamic modulus, whereas the dynamic modulus of asphalt mixtures with different types of aggregates and fillers showed an insignificant difference. Moreover, there was a good correlation between the bitumen/mastic complex modulus and the dynamic modulus of asphalt mixtures. Previous studies mainly investigated several material factors in developing prediction models, while few studies provide a model for the dynamic modulus prediction considering all aspects of the material properties.

Therefore, a prediction model adopted for Norwegian materials, which comprehensively considers the material influence on dynamic modulus of asphalt mixtures, has not been investigated. To contribute to this research gap, this work aims to investigate the influence of material factors (i.e., maximum aggregate size, binder content, rheological properties of bitumen, bulk density and void characteristics of asphalt mixtures) on the dynamic modulus and establish an innovative prediction model for Norwegian asphalt mixtures.

In this research, the 20 types of asphalt mixtures commonly used for the construction of Norwegian roads were investigated. The dynamic moduli of the asphalt mixtures were determined by using the CITT. A regression model of the experimental data was developed based on the sigmoidal function. The bitumen viscosity was measured by the plate method and the experimental data were fitted to a temperature-dependent log-linear relationship. The bitumen complex modulus was obtained by performing a frequency sweep test using a Dynamic Shear Rheometer (DSR) and modelled based on the modified Huet-Sayegh formulation. The grey relational analysis was used to evaluate the degree of influence that each material factor (i.e., maximum aggregate size, binder content, rheological properties of bitumen, bulk density and void characteristics of asphalt mixtures) exerted on the dynamic modulus. The relationship between bitumen viscosity, bitumen complex modulus and dynamic modulus of asphalt mixtures was investigated and a prediction model for the master curve parameters was established. Statistical analysis was used to estimate the quality of the model. The results reveal the correlation between dynamic modulus and material factors and thus provide an accurate and convenient method to predict the dynamic modulus for use in the ME pavement design system.

2. Materials and methods

2.1. Materials

2.1.1. Bitumen

Three types of bitumen commonly used for Norwegian roads were investigated. The first type included bituminous binders with penetration of 70 – 100, 160 – 220 and 330 – 430 (0.1 mm at 25 °C). The second type was Polymer Modified Bitumen (PMB) with penetration of 65 – 105 (0.1 mm at 25 °C) and softening point higher than 60 °C. The third type comprised soft bitumen with viscosity values equal to 1500, 3000, 6000, 9000 and 12000 mm^2/s at 60 °C named V1500, V3000, V6000, V9000 and V12000, respectively. The physical properties of the investigated binders are shown in Table 1 and fulfil the requirements set by EN 12,591 [22]. The bitumen 70/100 and 160/220 were supplied by Veidekke company (Trondheim, Norway), and the other types were provided by Nynas company (Göteborg, Sweden).

2.1.2. Rock aggregates

Two types of aggregates were used in this study. The first type was a crushed rock from the Vassfjell area and supplied by Franzefoss company (Heimdal, Norway). This material is characterised by very good mechanical properties and is largely used for road construction in the central part of Norway [26,27]. The second type of aggregates used in this study was natural gravel and supplied by Forset Grus company (Tanem, Norway). This material has a poorer mechanical performance and is used for low-volume roads. The resistance to wear (abrasion value and Micro-Deval coefficient) and fragmentation (Los Angeles value) of the aggregates are specified in Table 2. The strength of the crushed rock aggregates fulfils the requirements set by the Norwegian pavement design code “N200” for high Annual Average Daily Traffic (AADT) of around 15 000 [28]. For asphalt mixtures used for roads with a lower AADT, 30 % to 50 % fine aggregates consist of natural gravel.

2.2. Specimen fabrication

In this study, the 20 asphalt mixture types, mostly used for Norwegian roads were investigated. They included five kinds of grading and nine types of bitumen. In terms of grading, they included Asphalt Concrete (AC), Stone Matrix Asphalt (SMA), Soft Asphalt (MA) for the low traffic volume road, Asphalt Gravel (AG) for the base layer and Asphalt Crushed Stone (AP) with a high air void content also for the base layer. All asphalt mixtures were prepared in the laboratory based on the average values of the upper and lower limits of the grading curves set by

Table 1
Physical properties of bitumen.

Bitumen type		Penetration at 25 °C [0.1 mm]		Softening point [°C]		Dynamic or kinematic viscosity at 60 °C [Pa·s or mm²/s]	
		EN 1426 [23]		EN 1427 [24]		EN 13,702 [25]	
		Value	Specification	Value	Specification	Value	Specification
Neat bitumen	70/100	92	70 – 100	46.0	43 – 51	235.7 Pa·s	≥ 90 Pa·s
	160/220	189	160 – 220	38.1	68 – 43	102.6 Pa·s	≥ 30 Pa·s
	330/430	–	–	–	–	44.5 Pa·s	≥ 12 Pa·s
PMB	65/105–60	88	65 – 105	62.6	≥ 60	391.8 Pa·s	–
Soft bitumen	V1500	–	–	–	–	1708 mm²/s	1000 – 2000 mm²/s
	V3000	–	–	–	–	2815 mm²/s	2000 – 4000 mm²/s
	V6000	–	–	–	–	5450 mm²/s	4000 – 8000 mm²/s
	V9000	–	–	–	–	8990 mm²/s	6000 – 12000 mm²/s
	V12000	–	–	–	–	14036 mm²/s	8000 – 16000 mm²/s

Table 2
Resistance to wear and fragmentation of rock aggregates.

Strength property	Abrasion value EN 1097-9 [29]	Micro-Deval coefficient EN 1097-1 [30]	Los Angeles value EN 1097-2 [31]
Crushed rock	7.8	14.2	18.2
Natural gravel	17.3	17.3	27.7

the Norwegian pavement design code "Nr. 670" [32] and the Optimum Binder Contents (*OBC*) determined by the Marshall mix design method [33]. The grading curves and the *OBC* of the 20 asphalt mixture types are given in Table 3.

Based on the grading curves and *OBC*, all asphalt mixture specimens were prepared according to the procedure shown in Fig. 1. The bitumen and aggregates were preheated at the conditioning time and temperature in accordance with EN 12697-35 [34]. After preheating process, the bitumen and aggregates were mixed in a continuously heated blender for 3 – 5 min to obtain the asphalt mixtures. The asphalt mixture was poured into a preheated mould to prepare asphalt slabs with dimensions 305 mm × 305 mm × 57 mm using a roller compactor. This device compressed the asphalt slab according to four sequences with the table moving velocity of 250 ± 100 mm/s and applying pressures of 2 bar, 4 bar, 6 bar and 0 bar, respectively [35]. Each stage consisted of four passes and vibration was used during the last passes of the fourth stage to ensure adequate compaction. Moreover, a 3 mm resin plate was placed at the bottom of the mould to protect the mould during the following sample coring operations. From the compacted slab, specimens with a diameter of 100 mm and a height of 40 mm were cored and cut from the asphalt slabs [36]. At least four testing specimens were obtained from each asphalt plate. The density and void characteristics including Air Void Content (V_a), Voids in the Mineral Aggregate (*VMA*) and Voids Filled with Bitumen (*VFB*) of testing specimens are given in Table 4.

2.3. Characterisation of material properties

2.3.1. Viscosity of bitumen by DSR rotational plate method

The dynamic viscosity of the bitumen was determined by a DSR based on the plate method [25,39]. The bitumen samples were placed between two 25 mm diameter plates. The rotation was conducted at a shear rate of 10 rad/s and a shear strain of 1 %. The shear stress was measured by the DSR. Based on Newton's internal friction law, the dynamic viscosity was calculated by Eq. (1).

$$\eta = \frac{\tau}{\dot{\gamma}} \tag{1}$$

where η is the dynamic viscosity, τ is the shear stress and $\dot{\gamma}$ is the shear rate. The viscosity test was performed at 40 °C, 60 °C, 80 °C and 100 °C to assess the relationship between viscosity and temperature. The bitumen types 70/100, 160/220, 330/430 and PMB were tested at 60 °C, 80 °C and 100 °C, while the soft bitumen of V1500, V3000, V6000, V9000 and V12000 were investigated at 40 °C, 60 °C and 80 °C. The testing temperatures were selected to ensure the bitumen behaviour

Table 3
Used grading curves and *OBC* of asphalt mixtures.

Mixture code	Passing percentage [%]									*OBC* [%]
	22.4 mm	16 mm	11.2 mm	8 mm	4 mm	2 mm	1 mm	0.25 mm	0.063 mm	
AC 11–70/100		100	95	70	47.5	33.5	25.5	12.5	7.5	5.1
AC 11–160/220		100	95	77	56	41.5	31.5	15	7.5	5.2
AC 11–330/430		100	95	77	56	41.5	31.5	15	7.5	5.8
AC 11-PMB		100	95	70	47.5	33.5	25.5	12.5	7.5	5.2
AC 16–70/100	100	95	71	58		31.5	24.5	13.5	8	4.9
AC 16–160/220	100	95	76	65		35.5	24.5	12.5	5.5	5.0
AC 16–330/430	100	95	76	65		35.5	24.5	12.5	5.5	5.6
AC 16-PMB	100	95	71	58		31.5	24.5	13.5	8	4.9
SMA 11–70/100		100	95	55.5	37.5	26		16	11	5.3
SMA 11-PMB		100	95	55.5	37.5	26		16	11	5.3
SMA 16–70/100	100	95	56	37		22.5		13.5	10	5.1
SMA 16-PMB	100	95	56	37		22.5		13.5	10	5.2
MA 11-V1500		100	94.5	79.5	60	43.5	34	17	6	4.3
MA 11-V6000		100	94.5	79.5	60	43.5	34	17	6	4.2
MA 16-V3000	100	92.5	80.5		46	31	21	8	5	4
MA 16-V9000	100	92.5	80.5		46	31	21	8	5	4.2
MA 16-V12000	100	92.5	80.5		46	31	21	8	5	4.2
AG 16–70/100	100	95	75			35.5		12.5	6	4.7
AG 16–160/220	100	95	75			35.5		12.5	6	4.6
AP 16–70/100	100	95	45	34.5		17		6.5	5	2.8

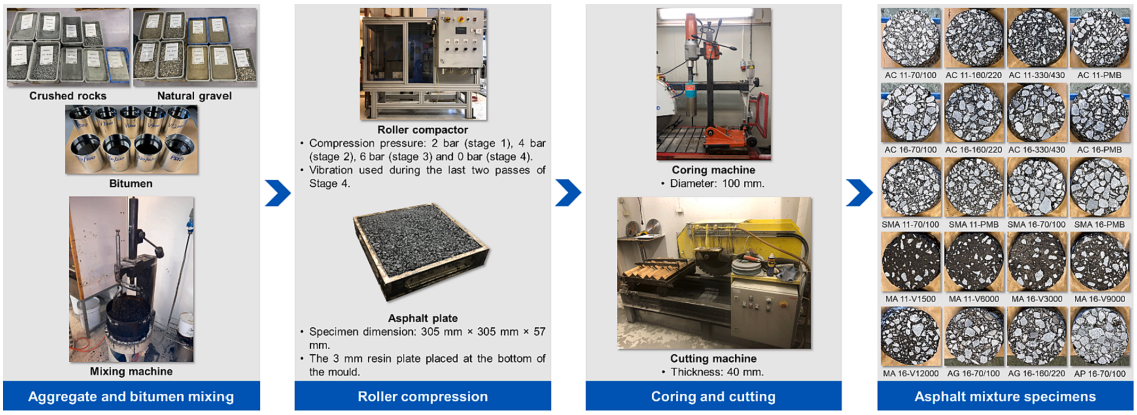

Fig. 1. Specimen preparation procedure.

Table 4
Density and void characteristics of testing specimens.

Mixture code	Density [Mg/m^3]	V_a [%]	*VMA* [%]	*VFB* [%]
	EN 12697-6 [37]	EN 12697-8 [38]		
AC 11-70/100	2.655	3.5	16.9	79.1
AC 11-160/220	2.557	3.0	16.1	81.7
AC 11-330/430	2.539	2.7	17.2	84.6
AC 11-PMB	2.684	2.3	16.1	85.7
AC 16-70/100	2.686	2.9	16.0	81.7
AC 16-160/220	2.647	2.8	15.9	82.6
AC 16-330/430	2.574	4.4	18.7	76.4
AC 16-PMB	2.697	2.5	15.6	83.8
SMA 11-70/100	2.597	5.2	18.8	72.5
SMA 11-PMB	2.676	2.3	16.4	85.8
SMA 16-70/100	2.650	3.9	17.3	77.5
SMA 16-PMB	2.689	2.3	16.2	85.6
MA 11-V1500	2.684	3.7	15.6	76.4
MA 11-V6000	2.635	5.7	17.0	66.3
MA 16-V3000	2.629	6.3	17.2	63.1
MA 16-V9000	2.631	6.0	17.3	65.1
MA 16-V12000	2.594	7.4	18.5	60.2
AG 16-70/100	2.563	7.9	19.9	60.0
AG 16-160/220	2.565	8.1	19.7	59.2
AP 16-70/100	2.430	15.8	22.6	30.0

within the Linear Viscoelastic (LVE) range. Three replicate specimens were tested for each type of bitumen and the mean value of dynamic viscosity was assessed, i.e., a total of 27 specimens were tested.

The kinematic viscosity is calculated as the dynamic viscosity divided by the bitumen density, which varies from 980 kg/m^3 to 1 010 kg/m^3 for the binders selected in this study. The kinematic viscosity expressed in mm/s^2 is therefore close to 1 000 times the associated dynamic viscosity expressed in Pa·s.

2.3.2. Complex modulus of bitumen by DSR frequency sweep method

The complex modulus of bitumen was also determined using the DSR by performing measurements at different loading frequencies and temperatures [40]. The bitumen samples were placed between two parallel plates with a diameter of 10 mm and a gap of 2 mm at low temperatures (<30 °C) and with a diameter of 25 mm and a gap of 1 mm at high temperatures (≥30 °C). The test temperatures ranged from −10 °C to 80 °C with intervals of 10 °C. The frequency was swept logarithmically down from 400 rad/s to 0.1 rad/s. The shear strain was controlled to keep all bitumen within the LVE range. The shear strain of the bitumen 70/100, 160/220, 330/430 and PMB was 1 %. The shear strain of the soft bitumen of V1500, V3000, V6000, V9000 and V12000 was 1 % and 2 % for temperatures lower or higher than 30 °C, respectively. The average results derived from the three replicate specimens were presented for a total of 54 samples that were tested.

2.3.3. Dynamic modulus by CITT method

The CITT was performed by a servo-pneumatic universal testing machine applying a controlled harmonic sinusoidal load. Two Linear Variable Differential Transformers (LVDT) were located on each side in the horizontal direction to obtain the corresponding deformation. The testing temperatures and frequencies vary from region to region according to local climatic and traffic conditions. In the United States, the testing temperatures of −12, 4, 21, 38 and 54 °C the testing frequencies from 0.1 Hz to 25 Hz are adopted based on the ME pavement design guide [11]. In Australia, the testing was carried out at four temperatures of 5, 20, 35 and 50 °C and six frequencies of 0.1, 0.5, 1, 5 10 and 25 Hz [16]. However, in Norway, the dynamic modulus of asphalt mixtures at low temperatures is of more concern. Thus, lower temperatures of −15, −10, 0, 15 and 30 °C and the frequencies of 0.1, 0.3, 1, 3, 5 and 10 Hz in accordance with EN 12697–26 were selected for the dynamic modulus test in this study [41]. The applied loads were adjusted to make sure that the initial horizontal strain amplitude was in a range comprised between 50 and 100 με for each testing frequency and temperature; this requirement ensured that the asphalt mixture specimens were in the LVE range. The dynamic modulus of the asphalt mixtures was determined based on the deviator stress and strain in the horizontal direction, and was calculated by the formula [42,43].

$$|E^*| = \frac{P}{t\Delta H}(\nu + 0.27) \tag{2}$$

where $|E^*|$ is the dynamic modulus, P is the vertical harmonic sinusoidal load, ν is the Poisson's ratio, t is the thickness of the asphalt mixture samples and ΔH is the horizontal deformation. To reduce random variation, four replicate samples were tested and the average values of the dynamic modulus were calculated; overall, a total of 80 CITT specimens were tested.

2.4. Master curve approach

2.4.1. Master curve construction for bitumen complex modulus

The master curve is constructed according to the time–temperature superposition principle by shifting the experimental results based on a selected reference temperature [44], which aims at predicting the stiffness for a wider frequency and temperature ranges than the tested ones. In this research, the Modified Huet-Sayegh (MHS) model was used to describe the master curve of bitumen expressed as [45,46]:

$$G^*(\omega) = \left\{ \left[G_0 + \frac{G_\infty - G_0}{1 + \delta_1 (i\omega\tau_1)^{-m_1} + \delta_2 (i\omega\tau_2)^{-m_2}} \right]^{-1} - \frac{i}{\eta_3 \omega} \right\}^{-1} \quad (3)$$

where $G^*(\omega)$ is the complex modulus, ω is the angular frequency, G_0 and G_∞ are the complex moduli at the infinitesimal and infinite frequencies, respectively, τ_1 and τ_2 are time constants for the parabolic dashpots and m_1, m_2, δ_1 and δ_2 are model parameters. The number of parameters can be decreased using one time constant $\tau = \tau_1 = \tau_2$. The Willian, Landel and Ferry (WLF) equation was used to shift the measured values based on the reference temperature of 15 °C given in Eq. (4) [47].

$$\log[\alpha(T)] = \frac{-C_1 (T - T_r)}{C_2 + (T - T_r)} \quad (4)$$

where $\alpha(T)$ is the shift factor, T is the testing temperature, T_r is the reference temperature and C_1 and C_2 are the model parameters. The fitting result was obtained by calculating the minimum error between the measured and modelled value.

2.4.2. Master curve construction for asphalt mixture dynamic modulus

The sigmoidal function was used to construct the master curve for the asphalt mixtures described in the ME pavement design guide [11], which also had better goodness of fit for the Norwegian AC and SMA mixtures [48], expressed as:

$$\log(|E^*|) = \delta + \frac{\alpha}{1 + e^{\beta - \gamma \log(f)}} \quad (5)$$

where $|E^*|$ is the dynamic modulus, f is the frequency, δ and $\delta + \alpha$ are the dynamic moduli at the infinitesimal and infinite frequencies, respectively and β and γ are the model parameters. The WLF equation (Eq. (4)) was also used to shift the measured value based on the same reference temperature of 15 °C. The fitting result was calculated by minimizing the error between the measured and modelled values.

2.5. Grey relational analysis method

The grey relational analysis is a statistical technique, which is mainly used to elaborate the closeness of the relationship between main factors and sub-factors in a system as well as to evaluate the degree of influence that each sub-factor exerts on the main factor [49]. In recent research, it has been applied in the field of bituminous binders [50,51]. In this study, the grey relational analysis method was used to investigate the degree of influence that each material parameter (i.e., maximum aggregate size, binder content, rheological properties of bitumen, bulk density and void characteristics of asphalt mixtures) had on the dynamic modulus of asphalt mixtures. In total, there were m material parameters and n sets of data. The ith material parameters can be expressed as x_{ij}, where $i = 1, 2, \ldots, m$ and $j = 1, 2, \ldots, n$.

Since the numerical values of the material parameters are in different ranges, the min–max value method was used for the dimensionless processing of variables by Eq. (6).

$$X_{ij} = \frac{x_{ij} - \min(x_{ij})}{\max(x_{ij}) - \min(x_{ij})} \quad for\ i = 1, 2, \ldots, m\ and\ j = 1, 2, \ldots, n \quad (6)$$

where X_{ij} is the comparability sequence from 0 to 1, $\min(x_{ij})$ is the minimum value of the x_{ij} matrix and $\max(x_{ij})$ is the maximum value of the x_{ij} matrix. The dynamic modulus sequence was defined as the reference sequence X_{0j}. The difference between material parameter sequence, X_{ij}, and reference sequence, X_{0j}, is $\Delta_{ij} = |X_{0j} - X_{ij}|$. The grey relational coefficient is used to determine how close X_{ij} is to X_{0j}, which can be calculated by Eq. (7).

$$\gamma(X_{0j}, X_{ij}) = \frac{\min(\Delta_{ij}) + \zeta \max(\Delta_{ij})}{\Delta_{ij} + \zeta \max(\Delta_{ij})} \quad for\ i = 1, 2, \ldots, m\ and\ j = 1, 2, \ldots, n \quad (7)$$

where $\gamma(X_{0j}, X_{ij})$ is the grey relational coefficient, $\min(\Delta_{ij})$ is the minimum value of Δ_{ij} matrix, $\max(\Delta_{ij})$ is the maximum value of Δ_{ij} matrix and ζ is the resolution coefficient between 0 and 1 to reflect the difference in the correlation and the value of 0.3 is selected in this study [20]. The grey relational grade between the ith material parameter sequence, X_i, and the dynamic modulus sequence, X_0, can be then calculated by Eq. (8).

$$\gamma(X_0, X_i) = \frac{1}{n} \sum_j^n \gamma(X_{0j}, X_{ij}) \text{ for } i = 1, 2, \ldots, m \quad (8)$$

where $\gamma(X_0, X_i)$ is the grey relational grade between 0 and 1, and the closer its value is to 1, the better the correlation between the material parameter and the dynamic modulus.

3. Results and discussion

3.1. Analysis of material properties

3.1.1. Viscosity-temperature curve of bitumen

The viscosities of the nine types of bitumen are presented in Fig. 2, with PMB being associated with the highest values in the range of 40 °C to 100 °C due to the network structure of the polymer in the bitumen [46,52]. Soft bitumen has the lowest viscosity, which presents a flow state at room temperature. The neat bitumen is characterised by average values, and its viscosity decreases as the penetration increases. The log value of viscosity is linear with temperature, as shown in Table 5. All R^2 are higher than 0.989, which indicates almost perfect fits. Therefore, the viscosity of the bitumen at a given temperature can be predicted by the linear regression model, which is used as a material factor influencing the dynamic modulus of asphalt mixtures.

3.1.2. Complex modulus master curve of bitumen

The complex moduli of the nine types of bitumen are shown in Fig. 3. The complex modulus of neat bitumen is higher than the one of soft bitumen. In terms of neat bitumen, the values of complex modulus decreased with increasing penetration. Regarding the soft bitumen, the values of complex modulus decreased with decreasing viscosity. The complex modulus of PMB is lower than the one of neat bitumen at high frequencies (low temperatures) and higher than that of neat bitumen at low frequencies (high temperatures). This is connected that the polymer increases the flexibility of the binder at low temperatures and the network structure of the polymer provides the elasticity in neat bitumen at high temperatures [53,54]. The MHS model and WLF equation parameters of nine bitumen are given in Table 6. The results display good goodness of fit as all R^2 values are higher than 0.968. Therefore, the complex modulus of bitumen at an arbitrary condition can be obtained by the master curves and used as a material factor for evaluating the dynamic modulus.

3.1.3. Dynamic modulus master curve of asphalt mixtures

The dynamic modulus master curves of asphalt mixtures were constructed using the sigmoidal function and the WLF equation based on the measured values of dynamic modulus at different frequencies and temperatures as shown in Fig. 4. Furthermore, Fig. 4 also documents that the dynamic modulus master curves of asphalt mixtures containing the bitumen types belonging to the same group (i.e., neat, PMB, soft) are relatively close. Moreover, the order of dynamic modulus of asphalt mixtures with different bitumen was in accordance with that of the viscosity and complex modulus of corresponding bitumen under the same testing conditions. This can be explained considering that the viscoelastic behaviour of asphalt mixture is highly determined by the rheological properties of bitumen [7–10]. The fitting parameters of both sigmoidal function and WLF equation are given in Table 7. All results display a high goodness of fit $R^2 \geq 0.973$. Since the viscosity of soft

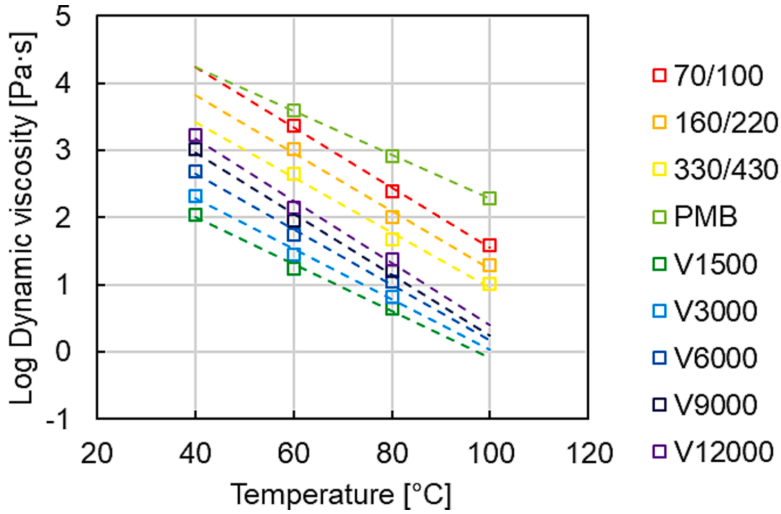

Fig. 2. Viscosity of bitumen.

Table 5
Linear regression of viscosity, η, with temperature, T.

Bitumen		Linear regression equation	R^2
Neat bitumen	70/100	$\log(\eta) = -0.0448 \cdot T + 6.0315$	0.997
	160/220	$\log(\eta) = -0.0430 \cdot T + 5.5481$	0.992
	330/430	$\log(\eta) = -0.0408 \cdot T + 5.0483$	0.989
PMB	65/105–60	$\log(\eta) = -0.0325 \cdot T + 5.5327$	0.999
Soft bitumen	V1500	$\log(\eta) = -0.0348 \cdot T + 3.3888$	0.992
	V3000	$\log(\eta) = -0.0376 \cdot T + 3.7867$	0.991
	V6000	$\log(\eta) = -0.0411 \cdot T + 4.2923$	0.991
	V9000	$\log(\eta) = -0.0454 \cdot T + 4.7810$	0.991
	V12000	$\log(\eta) = -0.0461 \cdot T + 5.0168$	0.991

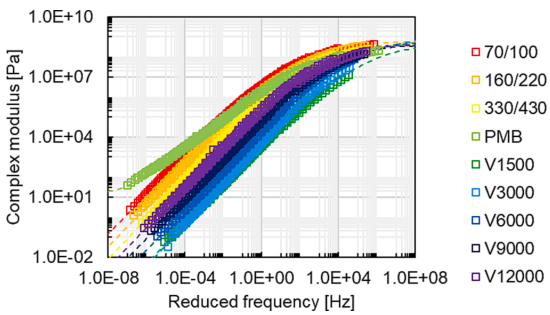

Fig. 3. Complex modulus of bitumen.

bitumen is very small at high temperatures, the dynamic modulus of the corresponding asphalt mixtures varies at high temperatures (≥15 °C) resulting in an R^2 lower than the ones of other mixtures.

3.2. Grey relational analysis of material factors

In this research, only bitumen 70/100, 160/220 and PMB are characterised by the following parameters of the penetration at 25 °C, $Pen_{25\,°C}$, and softening point tested in the water, $T_{R\&B}$. Thus, the grey relational grad was assessed regarding the correlation between the dynamic modulus of asphalt mixtures and the following available material parameters: maximum aggregate size, P_{max}, binder content, B, bitumen viscosity, $\eta(T)$, bitumen complex modulus, $|G^*|(T,f)$, asphalt mixture density, ρ_{mix}, V_a, VMA and VFB. The bitumen viscosity and complex modulus obtained at the same testing conditions adopted for the evaluation of the dynamic modulus are calculated according to the regression and MHS models illustrated in Section 3.1.1 and Section 3.1.2, respectively. The 20 asphalt mixtures were analysed and their dynamic moduli were measured for 30 combinations of frequencies and temperatures for neat bitumen and PMB and 24 combinations for soft bitumen. Thus, the grey relational analysis was conducted for a total of 570 sets of data leading to the result shown in Fig. 5. The grey relational degree is ranked as follows in descending order: $|G^*|(T,f)$, $\eta(T)$, VFB, V_a, $\eta_{60\,°C}$, B, ρ_{mix}, P_{max}, and VMA. The result indicates that the dynamic modulus is greatly affected by the bitumen complex modulus and its viscosity as the two corresponding factors are higher than 0.7, followed by the void characteristics of VFB and V_a with values of 0.595 and 0.592. Other factors, such as bitumen properties and binder content, have a relatively low effect on the dynamic modulus since their values range from 0.428 to 0.562. On the one hand, this outcome can be explained considering that the rheological properties of bitumen dominate the viscoelastic behaviour of asphalt mixtures. On the other hand, the factors of bitumen complex modulus and viscosity, resembling dynamic modulus, change with frequency and temperature, whereas others are not dependent on these two conditions and therefore do not vary, e.g., VFB, V_a, $\eta_{60\,°C}$, B, ρ_{mix}, P_{max}, and VMA.

Considering the effect of $Pen_{25\,°C}$ and $T_{R\&B}$, 13 asphalt mixtures with these two parameters were selected for the grey relational analysis; the corresponding 390 sets of data were analysed. The results are presented in Fig. 6, which are similar to the findings already reported in Fig. 5. The effect of $Pen_{25\,°C}$ and $T_{R\&B}$ on the dynamic modulus of asphalt mixtures are close to $\eta_{60\,°C}$, and are ranked according to the descending order: $|G^*|(T,f)$, $\eta(T)$, VFB and V_a.

The results of grey relational analysis illustrate that the most influential factor in the determination of the dynamic modulus of asphalt mixtures is represented by the rheological properties of the bitumen, which change with frequency and temperature. The void characteristics of VFB and V_a as well as $\eta_{60\,°C}$, $Pen_{25\,°C}$ and $T_{R\&B}$ of the binders are the other parameters exerting the largest influence.

Table 6
MHS model and WLF equation parameters of complex modulus.

Bitumen		MHS model								WLF equation		R^2
		G_0	G_∞	τ	m_1	m_2	δ_1	δ_2	η_3	C_1	C_2	
Neat bitumen	70/100	4.51×10^{-2}	3.52×10^{8}	6.30×10^{-3}	0.55	1.00	15.04	1.00	1.00×10^{50}	13.44	108.37	0.968
	160/220	4.01×10^{-103}	5.59×10^{8}	9.16×10^{-4}	0.45	1.00	12.57	1.00	9.97×10^{49}	14.23	125.06	0.994
	330/430	3.54×10^{-97}	5.82×10^{8}	2.18×10^{-4}	0.34	1.00	13.25	6.55	3.60×10^{50}	11.26	100.32	0.985
PMB	65/105–60	1.62×10^{1}	3.48×10^{9}	3.35×10^{-6}	0.22	0.70	29.03	5.59	1.00×10^{300}	13.53	104.01	0.984
Soft bitumen	V1500	1.09×10^{-6}	3.30×10^{8}	1.76×10^{-6}	0.49	1.00	10.11	1.00	3.24×10^{49}	8.34	100.91	0.991
	V3000	2.15×10^{-16}	7.70×10^{8}	9.86×10^{-7}	0.48	1.00	7.17	1.00	1.83×10^{49}	7.53	92.78	0.988
	V6000	3.23×10^{-163}	5.22×10^{8}	6.83×10^{-6}	0.5	1.00	7.98	1.00	8.64×10^{105}	9.34	102.05	0.987
	V9000	1.60×10^{-205}	3.71×10^{8}	3.22×10^{-5}	0.48	0.99	9.00	1.00	9.98×10^{49}	9.6	92.97	0.984
	V12000	5.46×10^{-281}	3.99×10^{8}	1.17×10^{-4}	0.5	1.00	12.42	1.04	1.10×10^{50}	10.95	99.83	0.978

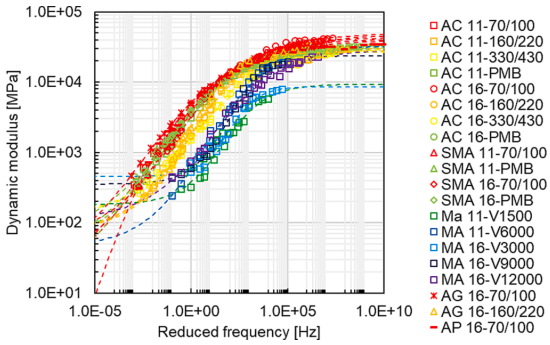

Fig. 4. Dynamic modulus master curves of asphalt mixtures.

3.3. Correlation between bitumen viscosity, bitumen complex modulus and dynamic modulus of asphalt mixtures

Based on the results of the grey relational analysis, the correlation between bitumen viscosity, bitumen complex modulus and dynamic modulus of asphalt mixtures was investigated. As shown in Fig. 4, the dynamic modulus of asphalt mixtures containing the different types of bitumen belonging to the same group is relatively close. Therefore, the asphalt mixtures were divided into nine types according to the type of bitumen. Based on the experimental data of the asphalt mixture dynamic modulus and the modelling data of the viscosity and complex modulus of the bitumen, Multiple Linear Regression (MLR) was performed to evaluate the correlation. The MLR model is given in Eq. (9).

$$\log[|E^*|(T,f)] = a_1 \cdot \log[\eta(T)] + a_2 \cdot \log[|G^*|(T,f)] + a_3 \tag{9}$$

where $|E^*|(T, f)$ is the dynamic modulus at different temperatures and frequencies, a_1, a_2 and a_3 are model parameters. $\eta(T)$ and $|G^*|(T, f)$ are obtained as illustrated in Section 3.1.1 and Section 3.1.2, respectively.

The model parameters are displayed in Table 8 and the results are illustrated in Fig. 7. All nine bitumen types have a good fit with $R^2 \geq 0.901$. The value of *Sig.* is the p-value, which indicates the significance of the independent variable in the model. The lower p-value shows the greater significance of the variable. Analysis of Variance (ANOVA) is used to verify the significance of the model. As shown in Table 8, the p-

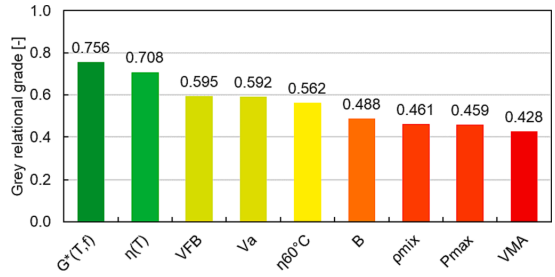

Fig. 5. Grey relational grade of material parameters except $Pen_{25\,^\circ C}$ and $T_{R\&B}$.

Table 7
Fitting parameter of sigmoidal function and WLF equation for dynamic modulus.

Mixture code	Sigmoidal function				WLF equation		R^2
	δ	α	β	γ	C_1'	C_2'	
AC 11–70/100	0.72	3.97	−0.98	0.38	17.87	123.47	0.999
AC 11–160/220	1.89	2.60	−0.09	0.63	9.39	82.16	0.995
AC 11–330/430	2.16	2.27	0.23	0.64	10.33	79.76	0.988
AC 11-PMB	1.74	2.73	−0.59	0.57	12.14	86.34	0.994
AC 16–70/100	0.90	3.80	−0.92	0.42	13.20	92.23	0.991
AC 16–160/220	1.87	2.67	−0.08	0.63	8.51	77.17	0.990
AC 16–330/430	2.02	2.46	0.07	0.50	11.60	83.09	0.990
AC 16-PMB	1.76	2.77	−0.65	0.49	11.40	74.07	0.997
SMA 11–70/100	1.40	3.21	−0.71	0.49	12.30	92.50	0.999
SMA 11-PMB	0.85	3.69	−1.04	0.42	9.94	69.26	0.998
SMA 16–70/100	1.74	2.89	−0.46	0.53	12.24	91.17	0.998
SMA 16-PMB	1.59	2.91	−0.78	0.51	12.20	83.56	0.997
MA 11-V1500	2.26	1.71	1.47	0.89	1.11	41.09	0.973
MA 11-V6000	1.65	2.86	0.45	0.61	5.50	70.76	0.977
MA 16-V3000	2.66	1.28	2.53	1.31	1.85	44.84	0.994
MA 16-V9000	2.55	1.83	1.97	1.02	18.41	167.42	0.980
MA 16-V12000	2.05	2.41	0.63	0.56	33705.31	180907.61	0.990
AG 16–70/100	1.17	3.43	−1.06	0.42	23.02	149.73	0.997
AG 16–160/220	1.91	2.53	−0.28	0.76	4.91	50.67	0.981
AP 16–70/100	−4.86	9.43	−2.26	0.36	8.20	57.47	0.996

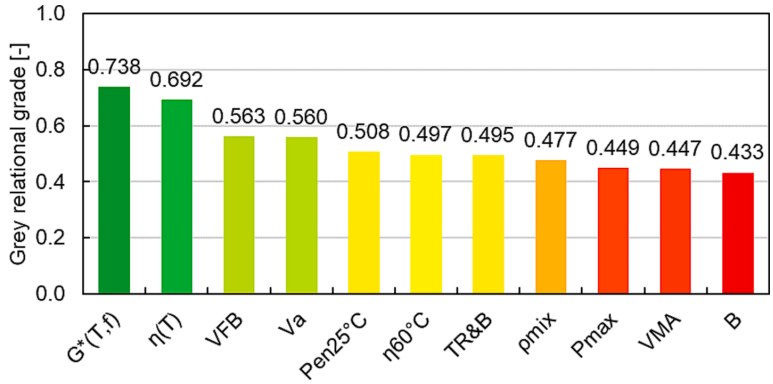

Fig. 6. Grey relational grade of material parameters containing $Pen_{25\ ^\circ C}$ and $T_{R\&B}$.

Table 8
MLR model parameters of Eq. (9) calculated for the nine bitumen types.

Bitumen type		Coefficient						ANOVA		Model summary
		a_1	*Sig.*	a_2	*Sig.*	a_3	*Sig.*	*F*	*Sig.*	R^2
Neat bitumen	70/100	0.041	0.057	0.463	0.000	6.385	0.000	7614.192	0.000	0.989
	160/220	0.086	0.039	0.452	0.000	6.212	0.000	2309.521	0.000	0.982
	330/430	0.300	0.000	0.320	0.000	6.385	0.000	2269.337	0.000	0.988
PMB	65/105–60	−0.009	0.837	0.501	0.000	6.442	0.000	4041.070	0.000	0.986
Soft bitumen	V1500	−0.131	0.411	0.336	0.000	38.213	0.000	95.217	0.000	0.901
	V3000	0.111	0.369	0.259	0.000	7.453	0.000	124.104	0.000	0.922
	V6000	0.024	0.719	0.429	0.000	6.858	0.000	1095.766	0.000	0.991
	V9000	0.093	0.437	0.407	0.000	6.511	0.000	285.341	0.000	0.965
	V12000	0.258	0.019	0.370	0.000	6.128	0.000	364.748	0.000	0.972

values of a_2 are all 0, reflecting the significance of bitumen complex modulus in the model. Whereas the p-values of a_1 are from 0 to 0.837, and neat bitumen shows a lower value than the other bitumen. This result indicates that the effect of viscosity on dynamic modulus depends on bitumen types. The ANOVA results indicate that the models for all bitumen have a good correlation with the test results. The R^2 of soft bitumen is more variable when compared to neat bitumen and PMB. This might be caused by the relatively unstable test results of the asphalt mixtures containing the soft bitumen, causing fluctuations, especially at high temperatures [55]. Nevertheless, the dynamic modulus of asphalt mixtures can be predicted with high reliability by the viscosity and complex modulus of the bitumen for certain loading frequency and temperature conditions. This method can save testing time and the required materials for performing the dynamic modulus test.

3.4. Dynamic modulus prediction model by master curve parameter modelling

Although the method illustrated in Section 3.3 can well predict the dynamic modulus of asphalt mixtures, it is necessary to assess the viscosity and complex modulus of bitumen, which are evaluated by means of laboratory devices requiring highly specialized equipment and well-trained operating skills. While the dynamic modulus varies with loading frequency and temperature, some other material parameters (i.e., P_{max}, B, $\eta_{60\ ^\circ C}$, ρ_{mix}, V_a, *VMA*, *VFB*, *Pen* and $T_{R\&B}$) do not vary. The sigmoidal function fits the dynamic modulus well and its fitting parameters are also fixed for one material. Thus, the material parameters can be used to predict the fitting parameters of the sigmoidal function and thus estimate the dynamic modulus. In this case, the selected material parameters were P_{max}, B, $\eta_{60\ ^\circ C}$, ρ_{mix}, V_a, *VMA*, *VFB*, *Pen* and $T_{R\&B}$, while δ, α, β and γ were chosen as the fitting parameters of sigmoidal function. The MLR was also used to find the correlation between material parameters and fitting parameters of sigmoidal function as expressed in Eq. (10) in two ways: one for the material parameters without *Pen* and $T_{R\&B}$ (Eq. (10.1)) and another one for all obtained material parameters (Eq. (10.2)).

For material parameters without *Pen* and $T_{R\&B}$

$$\delta, \alpha, \beta \text{ and } \gamma = b_1 \cdot P_{\max} + b_2 \cdot B + b_3 \cdot \eta_{60^\circ C} + b_4 \cdot \rho_{mix} + b_5 \cdot V_a + b_6 \cdot VMA + b_7 \cdot VFB + b_8 \tag{10.1}$$

For material parameters with *Pen* and $T_{R\&B}$

$$\delta, \alpha, \beta \text{ and } \gamma = b_1' \cdot P_{\max} + b_2' \cdot B + b_3' \cdot Pen_{25\ ^\circ C} + b_4' \cdot T_{R\&B} + b_5' \cdot \eta_{60\ ^\circ C} + b_6' \cdot \rho_{mix} + b_7' \cdot V_a + b_8' \cdot VMA + b_9' \cdot VFB + b_{10}' \tag{10.2}$$

where $b_{1\text{-}10}'$ and $b_{1\text{-}8}$ are the regression parameters and all material parameters are in the international system of units. The MLR model parameters of Eq. (10) are given in Table 9. The results indicate that there is a good fit between parameters δ, α, β and material parameters. The correlation between γ and material parameters is relatively poor. This reflects the γ is less affected by the material properties. Nevertheless, in the MLR model with material parameters containing *Pen* and $T_{R\&B}$, the R^2 of γ is also as high as 0.837, showing a certain dependence of γ on the material parameters. Furthermore, in this MLR model, the variables of $\eta_{60\ ^\circ C}$ and V_a were excluded. This is due to the small correlation between $\eta_{60\ ^\circ C}$ and fitting parameters of master curve, which can also be verified by small values of b_3 for the MLR model without *Pen* and $T_{R\&B}$. The variable of V_a is excluded due to a higher variance inflation factor, which is caused by the correlation between V_a, *VMA* and *VFB*.

The dynamic modulus of the asphalt mixtures predicted by the sigmoidal function fitted with the material parameters and Witczak 1-

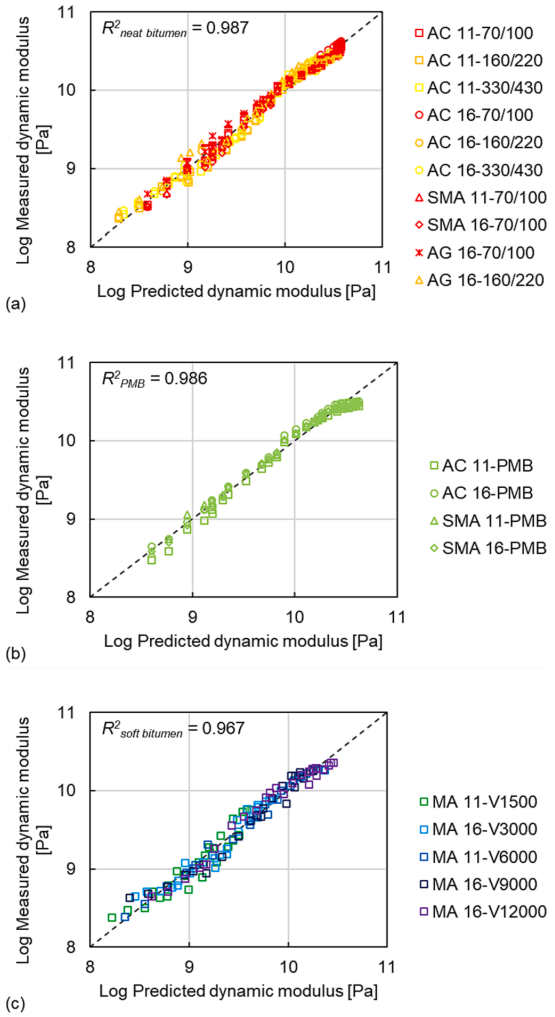

Fig. 7. Results of multiple linear regression of Eq. (6): (a) Neat bitumen, (b) PMB and (c) Soft bitumen.

37A, Witczak 1-40D, Hirsch, Al-Khateeb, global and simplified global models for comparison are shown in Fig. 8. The R^2 of the MLR without and with *Pen* and $T_{R\&B}$ are 0.973 and 0.993, respectively, which can reasonably predict the dynamic modulus for more types of asphalt mixtures [20]. The soft bitumen displays a lower R^2 than the other types, especially at low frequencies (high temperatures). This can be interpreted by taking into consideration the small contribution of soft bitumen to the elasticity of the asphalt mixture at high temperatures. In this condition, the stiffness is provided mainly by the aggregate skeleton, thus defining estimated actual stiffness, which deviates from the dynamic modulus predicted by the material parameters. Compared with the Witczak 1-37A (R^2 = 0.707), Witczak 1-40D (R^2 = 0.926), Hirsch (R^2 = 0.815), Al-Khateeb (R^2 = 0.814), global (R^2 = 0.906) and simplified global (R^2 = 0.891) models, the prediction results of the MLR model in this research shows a better fit. Furthermore, the empirical model of Witczak 1-40D is more suitable for Norwegian asphalt mixtures.

For each type of asphalt mixture, Fig. 9 shows that the MLR model

Table 9
MLR model parameters of Eq. (10).

Master curve parameter		Coefficient																		ANOVA		Model summary
		b_1	Sig.	b_2	Sig.	b_3	Sig.	b_4	Sig.	b_5	Sig.	b_6	Sig.	b_7	Sig.	b_8	Sig.						
																		b_9'	Sig.	b_{10}'	Sig.	F	Sig.	R^2
MLR without *Pen* and $T_{R\&B}$	δ	0.129	0.049	−4.738	0.350	0.001	0.564	−0.018	0.193	−5.533	0.026	−0.647	0.001	2.580	0.234	99.76	0.027					24.08	0.000	0.934
	α	−0.145	0.069	8.730	0.171	−0.001	0.615	0.028	0.119	7.176	0.021	0.646	0.003	−4.188	0.124	−118.0	0.033					17.12	0.000	0.909
	β	0.118	0.039	−14.79	0.004	0.000	0.856	−0.038	0.006	−7.602	0.002	−0.303	0.029	6.063	0.005	121.9	0.004					16.30	0.000	0.905
	γ	0.024	0.271	−2.481	0.175	0.000	0.831	−0.007	0.160	−1.303	0.117	−0.063	0.234	0.970	0.207	24.66	0.104					2.906	0.050	0.629
MLR with *Pen* and $T_{R\&B}$		b_1'	Sig.	b_2'	Sig.	b_3'	Sig.	b_4'	Sig.	b_5'	Sig.	b_6'	Sig.	b_7'	Sig.	b_8'	Sig.	b_9'	Sig.	b_{10}'	Sig.	F	Sig.	R^2
	δ	0.107	0.163	8.187	0.005	125.7	0.029	0.062	0.041	–	–	0.011	0.119	–	0.942	−0.575	0.027	−2.375	0.038	11.52	0.571	43.01	0.000	0.984
	α	−0.110	0.176	−8.242	0.006	−150.0	0.020	−0.074	0.029	–	–	−0.010	0.156	–	0.963	0.576	0.034	2.3655	0.048	−7.046	0.744	38.06	0.000	0.982
	β	0.036	0.430	1.248	0.302	72.37	0.041	0.005	0.724	–	–	0.001	0.828	–	0.683	−0.064	0.613	−0.294	0.608	−0.714	0.955	9.808	0.012	0.932
	γ	0.005	0.728	0.093	0.799	31.67	0.013	0.005	0.314	–	–	0.001	0.636	–	0.678	−0.002	0.954	0.024	0.893	−2.381	0.562	3.669	0.086	0.837

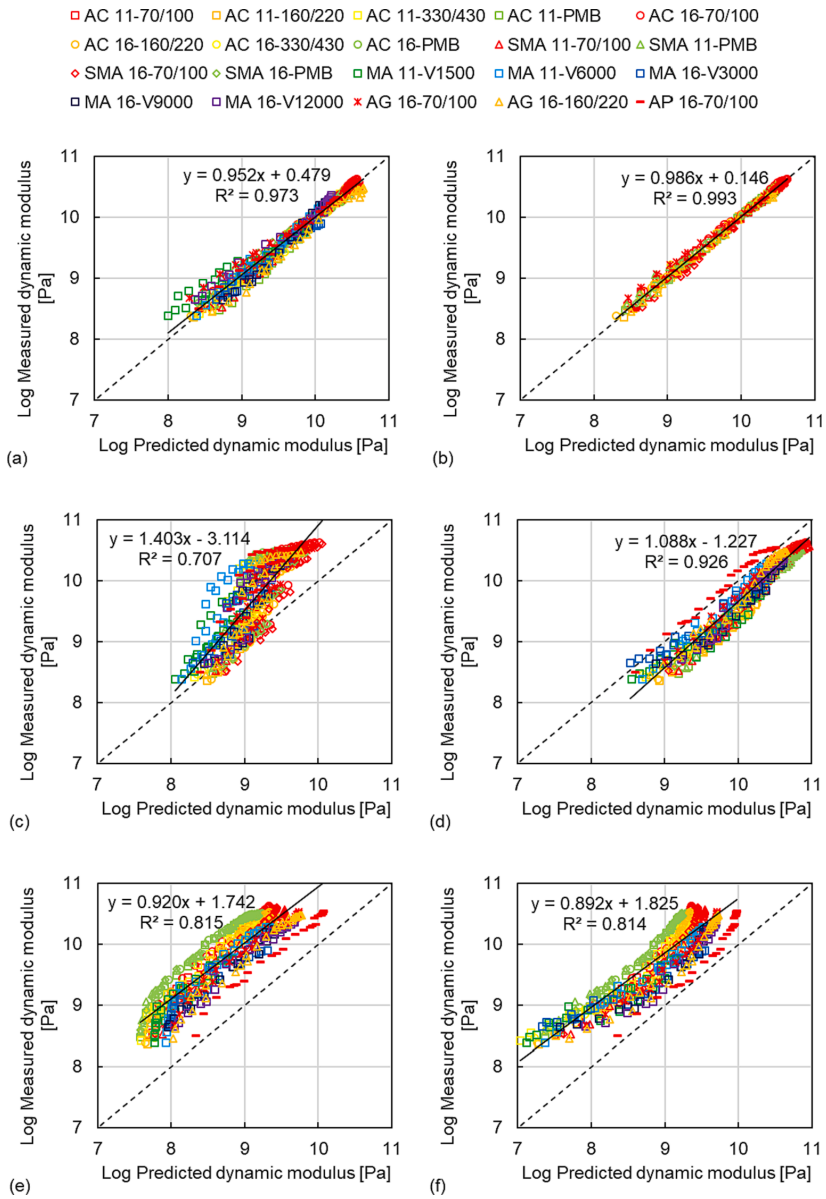

Fig. 8. Comparison between the predicted and measured dynamic modulus: (a) MLR model without *Pen* and $T_{R\&B}$, (b) MLR model with *Pen* and $T_{R\&B}$, (c) Witczak 1-37A model, (d) Witczak 1-40D model, (e) Hirsch model, (f) Al-Khateeb model, (g) Global model and (h) Simplified global model.

offers a better fit for stiffer bitumen. This relates to the larger variation in the dynamic modulus test for the asphalt mixtures containing soft bitumen. In summary, the dynamic modulus of asphalt mixtures can be predicted based on the material parameters by this MLR model.

4. Conclusions

In this study, the dynamic modulus was measured using the cyclic indirect tensile test for the 20 kinds of asphalt mixtures containing nine types of bitumen that are mostly used for Norwegian roads and corresponding master curves were constructed. The influence of different material factors (i.e., maximum aggregate size, binder content, rheological properties of bitumen, bulk density and void characteristics of asphalt mixtures) on the dynamic modulus was investigated. New prediction models for the dynamic modulus of asphalt mixtures were proposed based on the experimental test data. The testing results are used to create a database of asphalt materials for the "VegDim" project and the findings can be incorporated into the development of a ME pavement

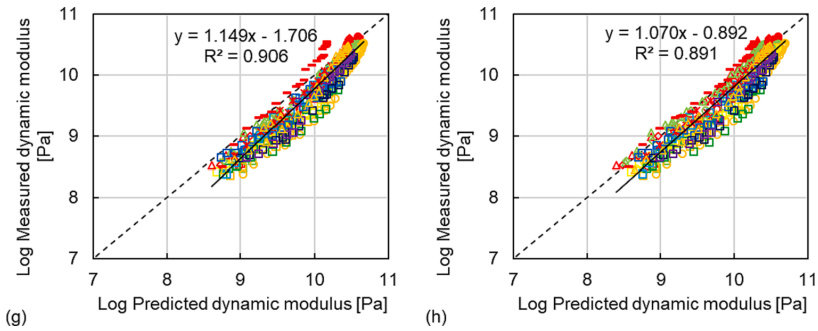

Fig. 8. (*continued*).

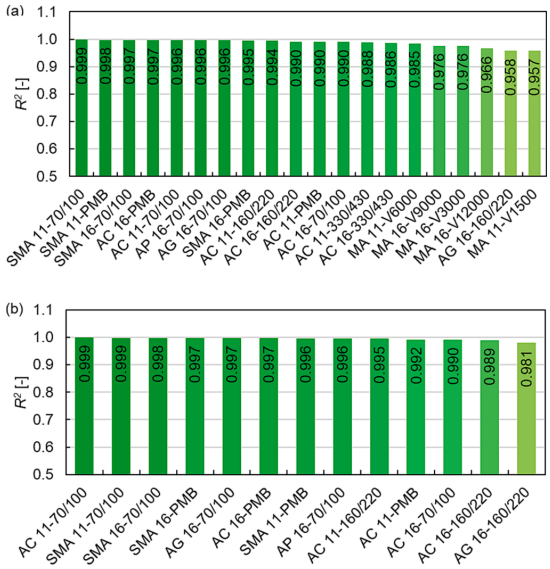

Fig. 9. Goodness of fit R^2 for each type of asphalt mixture: (a) MLR model without *Pen* and $T_{R\&B}$ and (b) MLR model with *Pen* and $T_{R\&B}$.

design for Norwegian conditions. The conclusions are summarised as follows.

- Regarding the nine types of bituminous binders, a log-linear relationship was used to model the relationship between viscosity and temperature, whereas the complex modulus was modelled based on the modified Huet-Sayegh formulation. As for the 20 types of asphalt mixtures, their dynamic moduli were modelled by using the sigmoidal function. The reliability associated with all the formulations was good showing Coefficient of Determination (R^2) $\geq$ 0.968.
- According to the grey relational analysis results, the dynamic modulus of asphalt mixtures is greatly affected by the viscosity and complex modulus of bitumen, followed by the void characteristics of void filled with bitumen and air void content, and then by the bitumen penetration and softening point.
- The dynamic moduli of asphalt mixtures containing the same bitumen type were close. The order of dynamic modulus of asphalt mixtures was in accordance with that of the viscosity and complex modulus of corresponding bitumen under the same testing conditions. The correlation between the dynamic modulus and bitumen viscosity and complex modulus was established by Multiple Linear Regression (MLR). The prediction model had the goodness of fit values $R^2 \geq 0.901$.
- The prediction model of the fitting parameters of the sigmoidal function had a good correlation with $R^2 \geq 0.973$ and asphalt mixtures with stiffer bitumen showed a better fit. This value was higher than the corresponding R^2 obtained for the other empirical prediction models. Moreover, this method accurately predicts the dynamic modulus of asphalt mixtures without involving the rheological properties of bitumen. This can reduce the tedious testing of bituminous rheological properties when predicting the dynamic modulus of asphalt mixtures.

The MLR results for master curve parameters show that some material factors have a significant influence on the prediction model for some asphalt mixtures, while they have little effect on other asphalt mixtures. Therefore, the types of material factors can be further optimised for a specific asphalt mixture to improve the accuracy of the prediction model and reduce the workload in future studies. In addition, since the current specification in many regions is based on a cyclic compression test for the circular cylinder to measure the dynamic modulus of asphalt mixtures, further research can focus on the difference and connection between compressive and indirect tensile modes in dynamic modulus results for optimising the prediction model.

CRediT authorship contribution statement

Hao Chen: Conceptualization, Methodology, Software, Formal analysis, Investigation, Data curation, Writing – original draft. **Rabbira Garba Saba:** Project administration, Resources, Writing – review & editing, Supervision. **Gang Liu:** Methodology, Writing – review & editing, Supervision. **Diego Maria Barbieri:** Investigation, Writing – review & editing. **Xuemei Zhang:** Investigation, Writing – review & editing. **Inge Hoff:** Resources, Writing – review & editing, Supervision.

Declaration of Competing Interest

The authors declare that they have no known competing financial interests or personal relationships that could have appeared to influence the work reported in this paper.

Data availability

Data will be made available on request.

Acknowledgements

This research work was supported by the VegDim project of the Norwegian Public Roads Administration. The financial support provided

by China Scholarship Council (No. 201806950077) and Department of Civil and Environmental Engineering, Norwegian University of Science and Technology (No. K-649105) is highly acknowledged. The support kindly provided by the laboratory technicians Bent Lervik and Jan Erik Molde is greatly acknowledged.

References

[1] L. Cong, F. Yang, G. Guo, M. Ren, J. Shi, L. Tan, The use of polyurethane for asphalt pavement engineering applications: A state-of-the-art review, Constr. Build. Mater. 225 (2019) 1012–1025.
[2] J. Hu, X. Gao, R. Wang, S. Sun, Research on comfort and safety threshold of pavement roughness, Transp. Res. Rec. 2641 (1) (2017) 149–155.
[3] F. Guo, J. Pei, J. Zhang, R. Li, B. Zhou, Z. Chen, Study on the skid resistance of asphalt pavement: A state-of-the-art review and future prospective, Constr. Build. Mater. 303 (2021), 124411.
[4] R. Garba Saba, Analytical Design of Pavement Structures: Evaluation and Choice of a System for, Norwegian Conditions (2019).
[5] Y.H. Huang, Pavement analysis and design, Pearson Prentice Hall Upper Saddle River, NJ, 2004.
[6] X. Zhang, I. Hoff, H. Chen, Characterization of various bitumen exposed to environmental chemicals, J. Clean. Prod. 337 (2022), 130610.
[7] E. Hesami, B. Birgisson, N. Kringos, Numerical and experimental evaluation of the influence of the filler–bitumen interface in mastics, Mater. Struct. 47 (8) (2014) 1325–1337.
[8] X. Lu, U. Isacsson, Modification of road bitumens with thermoplastic polymers, Polym. Test. 20 (1) (2000) 77–86.
[9] C. Brovelli, L. Hilliou, Y. Hemar, J. Pais, P. Pereira, M. Crispino, Rheological characteristics of EVA modified bitumen and their correlations with bitumen concrete properties, Constr. Build. Mater. 48 (2013) 1202–1208.
[10] X. Zhang, H. Chen, D.M. Barbieri, I. Hoff, Laboratory Evaluation of Mechanical Properties of Asphalt Mixtures Exposed to Sodium Chloride, Transp. Res. Rec. 03611981221082579 (2022).
[11] NCHRP, Guide for mechanistic-empirical design of new and rehabilitated pavement structures, NCHRP 1-37A Final Rep. (2004).
[12] D. Andrei, M. Witczak, M. Mirza, Development of a revised predictive model for the dynamic (complex) modulus of asphalt mixtures, Development of the 2002 guide for the design of new and rehabilitated pavement structures, NCHRP (1999).
[13] D. Christensen Jr, T. Pellinen, R. Bonaquist, Hirsch model for estimating the modulus of asphalt concrete, J. Assoc. Asphalt Paving Technol. 72 (2003).
[14] G. Al-Khateeb, A. Shenoy, N. Gibson, T. Harman, A new simplistic model for dynamic modulus predictions of asphalt paving mixtures, J. Assoc. Asphalt Paving Technol. 75 (2006).
[15] M.S. Sakhaeifar, Y.R. Kim, P. Kabir, New predictive models for the dynamic modulus of hot mix asphalt, Constr. Build. Mater. 76 (2015) 221–231.
[16] S. Yousefdoost, B. Vuong, I. Rickards, P. Armstrong, B. Sullivan, Evaluation of dynamic modulus predictive models for typical Australian asphalt mixes, in: Proceedings of the 15th AAPA International Flexible Pavements Conference, 2013, pp. 22–25.
[17] C. Zhang, S. Shen, X. Jia, Modification of the Hirsch dynamic modulus prediction model for asphalt mixtures, J. Mater. Civ. Eng. 29 (12) (2017) 04017241.
[18] Y. Ali, M. Irfan, S. Ahmed, S. Khanzada, T. Mahmood, Investigation of factors affecting dynamic modulus and phase angle of various asphalt concrete mixtures, Mater. Struct. 49 (3) (2016) 857–868.
[19] X. Shu, B. Huang, Micromechanics-based dynamic modulus prediction of polymeric asphalt concrete mixtures, Compos. B Eng. 39 (4) (2008) 704–713.
[20] M. Zhang, H. Zhao, L. Fan, J. Yi, Dynamic modulus prediction model and analysis of factors influencing asphalt mixtures using gray relational analysis methods, J. Mater. Res. Technol. (2022).
[21] Y. Bi, F. Guo, J. Zhang, J. Pei, R. Li, Correlation analysis between asphalt binder/asphalt mastic properties and dynamic modulus of asphalt mixture, Constr. Build. Mater. 276 (2021), 122256.
[22] CEN, EN 12591 Bitumen and bituminous binders, Specifications for paving grade bitumens, Brussels, Belgium, (2011).
[23] CEN, EN 1426 Bitumen and bituminous binders, Determination of needle penetration, Brussels, Belgium, (2015).
[24] CEN, EN 1427 Bitumen and bituminous binders, Determination of the softening point, Ring and Ball method, Brussels, Belgium, (2015).
[25] CEN, EN 13702 Bitumen and bituminous binders, Determination of dynamic viscosity of bitumen and bituminous binders by the cone and plate method, Brussels, Belgium, (2018).
[26] D. Barbieri, I. Hoff, H. Mork, Laboratory investigation on unbound materials used in a highway with premature damage, Bearing capacity of Roads, Railways and Airfields, CRC Press (2017) 101-108.
[27] D.M. Barbieri, I. Hoff, M.B.E. Mørk, Mechanical assessment of crushed rocks derived from tunnelling operations, Civil Infrastructures Confronting Severe Weathers and Climate Changes Conference (2018) 225–241.
[28] NPRA, N200 Road construction, Norway, (2018).
[29] CEN, EN 1097-9 Tests for mechanical and physical properties of aggregates, Part 9 Determination of the resistance to wear by abrasion from studded tyres, Nordic test, Brussels, Belgium, (2014).
[30] CEN, EN 1097-1 Tests for mechanical and physical properties of aggregates, Part 1 Determination of the resistance to wear (micro-Deval), Brussels, Belgium, (2011).
[31] CEN, EN 1097-2 Tests for mechanical and physical properties of aggregates, Part 2 Methods for the determination of resistance to fragmentation, Brussels, Belgium, (2020).
[32] R.E. Asbjørn Arnevik, Nils Sigurd Uthus, Joralf Aurstad, Jostein Aksnes, Torbjørn Jørgensen, Nr. 670 Guidelines asphalt 2019, Norway, (2019).
[33] S. Anastasio, I. Hoff, C.C. Thodesen, H.U. Bahia, Laboratory testing methods for evaluating the moisture damage on the aggregate-asphalt system, in: 8th RILEM International Symposium on Testing and Characterization of Sustainable and Innovative Bituminous Materials, Springer, 2016, pp. 533–543.
[34] CEN, EN 12697-35 Bituminous mixtures, Test methods, Part 35 Laboratory mixing, Brussels, Belgium, (2016).
[35] CEN, EN 12697-33 Bituminous mixtures, Test method, Part 33 Specimen prepared by roller compactor, Brussels, Belgium, (2019).
[36] H. Chen, D.M. Barbieri, I. Hoff, H. Mork, P. Wathne, G. Liu, Construction of asphalt mixture master curves for a Norwegian mechanistic-empirical pavement design system, Eleventh International Conference on the Bearing Capacity of Roads, Railways and Airfields, Volume 2, CRC Press (2022) 423-434.
[37] CEN, EN 12697-6 Bituminous mixtures, Test methods, Part 6 Determination of bulk density of bituminous specimens, Brussels, Belgium, (2020).
[38] CEN, EN 12697-8 Bituminous mixtures, Test methods, Part 8 Determination of void characteristics of bituminous specimens, Brussels, Belgium, (2018).
[39] H. Luo, X. Huang, T. Rongyan, H. Ding, J. Huang, D. Wang, Y. Liu, Z. Hong, Advanced method for measuring asphalt viscosity: Rotational plate viscosity method and its application to asphalt construction temperature prediction, Constr. Build. Mater. 301 (2021), 124129.
[40] CEN, EN 14770 Bitumen and bituminous binders, Determination of complex shear modulus and phase angle, Dynamic Shear Rheometer (DSR), Brussels, Belgium, (2012).
[41] CEN, EN 12697-26 Bituminous mixtures, Test methods, Part 26 Stiffness, Brussels, Belgium, (2018).
[42] R. Schmidt, A practical method for measuring the resilient modulus of asphalt-treated mixes, Highw. Res. Rec. 404 (1972).
[43] Y.R. Kim, Y. Seo, M. King, M. Momen, Dynamic modulus testing of asphalt concrete in indirect tension mode, Transp. Res. Rec. 1891 (1) (2004) 163–173.
[44] E. Behzadfar, S.G. Hatzikiriakos, Viscoelastic properties and constitutive modelling of bitumen, Fuel 108 (2013) 391–399.
[45] M. Woldekidan, M. Huurman, A. Pronk, A modified HS model: Numerical applications in modeling the response of bituminous materials, Finite Elem. Anal. Des. 53 (2012) 37–47.
[46] G. Liu, G. Leegwater, E. Nielsen, J. Komacka, M. van de Ven, Evaluating the rheological properties of PMB-containing RA binders from surface-layer asphalt mixtures to be recycled, Constr. Build. Mater. 49 (2013) 8–14.
[47] M.L. Williams, R.F. Landel, J.D. Ferry, The temperature dependence of relaxation mechanisms in amorphous polymers and other glass-forming liquids, J. Am. Chem. Soc. 77 (14) (1955) 3701–3707.
[48] H. Chen, D.M. Barbieri, X. Zhang, I. Hoff, Reliability of Calculation of Dynamic Modulus for Asphalt Mixtures Using Different Master Curve Models and Shift Factor Equations, Materials 15 (12) (2022) 4325.
[49] Y. Kuo, T. Yang, G.-W. Huang, The use of grey relational analysis in solving multiple attribute decision-making problems, Comput. Ind. Eng. 55 (1) (2008) 80–93.
[50] X. Hou, B. Liang, F. Xiao, J. Wang, T. Wang, Characterizing asphalt aging behaviors and rheological properties based on spectrophotometry, Constr. Build. Mater. 256 (2020), 119401.
[51] J. Li, F. Xiao, S.N. Amirkhanian, High temperature rheological characteristics of plasma-treated crumb rubber modified binders, Constr. Build. Mater. 236 (2020), 117614.
[52] F. Guo, J. Zhang, J. Pei, B. Zhou, A.C. Falchetto, Z. Hu, Investigating the interaction behavior between asphalt binder and rubber in rubber asphalt by molecular dynamics simulation, Constr. Build. Mater. 252 (2020), 118956.
[53] V. Bulatović, V. Rek, K. Marković, Polymer modified bitumen, Mater. Res. Innov. 16 (1) (2012) 1–6.
[54] G. Liu, Y. Liang, H. Chen, H. Wang, J. Komacka, X. Gu, Influence of the chemical composition and the morphology of crumb rubbers on the rheological and self-healing properties of bitumen, Constr. Build. Mater. 210 (2019) 555–563.
[55] J. Ekblad, R. Lundström, Soft bitumen asphalt produced using RAP, Mater. Struct. 50 (1) (2017) 1–14.

APPENDIX D – PAPER IV

Chen, Hao*; Alamnie, Mequanent Mulugeta; Barbieri, Diego Maria; Zhang, Xuemei; Liu, Gang; Hoff, Inge.

Comparative study of indirect tensile test and uniaxial compression test on asphalt mixtures: Dynamic modulus and stress-strain state.

Published in the Journal of Construction and Building Materials, 366, 130187, 2023.

Construction and Building Materials 366 (2023) 130187

Contents lists available at ScienceDirect

Construction and Building Materials

journal homepage: www.elsevier.com/locate/conbuildmat

Comparative study of indirect tensile test and uniaxial compression test on asphalt mixtures: Dynamic modulus and stress-strain state

Hao Chen [a,*], Mequanent Mulugeta Alamnie [b], Diego Maria Barbieri [a,c], Xuemei Zhang [a], Gang Liu [d], Inge Hoff [a]

[a] Department of Civil and Environmental Engineering, Norwegian University of Science and Technology, Trondheim 7491, Norway
[b] Department of Engineering Sciences, University of Agder, Grimstad 4879, Norway
[c] Department of Mechanical and Structural Engineering and Materials Science, University of Stavanger, Stavanger 4021, Norway
[d] School of Materials Science and Engineering, Wuhan University of Technology, Wuhan 430070, China

ARTICLE INFO

Keywords:
Indirect tensile test
Uniaxial compression test
Asphalt mixture
Master curve
Dynamic modulus
Stress–strain state

ABSTRACT

Dynamic modulus is an essential parameter for the performance characterisation of asphalt materials for performance prediction and pavement design. The Indirect Tensile (IDT) test and the Uniaxial Compression (UC) test are both well-known experiments performed in the laboratory to characterise the dynamic modulus of asphalt mixtures over a range of temperatures and loading frequencies. A considerable amount of research has investigated the difference between two test modes, while few studies analysed the fundamental difference in stress–strain distributions for the two test setups. This work aims at comparing the effect of the two test methods on dynamic modulus of asphalt mixtures, as well as stress–strain state. For these purposes, two types of mixtures commonly employed to build road surface layers, namely Asphalt Concrete (AC) and Stone Mastic Asphalt (SMA), were created and tested. The specimens were prepared with a gyratory compactor. The master curves of dynamic modulus and the stress–strain states obtained from the two testing procedures were compared. The dynamic modulus and phase angle results are almost identical for medium frequency and temperature, whereas the results exhibit significant discrepancies for lower and higher frequency values. AC 11 and SMA 11 mixtures show differences in comparison between the two tests. Moreover, the strains measured by the IDT test are variable and the strains obtained from the UC test stabilise around 40 με. Similarly, both tests have poor strain control at 40 °C. The values of normalised stresses measured by the IDT test are approximately 3.26 and 2.34 times greater than the ones measured by the UC test for AC 11 and SMA 11 mixtures, respectively. In general, the results of the mechanical characterisation of the asphalt mixtures conducted using both tests are similar. The IDT test has the advantage of sample size for sample preparation methods in both laboratory and field, and the UC test has a better deformation control at low and medium temperatures.

1. Introduction

In the development of pavement design, the Mechanistic-Empirical (ME) pavement design approach applicable to various materials and environmental conditions has been gradually adopted to replace previous empirical design approaches [1,2]. The mechanical characterisation of road construction materials is necessary to predict the response of the structure according to the ME pavement design. When it comes to asphalt materials, the dynamic modulus is an essential parameter for engineering computations [3]. The dynamic modulus of asphalt mixtures mainly depends on the temperature and the loading time due to its viscoelastic properties [4–6]. The Uniaxial Compression (UC) test, which can be conducted at different temperatures and frequencies with a dynamic loading form, is the standard test method for the determination of dynamic modulus of asphalt mixture in the ME pavement design guide [7]. The dynamic modulus is calculated by dividing the peak-to-peak stress by the peak-to-peak strain for the asphalt mixture subjected to a sinusoidal load. Afterwards, the dynamic modulus master curve is constructed according to the time–temperature superposition principle [8] to predict the dynamic modulus of asphalt mixture over a

* Corresponding author.
E-mail addresses: hao.chen@ntnu.no (H. Chen), mequanent.m.alamnie@uia.no (M.M. Alamnie), diegomb271@gmail.com (D.M. Barbieri), xuemei.zhang@ntnu.no (X. Zhang), liug@whut.edu.cn (G. Liu), inge.hoff@ntnu.no (I. Hoff).

https://doi.org/10.1016/j.conbuildmat.2022.130187
Received 10 October 2022; Received in revised form 25 November 2022; Accepted 20 December 2022
Available online 26 December 2022

Table 1
Physical properties of bitumen 70/100.

Physical property	Unit	Bitumen 70/100	Test standard
Penetration at 25 °C	0.1 mm	92	EN 1426:2015 [22]
Softening point (Ring and Ball)	°C	46.0	EN 1427:2015 [23]

Table 2
Resistance to wear and fragmentation of crushed rock aggregates.

Property	Value	Requirements for AADT > 15 000	Test standard
Micro-Deval coefficient	14.2	≤ 20	EN 1097–1:2011 [24]
Los Angeles value	18.2	≤ 15	EN 1097–2:2020 [25]

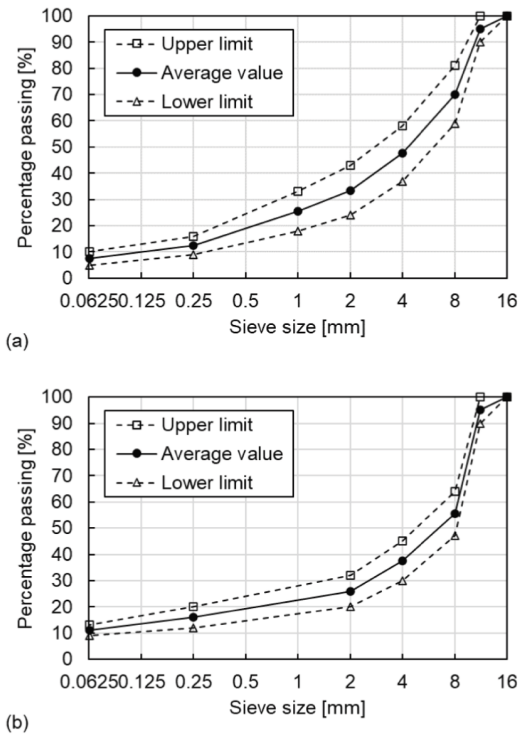

Fig. 1. Grading curves of (a) AC 11 and (b) SMA 11.

Table 3
OBC and voids characteristics of AC 11 and SMA 11.

Asphalt mixture	*OBC* [%]	Void characteristic (EN 12697–8:2018 [29])			
		V_a [%]	Standard deviation	*VFB* [%]	Standard deviation
AC 11	5.1 %	3.8 %	0.2 %	77.0 %	1.3 %
SMA 11	5.3 %	4.0 %	0.3 %	77.1 %	1.6 %

wide frequency range. This test method is widely used not only for traditional materials but also for innovative and recycled construction resources [9–11].

The dynamic modulus can be tested on samples produced in the laboratory or from samples cored from a real pavement. However, the thickness of the core sample extracted from the existing pavement is often less than the required height of the UC test. Differently, the Indirect Tensile (IDT) test determines the dynamic modulus according to a biaxial stress state on a thinner specimen [12]. Compared with UC test, the IDT test is largely used thanks to the easiness of operation (e.g., smaller samples) and its suitability to characterise core road samples. Even though the IDT test is commonly used for the evaluation of resilient modulus, strength and fatigue of asphalt mixture, it has been also performed to assess the dynamic modulus. Zaumanis et al. [13] conducted IDT investigation to determine the dynamic modulus of 100 % recycled asphalt mixtures while appraising the suitability of the IDT setup to characterise highly recycled asphalt mixtures. Mollenhauer et al. [14] obtained the stiffness of asphalt mixtures by conducting IDT tests to develop a German ME pavement design. Zhang et al. [15] have adopted the IDT test to compare the change in dynamic modulus of asphalt mixture before and after chemical ageing. The Norwegian Public Roads Administration (NPRA) is currently developing a ME pavement design system and, therefore, needs the creation of a database defining the dynamic modulus for the asphalt mixtures employed in the Nordics pavements [16].

Although both IDT and UC tests can measure the dynamic modulus of asphalt materials, their results show some discrepancies due to the different stress–strain states and test conditions [17]. Understanding these differences is important to select the correct material characterisation testing and to define the pavement design system more accurately. Kim et al. [18] developed an analytical solution to assess the dynamic modulus from the IDT test. In this regard, twelve asphalt mixtures used in North Carolina were tested according to both IDT and UC procedures. The results displayed a little discrepancy in the dynamic modulus master curves. However, Qin et al. [19] found some differences between the two tests in dynamic modulus, phase angle, and shift factor. The dynamic modulus and shift factor measured using the UC test were higher than the corresponding values obtained using the IDT test. As very few studies shed light on the differences between the IDT and the UC testing procedures from the perspective of stress–strain states for Norwegian asphalt mixtures, this work addresses this gap as well as delves into the fundamental difference in stress–strain distributions for the two test setups and provides guidance on test methods for the development of Norwegian ME pavement design.

In this study, Asphalt Concrete (AC) and Stone Mastic Asphalt (SMA) mixtures were characterised as they were commonly used for surfacing road pavements. The mixtures were compressed using a gyratory compactor and the samples were drilled and cut according to the testing requirements. The IDT and UC tests were conducted in the laboratories of the Norwegian University of Science and Technology (NTNU) and the University of Agder (UiA), respectively. The master curves were constructed based on the ME pavement design guide and shift factor function defined by the Williams-Landel-Ferry (WLF) equation. The differences in the values of dynamic modulus, phase angle, shift factor as well as the discrepancies in the stress–strain states for the two tests were analysed.

2. Materials and test methods

2.1. Materials

The bituminous binder employed was type 70/100, which is the most used in Norwegian asphalt pavements. Crushed rocks having magmatic and metamorphic origin as well as limestone filler were used as aggregates [20,21]. The main physical properties of the binder are given in Table 1. The resistance of aggregates to wear and fragmentation is

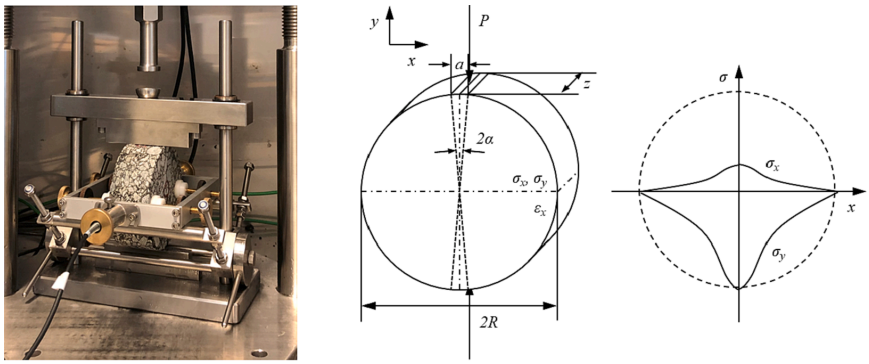

Fig. 2. (a) IDT test setup using UTM, (b) scheme of IDT test specimen subjected to a vertical load and (c) stress distribution.

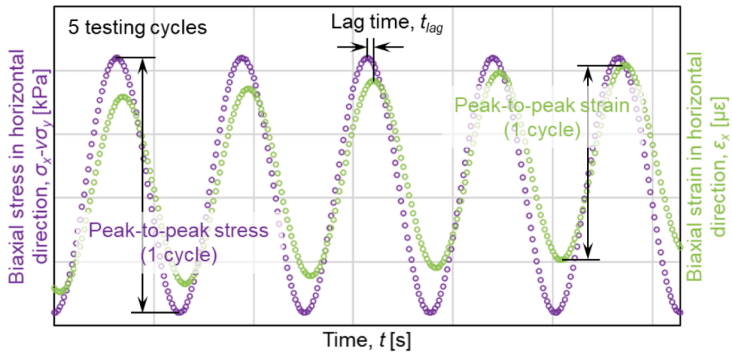

Fig. 3. Schematic trend of stress and strain for IDT test.

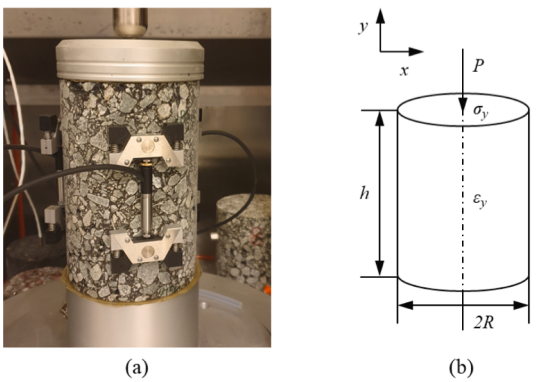

Fig. 4. (a) UC test setup using UTM-130 and (b) scheme of UC specimen subjected to a vertical load.

specified in Table 2, which fulfils the Norwegian requirements of AC and SMA mixtures with an Annual Average Daily Traffic (AADT) higher than 15 000.

2.2. Sample preparation

Sample preparation is very important for the results from laboratory testing of asphalt and special care was taken to produce samples as homogeneous as possible to compare the two testing methods without any bias from the sample preparation.

The particle size distributions are given in Fig. 1 and the average gradation curves are selected to prepare the tested samples. The Optimum Binder Content (*OBC*) was determined by the Marshall mixture design. The asphalt mixture specimens were prepared in the laboratory of NTNU using a gyratory compactor (ICT-150RB produced by Invelop Oy, Savonlinna, Finland). The compaction pressure was 620 kPa, and the gyratory angle was set to 17 mrad (0.97°) [26]. The 100 and 115 design gyrations were applied for the AC 11 and SMA 11, respectively [27]. Asphalt cylinders with a diameter of 150 mm and a height of 180 mm were thus obtained; afterwards, IDT specimens (diameter = 100 mm, height = 40 mm) and UC specimens (diameter = 100 mm, height = 150 mm) were drilled and cut. The *OBC* and the void characteristics including the Air Voids Content (V_a) and the Voids Filled with Binder (*VFB*) are shown in Table 3, which fulfil the corresponding requirements [28]. Four replicate samples were created for each asphalt mixture type.

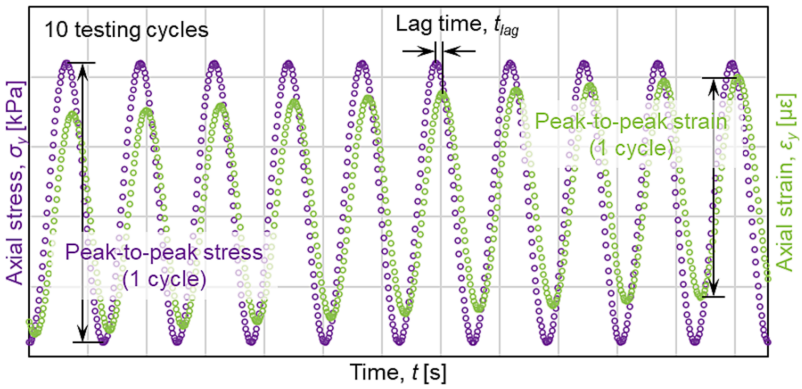

Fig. 5. Schematic trend of stress and strain for UC test.

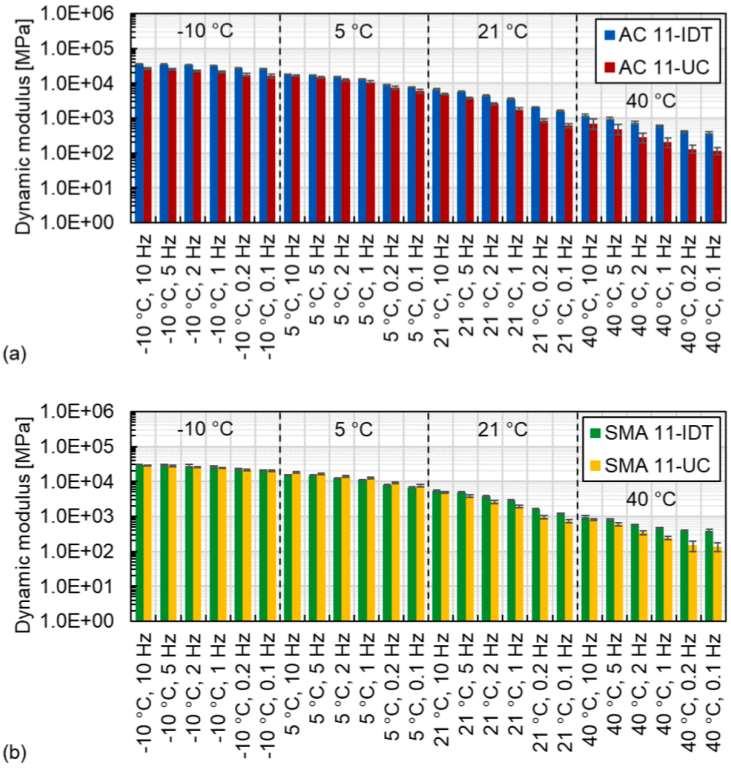

Fig. 6. Dynamic modulus results: (a) AC 11 and (b) SMA 11.

A total of 16 samples were tested and they were denominated as AC 11-IDT, AC 11-UC, SMA 11-IDT and SMA 11-UC.

2.3. Dynamic modulus tests

2.3.1. Indirect tensile test

The cyclic IDT test was performed by a servo-pneumatic Universal Testing Machine (UTM) produced by Cooper Technology exerting a controlled harmonic sinusoidal load with a haversine wave. Two Linear Variable Differential Transformers (LVDT) were used on both sides in the horizontal direction. The test was conducted in accordance with EN 12697–26 [30] at frequencies of 10, 5, 2, 1, 0.2 and 0.1 Hz and the temperatures of −10, 5, 21 and 40 °C to obtain a broad and continuous dynamic modulus master curve for measured values. The applied loads were adjusted to keep the initial horizontal strain amplitude in a range between 50 με to 100 με for every testing temperature and frequency. The IDT test is regarded as a stress–strain dual control test.

The scheme of the IDT test is shown in Fig. 2; the x and y axes are

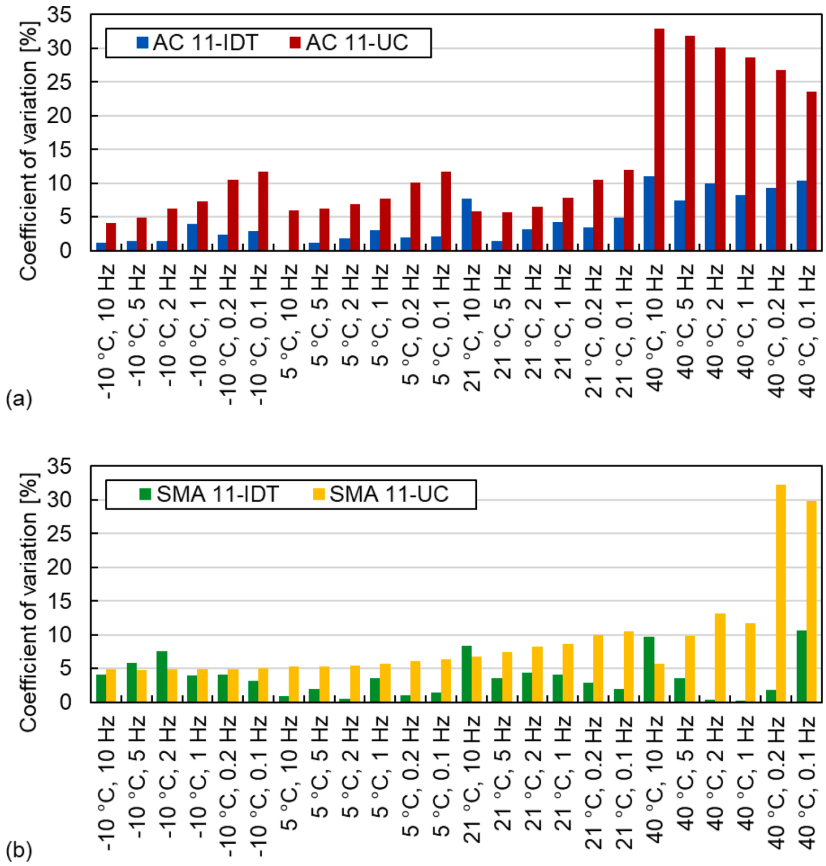

Fig. 7. Coefficient of variation of dynamic modulus results: (a) AC 11 and (b) SMA 11.

defined as the horizontal and vertical direction, respectively. Based on the linear viscoelastic solution the stress and strain in the horizontal direction of the IDT test specimen are used to calculate the dynamic modulus [18]. The stress distribution is presented in Fig. 2(c). The coordinate axis between the position in the horizontal direction and the stress at this position was established. The IDT test specimen was applied a vertical harmonic sinusoidal load, P, which can be expressed as shown in Eq. (1). Along the horizontal diameter of the IDT specimen the horizontal stress, $\sigma_x(x)$, and the vertical stress, $\sigma_y(x)$, can be evaluated as defined by Eq. (2) and Eq. (3), respectively [31–33].

$$P = P_0 \cdot e^{i\omega t} = P_0[\cos(\omega t) + i\sin(\omega t)] \tag{1}$$

$$\sigma_x(x) = \frac{2P}{\pi a z}\left[\frac{(1 - x^2/R^2)\sin 2\alpha}{1 + 2(x^2/R^2)\cos 2\alpha + x^4/R^4} - \tan^{-1}\left(\frac{1 - x^2/R^2}{1 + x^2/R^2}\tan\alpha\right)\right] = \frac{2P}{\pi a z}[f(x) - g(x)] \tag{2}$$

$$\sigma_y(x) = -\frac{2P}{\pi a z}\left[\frac{(1 - x^2/R^2)\sin 2\alpha}{1 + 2(x^2/R^2)\cos 2\alpha + x^4/R^4} + \tan^{-1}\left(\frac{1 - x^2/R^2}{1 + x^2/R^2}\tan\alpha\right)\right] = -\frac{2P}{\pi a z}[f(x) + g(x)] \tag{3}$$

where x is the distance from the origin along the abscissa, P_0 is the amplitude of the sinusoidal load, ω is the angular frequency of the sinusoidal load, t is time, a is the loading strip width, z is the thickness of the sample and R is the radius of the sample. The horizontal strain, $\varepsilon_x(x, t)$, is expressed:

$$\varepsilon_x(x,t) = \frac{1}{E^*}[\sigma_x(x) - \nu\sigma_y(x)] = \frac{2P_0}{E^*\pi a z}e^{i(\omega t - \varphi)}[(\nu + 1)f(x) + (\nu - 1)g(x)] \tag{4}$$

where E^* is the dynamic modulus, φ is the phase angle and ν is the Poisson's ratio. The total deformation between $-R$ and R at the horizontal central axis, $\Delta H(t)$, is given:

$$\Delta H(t) = \int_{-R}^{R}\varepsilon_x(x,t)dx = \frac{2P_0}{E^*\pi a z}e^{i(\omega t - \varphi)}\left[(\nu + 1)\int_{-R}^{R}f(x)dx + (\nu - 1)\int_{-R}^{R}g(x)dx\right] = \frac{2P_0}{E^*\pi a z}e^{i(\omega t - \varphi)}A \tag{5}$$

Therefore, in the IDT mode, the dynamic modulus from the horizontal deformation can be expressed as:

$$E^* = |E^*| \cdot e^{i\varphi} = \frac{2P_0\sin(\omega t - \varphi)}{\pi a z \Delta H(t)}A \tag{6}$$

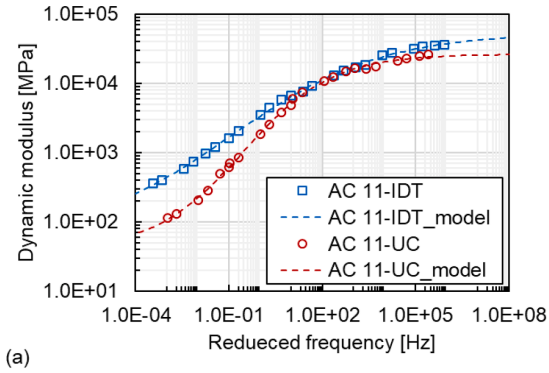

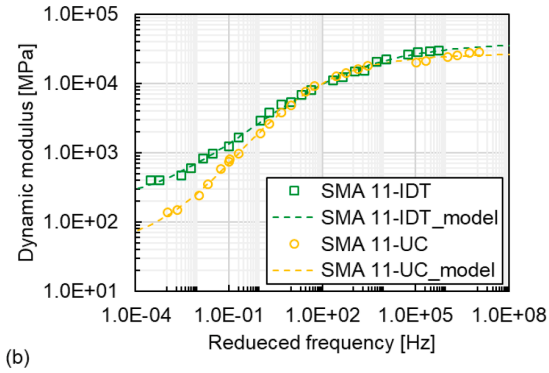

Fig. 8. Master curves of dynamic modulus: (a) AC 11 and (b) SMA 11.

Table 4
The fitting parameters and statistical parameters of the dynamic modulus master curves for asphalt mixtures.

Fitting parameter		AC 11-IDT	SMA 11-IDT	AC 11-UC	SMA 11-UC
Sigmoidal function	δ	1.755	2.152	1.594	1.575
	α	2.974	2.431	2.823	2.847
	β	−0.382	−0.106	−0.385	−0.432
	γ	0.413	0.504	0.701	0.650
WLF equation	C_1	33.802	49.893	19.297	11.018
	C_2	243.539	356.001	166.369	87.622
Goodness of fit statistics					
S_e		724.649	673.983	798.555	1098.795
S_y		12566.958	10345.098	8937.466	10067.358
S_e/S_y		0.058	0.065	0.089	0.109
R^2		0.997	0.996	0.992	0.988

where $|E^*|$ is the norm of the dynamic modulus.

The schematic trend of the stress–strain state for the IDT test is shown in Fig. 3. In the IDT test mode, the value of biaxial stress and strain in the horizontal direction were recorded. The peak-to-peak stress and strain of the specified five cycles per test condition according to EN 12697–26 [30] are used to determine the dynamic modulus. For the cyclic IDT test, the vertical load and the peak-to-peak deformation were recorded to calculate the dynamic modulus based on Eq. (6). The test data is analysed to obtain the dynamic modulus of the IDT test specimen under a certain test condition. The strain response lags to the stress due to the viscoelastic behaviour of asphalt materials, as shown in Fig. 3. The phase angle is to describe the lag of the strain response, which is equal to the lag time, t_{lag}, multiplied by the angular frequency. The stress and

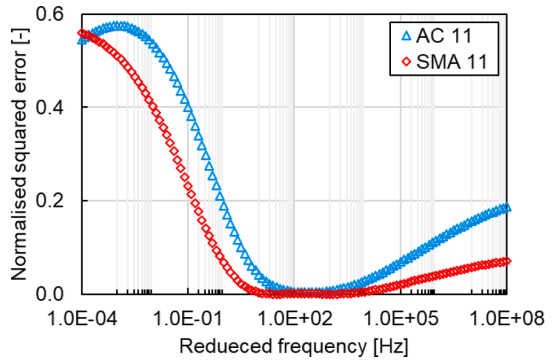

Fig. 9. *NSE* of dynamic modulus between two test modes for AC 11 and SMA 11.

strain as a function of the time are expressed in Eq. (7) and Eq. (8).

$$\varepsilon(t) = \varepsilon_0 \sin(\omega t) \tag{7}$$

$$\sigma(t) = \sigma_0 \sin(\omega t - \varphi) \tag{8}$$

where σ_0 is the stress amplitude, and ε_0 is the strain amplitude.

2.3.2. Uniaxial compression test

The UC test was performed using the servo-hydraulic UTM (UTM-130) manufactured by IPC global®. The machine is capable of exerting sinusoidal axial load over a wide range of frequencies. Three LVDT with 70 mm gauge lengths installed at 120°apart were used. The test was conducted in accordance with AASHTO T378-17 [34] at the same test conditions as the IDT test. The UC dynamic modulus test was performed in a controlled-strain mode with a target strain of 50 με or less.

The illustration of the UC test is shown in Fig. 4. Differently from the IDT test, the UC test determines the dynamic modulus uniaxially as it measures the vertical stress, $\sigma_y(t)$, and strain, $\varepsilon_y(t)$, along the direction of the applied load as shown in Fig. 5., which is expressed as follows.

$$E^* = |E^*| \cdot e^{i\varphi} = \frac{\sigma_y(t)}{\varepsilon_y(t)} = \frac{\sigma_0 \sin(\omega t - \varphi)}{\varepsilon_0 \sin(\omega t)} \tag{9}$$

In the UC test, the value of axial stress and strain were recorded. The mean value of stiffness from the 10 testing cycles determined the dynamic modulus of the UC test specimen at a certain test condition. As the same as the IDT test, the phase angle can be determined by the lag time between stress and strain.

2.4. Master curve construction

The master curve was constructed by fitting the experimental test data of dynamic modulus according to the sigmoidal function described in the ME pavement design guide was selected as expressed in Eq. (10) and Eq. (11). The WLF equation given in Eq. (12) was used to describe the relationship between shift factor and temperature above the glass transition temperature (T_g) [35].

$$\log(|E^*|) = \delta + \frac{\alpha}{1 + e^{\beta - \gamma(\log f_r)}} \tag{10}$$

$$\log(f_r) = \log(f) + \log[\alpha(T)] \tag{11}$$

where f_r is the frequency at the reference temperature, T_r, T is the test temperature, $\alpha(T)$ is the shift factor, δ, α, β and γ are the fitting parameters.

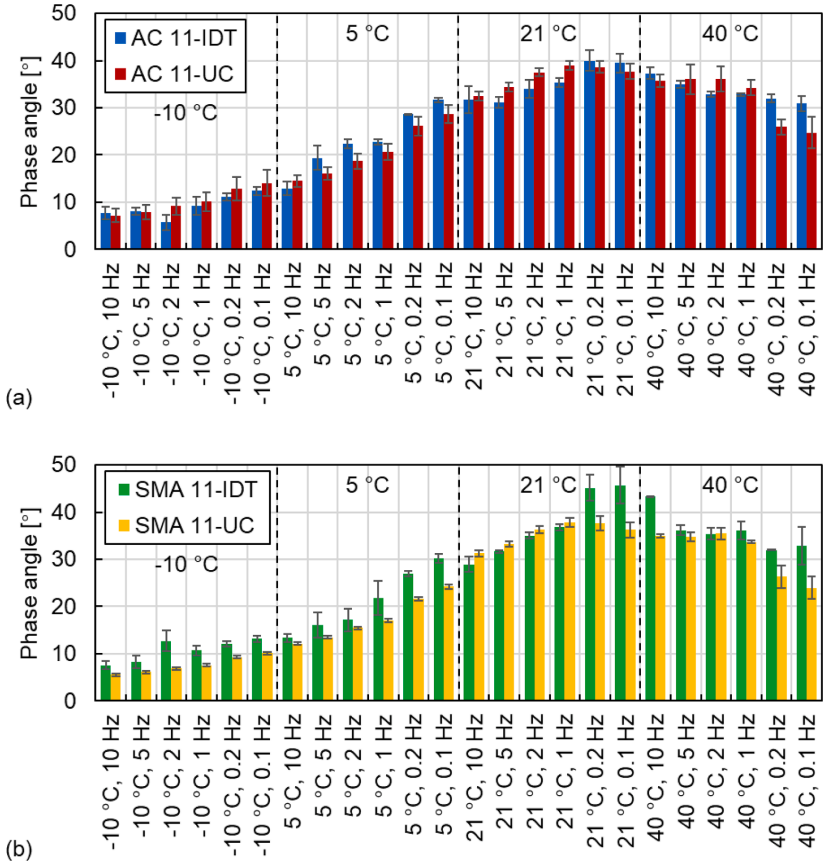

Fig. 10. Phase angle results: (a) AC 11 and (b) SMA 11.

$$\log[\alpha(T)] = \frac{-C_1(T - T_r)}{C_2 + (T - T_r)} \tag{12}$$

where C_1 and C_2 are the fitting parameters. The reference temperature of master curve construction for both tests was the same at 21 °C.

The phase angle master curve was constructed through the Lorentzian equation, denoted as Eq. (13) [36,37]:

$$\varphi = \frac{k_p \cdot k_g^2}{[\log(f_r) - k_c]^2 + k_g^2} \tag{13}$$

where φ is the phase angle, k_p is the peak value, k_g is the growth rate and k_c is the critical point. The master curves of both tests were constructed using the Solver add-in tool in Microsoft Excel. The non-linear least squares regression was performed to fit the test data based on the sigmoidal function, WLF equation and Lorentzian equation [38,39].

3. Results and discussion

3.1. Master curve of dynamic modulus and phase angle

3.1.1. Dynamic modulus

The dynamic modulus results of the IDT and the UC tests are shown in Fig. 6. Fig. 6(a) displays that the dynamic moduli of AC 11 mixtures measured by both tests are similar at 5 °C and there are some differences at higher and lower temperatures. The dynamic moduli of SMA 11 mixtures obtained by two tests are similar at low temperatures (-10 and 5 °C) and different at higher temperatures. The Coefficients of Variation (*CoV*) of the dynamic modulus results are given in Fig. 7. The *CoV* of AC 11-IDT, AC 11-UC, SMA 11-IDT and SMA 11-UC are smaller at −10, 5, 21 °C, which are around 10 % or less. The *CoV* of AC 11-IDT, SMA 11-IDT and SMA 11-UC are bigger at 40 °C, which is up to 30 %. This indicates that the dynamic modulus test has a smaller variation at low temperatures and a bigger variation at high temperatures. Furthermore, the *CoV* of SMA 11 mixtures are lower than the ones of AC 11 mixtures, which displays that the grading type of mixtures has an influence on the test variation.

To compare the two test methods under a wider range of conditions, dynamic modulus master curves of asphalt mixtures are constructed. The dynamic modulus master curves of AC 11-IDT, SMA 11-IDT, AC 11-UC and SMA 11-UC are presented in Fig. 8. The fitting parameters and the goodness of fit statistics [40], including the standard error of estimation (S_e), the standard error of deviation (S_y), the standard error ratio (S_e/S_y) and the coefficients of determination (R^2), are given in Table 4. All master curves have good fits. The R^2 of dynamic modulus are over 0.988. Both R^2 of dynamic modulus for AC 11-IDT and SMA 11-IDT are bigger than the R^2 values of AC 11-UC and SMA 11-UC. Meanwhile, both the S_e/S_y of dynamic modulus for AC 11-IDT and SMA 11-IDT are smaller than the S_e/S_y of AC 11-UC and SMA 11-UC. These outcomes

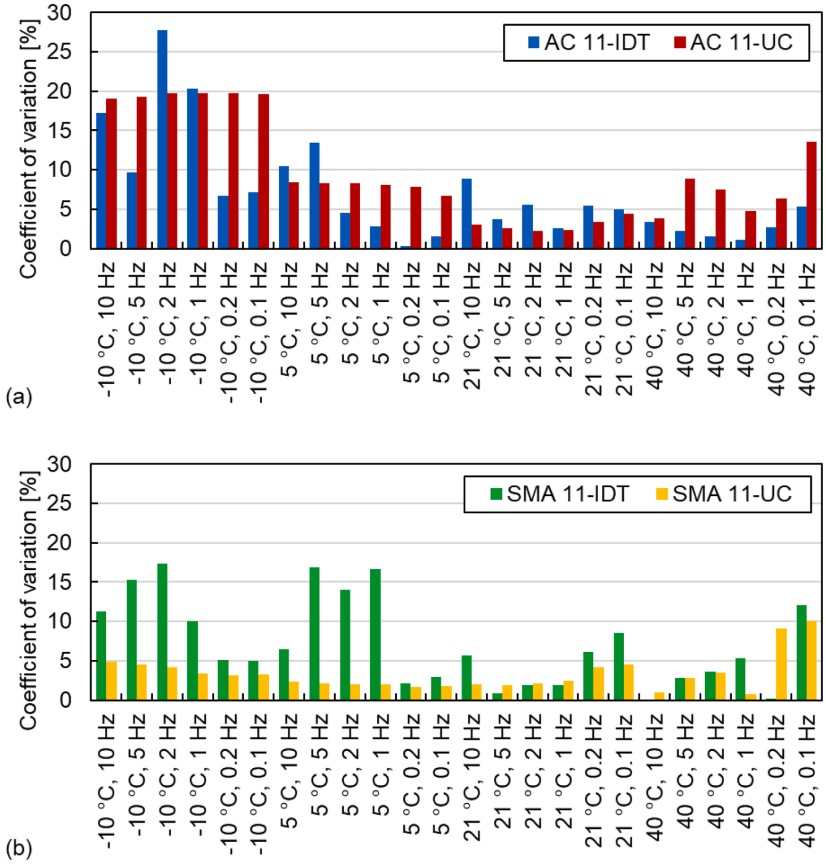

Fig. 11. Coefficient of variation of phase angle results: (a) AC 11 and (b) SMA 11.

indicate that the dynamic modulus master curves have a better fit for IDT test data. Furthermore, it can be observed from Fig. 8 that the dynamic moduli obtained by the two tests are relatively consistent in the frequency range from 10 Hz to 10^4 Hz. When the frequency is higher than 10^4 Hz or lower than 10 Hz, the dynamic moduli display differences. Compared with SMA 11, two tests induce a more severe difference in dynamic modulus at both higher and lower frequencies for AC 11. This result indicates that AC 11 structure tends to expand the difference in dynamic modulus caused by the two tests compared to SMA 11 structure.

As all the dynamic modulus master curves of the four asphalt mixtures have a good fit, the dynamic modulus predicted by the master curves at each frequency is compared by the Normalized Squared Error (*NSE*) following Eq. (14). The smaller the *NSE* value, the more consistent the two test results.

$$NSE = \frac{\left(|E^*|_{IDT} - |E^*|_{UC}\right)^2}{|E^*|_{IDT}^2} \tag{14}$$

where $|E^*|_{IDT}$ is the dynamic modulus obtained by the IDT test, $|E^*|_{UC}$ is the dynamic modulus obtained by the UC test. The *NSE* between two tests of AC 11 and SMA 11 is illustrated in Fig. 9. The dynamic moduli obtained by the two tests are considered relatively consistent with a *NSE* less than 0.005.

As presented in Fig. 9, the dynamic moduli obtained from both tests for the AC 11 are consistent in the frequency range from 10^2 Hz to 10^3 Hz. The dynamic modulus evaluated from both tests for the SMA 11 is consistent in the frequency range from 10 Hz to 10^4 Hz. Meanwhile, the *NSE* of the two mixtures increase gradually with the increase of the frequency over 10^4 Hz or decrease of the frequency less than 10 Hz. The *NSE* of SMA 11 is smaller than that of the *NSE* of AC 11. These results indicate that the dynamic moduli of asphalt mixtures measured by the two tests are almost the same in the reduced frequency range from 10 Hz to 10^4 Hz. On the contrary, differences are found at high and low frequencies (temperatures) where the dynamic moduli measured by the IDT test are greater than those obtained with UC test. Fig. 9 shows that the *NSE* of the two mixtures is large at extreme frequencies, particularly at very low reduced frequencies. This might be connected to the various stress–strain responses of the specimens under the two test modes at relatively high temperatures. The difference in *NSE* between the two asphalt mixtures might be caused by the distinct physical structures. Comparing with AC 11 mixture, SMA 11 has an embedded structure between large size aggregates and its dynamic modulus is less affected by temperature [41].

3.1.2. Phase angle

Fig. 10 presents the phase angle results of the IDT test and the UC test. The phase angles obtained by both tests are similar at 21 °C for AC 11 and SMA 11 mixtures. The differences in phase angles between the

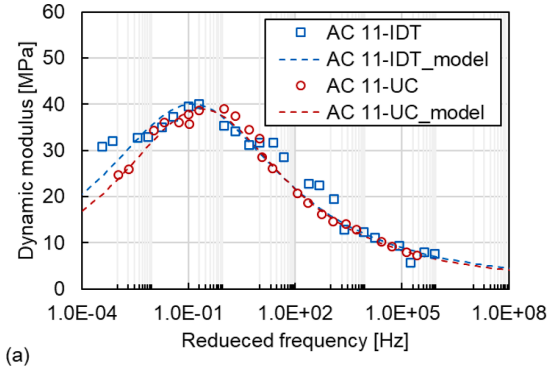

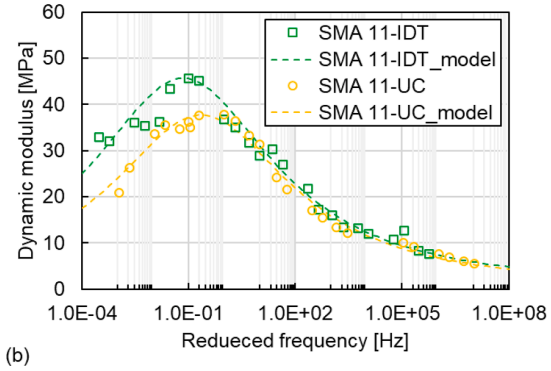

Fig. 12. Master curves of phase angle: (a) AC 11 and (b) SMA 11.

Table 5
The fitting parameters and statistical parameters of the phase angle master curves for asphalt mixtures.

Fitting parameter		AC 11-IDT	SMA 11-IDT	AC 11-UC	SMA 11-UC
Lorentzian equation	k_p	40.006	45.656	38.960	37.745
	k_g	3.167	3.141	2.946	3.114
	k_c	−0.910	−1.154	−0.639	−0.653
Goodness of fit statistics					
S_e		2.961	2.661	1.299	1.611
S_y		11.358	12.273	11.223	11.934
S_e/S_y		0.261	0.217	0.116	0.135
R^2		0.932	0.953	0.987	0.982

two tests occur at higher and lower temperatures. The *CoV* of phase angle results are smaller at 21 °C as shown in Fig. 11, which indicates that the two test modes are stable at 21 °C leading to fewer result differences of both tests in the properties of the same materials.

Similar to the dynamic modulus, phase angle master curves are constructed to compare the differences between the two test methods over a wider range of conditions. The phase angle master curves of AC 11-IDT, SMA 11-IDT, AC 11-UC and SMA 11-UC are presented in Fig. 12. The fitting parameters and the goodness of fit statistics are given in Table 5. The statistical parameters of phase angle for the two tests are different from the ones of dynamic modulus. Both R^2 of phase angle for AC 11-IDT and SMA 11-IDT are smaller than R^2 of AC 11-UC and SMA 11-UC shown in Table 5. Both S_e/S_y of phase angle for AC 11-IDT and SMA 11-IDT exceed S_e/S_y of AC 11-UC and SMA 11-UC. Thus, the phase

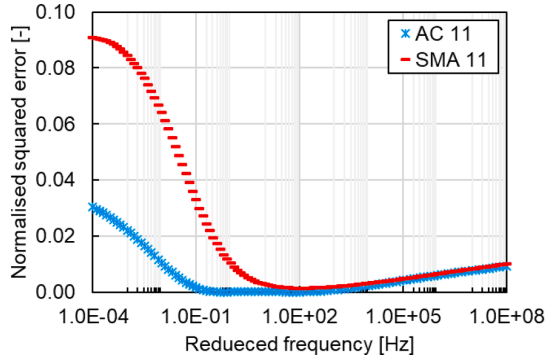

Fig. 13. *NSE* of phase angle between two test modes for AC 11 and SMA 11.

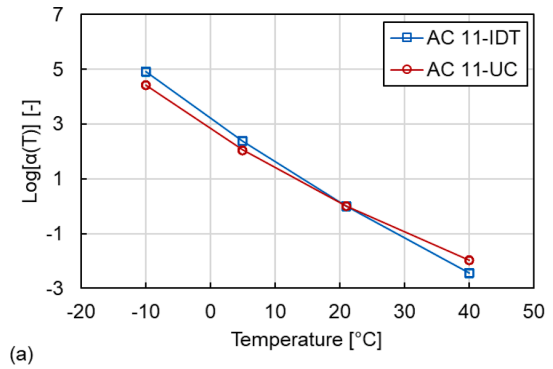

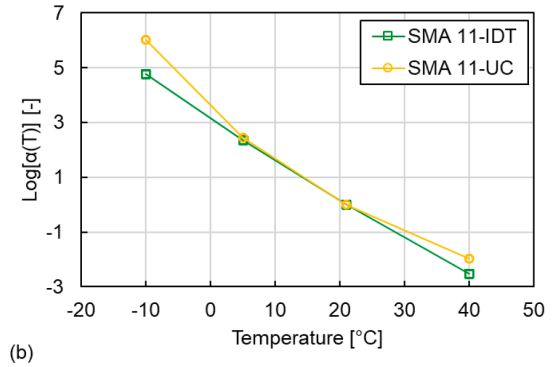

Fig. 14. Shift factors for specimens: (a) AC 11 and (b) SMA 11.

angle master curves of the UC test data have a better fit than that of the IDT test data. As shown in Fig. 12, the phase angle master curves for both tests are similar at high frequencies and show differences at lower frequencies. This difference is more severe for the SMA 11 mixtures than for the AC 11 mixtures.

The *NSE* of the phase angle is calculated from the Lorentzian equation and is also utilised to compare the phase angle at each frequency as similar to the comparison of dynamic modulus. Fig. 13 presents the *NSE* of phase angle for AC 11 and SMA 11. A smaller *NSE* value is obtained at a higher frequency and a bigger *NSE* value emerged at a lower

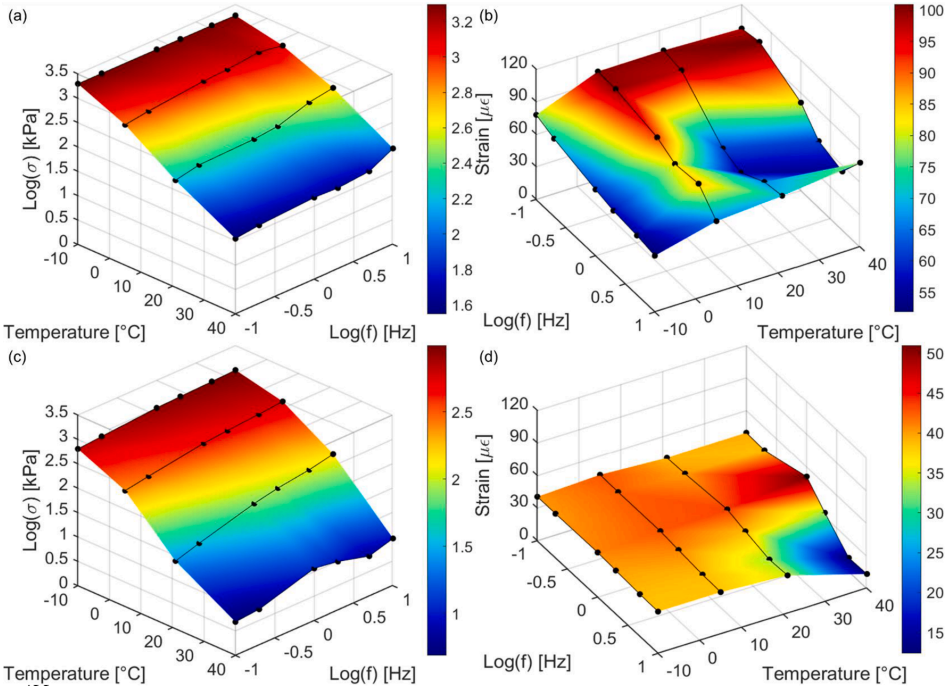

Fig. 15. Stress–strain states of AC 11 in IDT test and UC test at various conditions: (a) AC 11-IDT stress, (b) AC 11-IDT strain, (c) AC 11-UC stress and (d) AC 11-UC strain.

frequency. Meanwhile, the *NSE* of AC 11 is less than 0.005 in the range of 0.1 Hz to 10^5 Hz, showing the consistency of the phase angle of the two tests in this range. For the SMA 11 mixtures, the consistent range of phase angles from 10 Hz to 10^5 Hz for both tests is smaller than the range for the AC 11 mixtures. Furthermore, the *NSE* values of SMA 11 mixtures are bigger than the ones of AC 11 mixtures in the low frequency range. This phenomenon indicates that the difference in phase angle between the two test methods is larger for SMA 11 mixtures than for AC 11 mixtures. Besides, the phase angle of the IDT test is larger than that of the UC test, which is consistent with Kim's research [18]. The horizontal phase angles of the IDT test are generally higher than the phase angles determined from the UC test. The averaged phase angles from horizontal direction and vertical direction are close to the values from the UC test. It can be interpreted that the IDT test only considers the phase angle in the horizontal direction.

3.1.3. Shift factor

The results of the shift factor are also investigated, as shown in Fig. 14. The shift factor reflects how far the measured values have moved relative to the dynamic modulus at the reference temperature, resulting in an impact on the modelling values of the master curves. In terms of AC 11 mixtures, the slope of the shift factor of AC 11-IDT is higher than the one of AC 11-UC, which means that the curve of AC 11-IDT is shifted more in the construction of the master curve than that of AC 11-UC. However, for the SMA 11 mixtures, the measured values of SMA 11-UC move more at high frequencies relative to SMA 11-IDT. When the measured values are higher, moving more distance to high and low frequencies widens the difference, reflecting that the difference in dynamic modulus of the two test methods is greater for the AC 11 mixtures than for the SMA 11 mixtures. This result reveals that the structure of the tested asphalt mixture has a great impact on the results obtained with the two test procedures. The SMA mixtures with the embedded structure are less affected by the test than the AC mixtures with the dense structure.

3.2. Comparison of stress–strain state

3.2.1. Stress–strain response

The stress–strain states are obtained based on Section 2.3. The stress amplitude of the IDT test is expressed in Eq. (15). The stress amplitude of the UC test and the strain amplitudes of the two tests can be obtained from the testing programs.

$$\begin{aligned}\sigma_0 &= \sigma_{0x} - \nu\sigma_{0y} \\ &= \frac{2P_0}{\pi az}(\sin 2\alpha - \alpha) - \nu\left[-\frac{2P_0}{\pi az}(\sin 2\alpha + \alpha)\right] \\ &\approx \frac{P_0}{\pi Rz} + \nu\frac{3P_0}{\pi Rz}\end{aligned} \tag{15}$$

The stress–strain states of AC 11 mixtures for the two tests are represented in Fig. 15 at various temperature and frequency conditions. Fig. 16 shows the *CoV* of the stress and strain results. As shown in Fig. 15 (a, c), the stresses of both test modes for AC 11 decrease as the temperature increases. This is explained that both test modes control the strain in a certain range to ensure that the tested asphalt mixture is in the linear viscoelastic range. The increase in temperature causes the softening of the asphalt mixture yet the strain range does not change. The strains of two tests for AC 11 are shown in Fig. 15(b, d). It is observed

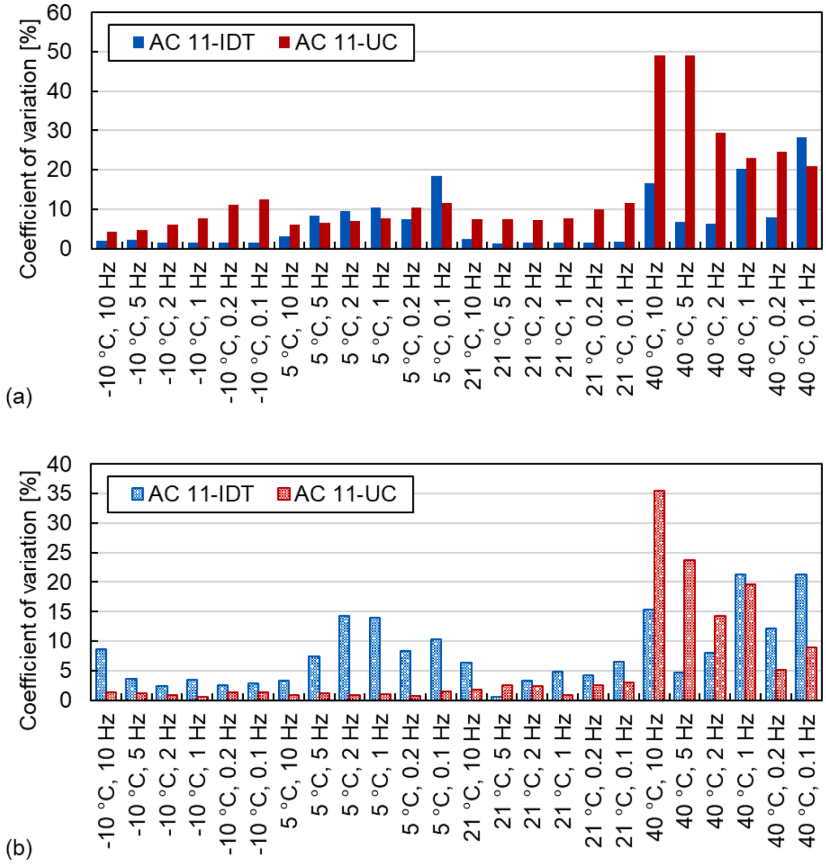

Fig. 16. Coefficient of variation of stress and strain results of AC 11 mixtures: (a) stress and (b) strain.

that the strains of the UC test are maintained around 40 με at all temperatures except for 40 °C. However, the strains of the IDT test are not stable at a certain value with the temperature changing, and there is no intuitive changing trend between the strain and the temperature. This indicates that the UC test controls the strain better than the IDT test and the strains of both tests are varied at the high temperatures.

Fig. 15 also shows the changes in stress and strain with the frequency. At low temperatures, the stresses measured for both tests are maintained at a relatively constant stress level as the frequency changes. The stresses are gradually affected by frequency as the temperature increases. For high temperatures, the stress values fluctuate more with various frequencies for both tests. The variation in the trends of strain and stress with frequency for the IDT test is similar, while the strain in the UC test is stable at an average of 40 με. When it comes to the changes in strains, the UC test has better deformation control than the IDT test. However, both approaches do not control the deformation well at high temperatures due to the viscous properties of the asphalt mixture at high temperatures. The change in the stress–strain state with temperature and frequency can be explained by considering the viscoelastic behaviour of asphalt materials. At low temperatures, the elastic component plays a major role; therefore, the dynamic modulus does not change much with frequency, and the stress and strain are stable. At high temperatures, the viscous component plays a more important role, and the dynamic modulus as well as the stress–strain state are highly related to temperature values. It is worth noting that the strain value measured during the IDT test at a high temperature and low frequency is close to the upper limit. Therefore, it is difficult to ensure that the asphalt material specimen is within the linear viscoelastic range at high temperatures when investigated with the IDT test.

Fig. 16 indicates that the *CoV* of stress and strain results for AC 11 mixtures are small at −10, 5, 21 °C and high at 40 °C, which is consistent with the *CoV* of dynamic modulus results. This result further reflects that the mechanical properties of asphalt mixtures are more stably determined at low and medium temperatures by both two test modes. The larger variations occur at high temperatures.

The stress–strain states measured for SMA 11 mixtures and their *CoV* are shown in Fig. 17 and Fig. 18, respectively. The trend of stress–strain states for SMA 11 is similar to the one for AC 11, indicating the major relevance of the viscoelastic properties of asphalt materials. However, there are still some distinctions between the two asphalt mixtures. At low temperatures, the stress of the SMA 11 is larger than that of the AC 11 except for 10 Hz in the IDT test. The strain of the SMA 11 is bigger than that of the AC 11 except for 10 Hz in the IDT test. Meanwhile, the stresses of the UC test grow slowly with the increase in frequency, and

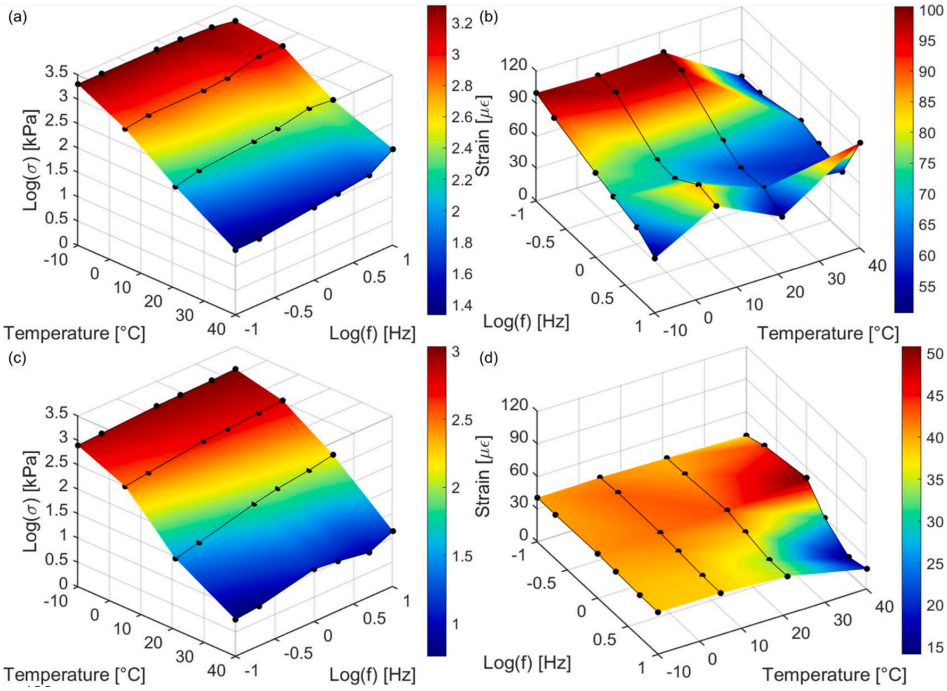

Fig. 17. Stress–strain states of SMA 11 in IDT test and UC test at various conditions: (a) SMA 11-IDT stress, (b) SMA 11-IDT strain, (c) SMA 11-UC stress and (d) SMA 11-UC strain.

the strains remain around 40 με for both AC 11 and SMA 11. Thus, this finding illustrates that the UC test has better control of stress and strain than the IDT test. Comparing the results depicted in Fig. 15(a, c) and Fig. 17(a, c) for high temperatures, the IDT test stress values measured for the SMA 11 samples are smaller than the ones for the AC 11 specimens. At 40 °C, the stress values of the SMA 11 in the IDT test decrease on average by about 15 % relative to the AC 11. However, the stress of the SMA 11 is almost the same as that of the AC 11 in the UC test at 40 °C. The trends of the strain values measured for both SMA 11 and AC 11 asphalt mixtures are similar at high temperatures.

The *CoV* of stress and strain results for SMA 11 mixtures have a similar trend to that for AC 11 mixtures as presented in Fig. 18. It is worth finding that the *CoV* of the UC test strain is very small at −10, 5, 21 °C and is relatively large at 40 °C for both asphalt mixtures. This reflects that the UC test has a very stable control on strain at −10, 5, 21 °C and controls strain unstably at high temperatures.

3.2.2. Normalised stress and strain

As the different modes of control strain for the two tests, the stress and the strain are normalised by dividing by the maximum value method for comparison. The normalised stresses at every temperature are used to reflect the changing trend of the stress. The exponential formulations used to fit the experimental values of mean stress and temperature are shown in Fig. 19. The high R^2 values validate the reliability of the relationship. The normalised stresses at −10 °C are similar for both tests and the difference occurs at high temperatures. At 40 °C, the values of normalised stresses measured by the IDT test are approximately 3.26 and 2.34 times greater than the ones measured by the UC test for AC 11 and SMA 11 mixtures, respectively. Compared with UC test, the results indicate that the stress level of the IDT test is higher and the difference between the two tests of AC 11 is greater than that of SMA 11 in terms of stress.

The relationship between normalised strain and temperature is shown in Fig. 20. At −10 °C, the normalized strain of the UC test has a stable value of around 0.8, which corresponded to 40 με. The strain difference with frequencies increases gradually with the increase in temperature. At 40 °C, the strains of the UC test at six frequencies are quite different. The normalised strain of the IDT test shows large deviations at all four test temperatures. The strain deviation under different frequencies of the IDT test is greater than that of the UC test at −10, 5 and 21 °C and smaller than that of the UC test at 40 °C. The results indicate that the changing trend of strain with temperature for the UC test is smaller than that of the IDT test at low and medium temperatures, while higher at high temperatures. This result demonstrates a better control over strain of the UC test at low and medium temperatures, which is consistent with the *CoV* of strain results.

3.3. Comparison between IDT test and UC test

The main features of the IDT test and UC test setups and result trends are summarised in Table 6. Due to the smaller dimension (weight) of the test specimen dimension (weight) the IDT test is more convenient for testing field core samples and for sample preparation in the laboratory, e.g., making plate samples and core and cut from them. The biaxial stress of the IDT test involves Poisson's ratio. In this test, the stress–strain response in horizontal direction is only considered and Poisson's ratio is

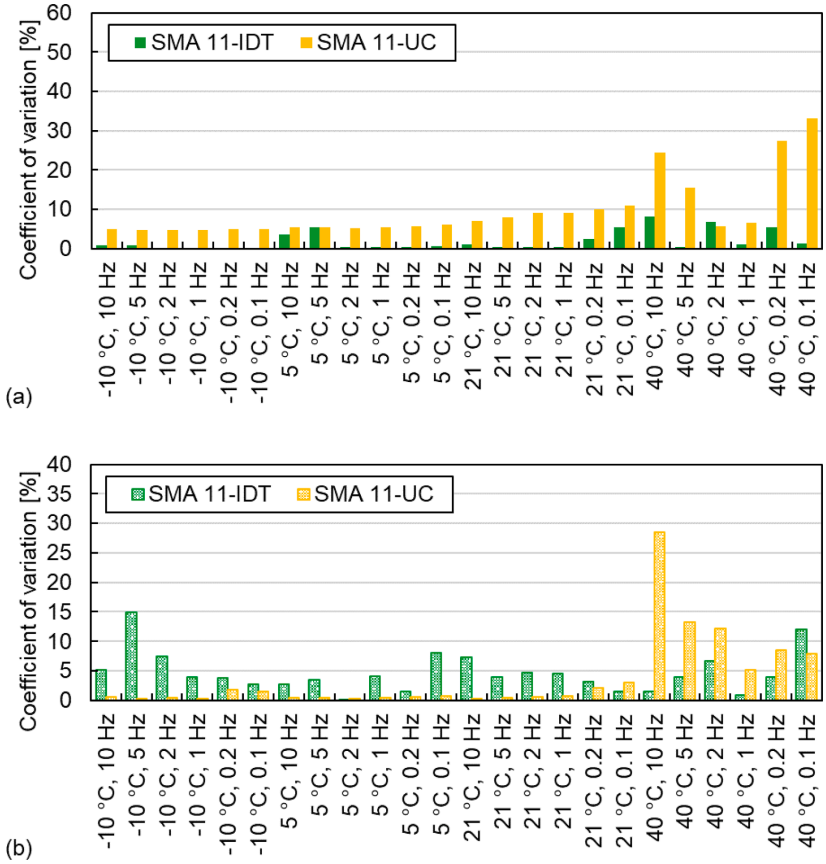

Fig. 18. Coefficient of variation of stress and strain results of SMA 11 mixtures: (a) stress and (b) strain.

selected as a constant value of 0.35 according to the standard (EN 12697–26). Differently from IDT test, the UC test takes account into stresses in a single direction (vertical direction) less affected by Poisson's ratio. Moreover, the UC test employs confining pressure, which can better simulate real service conditions of road pavement [42]. However, the UC test needs more time to condition temperature due to the larger size of the sample. Nevertheless, both IDT test and UC test can work well at intermediate temperatures. Considering the dynamic moduli, the results from the two tests are almost identical for intermediate frequency and temperature ranges, and slightly different at extreme temperatures. Regarding the phase angle, the UC test results are more accurate than IDT test results. Besides, the stress–strain states for IDT test and UC test are different. This is due to the different force forms and strain control modes of the two tests. The biaxial and uniaxial loads are applied to the IDT and UC tests, respectively. The initial strain of IDT test is controlled manually, while the strain of UC test is controlled by the software in the whole test procedure. Furthermore, the greater number of analysed cycles for the UC test also reflects better stability than the IDT test. Therefore, the UC test shows better deformation control at low and medium temperatures.

4. Conclusions

This study compares the two standard laboratory tests used for the mechanical characterisation of bituminous asphalt, namely Indirect Tensile (IDT) test and Uniaxial Compression (UC). The performance of two mixtures commonly employed for road surfacing, Asphalt Concrete (AC) and Stone Mastic Asphalt (SMA), are compared in terms of dynamic modulus, phase angle, shift factor and stress–strain state. Based on the attained results, the conclusions are drawn as follows:

- The dynamic moduli measured using both tests at medium frequency (temperature) range are the same. Moreover, the values obtained from IDT test are higher than the ones assessed by UC test at extreme frequencies (temperatures). The different mesoscopic structures of the asphalt mixture can account for the discrepancies in the results attained with the two test methods. The difference in dynamic modulus of SMA mixtures measured by both tests is smaller than that of AC mixtures.
- Compared with IDT test, the phase angle master curve has a better fit for UC test and has lower values.
- The shift factor of SMA 11-UC is bigger than that of SMA 11-IDT at low temperatures, which is different from the situation for AC 11

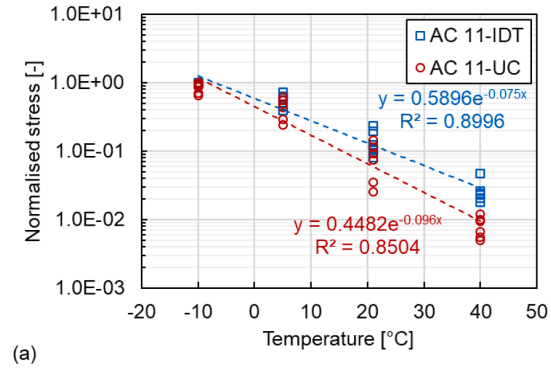

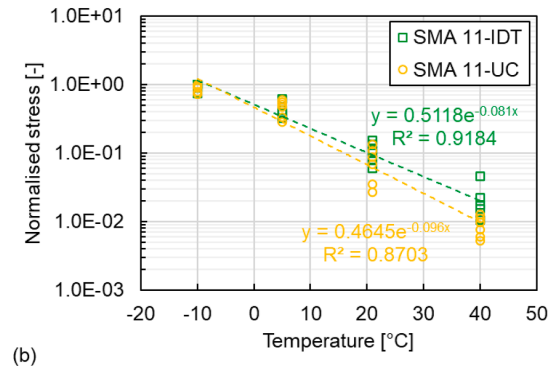

Fig. 19. Relationship between normalised stress and temperature: (a) AC 11 and (b) SMA 11.

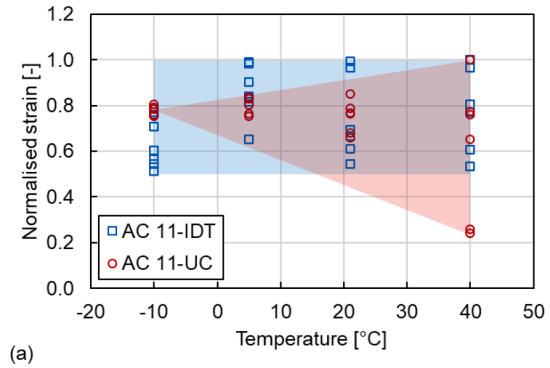

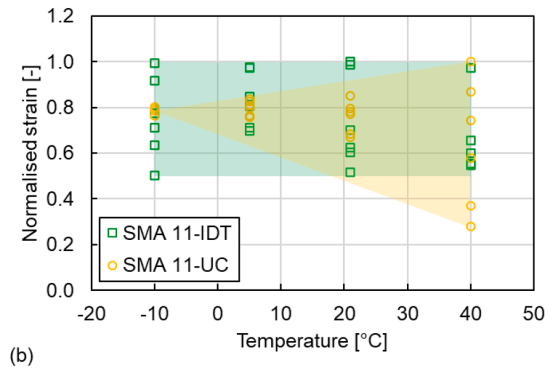

Fig. 20. Relationship between normalised strain and temperature: (a) AC 11 and (b) SMA 11.

mixtures. The measured dynamic modulus and the shifting situation cause a smaller difference between the two test methods in modelling dynamic modulus for the SMA 11 mixtures.

- The stress level pertaining to the IDT test is bigger than the one achieved during UC test. The IDT test strain values are various at all four test temperatures. Although the variation of strain obtained from the UC test is based on the frequency largens as the temperature increases, the stress–strain states are stable at low and medium temperatures, showing a better strain control than the IDT test.
- The coefficients of variation of dynamic modulus, stress and strain results are small at −10, 5, 21 °C and higher at 40 °C indicating that both test modes are more stable for testing the mechanical properties of asphalt mixtures at low and medium temperatures. The phase angle results only show small variations at 21 °C.

In general, both tests can be used to properly characterise the dynamic modulus of asphalt materials. The IDT test can be efficiently used for the characterisation of road surfaces built in cold regions. Moreover, the IDT test plays an important role when it comes to the mechanical characterisation of existing asphalt pavements since the dimensions of the field samples normally meet the size requirements. The UC test controls strain better for low and medium temperature ranges compared with IDT test, resulting in more accurate results. A confining pressure can be applied for UC test, which better simulates real field conditions. For Norwegian conditions as a basis for practical design, the IDT test seems to be the best choice due to easier/more realistic sample preparation and to compare with field cored samples.

The comparison between IDT and UC modes in dynamic modulus tests for AC 11 and SMA 11 mixtures was focused on in this study. Further studies involving more types of asphalt mixtures are recommended to investigate the effect of materials on the difference between the two test modes and fully understand the two modes of dynamic modulus tests. Moreover, the connection of the IDT and UC tests under extreme environmental conditions will be established to develop the wide application of the IDT test in ME pavement design.

5. Data availability

Data will be made available on request.

CRediT authorship contribution statement

Hao Chen: Conceptualization, Methodology, Software, Formal analysis, Investigation, Data curation, Writing – original draft. **Mequanent Mulugeta Alamnie:** Conceptualization, Methodology, Investigation, Data curation, Writing – review & editing. **Diego Maria Barbieri:** Investigation, Writing – review & editing. **Xuemei Zhang:** Investigation, Writing – review & editing. **Gang Liu:** Methodology, Writing – review & editing, Supervision. **Inge Hoff:** Resources, Writing – review & editing, Supervision.

Table 6
Summarised comparison between IDT test and UC test.

Item			IDT test	UC test
Standard			EN 12697–26:2018	AASHTO T378-17
Cylindrical specimen dimension	Diameter		100 mm	100 mm
	Thickness (height)		40 mm	150 mm
Conditioning temperature time			≥ 4 h (Better for low temperature)	−10 °C ~ Overnight 5 °C ~ 4 h or Overnight 21 °C ~ 3 h 40 °C ~ 2 h (Suitable for intermediate and high temperature)
Test temperature (this study)			−10 °C, 5 °C, 21 °C, 40 °C	
Test frequency (this study)			10 Hz, 5 Hz, 2 Hz, 1 Hz, 0.2 Hz, 0.1 Hz	
Applied load			Harmonic sinusoidal load	
Load control mode			Controlled stress–strain	Controlled strain
Number of analysed cycles			5 cycles	10 cycles
Dynamic modulus	f_r: 10^{-4} ~ 10 Hz	AC 11	255 ~ 6379 MPa	67 ~ 5072 MPa
		CoV	1.4 % ~ 11.0 %	5.7 % ~ 32.9 %
		SMA 11	292 ~ 5341 MPa	74 ~ 5028 MPa
		CoV	0.2 % ~ 10.6 %	5.7 % ~ 32.3 %
	f_r: 10 ~ 10^4 Hz	AC 11	6379 ~ 24329 MPa	5072 ~ 20224 MPa
		CoV	0.1 % ~ 7.7 %	5.8 % ~ 11.7 %
		SMA 11	5341 ~ 21066 MPa	5028 ~ 19546 MPa
		CoV	0.5 % ~ 8.3 %	5.3 % ~ 6.7 %
	f_r: 10^4 ~ 10^8 Hz	AC 11	24329 ~ 45411 MPa	20224 ~ 25731 MPa
		CoV	1.1 % ~ 3.9 %	4.1 % ~ 6.2 %
		SMA 11	21066 ~ 35123 MPa	19546 ~ 25808 MPa
		CoV	4.0 % ~ 7.5 %	4.8 % ~ 4.9 %
	S_e/S_y	AC 11	0.058	0.089
		SMA 11	0.065	0.109
	R^2	AC 11	0.997	0.992
		SMA 11	0.996	0.988
Phase angle	f_r: 10^{-4} ~ 10 Hz	AC 11	20 ~ 40°	17 ~ 39°
		CoV	1.0 % ~ 5.5 %	2.2 % ~ 13.6 %
		SMA 11	25 ~ 46°	18 ~ 38°
		CoV	0.1 % ~ 12.1 %	0.8 % ~ 10.0 %
	f_r: 10 ~ 10^4 Hz	AC 11	12 ~ 29°	11 ~ 30°
		CoV	0.3 % ~ 13.4 %	3.0 % ~ 19.8 %
		SMA 11	12 ~ 31°	12 ~ 29°
		CoV	2.1 % ~ 16.9 %	1.7 % ~ 2.4 %
	f_r: 10^4 ~ 10^8 Hz	AC 11	4 ~ 12°	4 ~ 11°
		CoV	9.7 % ~ 27.8 %	19.0 % ~ 19.7 %
		SMA 11	5 ~ 12°	4 ~ 11°
		CoV	10.1 % ~ 17.4 %	3.1 % ~ 4.9 %
	S_e/S_y	AC 11	0.261	0.116
		SMA 11	0.217	0.135
	R^2	AC 11	0.932	0.987
		SMA 11	0.953	0.982
Shift factor	$T < T_r$	AC 11	2.4 ~ 4.9	2.0 ~ 4.4
		SMA 11	2.3 ~ 4.8	2.5 ~ 6.0
	$T \geq T_r$	AC 11	−2.4 ~ 0	−2.0 ~ 0
		SMA 11	−2.5 ~ 0	−2.0 ~ 0
Stress	Direction		Horizontal and vertical (biaxial)	Vertical (uniaxial)
	$T < T_r$	AC 11	766 ~ 1982 kPa	240 ~ 987 kPa
		CoV	1.5 % ~ 18.4 %	4.3 % ~ 12.5 %
		SMA 11	665 ~ 2047 kPa	306 ~ 1087 kPa
		CoV	0.1 % ~ 5.5 %	4.7 % ~ 6.2 %
	$T \geq T_r$	AC 11	35 ~ 468 kPa	5 ~ 143 kPa
		CoV	1.2 % ~ 28.3 %	7.3 % ~ 49.2 %
		SMA 11	22 ~ 310 kPa	6 ~ 146 kPa
		CoV	0.3 % ~ 8.3 %	5.6 % ~ 33.2 %
Strain	Direction		Horizontal	Vertical
	$T < T_r$	AC 11	52 ~ 100 με	38 ~ 43 με
		CoV	2.3 % ~ 14.3 %	0.6 % ~ 1.5 %
		SMA 11	51 ~ 100 με	38 ~ 43 με
		CoV	0.1 % ~ 14.9 %	0.3 % ~ 1.8 %
	$T \geq T_r$	AC 11	54 ~ 101 με	12 ~ 51 με
		CoV	0.5 % ~ 21.3 %	0.8 % ~ 35.5 %
		SMA 11	52 ~ 101 με	14 ~ 51 με
		CoV	0.8 % ~ 11.9 %	0.3 % ~ 28.5 %

Declaration of Competing Interest

The authors declare that they have no known competing financial interests or personal relationships that could have appeared to influence the work reported in this paper.

Data availability

Data will be made available on request.

Acknowledgements

This research work was supported by the VegDim project of the Norwegian Public Roads Administration. The financial support provided by China Scholarship Council (No. 201806950077) and Department of Civil and Environmental Engineering, Norwegian University of Science and Technology (No. K-649105) is highly acknowledged. The support kindly provided by the laboratory technicians Bent Lervik and Jan Erik Molde is greatly acknowledged.

References

[1] Y.H. Huang, Pavement analysis and design, Pearson Prentice, Hall Upper Saddle River, NJ, 2004.
[2] A. Maji, A. Das, Reliability considerations of bituminous pavement design by mechanistic–empirical approach, Int. J. Pavement Eng. 9 (1) (2008) 19–31.
[3] Nchrp, Guide for Mechanistic-Empirical Design of New and Rehabilitated Pavement Structures, NCHRP 1–37A Part 2 Design Inputs Chapter 2 Material Characterization, Transportation Research Board, Washington, D.C., 2004.
[4] D. Lesueur, J.F. Gerard, P. Claudy, J.M. Letoffe, J.P. Planche, D. Martin, A structure-related model to describe asphalt linear viscoelasticity, J. Rheol. 40 (5) (1996) 813–836.
[5] D.D. Li, M.L. Greenfield, Viscosity, relaxation time, and dynamics within a model asphalt of larger molecules, J. Chem. Phys. 140 (3) (2014), 034507.
[6] X. Zhang, H. Chen, D.M. Barbieri, B. Lou, I. Hoff, The classification and reutilisation of recycled asphalt pavement binder: Norwegian case study, Case Stud. Constr. Mater. 17 (2022) e01491.
[7] T. Officials, AASHTO Guide for Design of Pavement Structures, AASHTO (1993).

[8] C.W. Schwartz, N. Gibson, R.A. Schapery, Time-temperature superposition for asphalt concrete at large compressive strains, Transp. Res. Rec. 1789 (1) (2002) 101–112.
[9] H. Yao, Z. You, L. Li, C.H. Lee, D. Wingard, Y.K. Yap, X. Shi, S.W. Goh, Rheological properties and chemical bonding of asphalt modified with nanosilica, J. Mater. Civ. Eng. 25 (11) (2013) 1619–1630.
[10] T. Chen, Y. Luan, T. Ma, J. Zhu, X. Huang, S. Ma, Mechanical and microstructural characteristics of different interfaces in cold recycled mixture containing cement and asphalt emulsion, J. Clean. Prod. 258 (2020), 120674.
[11] J. Zhu, T. Ma, J. Fan, Z. Fang, T. Chen, Y. Zhou, Experimental study of high modulus asphalt mixture containing reclaimed asphalt pavement, J. Clean. Prod. 263 (2020), 121447.
[12] D.W. Christensen, R.F. Bonaquist, Evaluation of indirect tensile test (IDT) procedures for low-temperature performance of hot mix asphalt, Transp. Res. Board (2004).
[13] M. Zaumanis, M.C. Cavalli, L.D. Poulikakos, How not to design 100% recycled asphalt mixture using performance-based tests, Road Mater. Pavement Des. 21 (6) (2020) 1634–1646.
[14] K. Mollenhauer, P. Plachkova-Dzhurova, Categories for stiffness and fatigue based on cyclic indirect tensile tests and their applicability in construction contracts. 6th Eurasphlat & Eurobitumen Congress, 2016.
[15] X. Zhang, H. Chen, D.M. Barbieri, I. Hoff, Laboratory Evaluation of Mechanical Properties of Asphalt Mixtures Exposed to Sodium Chloride, 03611981221082579, Transp. Res. Rec. (2022).
[16] R.G. Saba, Analytical Design of Pavement Structures, NPRA reports, Norway, (2019).
[17] H. Cheng, Y. Wang, L. Liu, L. Sun, Y. Zhang, R. Yang, Estimating tensile and compressive moduli of asphalt mixture from indirect tensile and four-point bending tests, ASCE J. Mater. Civ. Eng. 33 (1) (2021) 04020402.
[18] Y.R. Kim, Y. Seo, M. King, M. Momen, Dynamic modulus testing of asphalt concrete in indirect tension mode, Transp. Res. Rec. 1891 (1) (2004) 163–173.
[19] X. Qin, L. Ma, H. Wang, Comparison analysis of dynamic modulus of asphalt mixture: indirect tension and uniaxial compression test, Transportmetrica A 15 (1) (2019) 165–178.
[20] D. Barbieri, I. Hoff, H. Mork, Laboratory investigation on unbound materials used in a highway with premature damage, Bearing capacity of Roads, Railways and Airfields, CRC Press, 2017, pp. 101–108.
[21] D.M. Barbieri, I. Hoff, M.B.E. Mørk, Mechanical assessment of crushed rocks derived from tunnelling operations, in: Civil Infrastructures Confronting Severe Weathers and Climate Changes Conference, Springer, 2018, pp. 225–241.
[22] CEN, EN 1426:2015 Bitumen and bituminous binders Determination of needle penetration, Brussels, Belgium, (2015).
[23] CEN, EN 1427:2015 Bitumen and bituminous binders Determination of the softening point Ring and Ball method, Brussels, Belgium, (2015).
[24] CEN, EN 1097-1:2011 Tests for mechanical and physical properties of aggregates Part 1: Determination of the resistance to wear (micro-Deval), Brussels, Belgium, (2011).
[25] CEN, EN 1097-2:2020 Tests for mechanical and physical properties of aggregates Part 2: Methods for the determination of resistance to fragmentation, Brussels, Belgium, (2020).
[26] CEN, EN 12697-31:2019 Bituminous mixtures Test methods Part 31: Specimen preparation by gyratory compactor, Brussels, Belgium, (2019).
[27] M.M. Alamnie, E. Taddesse, I. Hoff, Thermo-piezo-rheological characterization of asphalt concrete, Constr. Build. Mater. 329 (2022), 127106.
[28] R.E. Asbjørn Arnevik, Nils Sigurd Uthus, Joralf Aurstad, Jostein Aksnes, Torbjørn Jørgensen, Guidelines asphalt 2019, NPRA reports, Norway, (2019).
[29] CEN, EN 12697-8:2018 Bituminous mixtures Test methods Part 8: Determination of void characteristics of bituminous specimens, Brussels, Belgium, (2018).
[30] CEN, EN 12697-26:2018 Bituminous mixtures Test methods Part 26: Stiffness, Brussels, Belgium, (2018).
[31] G. Cerni, E. Bocci, F. Cardone, A. Corradini, Correlation between asphalt mixture stiffness determined through static and dynamic indirect tensile tests, Arab. J. Sci. Eng. 42 (3) (2017) 1295–1303.
[32] F. Olard, F. Noël, F. Loup, Modulus testing in indirect tension mode, Road Mater. Pavement Des. 7 (4) (2006) 543–554.
[33] P. Ghasemi, S. Lin, D.K. Rollins, R.C. Williams, Predicting dynamic modulus of asphalt mixture using data obtained from indirect tension mode of testing, arXiv preprint arXiv:1905.06810 (2019).
[34] AASHTO, T 378-17 Standard Method of Test for Determination the Dynamic Modulus and Flow Number for Asphalt Mixtures Using the Asphalt Mixture Performance Tester (AMPT), Washington, D.C., (2017).
[35] M.L. Williams, R.F. Landel, J.D. Ferry, The temperature dependence of relaxation mechanisms in amorphous polymers and other glass-forming liquids, J. Am. Chem. Soc. 77 (14) (1955) 3701–3707.
[36] R. Nemati, E.V. Dave, Nominal property based predictive models for asphalt mixture complex modulus (dynamic modulus and phase angle), Constr. Build. Mater. 158 (2018) 308–319.
[37] A.R. Archilla, J.P. Corrales-Azofeifa, J.P. Aguiar-Moya, Comprehensive Model for the Prediction of the Phase Angle Master Curve of Asphalt Concrete Mixes, in: RILEM International Symposium on Bituminous Materials, Springer, 2020, pp. 473–479.
[38] T.K. Pellinen, M.W. Witczak, R.F. Bonaquist, Asphalt mix master curve construction using sigmoidal fitting function with non-linear least squares optimization, Recent advances in materials characterization and modeling of pavement systems (2004) 83-101.
[39] H. Chen, D.M. Barbieri, X. Zhang, I. Hoff, Reliability of Calculation of Dynamic Modulus for Asphalt Mixtures Using Different Master Curve Models and Shift Factor Equations, Materials 15 (12) (2022) 4325.
[40] M.W. Witzcak, Simple performance test for superpave mix design, Transportation Research Board (2002).
[41] I.M. Asi, Laboratory comparison study for the use of stone matrix asphalt in hot weather climates, Constr. Build. Mater. 20 (10) (2006) 982–989.
[42] H.L. Von Quintus, J. Rauhut, T. Kennedy, Comparisons of asphalt concrete stiffness as measured by various testing techniques (with discussion), Association of Asphalt Paving Technologists Proceedings, (1982).

APPENDIX E – PAPER V

Chen, Hao; Hoff, Inge; Liu, Gang[*]; Zhang, Xuemei[**]; Barbieri, Diego Maria; Wang, Fusong; Liu, Jianan.

Development of finite element model based on indirect tensile test for various asphalt mixtures.

Submitted to the Journal of Construction and Building Materials.

This paper is awaiting publicaton and is not included in NTNU Open

ISBN 978-82-326-7116-8 (printed ver.)
ISBN 978-82-326-7115-1 (electronic ver.)
ISSN 1503-8181 (printed ver.)
ISSN 2703-8084 (online ver.)

NTNU

Norwegian University of
Science and Technology